

Protein-Based Particles Structure-Function Relationships

Franziska Maria Hartinger

Vollständiger Abdruck der von der TUM School of Life Sciences der Technischen Universität München zur Erlangung einer
Doktorin der Ingenieurwissenschaften (Dr.-Ing.)
genehmigten Dissertation.

Vorsitz: Prof. Dr. Mirjana Minceva

Prüfer*innen der Dissertation:

1. Prof. Dr.-Ing. Ulrich Kulozik
2. Prof. Dr.-Ing. Heiko Briesen

Die Dissertation wurde am 01.12.2022 bei der Technischen Universität München eingereicht und durch die TUM School of Life Sciences am 07.03.2023 angenommen.

Für meine Familie

Acknowledgements

Die vorliegende Arbeit entstand während meiner Zeit als wissenschaftliche Mitarbeiterin am Lehrstuhl für Lebensmittel- und Bio-Prozesstechnik der Technischen Universität München unter Leitung von Herrn Professor Dr.-Ing. Ulrich Kulozik.

Zunächst möchte ich bei Herrn Professor Dr.-Ing. Ulrich Kulozik für sein entgegengebrachtes Vertrauen, die zur Verfügung gestellte hervorragende technische und analytische Ausstattung sowie den wissenschaftlichen Austausch bedanken.

Ein ganz besonderer Dank gilt Jannika Dombrowski, Joseph Dumpler und Martin Hartinger für die zahlreichen Diskussionen und die ständige Unterstützung auch außerhalb ihrer Lehrstuhlzeit, die maßgeblich zum Gelingen dieser Arbeit beigetragen haben.

Darüber hinaus möchte ich mich bei allen Kolleginnen und Kollegen des Lehrstuhls für das angenehme und unterstützende Umfeld, für die Zeit und das Wissen, die sie in diese Arbeit investiert haben bedanken. Ein besonderer Dank gilt hierbei Hermine Roßgoderer und Claudia Hengst für die experimentelle Unterstützung! Für die Unterstützung bei administrativen Angelegenheiten möchte ich mich bei Sabine Becker und Friederike Schöpflin bedanken. Sabine Grabbe danke ich von Herzen für die unersetzliche Unterstützung bei all meinen IT-Fragen. Ganz großer Dank gilt meinen Kollegen, die im Laufe der Jahre zu Freunden geworden sind und somit diese Zeit unvergessen machen! Danke an: Simon, Joseph and Andy (E.25 beste); Martin, Claudi, Regina, Roland, Christian und Malou.

Ein besonderer Dank gilt meinen Studenten, die maßgeblich zum Erfolg dieser Arbeit beigetragen haben. Insbesondere danke ich hierbei Christina Kiener, Vera Reitberger und Christina Dormeier.

Dafür, dass sie mir die beste Work-Life-Balance ermöglicht haben, möchte ich Aline, Maria, Yvonne, Michi, Vreni, Kessi und Eva, meinen lieben Freunden „außerhalb des Lehrstuhls“, danken!

Ein ganz besonderer Dank aus tiefstem Herzen gilt meinen „Teilzeit-Eltern“ Franz und Marianne (†) für die große persönliche Unterstützung und die unvergesslich schöne gemeinsame Zeit in Pulling. Ein weiterer besonderer Dank gilt Edgar (†), der mir beigebracht hat, an mich selbst zu glauben. Umso mehr stimmt es mich traurig, dass nicht alle den Abschluss dieser Arbeit erleben durften.

Mein größter Dank gilt meiner Familie! Mama und Papa, Kathi und Tobi, Marina und Florian, Martin und Selina, Anna, Xaver, Laura, Josefa und Eva, und „meinem“ Martin. Danke für eure Geduld, euer Verständnis, eure Unterstützung und besonders dafür, dass ihr mich immer daran erinnert habt, dass es Dinge im Leben gibt, die wichtiger sind als Proteinpartikel.

Contents

Acknowledgements	V
Contents	VII
Abbreviations	XI
Summary & Zusammenfassung	XV
<i>Summary</i>	XV
<i>Zusammenfassung</i>	XIX
1 General Introduction	1
1.1 <i>Proteins</i>	3
1.1.1 Structural Properties of Proteins	3
1.1.2 Whey Proteins	3
1.1.3 Plant Proteins – Patatin: Molecular and Structural Properties	6
1.2 <i>Heat-Induced Generation of β-Lg-Based Particles</i>	6
1.2.1 Mechanism of β -Lg Unfolding and Aggregation	7
1.2.2 Molecular Interactions During Heat Treatment	8
1.2.3 Selected Environmental Factors Affecting the Thermally-Induced Denaturation and the Resulting β -Lg Particle Properties.....	8
1.3 <i>Stabilization of Interfaces</i>	13
1.3.1 General Aspects Relating to Interfaces.....	13
1.3.2 Surface Active Molecules: Proteins at Interfaces	15
1.4 <i>Foaming and Emulsifying Properties of Proteins and Protein-Based Particles</i>	19
1.4.1 Foams: Formation and Structure	19
1.4.2 Emulsions: Formation and Structure	21
1.4.3 Foam and Emulsion Stabilization.....	22
1.4.4 Foam and Emulsion Destabilization Mechanisms	24
1.4.5 Factors Affecting the Interfacial, Foaming and Emulsifying Properties of Proteins	28
2 Motivation and Objectives	33
3 RP-HPLC Method for Simultaneous Quantification of Free and Total Thiol Groups in Native and Heat Aggregated Whey Proteins	35
<i>Summary and Contribution of the Doctoral Candidate Franziska Maria Hartinger (Name at Birth: Kurz)</i>	35
<i>Abstract</i>	36
3.1 <i>Background Information</i>	38
3.2 <i>Method Protocol</i>	40
3.2.1 Preparation and Storage of 40 mM 4,4'-dithiodipyridine Stock Solution	40
3.2.2 Buffer and Sample Preparation for Free Thiols	41
3.2.3 Buffer and Sample Preparation for Free Thiols and Disulfide Bonds (Total Thiols).....	42
3.2.4 Calibration and Analysis of Thiols by RP-HPLC.....	44
3.2.5 Calculation of Parameters for Characterization of Thiol-Disulfide Reactions During Processing.....	45
3.3 <i>Method Validation</i>	46
3.3.1 Buffer Composition.....	46
3.3.2 DTDP Concentration	49

3.3.3	Recovery Rates	51
3.3.4	Reproducibility of the Method	52
3.3.5	Thiol Reactivity and Disulfide Formation/ Degradation during Heat Treatment.....	52
4	Correlation between Physico-Chemical Characteristics of Particulated β-Lactoglobulin and Its Behavior at Air/Water and Oil/Water Interfaces.....	55
	<i>Summary and Contribution of the Doctoral Candidate Franziska Maria Hartinger (Name at Birth: Kurz).</i>	<i>55</i>
	<i>Abstract.....</i>	<i>57</i>
4.1	<i>Introduction</i>	<i>58</i>
4.2	<i>Materials and Methods</i>	<i>60</i>
4.2.1	Materials.....	60
4.2.2	Production of β -Lactoglobulin Particles by Thermal Treatment and Particle Concentration	60
4.2.3	Quantification of Protein Thiols and Disulfide Bonds	62
4.2.4	Particle Size and Zeta Potential Measurements	62
4.2.5	Viscosity Measurements.....	62
4.2.6	Surface and Interfacial Tension	63
4.2.7	Foaming and Characterization of Foam Stability.....	63
4.2.8	Emulsification and Measurement of Oil Droplet Size	64
4.3	<i>Results and Discussion</i>	<i>65</i>
4.3.1	Preparation and Structural Characterization of β -Lg Particles	65
4.3.2	β -Lg Particles at the Air/Water Interface: Interfacial Properties and Foam Structure Dynamics	69
4.3.3	β -Lg Particles at the Oil/Water Interface: Interfacial Properties and Emulsion Stabilization	74
4.3.4	Comparison of the Properties of β -Lg Particles at the Air/Water and the Oil/Water Interfaces.....	78
4.4	<i>Conclusion.....</i>	<i>80</i>
4.5	<i>Appendix A.....</i>	<i>81</i>
5	Technofunctionality of β-Lg and β-Lg Nanosized Particles at Air/Water and Oil/Water Interfaces as a Function of Structural and Surface Characteristics	83
	<i>Summary and Contribution of the Doctoral Candidate Franziska Maria Hartinger (Name at Birth: Kurz).</i>	<i>83</i>
	<i>Abstract.....</i>	<i>84</i>
5.1	<i>Introduction</i>	<i>85</i>
5.2	<i>Materials and Methods</i>	<i>87</i>
5.2.1	Materials.....	87
5.2.2	β -Lg Particle Preparation	87
5.2.3	Purification of the β -Lg Particles by Membrane Filtration in Diafiltration Mode	88
5.2.4	Particle Size.....	89
5.2.5	Zeta Potential	89
5.2.6	Degree of Disulfide Cross-Linking	89
5.2.7	Hydrophobicity of the Particle Surface.....	90
5.2.8	Viscosity.....	90
5.2.9	Surface and Interfacial Tension	90
5.2.10	Foam Formation and Stability	91
5.2.11	Emulsion Formation and Stability.....	92

5.2.12	Statistical Analysis.....	92
5.3	<i>Results and Discussion</i>	92
5.3.1	β -Lg Particle Generation, Purification, and Characterization.	92
5.3.2	Behavior of β -Lg Particles at the Air/Water and Oil/Water (MCT and SF) Interface	93
5.3.3	β -Lg Particles: Foaming and Emulsifying Properties	97
6	Impact of the pH Value on the Techno-Functionality of Native and Particulated β-Lg	105
6.1	<i>Introduction</i>	105
6.2	<i>Material and Methods</i>	107
6.2.1	Materials.....	107
6.2.2	Native (Non-Particulated) β -Lg Solutions	107
6.2.3	β -Lg Particle Preparation and Purification.....	107
6.2.4	Particle Size and Zeta Potential	108
6.2.5	Viscosity	108
6.2.6	Surface Tension	108
6.2.7	Foam Formation and Stability	108
6.3	<i>Results and Discussion</i>	109
6.3.1	Interfacial Properties	109
6.3.2	Foaming Properties.....	111
7	Overall Discussion and Main Findings	115
7.1	<i>β-Lg Particles: Generation and Purification</i>	115
7.1.1	Impact of pH Value and Ionic Strength Upon Heating on the Resulting β -Lg Particles Characteristics	115
7.1.2	Comparison of Purification Methods.....	117
7.2	<i>Influence of Specific Particle Characteristics on the Techno-Functional Properties of β-Lg and β-Lg Particles at the Air/Water Interface</i>	119
7.2.1	Understanding Protein Adsorption at the Air/Water Interface.....	119
7.2.2	Understanding Foam Formation.....	122
7.2.3	Understanding Foam Stabilization.....	123
7.2.4	Correlation between Interfacial and Foaming Properties	126
7.2.5	Comparison of Techno-Functionality as Affected by the Purification Method	127
7.3	<i>Transferability of Results from Air/Water to Oil/Water Interfaces</i>	129
8	Appendix	133
	<i>Peer Reviewed Publications (included in this thesis)</i>	133
	<i>Peer Reviewed Publications (not included in this thesis)</i>	133
	<i>Non Reviewed Publications</i>	133
	<i>Oral and Poster Presentations</i>	134
9	References	135

Abbreviations

Main Latin Symbols

A	area, mean bubble area	m ²
a/w	air/water interface	
ACN	acetonitrile	
Bo	Bond number	-
BSA	bovine serum albumin	
c	concentration	kg m ⁻³ , mol L ⁻¹
CYS	cysteine	
d	diameter	m
d _{3.2}	the Sauter, surface weighted mean diameter	m
d _{50.3}	volume-based median particle diameter	m
D	diffusion coefficient	N m ⁻¹ s ^{-0.5}
DC	degree of disulfide cross-linking	%, -
DD	degree of denaturation	%
DF	diafiltration	
DTDP	4,4'-dithiodipyridine	
DTNB	5,5'-di-thiobis(2-nitrobenzoic acid)	
DTT	dithiothreitol	
E	energy	J
EDTA	ethylenediaminetetraacetic acid	
ff	flocculation factor	-
FA	foamability	%
FD	foam drainage	%
FS	normalized foam stability	%
g	gravity	m s ⁻²
G	Gibbs free energy	J

GdnHCl	guanidine hydrochloride	
h	height	m
HCl	hydrochloric acid	
I	ionic strength	mol L ⁻¹
IgG	immunoglobulin G	
KH ₂ PO ₄	potassium phosphate monobasic	
L	length	m
M _w	molecular weight	kg mol ⁻¹
MCT	medium chain triglyceride	
n	number of replications, number of moles	
n.d.	not determined	
Na ₂ HPO ₄	sodium phosphate dibasic	
NaBH ₄	sodium borohydride	
NaCl	sodium chloride	
NaOH	sodium hydroxide	
NTP	p-nitrothiophenol	
o/w	oil/water interface	
P, p	pressure	Pa
PDI	polydispersity index	-
r	radius	m
Re	Reynolds number	
RI	refractive index	
RP-HPLC	reversed-phase high performance liquid chromatography	
PRODAN	N,N-dimethyl-6-propionyl-2-naphthylamine dimethyl-6-propionyl-2-naphthylamine	
RSH	free thiol	
RSSR	disulfide bond	

S	entropy	J K^{-1}
S_0	surface hydrophobicity	-
SDS	sodium dodecyl sulfate	
SDS-PAGE	sodium dodecyl sulfate polyacrylamide gel electrophoresis	
SF	sunflower	
SH	thiol group	
SS	disulfide bond	
t	time	s
T	absolute temperature	K
TFA	trifluoroacetic acid	
total	total thiols	
4-TP	4-thiopyridine	
v	velocity	m s^{-1}
V	volume	m^3
\dot{V}	film drainage	$\text{m}^3 \text{s}^{-1}$
WPC	whey protein concentrate	
WPI	whey protein isolate	
x	time	s
z	charge number	-
ZP	zeta potential	mV

Main Latin Indices

0	initial, unheated
50.3	volume based median
dyn	dynamic
RSH	free thiols

RSSR	disulfide bond
SH	thiol
t	time dependent

Main Greek Symbols and Indices

α	coarsening exponent/ factor	-
α -La	α -lactalbumin	
β -Lg	β -lactoglobulin	
γ	interfacial tension	N m^{-1}
δ	thickness	m
ε	molar extinction coefficient	$\text{M}^{-1} \text{cm}^{-1}$
η	viscosity	Pa s
ϑ	temperature	$^{\circ}\text{C}$
θ	contact angle	$^{\circ}$
κ	electrical conductivity	mS cm^{-1}
λ	wavelength	m
μ	chemical potential	J
π^*	normalized interfacial pressure	-
π_{γ}	interfacial pressure	N m^{-1}
π_{σ}	surface pressure	N m^{-1}
Π	disjoining pressure	N m^{-1}
ρ	density	kg m^{-3}
σ	surface tension	N m^{-1}
φ	dispersed phase volume fraction	%, -

Summary & Zusammenfassung

Summary

A variety of food products is produced in the form of thermodynamically unstable colloidal dispersions, e.g., as foams or emulsions. Inorganic, solid particles can be used as interfacial stabilizers. For a high stability of the colloidal dispersions, the particles' properties, i.e., the contact angle between the particles' surface and the surrounding two immiscible phases, and the particle size are the main factors. This concept is often referred to as the 'Pickering theory' (Pickering, 1907). However, due to clean-label issues, applications for these inorganic 'Pickering particles' are mainly limited to the non-food sector.

This resulted in the idea of combining the effectiveness in creating long-lasting stability with a 'clean label', i.e., to create biogenic particles with techno-functional properties similar to those of inorganic particles. However, due to the deformable and porous structure of organic (e.g., protein-based) particles, the contact-angle theory (i.e., the 'Pickering theory') cannot be directly transferred to organic particles (Schmidt et al., 2011). Therefore, new explanatory approaches are needed. The hypothesis of this thesis is that similar to the 'Pickering theory' structural attributes of organic (protein-based) particles are linked to their respective techno-functionality.

Besides the foaming/ emulsifying method and conditions, the foam and emulsion structure (e.g., bubble/ oil droplet size distribution) depends on the interfacial behavior (e.g., surface activity and surface film stability) of the surface active substance. The interfacial behavior in turn is linked to specific properties of the organic particle (e.g., surface charge, surface hydrophobicity, structural flexibility, and particle size) in combination with the environmental conditions (e.g., pH value and ionic strength). To verify the hypothesis, in a first step organic particles of defined properties needed to be created, which could be used to assess the effects of individual particle properties as well as their interrelations on the formation and stabilization of foams and emulsions.

Heat-treatment (80 °C, 90 min) of native β -lactoglobulin (β -Lg) solutions ($c_{\beta\text{-Lg}}$: 1%) at different pH values (5.8 – 8.5) and NaCl concentrations (0 – 60 mM) formed protein-based particles of defined characteristics (e.g., particle size and surface charge). The whey protein β -Lg was chosen as a model system due to its well-known molecular structure and aggregation behavior. In order to avoid interference of the heat-induced particles and remaining native molecules of β -Lg and NaCl a purification was required. Therefore, two different methods were used in dependence of the particle characteristics. A laboratory scale method based on isoelectric precipitation of the particles by minimizing the repulsive forces was used with particles of sizes similar to native β -Lg. In contrast, a pilot scale method based on membrane filtration in diafiltration mode, i.e., separation based on size, was used when resolubilization of the particle pellet formed by isoelectric precipitation was not possible. In this regard, it needs to be noted that the methods were proven to provide similar results.

In summary, large ($d_{50.3} \sim 100$ nm), non-covalently bound particles result from pH values close to the isoelectric point (\sim pH 5) and a high ionic strength during heating, whereas a pH far from the isoelectric point and a low ionic strength result in significantly smaller particles mainly cross-linked via disulfide bonds (i.e., low structural flexibility).

The characterization of the techno-functionality of the particles showed that a decreasing net zeta potential increased the protein particles' diffusion rate to the air/water interface and improved the adsorption behavior resulting in smaller initial mean bubble areas. This effect is related to a reduced electrostatic barrier against adsorption by reducing the net zeta potential, i.e., the proteins charge effective range. Furthermore, it is likely that a thicker, closely packed adsorbed layer is formed by the particles exhibiting a lower net zeta potential resulting in air bubbles more stable against destabilization, e.g., in terms of coalescence. However, this effect was shown to be also dependent on the particle size.

Increasing the particle size from 5 (native β -Lg) up to > 70 nm generally resulted in a decelerated diffusion to and adsorption at the interface and thus, in larger initial mean bubble areas. Despite the larger bubble area, foam stability increased with the particle size. Interestingly, no lamella blocking by large-sized particles could be observed and consequently no prevention of destabilization mechanisms such as drainage occurred due to the increasing particle size. This indicates that another factor may be of higher significance. In this context, the thickness of the adsorbed layer was assumed as a key factor for foam stabilization. Consequently, the effect of the zeta potential, which also affects the thickness of the adsorbed layer, becomes less important with increasing particle size. Moreover, the high stability found for larger-sized particles exhibiting a higher net zeta potential indicates the importance of the thickness of the liquid films and thereby, the interrelation between the individual particle characteristics. Due to the electrostatic repulsions between the particles foam stability may be enhanced by keeping the bubbles at distance. Thus, the foam stability in systems stabilized by organic particles cannot be directly correlated with a high surface activity, i.e., a small initial mean bubble area, but is more likely linked to the thickness of the adsorbed layer and the liquid films.

The aforementioned results point out that also the particle-particle interactions within the adsorbed layer might be of importance to the elasticity of the surface film and thus the foam stability. To be able to intensely interact, particles need to be structurally flexible within the adsorbed layer. A measure for this structural flexibility is the degree of disulfide cross-linking, which quantifies the concentration of covalent bonds between the individual protein strains within the particle and thus the particle's rigidity. To obtain the degree of disulfide cross-linking, a new RP-HPLC method based on the thiol detection reagent 4,4'-dithiodipyridine (DTDP) was developed within this thesis.

By this method, it was observed that the degree of disulfide cross-linking had no effect on the initial adsorption behavior, i.e., the air bubble size. In contrast to that, the

foam stability increased with the structural flexibility (i.e., low degree of disulfide cross-linking), as likely the particle-particle interactions within the surface film as well as between adsorbed and non-adsorbed particles of neighboring bubbles increased due to structural rearrangements at the interface based on the particles' high structural flexibility. This assumption is supported by the lower final ($t = 3600$ s) surface tension values of the less cross-linked particles, which may be related to a structural rearrangement after adsorption leading to lower coarsening factors.

Another important factor for the adsorption at the interface as well as for particle-particle interactions at the interface, is the surface hydrophobicity. In this regard, the particles interfacial and foaming properties were investigated as a function of the average surface hydrophobicity. Based on the observations, it is postulated that the distribution of the hydrophobic patches at the particle surface is more important for the surface activity, i.e., the initial size of the air bubbles, than a high average surface hydrophobicity per se. In contrast to the influence on the foam formation, surface hydrophobicity seems to be unimportant for the foam stability. It has to be noted that only the average surface hydrophobicity (but not the distribution of hydrophobic patches at the surface) of the pure protein particle dispersion (but not at the interface) could be characterized. Thus, to finally clarify the effect of the surface hydrophobicity, a direct method for determining the local distribution of hydrophobic patches at the surface of the particles at the respective interface would be required, which is not available to date.

Apart from the air/water interface, the effects of different particle properties on the oil/water interface were investigated. It could be shown that the same particle properties were decisive for the initial adsorption behavior at both types of interfaces and the resulting droplet size. However, this does not apply for the stability. While the foam stability increased with an increasing particle size and a decreasing cross-linking degree, the emulsion stability (i.e., oil droplet size and aggregation) decreased. This is most likely not directly linked to the kind of interface but to the disperse volume fraction φ of air or oil and the disperse volume to protein ratio. While the disperse volume fraction was 0.1 and the oil-to-protein ratio close to 10:1 in terms of emulsions, the air content was much higher in terms of foams with a value of 0.9 and an air-to-protein ratio close to 90:1. In terms of foams, the high disperse volume fraction may lead to the formation of closely packed systems, which enables the formation of a three-dimensional network between adsorbed particles at the interface and non-adsorbed particles in the continuous phase resulting in an increased stability. This network formation is favored by less cross-linked particles due to increased particle-particle interactions. In the case of emulsions with a low disperse volume fraction of 0.1, network formation between oil droplets favors aggregation and thus, creaming. In consequence, an increase in the disperse volume fraction of emulsions may also contribute to network formation and thus, to higher emulsion stability against creaming.

To conclude, the bottom-up approach, which included the formation of protein-particles of defined characteristics and the study of interfacial, foaming, and emulsifying properties, has proven to be an ideal base to clarify the correlation between protein physicochemical characteristics and techno-functionality. It could be shown that not a single particle property is decisive for its techno-functionality but rather the interaction between zeta potential, particle size, structural flexibility (i.e., degree of disulfide cross-linking), and surface hydrophobicity as well as the composition of the respective media forming the interface. The effect and the priority of the individual particle characteristics differs with regard to the scope of application.

This thesis clearly shows the limits of the Pickering theory when applied to organic particles, as these particles are not inert, i.e., interactions between particles within the interface are decisive for their techno-functionality. Thus, organic particles need to be designed individually for the respective type of interface and application. In this regard, this thesis provides a mechanistic understanding for the underlying stabilization mechanisms in food-based dispersions and can guide the practical optimization of the stabilization of foams and emulsions by non-particulated and particulated proteins.

Zusammenfassung

Eine Vielzahl von Lebensmitteln wird in Form von thermodynamisch instabilen kolloidalen Dispersionen, z. B. als Schäume oder Emulsionen, hergestellt. Zur Grenzflächenstabilisierung können anorganische, feste Partikel eingesetzt werden. Für eine hohe Stabilität der kolloidalen Dispersionen sind die Eigenschaften der Partikel, d. h. der Kontaktwinkel zwischen der Partikeloberfläche und den beiden umgebenden nicht mischbaren Phasen, und die Partikelgröße die wichtigsten Faktoren. Dieses Konzept wird häufig als "Pickering-Theorie" bezeichnet (Pickering, 1907). Aus Gründen des „clean Labelling“ sind die Anwendungen dieser anorganischen Pickering-Partikel jedoch hauptsächlich auf den Nicht-Lebensmittelbereich („non-food“ Sektor) beschränkt.

Daraus entstand die Idee, eine lang anhaltende Stabilität mit einem "clean Labelling" zu kombinieren, d. h. biogene Partikel mit technofunktionellen Eigenschaften zu schaffen, die denen anorganischer Partikel ähneln. Aufgrund der deformierbaren und porösen Struktur organischer (z. B. proteinbasierter) Partikel kann die Kontaktwinkeltheorie (d. h. die "Pickering-Theorie") jedoch nicht direkt auf organische Partikel übertragen werden (Schmidt et al., 2011). Daher werden neue Erklärungsansätze benötigt. Die Hypothese dieser Arbeit ist, dass ähnlich der "Pickering-Theorie" strukturelle Eigenschaften von organischen (proteinbasierten) Partikeln mit ihrer jeweiligen Technofunktionalität korrelieren.

Neben dem Schäumungs-/ Emulgierverfahren und den -bedingungen hängt die Schaum- und Emulsionsstruktur (z. B. die Größenverteilung der Blasen/Öltropfen) vom Grenzflächenverhalten (z. B. Grenzflächenaktivität und Grenzflächenfilmstabilität) der grenzflächenaktiven Substanz ab. Das Grenzflächenverhalten wiederum korreliert mit spezifischen Eigenschaften der organischen Partikel (z. B. Oberflächenladung, Oberflächenhydrophobie, strukturelle Flexibilität und Partikelgröße) in Kombination mit den Umgebungsbedingungen (z. B. pH-Wert und Ionenstärke). Um die Hypothese zu überprüfen, mussten in einem ersten Schritt organische Partikel mit definierten Eigenschaften hergestellt werden, mit denen der Einfluss der einzelnen Partikeleigenschaften sowie ihre Wechselbeziehungen auf die Bildung und Stabilisierung von Schäumen und Emulsionen bewertet werden konnten.

Durch Hitzebehandlung (80 °C, 90 min) von nativen β -Lactoglobulin (β -Lg)-Lösungen ($c_{\beta\text{-Lg}}$: 1%) bei unterschiedlichen pH-Werten (5,8 - 8,5) und NaCl-Konzentrationen (0 – 60 mM) wurden proteinbasierte Partikel mit definierten Eigenschaften (z.B. Partikelgröße und Oberflächenladung) gebildet. Das Molkenprotein β -Lg wurde hierfür aufgrund seiner bekannten Molekularstruktur und seines Aggregationsverhaltens als Modellsystem gewählt. Um eine Interferenz der hitzeinduzierten Partikel und der verbleibenden nativen Moleküle von β -Lg und NaCl zu verhindern, war eine Reinigung erforderlich. Hierfür wurden zwei verschiedene Methoden in Abhängigkeit von den Partikeleigenschaften angewandt. Eine Methode im Labormaßstab, die auf der isoelektrischen Fällung der Partikel durch Minimierung

der Abstoßungskräfte beruht, wurde bei Partikeln mit Größen verwendet, die dem nativen β -Lg ähnlich sind. Im Gegensatz dazu wurde eine Methode im Pilotmaßstab verwendet, die auf der Membranfiltration im Diafiltrationsmodus, d. h. auf der Trennung nach Größe, beruht, wenn eine Resolubilisierung des durch isoelektrische Fällung gebildeten Partikelpellets nicht möglich war. In diesem Zusammenhang ist anzumerken, dass die Methoden nachweislich ähnliche Ergebnisse liefern.

Zusammenfassend lässt sich sagen, dass große ($d_{50,3} \sim 100$ nm), nicht kovalent verknüpfte Partikel aus pH-Werten nahe dem isoelektrischen Punkt (\sim pH 5) und einer hohen Ionenstärke beim Erhitzen resultieren, während ein pH-Wert weit entfernt vom isoelektrischen Punkt und eine niedrige Ionenstärke zu deutlich kleineren Partikeln führen, die hauptsächlich über Disulfidbindungen vernetzt sind (d. h. geringe strukturelle Flexibilität).

Die Charakterisierung der Technofunktionalität der Partikel zeigte, dass eine Verringerung des Netto-Zeta-Potentials die Diffusionsrate der Proteinpartikel an die Luft/Wasser-Grenzfläche erhöht und das Adsorptionsverhalten verbessert, was zu kleineren mittleren initialen Blasenflächen führt. Dieser Effekt steht im Zusammenhang mit einer verringerten elektrostatischen Adsorptionsbarriere durch Verringerung des Netto-Zeta-Potentials, d. h. der effektiven Ladungsreichweite der Proteine. Darüber hinaus ist es wahrscheinlich, dass die Partikel mit einem niedrigeren Netto-Zeta-Potentials eine dickere, dicht gepackte adsorbierte Schicht bilden, was zu Luftblasen führt, die stabiler gegen Destabilisierung, z. B. in Form von Koaleszenz, sind. Es hat sich jedoch gezeigt, dass dieser Effekt auch von der Partikelgröße abhängig ist.

Eine Erhöhung der Partikelgröße von 5 (natives β Lg) auf > 70 nm führte im Allgemeinen zu einer verlangsamten Diffusion zur und Adsorption an der Grenzfläche und somit zu größeren mittleren initialen Blasenflächen. Trotz der größeren Blasenfläche nahm die Schaumstabilität mit der Partikelgröße zu. Interessanterweise konnte keine Verblockung der Lamellen durch große Partikel beobachtet werden und folglich auch keine Verhinderung von Destabilisierungsmechanismen wie Drainage durch die zunehmende Partikelgröße. Dies deutet darauf hin, dass ein anderer Faktor von größerer Bedeutung sein könnte. In diesem Zusammenhang wurde die Dicke der adsorbierten Schicht als ein Schlüsselfaktor für die Schaumstabilisierung angenommen. Folglich verliert die Wirkung des Zeta-Potentials, das ebenfalls die Dicke der adsorbierten Schicht beeinflusst, mit zunehmender Partikelgröße an Bedeutung. Die hohe Stabilität, die für größere Partikel mit einem höheren Netto-Zeta-Potentials festgestellt wurde, deutet zudem auf die Bedeutung der Dicke der Flüssigkeitsfilme und damit auf die Wechselbeziehung zwischen den einzelnen Partikeleigenschaften hin. Aufgrund der elektrostatischen Abstoßung zwischen den Partikeln kann die Schaumstabilität dadurch erhöht werden, dass die Blasen auf Abstand gehalten werden. Die Schaumstabilität in Systemen, die durch organische Partikel stabilisiert werden, kann also nicht direkt mit einer hohen Grenzflächenaktivität, d. h. einer kleinen mittleren

Anfangsfläche der Blasen, in Verbindung gebracht werden, sondern hängt eher mit der Dicke der adsorbierten Schicht und der Flüssigkeitsfilme zusammen.

Die oben genannten Ergebnisse weisen darauf hin, dass auch die Partikel-Partikel-Wechselwirkungen innerhalb der adsorbierten Schicht für die Elastizität des Grenzflächenfilms und damit für die Schaumstabilität von Bedeutung sein könnten. Um intensive Wechselwirkungen eingehen zu können, müssen die Partikel innerhalb der adsorbierten Schicht strukturell flexibel sein. Ein Maß für diese strukturelle Flexibilität ist der Grad der Disulfid-Quervernetzung, der die Konzentration der kovalenten Bindungen zwischen den einzelnen Proteinsträngen innerhalb des Partikels und damit die Steifigkeit des Partikels quantifiziert. Zur Bestimmung des Disulfid-Quervernetzungsgrades wurde im Rahmen dieser Arbeit eine neue RP-HPLC-Methode entwickelt, die auf dem Thiol-Detektionsreagenz 4,4'-Dithiodipyridin (DTDP) basiert.

Mit Hilfe dieser Methode wurde festgestellt, dass der Grad der Disulfid-Quervernetzung keinen Einfluss auf das anfängliche Adsorptionsverhalten, d.h. die Luftblasengröße, hat. Im Gegensatz dazu nahm die Schaumstabilität mit der strukturellen Flexibilität (d.h. niedrigem Disulfid-Quervernetzungsgrad) zu, da wahrscheinlich die Partikel-Partikel-Wechselwirkungen innerhalb des Grenzflächenfilms sowie zwischen adsorbierten und nicht adsorbierten Partikeln benachbarter Blasen durch strukturelle Umlagerungen an der Grenzfläche aufgrund der hohen strukturellen Flexibilität der Partikel zunahm. Diese Annahme wird durch die niedrigeren Endwerte ($t = 3600$ s) der Oberflächenspannung der weniger vernetzten Partikel gestützt, die möglicherweise mit einer strukturellen Umlagerung nach der Adsorption zusammenhängen, die zu niedrigeren Vergrößerungsfaktoren führt.

Ein weiterer wichtiger Faktor für die Adsorption an der Grenzfläche sowie für Partikel-Partikel-Wechselwirkungen an der Grenzfläche ist die Oberflächenhydrophobie. In diesem Zusammenhang wurden die Grenzflächen- und Schaumeigenschaften der Partikel in Abhängigkeit von der durchschnittlichen Oberflächenhydrophobie untersucht. Ausgehend von den Beobachtungen wird postuliert, dass die Verteilung der hydrophoben Stellen an der Partikeloberfläche für die Grenzflächenaktivität, d.h. die Anfangsgröße der Luftblasen, wichtiger ist als eine hohe durchschnittliche Oberflächenhydrophobie per se. Im Gegensatz zum Einfluss auf die Schaumbildung scheint die Oberflächenhydrophobie für die Schaumstabilität unwichtig zu sein. Es ist zu beachten, dass nur die durchschnittliche Oberflächenhydrophobie (aber nicht die Verteilung der hydrophoben Stellen an der Oberfläche) der reinen Proteinpartikeldispersion (aber nicht an der Grenzfläche) charakterisiert werden konnte. Um den Effekt der Oberflächenhydrophobie endgültig zu klären, wäre also eine direkte Methode zur Bestimmung der lokalen Verteilung der hydrophoben Stellen an der Oberfläche der Partikel an der jeweiligen Grenzfläche erforderlich, die bisher nicht verfügbar ist.

Neben der Luft/Wasser-Grenzfläche wurden auch die Auswirkungen unterschiedlicher Partikeleigenschaften auf die Öl/Wasser-Grenzfläche untersucht. Es konnte gezeigt werden, dass die gleichen Partikeleigenschaften für das anfängliche Adsorptionsverhalten an beiden Grenzflächentypen und die resultierende Tropfengröße entscheidend sind. Dies gilt jedoch nicht für die Stabilität. Während die Schaumstabilität mit zunehmender Partikelgröße und abnehmendem Quervernetzungsgrad zunahm, nahm die Emulsionsstabilität (d. h. Öltropfengröße und Aggregation) ab. Dies hängt höchstwahrscheinlich nicht direkt mit der Art der Grenzfläche zusammen, sondern mit dem dispersen Volumenanteil φ von Luft oder Öl und dem Verhältnis von dispersem Volumen zu Protein. Während der disperse Volumenanteil bei Emulsionen bei 0,1 und das Verhältnis von Öl zu Protein bei 10:1 lag, war der Luftanteil bei Schäumen mit einem Wert von 0,9 und einem Verhältnis von Luft zu Protein von fast 90:1 wesentlich höher. Bei Schäumen kann der hohe disperse Volumenanteil zur Bildung dicht gepackter Systeme führen, was die Bildung eines dreidimensionalen Netzwerks zwischen adsorbierten Teilchen an der Grenzfläche und nicht adsorbierten Teilchen in der kontinuierlichen Phase ermöglicht und zu einer erhöhten Stabilität führt. Diese Netzwerkbildung wird durch weniger stark quervernetzte Teilchen aufgrund verstärkter Teilchen-Teilchen-Wechselwirkungen begünstigt. Bei Emulsionen mit einem niedrigen dispersen Volumenanteil von 0,1 begünstigt die Netzwerkbildung zwischen Öltropfen die Aggregation und damit das Aufrahmen. Folglich kann eine Erhöhung des dispersen Volumenanteils von Emulsionen auch zur Netzwerkbildung und damit zu einer höheren Stabilität der Emulsion gegen Aufrahmung beitragen.

Zusammenfassend lässt sich sagen, dass der Bottom-up-Ansatz, der die Bildung von Proteinpartikeln mit definierten Eigenschaften und die Untersuchung der Grenzflächen-, Schaum- und Emulgiereigenschaften umfasste, sich als geeignete Grundlage für die Klärung des Zusammenhangs zwischen den physikochemischen Eigenschaften von Proteinen und ihrer Technofunktionalität erwiesen hat. Es wurde gezeigt, dass nicht eine einzelne Partikeleigenschaft für die Technofunktionalität ausschlaggebend ist, sondern vielmehr die Wechselwirkung zwischen Zeta-Potentials, Partikelgröße, struktureller Flexibilität (d.h. Grad der Disulfid-Quervernetzung) und Oberflächenhydrophobie sowie die Zusammensetzung der jeweiligen grenzflächenbildenden Medien. Die Wirkung und der Stellenwert der einzelnen Partikeleigenschaften ist je nach Anwendungsbereich unterschiedlich.

Diese Arbeit zeigt deutlich die Grenzen der Pickering-Theorie bei der Anwendung auf organische Partikel auf, da diese Partikel nicht inert sind, d.h. die Wechselwirkungen zwischen den Partikeln innerhalb der Grenzfläche sind entscheidend für deren Technofunktionalität. Organische Partikel müssen daher individuell für die jeweilige Art der Grenzfläche und Anwendung konzipiert werden. In dieser Hinsicht liefert diese Arbeit ein mechanistisches Verständnis für die zugrundeliegenden Stabilisierungsmechanismen in lebensmittelbasierten Dispersionen und kann die praktische Optimierung der Stabilisierung von Schäumen und Emulsionen durch nicht-partikulierte und partikulierte Proteine unterstützen.

1 General Introduction

A variety of food products exist in the form of colloidal dispersions such as foams and emulsions. (Liquid) Foams consist of air bubbles dispersed in a continuous liquid phase (e.g., milk foam) while emulsions are formed of liquid droplets dispersed in another liquid phase (e.g., salad dressing). In general, foams and emulsions are thermodynamically instable systems of two immiscible phases. In consequence, the systems tend to phase separation over time. Therefore, surface active substances are of importance to reduce the free energy and thus, to prolong the stability of such systems and to provide satisfying shelf life.

In this context, proteins are widely used in the food industry as amphiphilic macromolecules. This is mainly due to their ability to adsorb at the interface and to form viscoelastic interfacial films whereby the foam and emulsion stability can be increased tremendously.

Apart from proteins in their native state, inorganic, solid (non-deformable) colloidal particles are mentioned as effective, long-lasting interfacial stabilizers. After adsorption at the interface, a mechanical barrier is created, which protects against destabilization (mainly coalescence and disproportionation) (Dickinson, 2012). This mechanism is often referred to as 'Pickering theory' after the pioneering work of Pickering (1907). According to literature, the affinity of inorganic particles to the two phases depends on the contact angle (θ), which the particle encloses with the respective interface (Binks, 2002; Tcholakova, Denkov, & Lips, 2008). At a contact angle of $\sim 90^\circ$, the same fraction of the particle surface resides in the polar and in the non-polar phase. Once adsorbed at the interface, the adsorption is considered to be irreversible due to the high energy required for desorption of a spherical particle. In turn, the desorption energy mainly depends on the particle size and the contact angle as given by Eq. (1-1)) (Binks, 2002; Dickinson, 2012; Kaptay, 2006; Tang, Quinlan, & Tam, 2015):

$$E = \pi r^2 \gamma_{\alpha\beta} (1 \pm \cos\theta)^2 \quad (1-1)$$

E is the amount of energy required to remove a spherical solid particle from the interface, r is the radius of the spherical solid particle, θ is the contact angle, which the particle makes with the interface, and $\gamma_{\alpha\beta}$ is the tension of the pure interface, i.e., the interfacial energy between the two liquid in the case of emulsions or between liquid and gas in the case of foams. Consequently, increasing the particle size and approaching a contact angle of 90° results in a higher foam/ emulsion stability (Binks, 2002). If the particle is removed to the water bulk phase, the term $\cos\theta$ becomes negative, otherwise (i.e., when it is removed to the bulk gas or oil phase), it becomes positive (Kaptay, 2006).

For a long time, the focus of particle-stabilized disperse systems was on the use of inorganic particles (e.g., silicates). However, more recently, organic particles were

created for the application in the food sector in order to use them as biogenic, 'clean label' particles to substitute inorganic particles. In this regard, a theory for the techno-functionality of these organic particles was needed. However, a transfer of the classical 'Pickering theory' based on inorganic, solid particles to the deformable and porous organic (e.g., protein-based) particles was shown to be impossible (Dickinson, 2015; Schmidt et al., 2011). This is referred to the fact that no clear contact point between the organic particles' surface and the surrounding two immiscible phases can be defined as a consequence of the structural flexibility of organic particles.

Following this, new explanatory approaches are needed for the interfacial stabilization via deformable organic particles. The hypothesis of this thesis is that similar to the 'Pickering theory' structural attributes of organic (protein-based) particles are linked to their respective techno-functionality. In this regard, the specific organic (e.g., protein) particle properties such as size, surface hydrophobicity, deformability, and surface charge are mentioned to be crucial for the particle's techno-functionality. However, comparing studies on proteins and protein-based particles, no general consensus regarding the interrelation and the priority of the individual protein structural characteristics in terms of foam and emulsion formation and stabilization was found. This is mainly due to the following aspects. First, variable protein raw materials were processed by different particulation methods resulting in particles of variable structural attributes per se. Consequently, it is difficult to assess the specificity of the respective attribute due to the use of different particle formation methods as well as particle characterization methods. Second, most studies focused on either air/water or oil/water interfaces but lack a comparison of these two systems. Third, multiple foam and emulsion formation processes as well as bulk conditions are used. Thus, it is difficult to assess the impact of the individual structural property. As can be seen in Fig. 1.1, the interdependency of these different factors determines the foaming and emulsifying properties of proteins and protein-based particles.

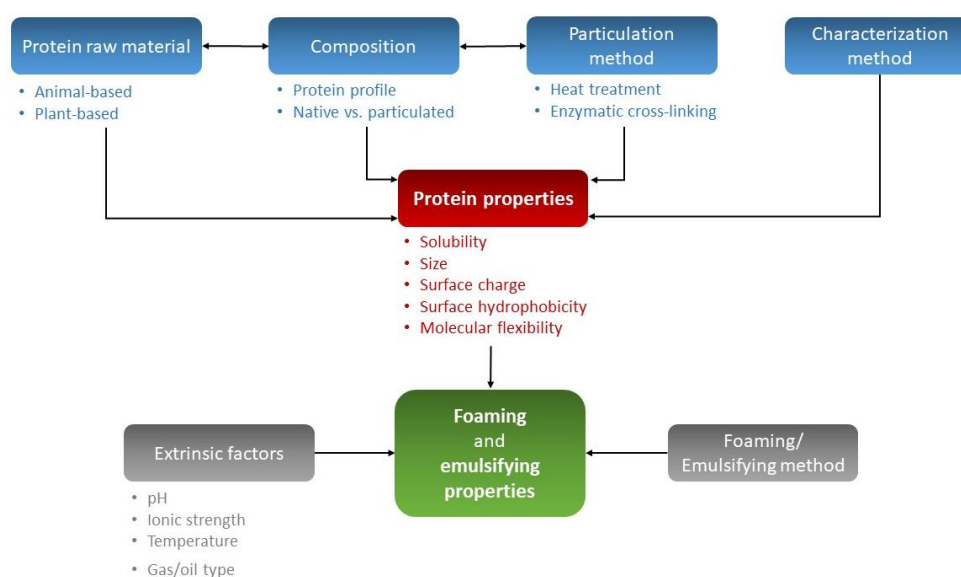


Fig. 1.1: Overview of the interdependency of the factors determining the foaming and emulsifying properties of proteins (modified according to Amagliani, Silva, Saffon, and Dombrowski (2021)).

To conclude, for a comprehensive explanation on this topic, a bottom up method with varying one parameter at a time is required to clarify structure-function relationships in the first step. Therefore, the concept of this thesis can be divided into different parts:

- Formation of highly pure (whey) protein-based particles varying only in one defined characteristic (e.g., size or surface charge)
- Investigation of correlations between physicochemical characteristics of particulated proteins and their behavior at air/water as well as oil/water interfaces. The protein in its native state serves as a reference.

Based on this, the priority and interrelations between the individual characteristics should be assessed to specifically design particles for each foam or emulsion system.

1.1 Proteins

In order to investigate the correlation between the structural attributes and techno-functionality of organic particles, animal-based proteins were chosen as raw material for the particulation. To understand the underlying mechanisms of protein particle stabilized foams and emulsions, the structural properties of proteins and the heat-induced particle formation need to be discussed first.

1.1.1 *Structural Properties of Proteins*

In general, proteins are formed by a repertoire of 20 amino acids. The individual amino acids are linked by peptide bonds. In turn, the amino acid sequence is referred to as the primary structure of a protein. The secondary structure describes spatial arrangement of amino acid residues to bigger assemblies. It is generated by regular structures of the polypeptide chain by formation of α -helixes, β -sheets, β -turns, and Ω -loops. The overall arrangement of the polypeptide chain (i.e., beyond the rather short-ranged secondary structure) is referred to as the tertiary structure. Among others, it can be stabilized by disulfide bridges. The quaternary structure describes the spatial arrangement of subunits (i.e., the protein complex may consist of more than one polypeptide chain) and the nature of their interactions with each other (Berg, Tymoczko, Stryer, & Gatto, 2014).

The structure of the globular whey and plant proteins used in this work are described in more detail below. In this regard, the main focus of this work was on the whey protein β -Lactoglobulin (β -Lg).

1.1.2 *Whey Proteins*

Whey is the serum phase of milk, which results from precipitation of the caseins, which form the main milk protein fraction. The two major whey proteins β -Lactoglobulin (β -Lg) and α -Lactalbumin (α -La) account for about 80% of the total whey protein fraction (Thompson, Singh, & Boland, 2009). The molecular structure of β -Lg and α -La are highlighted in the following.

1.1.2.1 β -Lactoglobulin: Molecular and Structural Properties

β -Lactoglobulin (β -Lg) is the major protein component in whey and is representing about 50% of the total whey protein in bovine milk (Fox & McSweeney, 1998; Kontopidis, Holt, & Sawyer, 2004). The primary structure of β -Lg contains 162 amino acids having a molecular weight of 18.3 kDa (Thompson et al., 2009). The isoelectric pH is around 5.1 (Verheul, Pedersen, Roefs, & Kruif, 1999). Of the 13 currently known variants, β -Lg A and β -Lg B are the most abundant ones (Sawyer, Kontopidis, & Wu, 1999). These two variants differ only at the positions 64 and 118 of their amino acid sequence. Instead of Asp₆₄ and Val₁₁₈ in variant A, variant B contains Gly₆₄ and Ala₁₁₈, respectively (Fox & McSweeney, 1998). This substitution of amino groups in the amino acid sequence of the protein affects several properties of β -Lg, e.g., the denaturation behavior (Dannenberg & Kessler, 1988). The secondary structure of β -Lg consists of 6-15% α -helix, 38-52% β -sheet, 8-10% turn, and 32-35% random coil (Qi et al., 1997; Sawyer & Kontopidis, 2000; Tolkach, 2007). The tertiary structure of β -Lg (Fig. 1.2) is stabilized by two intramolecular disulfide bridges (Cys₆₆-Cys₁₆₀ and Cys₁₀₆-Cys₁₁₉) (Sawyer & Kontopidis, 2000; Wit, 2009). Furthermore, a free thiol group (Cys₁₂₁), which is shielded by a α -helix in the native conformation of the β -Lg, is included in the globular structure. Consequently, the free thiol group is non-reactive in the native state (Kontopidis et al., 2004; Sawyer & Kontopidis, 2000). The reactivity of the free thiol group can be increased by thermal treatment (refer to Section 1.2). The correlation between the reactivity of the free thiol group and the subsequent formation of new, additional disulfide bonds and the techno-functionality of β -Lg particles will be discussed in detail in Section 3 and 5.

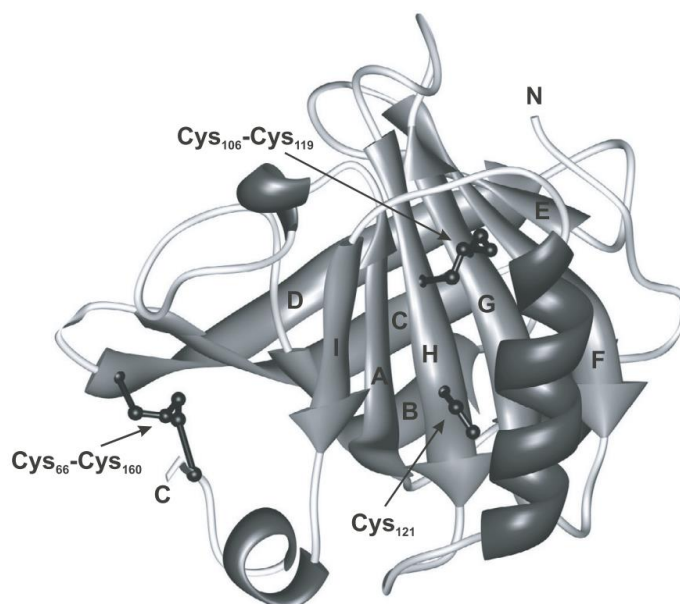


Fig. 1.2: Molecular structure of β -Lg with β -strands A to I, the C and the N terminus of the molecule, the α -helix, the position of the two disulfide bridges, and the free thiol group (adopted from Tolkach and Kulozik (2007)).

The quaternary structure of β -Lg is strongly dependent on environmental conditions such as pH, temperature, and ionic strength (Verheul et al., 1999). Under

milk's physiological conditions (\sim pH 6.8), β -Lg predominantly exists as a dimer. In dependence of the pH value and the temperature, conformational changes of β -Lg's structure occur. As can be seen in Fig. 1.3, at temperatures below 40 °C in the pH range of 3.7 to 5.2, the formation of β -Lg octamers occurs due to the minimization of electrostatic repulsive forces between the individual molecules. In the acidic pH range (2.0-3.7) and slightly acidic to neutral pH range (5.1-7.5), these octamers dissociate reversibly to dimers. Below pH 2.0 and above pH 7.5, the β -Lg dimer dissociates into its monomers. At pH values above 8.0, the protein irreversibly denatures (Pessen, Purcell, & Farrell, 1985; Tanford, Bunville, & Nozaki, 1959; Timasheff & Townend, 1964).

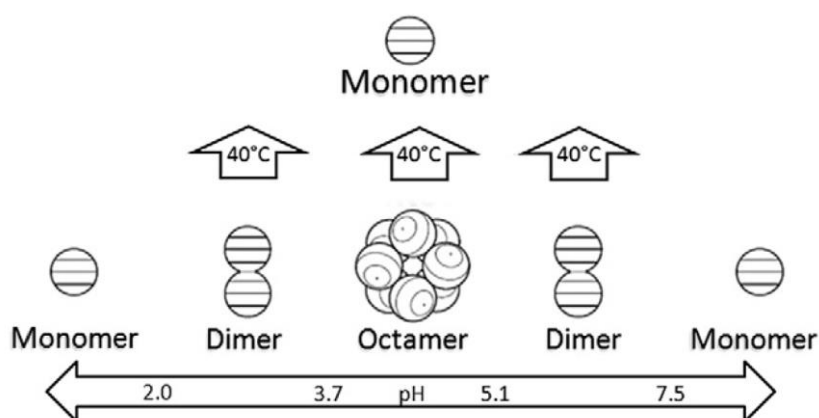


Fig. 1.3: Self-association and dissociation of β -Lg in dependence of the pH (adopted from Cheison, Lai, Leeb, and Kulozik (2011)).

The structural properties of β -Lg are of great importance with regard to their techno-functionality as will be addressed later on (Section 1.4.5). Alteration of these characteristics, e.g., by variation of the environmental conditions in combination with a heat-treatment, results in modified functional properties and consequently in modified techno-functional properties (compare Section 3 to 6).

1.1.2.2 α -Lactalbumin: Molecular and Structural Properties

α -Lactalbumin (α -La) is the second most abundant whey protein of cow's milk. It is composed of 123 amino acids and has a molecular weight of 14.2 kDa (Thompson et al., 2009). Its isoelectric point is around pH 4.2 to 4.5 (Suttiprasit, Krisdhasima, & McGuire, 1992). The α -La molecule consists of two subdomains, a α -helical (α) and a β -helical (β) domain, which are connected by a calcium binding loop (Fig. 1.4). In contrast to β -Lg, the tertiary structure of β -Lg is stabilized by four disulfide bonds (Cys₅₆ - Cys₁₂₀, Cys₆₁ - Cys₇₇, Cys₇₃ - Cys₉₁, and Cys₂₈ - Cys₁₁₁) and contains no free thiol group. The disulfide bridge between Cys₇₃ and Cys₉₁, held the two domains together and forms the calcium binding loop (Permyakov & Berliner, 2000; Suttiprasit et al., 1992).

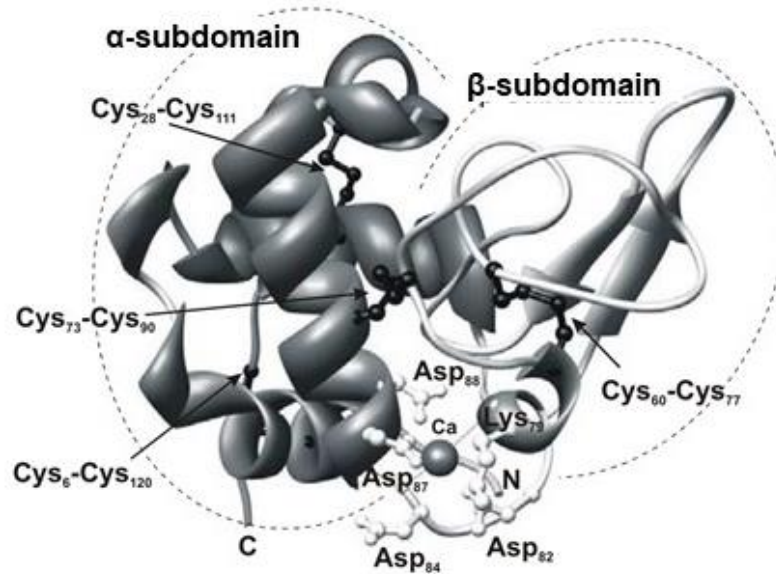


Fig. 1.4: Molecular structure of α -La with the C and the N terminus of the molecule, the position of the cysteines, and the bound calcium ion (modified according to Tolkach (2007)).

One of the most interesting features of α -La is its calcium-binding ability. The binding of Ca^{2+} (holo form) stabilizes the tertiary structure, resulting in higher thermal stability compared to the Ca^{2+} free apo form. In general, the removal of calcium results in negative charge-charge interactions in the calcium binding loop and thus, reduced stability (Griko & Remeta, 1999; Hendrix, Griko, & Privalov, 2000; Permyakov & Berliner, 2000). The release of calcium can be induced by adjusting pH values to < 4.0 (Patocka & Jelen, 1991).

1.1.3 Plant Proteins – Patatin: Molecular and Structural Properties

Patatin is the main protein from potato tuber. It has a molecular mass of around 40-42 kDa and four different isoforms are known (Pots, Gruppen, Hessing, van Boekel, & Voragen, 1999). The primary structure comprises 366 amino acids (Pots et al., 1999) and its isoelectric point is around 4.5 to 5.1 (Racusen & Foote, 1980). The secondary structure of the glycoprotein contains 45% β -stranded and 33% α -helical structures (Pots, Jongh, Gruppen, Hamer, & Voragen, 1998). In contrast to the whey proteins β -Lg and α -La, the structure of Patatin is not stabilized by internal disulfide bonds. However, one free thiol group is included in its structure as with β -Lg (Delahaije, Wierenga, Giuseppin, & Gruppen, 2015). In solutions around pH 7, Patatin mainly exists as a dimer (Racusen & Weller, 1984).

1.2 Heat-Induced Generation of β -Lg-Based Particles

To study the correlation between structural attributes and techno-functionality of organic (protein-based) particles compared to proteins in their native state (compare Section 4 to 6) and inorganic particles, protein-based particles must first be prepared. Therefore, different methods such as heat-induced or enzymatic cross-linking can be used (Dhayan, Delahaije, Vries, Gruppen, & Wierenga, 2015; Nicolai, Britten, & Schmitt, 2011).

Heat treatment of (whey) protein solutions is the most commonly applied method to alter the functional properties of the native proteins and thus, will be discussed in more detail in the following. In dependence of processing conditions (e.g., heating temperature and time) and environmental conditions (e.g., pH value, ionic strength, and protein concentration), particulated proteins of different size, shape, surface characteristics (e.g., hydrophobicity and charge), and structural flexibility (stabilization by covalent and non-covalent bonds) can be formed (Amagliani & Schmitt, 2017; Nicolai et al., 2011; Schmitt, Bovay, Rouvet, Shojaei-Rami, & Kolodziejczyk, 2007; Zuniga, Tolkach, Kulozik, & Aguilera, 2010).

1.2.1 Mechanism of β -Lg Unfolding and Aggregation

Thermal denaturation of β -Lg is a complex, multistage process, which has been subject to a number of publications (La Fuente, Singh, & Hemar, 2002; Leeb, Haller, & Kulozik, 2018; Tolkach & Kulozik, 2007; Verheul, Roefs, & Kruif, 1998; Wit, 2009; Wolz & Kulozik, 2015). Based on these works by Wit (2009) and Tolkach and Kulozik (2007), the main steps of β -Lg unfolding and aggregation are briefly presented in the following. As can be seen in Fig. 1.5, a reversible transition from the dimeric (N_2) β -Lg to the monomeric form ($2N$) takes place at temperatures above 40 °C (pH 6). In the temperature range between 40 and 55 °C (especially above pH 7.5), the monomer undergoes a reversible conformational change ($2N_R$), the so-called Tanford transition (Tanford et al., 1959; Tolkach & Kulozik, 2007; Wit, 2009). This state differs from the native state only by slight conformational changes of some side chains, resulting in a better accessibility of the free thiol group (Cys₁₂₁). However, the aggregation rate of monomers is rate is negligible. A further temperature increase above 60 up to 70 °C induces a reversible partial unfolding of the protein molecule by reaching the molten globule state ($2U_{MG}$). Thereby, the α -helix structure, which masked the free thiol group, is completely unfolded resulting in the exposure of the free thiol group and some parts of the hydrophobic core.

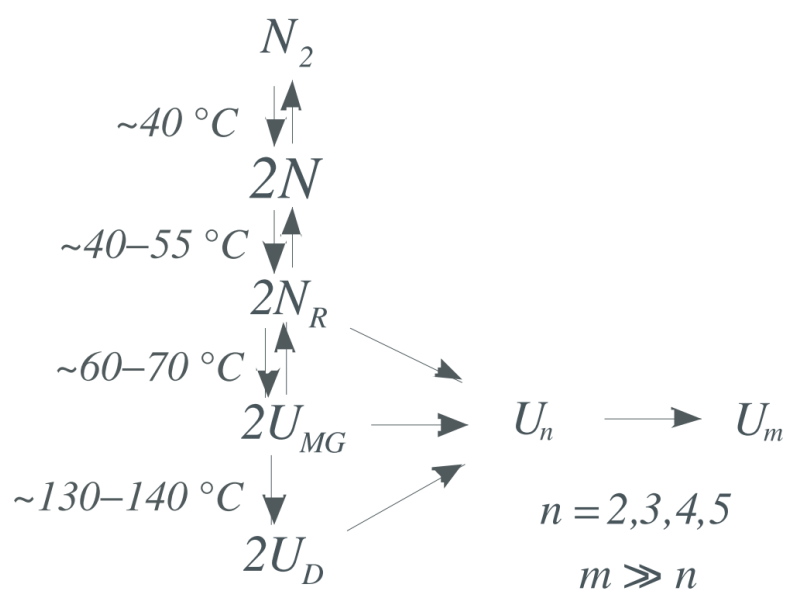
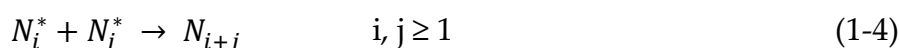
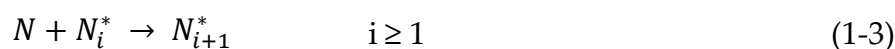


Fig. 1.5: Mechanism of the thermal denaturation of β -Lg. Adopted from Tolkach (2007).

In the further course of temperature, irreversible intermolecular interactions via thiol exchange reactions and hydrophobic bonds result in the formation of β -Lg particles (U_n , U_m) (irreversible aggregation). A further temperature increase up to 130-140 °C causes a complete destruction of the secondary structure of β -Lg (Tolkach & Kulozik, 2007; Wit, 2009). In this regard it is important to mention that the unfolding and aggregation reaction and thus, the properties of the thermally induced protein particles are strongly dependent on the processing and environmental (Section 1.2.3) conditions as will be discussed in detail in Section 4 to 6.

1.2.2 *Molecular Interactions During Heat Treatment*

A more detailed model for the aggregation of β -Lg during thermal denaturation in view of molecular interactions is given by Roefs and Kruif (1994). In general, this model proposes three steps (Eqs. (1-2) to (1-4)), an initiation step, a propagation step, and a termination step.



The initiation step (1-2) consists of reversible reactions, which result in the dissociation of the β -Lg dimers (N_2) into monomers (N). The initiation step is completed by the irreversible exposure of the free thiol group, i.e., the β -Lg monomer becomes reactive (N^*). The propagation step (1-3) includes the particulation (aggregation) via thiol-disulfide reactions, i.e., the reactive thiol group (N^*) reacts with one of the two intramolecular disulfide bonds of a non-denatured monomer (N). Thereby, a reactive covalent cross-linked dimer (N_2^*) is formed, which repeats the propagation step multiple times. In the termination step (1-4), the free thiol groups of two reactive intermediates (N^*) form a larger disulfide-linked particle and the particulation process is stopped.

Besides the free thiol group, initially masked hydrophobic groups are exposed during heat treatment favoring particulation via non-covalent bonds. The importance of covalent and non-covalent is thereby influenced by the processing and environmental conditions (Havea, Carr, & Creamer, 2004; Hoffmann & van Mil, 1997; Iametti, Cairoli, Gregori, & Bonomi, 1995; La Fuente et al., 2002; Moro, Gatti, & Delorenzi, 2001; Zuniga et al., 2010). This will be addressed in the following section.

1.2.3 *Selected Environmental Factors Affecting the Thermally-Induced Denaturation and the Resulting β -Lg Particle Properties*

In general, heat-induced denaturation and thus protein particulation is a complex mechanism in which the particles characteristics such as size, surface properties, and molecular interactions (covalent and/or non-covalent) are strongly influenced by the

heating milieu (Hoffmann & van Mil, 1997; La Fuente et al., 2002; Nicolai et al., 2011; Ryan, Zhong, & Foegeding, 2013). As the focus of this work was the impact of the environmental conditions (i.e., pH and ionic strength) on the particle properties, processing conditions are not addressed further.

The **pH value** is one of the most important factors influencing the thermal unfolding and denaturation behavior of β -Lg and thus, the resulting particle characteristics (i.e., size, degree of disulfide cross-links, surface hydrophobicity, and charge) (Ryan et al., 2013). The functional carboxyl-, phosphate-, and amino-residues of proteins are charged (protonated or deprotonated) as a function of the pH. Due to the fact that the charge of the molecules directly influences electrostatic interactions and thus, the heat-induced unfolding reaction (i.e., exposure of internal groups such as the free thiol group or the hydrophobic core), structural properties of the heat-induced β -Lg particles vary in dependence of the heating pH. In general, decreasing the heating pH from ~ 8 to the isoelectric point of β -Lg (\sim pH 5.1) reduces the electrostatic repulsion between the β -Lg molecules. In consequence, non-covalent bonds (e.g., hydrophobic interactions or interactions between unlike charges) become more dominant leading to an increased aggregation tendency of the monomers (Nicolai et al., 2011). Thereby, particles of larger size are formed due to decreased intermolecular repulsion (Dombrowski, Johler, Warncke, & Kulozik, 2016; Engelhardt et al., 2013; Hoffmann, Roefs, Verheul, van Mil, & Kruif, 1996; Hoffmann & van Mil, 1997; Nicolai et al., 2011; Schmitt et al., 2007; Zuniga et al., 2010). By contrast, an increase in the heating pH from 6.8 to 8.0 favors the Tanford transition and the deprotonation of the thiol group and thus, the exposure of the free thiol group favoring the formation of disulfide cross-linked particles (Hoffmann & van Mil, 1997; McSwiney, Singh, & Campanella, 1994; Tanford et al., 1959). Consequently, a method for the quantification of free and total thiol groups is required to investigate the techno-functionality of protein particles as a function of the degree of covalent cross-linking (refer to Section 3).

Concluding from the above, smaller-sized particles mainly stabilized by covalent bonds are formed at high pH values (> 6.8), whereas larger-sized particles mainly stabilized by non-covalent bonds result from the heat treatment at lower pH values (Hoffmann et al., 1996; Hoffmann & van Mil, 1997; Leeb et al., 2018; Monahan, German, & Kinsella, 1995; Nicolai et al., 2011; Schmitt et al., 2007; Shimada & Cheftel, 1989; Zuniga et al., 2010). This is schematically summarized in Fig. 1.6.

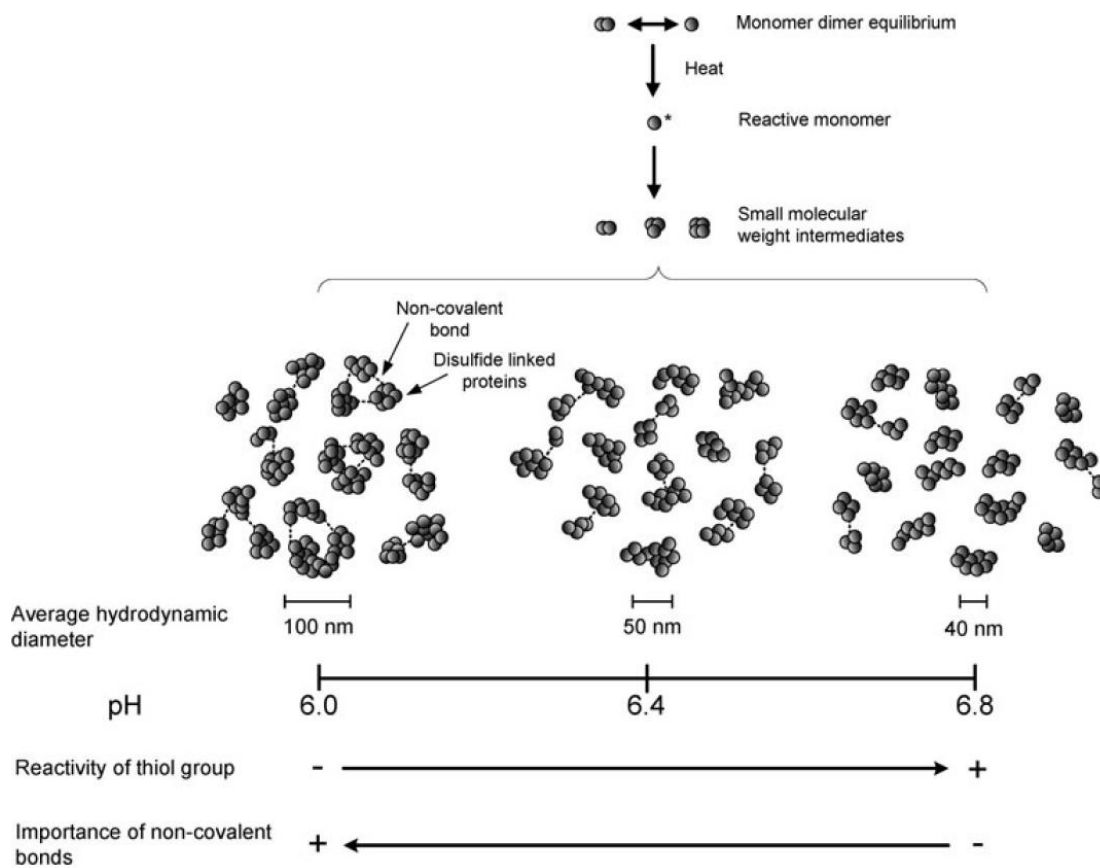


Fig. 1.6: Proposed scheme for formation of β -Lg particles during heat-treatment and type of bonding as a function of the heating pH. Adopted from Zuniga et al. (2010).

Moreover, the **ionic strength** influences the repulsive electrostatic interactions between proteins similar to the pH value and thus influences the unfolding and aggregation behavior of β -Lg (Verheul et al., 1998). In general, an increase in the molar salt concentration (c_i) as well as the charge number (z_i) of a specific ion results in an increase in the ionic strength (I) (Eq. (1-5)) whereby the molecules can approach each other more closely (Töpel, 2016).

$$I = \frac{1}{2} \sum_{i=1}^n c_i z_i^2 \quad (1-5)$$

In this regard, particles of larger size were formed by increasing the sodium chloride (NaCl) concentration due to shielded electrostatic repulsions, leading to favored aggregation subsequent to unfolding. Thereby, the critical NaCl concentration to observe such an effect increases with increasing heating pH ($>$ isoelectric pH), i.e., with increasing net surface charge (Dombrowski et al., 2016; Hoffmann et al., 1996; Hussain, Gaiani, Jeandel, Ghanbaja, & Scher, 2012; Schmitt et al., 2007; Unterhaslberger, Schmitt, Sanchez, Appolonia-Nouzille, & Raemy, 2006). Further on, surface hydrophobicity was found to increase during heat treatment due to exposure of the interior hydrophobic core of β -Lg (Dombrowski et al., 2016). With regard to the impact of ionic strength, surface hydrophobicity of the formed particles rather decreased with increasing the NaCl concentration during heat treatment (Hussain et al., 2012; Schmitt

et al., 2007). The reduced measurable surface hydrophobicity may be related to the increased increase in frequency of the aggregation via hydrophobic interactions (Hussain et al., 2012; Schmitt et al., 2007). Another explanation may be the limited accessibility of hydrophobic amino acid residues during salt-induced aggregation due to their location inside the molecule (Hussain et al., 2012; Moro et al., 2001; Schmitt et al., 2007). In the pH range of ~ 6.8 , the influence of the NaCl concentration on the content of accessible thiols seems to be less important. However, in the range of pH 6.2, the exposure of the free thiol group was reported to be more progressive with NaCl than that observed without salt (Schmitt et al., 2007). Therefore, the tendency to form particles based on covalent disulfide cross-links can be partially influenced by the salt concentration, which represents one of the main factors varied in this work in order to influence the resulting β -Lg-particle properties.

Apart from the pH value and the ionic strength, the **protein concentration** plays a major role in particle formation. An increase in the protein concentration without changing other processing and environmental conditions was shown to strongly increase the particle size by increasing the rate of aggregation (Hoffmann et al., 1996; Hoffmann, Sala, Olieman, & Kruif, 1997; Wolz & Kulozik, 2015).

Concluding from the above, the environmental conditions (i.e., pH, ionic strength, and protein concentration) display a powerful tool to generate β -Lg particles of different characteristics in terms of size, surface characteristics (e.g., surface hydrophobicity and zeta potential), and intermolecular interactions (i.e., covalent or non-covalent). However, due to a series of parallel and consecutive steps influencing the unfolding and aggregation reaction, formation of particles of defined characteristics is quite difficult. Therefore, a new approach has to be developed (compare Section 4) to produce particles varying in only one characteristic in order to elucidate the interrelation and priority of the different particle physico-chemical characteristics in terms of techno-functionality.

In this context, availability of standardized bulk (e.g., degree of denaturation, protein particle concentration) and environmental (e.g., ionic strength) conditions is vital to allow a meaningful comparison and to identify the decisive particle characteristics. However, due to differences in environmental conditions during the heat-induced generation of the protein particles, standardized conditions cannot necessarily be guaranteed (compare Section 4 to 6). Therefore, a purification step subsequent to the thermal treatment of protein solutions can be required to standardize the content of remaining native proteins and salt residues after heat-induced particulation.

There is a number of fractionation procedures in industrial and scientific application. The area of application of the respective methods essentially depends on the properties of the respective fractions to be separated. One option are solubility-based methods such as isoelectric (or enzymatic) precipitation (i.e., one component precipitates whereas the other remains soluble) followed by centrifugation to increase the separation velocity (Dannenberg & Kessler, 1988; Donato, Schmitt, Bovetto, &

Rouvet, 2009; Verheul et al., 1999). Following this, the separation efficiency is based on differences in the electrostatic, repulsive forces of the fractions to be separated whereas size differences are not decisive. The target fraction can be either around the supernatant or in the pellet. Thereby, multiple repetition of isoelectric precipitation - centrifugation (- resolubilization of the pellet) allow for the concentration (or purification) of the target fraction in the supernatant/sediment (refer to Section 4).

Another option are size-based separation methods such as membrane separation (Boye et al., 2010), which can be executed with or without filtration in diafiltration mode (Hartinger & Kulozik, 2020). In brief, during membrane filtration in diafiltration mode smaller-sized proteins are convectively transported through the membrane by the solvent, whereas the larger-sized fraction is retained and accumulates in the retentate. The resulting permeate is replaced by diafiltration medium (e.g., water or the serum phase of the retentate) to wash out the remaining smaller-sized protein fraction. One diafiltration step is reached when the volume of diafiltration medium and the volume of permeate obtained during the filtration in diafiltration mode equal the feed volume (refer to Section 5).

In this context, it is necessary to evaluate the applicability and possible influence of the purification method on the resulting techno-functional properties of the particles (refer to Section 7).

1.3 Stabilization of Interfaces

1.3.1 General Aspects Relating to Interfaces

The interface between two different bulk phases (e.g., gas/liquid (σ) or liquid/liquid (γ)) can be described as an interfacial region of thickness (δ) exhibiting properties which differ from those of the respective two bulk phases (a and b). According to the concept of Gibbs, the two bulk phases are assumed to have uniform thermodynamic properties up to a mathematical dividing line (Z^σ/Z^γ) as shown in Fig. 1.7 (Gibbs, 1961; Tadros, 2014).

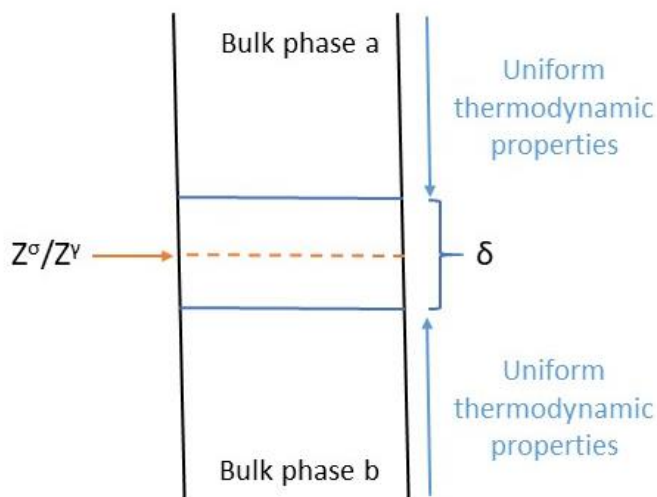


Fig. 1.7: Interfacial region (δ) between two different bulk phases (a and b) including the dividing line (Z^σ/Z^γ), where the two bulk phases are assumed to exhibit uniform thermodynamic properties according to the concept of Gibbs (modified according to Tadros (2014)).

Based on the Gibbs model, it is possible to obtain a definition of the surface (σ ; gas/liquid) or interfacial (γ ; liquid/liquid) tension, starting from the Gibbs-Duhem equation (Eq. (1-6)) (Tadros, 2014). To improve readability, in the following the indication in the equations is limited to the surface tension σ and the interfacial tension γ is only mentioned in the text as long as an equation is applicable for both σ and γ .

$$dG^\sigma = -S^\sigma dT + A d\sigma + \sum \mu_i dn_i \quad (1-6)$$

Hereby, G^σ (G^γ) is the surface (interfacial) free energy, S^σ (S^γ) is the entropy, A is the area of the interface, n_i is the number of moles of component i with chemical potential μ_i at the interface. At constant temperature and composition of the interface (i.e., without any adsorption), the surface (interfacial) tension σ (γ) can be defined as (Eq. (1-7)) (Tadros, 2014):

$$\sigma = \left(\frac{\delta G^\sigma}{\delta A} \right)_{T, n_i} \quad (1-7)$$

where G is the Gibbs free energy and A the area of the interface (Tadros, 2014).

Thermodynamic Stability of Dispersed Systems

Generally, dispersing a gas or liquid in another liquid phase with both phases being immiscible results in the formation of thermodynamically unstable systems, i.e., the contact between the molecules of the two phases is thermodynamically unfavorable (McClements, 2005; Stubenrauch & Klitzing, 2003; Tadros, 2009; Wilde, 2000). In consequence, the formation of a dispersed system requires an input of free energy to increase the thermodynamically unfavorable contact area between the immiscible phases. However, the system tends to rapidly undergo phase separation, i.e., to reduce the contact area to a minimum as soon as the energy input stops (McClements, 2005, 2012). This is due to the high interfacial free energy of the dispersed system (unlike microemulsions). Thereby, a specific value of the Gibbs' free energy can be assigned to each state, i.e., to the dispersed (G_d) and to the phase-separated system (G_s). The stable state of a system is the one, in which the free energy is minimal (McClements, 2005). The free energy ($\Delta G_{\text{formation}}$) associated with forming a disperse system (e.g., foam or emulsion) from the two bulk phases can be estimated by the difference between the interfacial free energy (ΔG_I) and the configuration entropy ($T\Delta S_{\text{config}}$) according to Eq. (1-8) (McClements, 2012):

$$\Delta G_{\text{formation}} = \Delta G_I - T\Delta S_{\text{config}} \quad (1-8)$$

At constant temperature (T), pressure (p), and interfacial chemical potential (n), the interfacial free energy term (ΔG_I) is equal to the increase in contact area between the two phases (ΔA) multiplied by the surface (interfacial) tension σ (γ) (McClements, 2012). In that case, Eq. (1-8) can be modified as follows (Eq. (1-9)).

$$\Delta G_{\text{formation}} = (\sigma\Delta A - T\Delta S_{\text{config}})_{T,p,n} \quad (1-9)$$

Concluding from Eq. (1-9), a decrease in the surface (interfacial) tension contributes to the formation of stable (i.e., $\Delta G_{\text{formation}} < 0$) dispersed systems. This can be achieved by using interfacial stabilizers (e.g., surface active surfactants and polymers) (McClements, 2005; Tadros, 2014). Thereby, different types of surface active substances can be distinguished (Berton-Carabin & Schroen, 2015; Binks, 2002; McClements & Jafari, 2018; Wilde, 2000):

- *Low molecular mass surfactants* such as Tween or monoacylglycerols
- *Surface active polymers* such as amphiphilic proteins (e.g., whey proteins) in their native state or protein-based particles
- *Solid colloidal particles* such as polystyrene particles

As the focus of this work was mainly on the stabilization of interfaces by proteins (native and particulated), these stabilization mechanisms are addressed in the following.

1.3.2 Surface Active Molecules: Proteins at Interfaces

The early works of Feijter and Benjamins (in Dickinson, 2005) and Graham and Phillips (1979) broke the complex process of adsorption of proteins at interfaces down to three steps. The first step involves the diffusion of the protein from the bulk to the interface, which is dependent on the protein bulk concentration. In dependence of the bulk concentration, a period of time may occur in which the surface (interfacial) tension does not change (induction time/ lag time) (Maldonado-Valderrama et al., 2005; Miller et al., 2000; Talansier et al., 2009; Tripp, Magda, & Andrade, 1995; Ulaganathan, Retzlaff, Won, Gochev, Gehin-Delval et al., 2017). In a second step, proteins adsorb at the interface. The third step refers to the film formation at the surface (interface) and rearrangement of adsorbed proteins within the surface layer. These steps result in a time-dependent decrease of surface (σ) (interfacial; γ) tension as can be exemplarily seen in Fig. 1.8. According to Tripp et al. (1995) for globular proteins adsorbing at the air/water interface, approximately half (50%) of the monolayer surface concentration must be attained before the surface tension will decrease significantly. The initial step decrease of surface tension (i.e., great $d\sigma/dt$) seen in the second step (II) (Fig. 1.8; II) indicates the period of half (50%) to full (100%) monolayer surface coverage. During the third regime (III), the slope ($d\sigma/dt$) values decrease by reaching the equilibrium state (i.e., $d\sigma/dt \sim 0$), the equilibrium conformation and surface concentration is achieved.

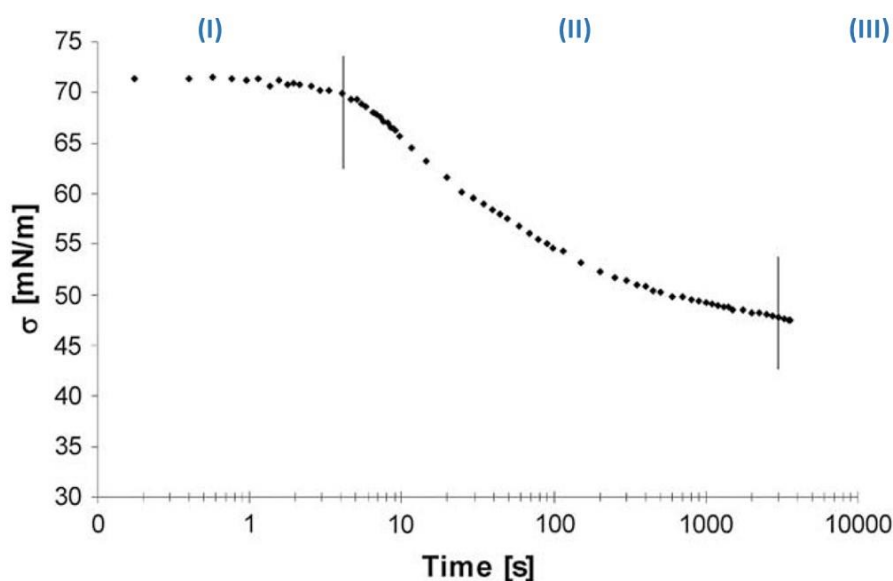


Fig. 1.8: Exemplary representation of the evolution of the surface tension (σ) of egg white proteins at the air/liquid interface including three successive steps of protein adsorption. First step (I): initiation (lag period) and diffusion. Second step (II): adsorption. Third step (III): rearrangement. Modified according to Talansier et al. (2009).

According to Graham and Phillips (1979), the protein adsorption rate is dependent on the diffusion rate to the interface and the ability of the protein to unfold upon adsorption at the interface. This is often linked to the so-called 'loop train' model in which the unfolded protein orients its hydrophobic parts to the nonpolar phase (air or

oil) and the hydrophilic parts to the polar phase (water) (Graham & Phillips, 1979; Wierenga & Gruppen, 2010). Accordingly, the unfolding is thought to be dependent on the molecular flexibility of the respective protein at the interface. In this regard, proteins with a high molecular flexibility such as caseins are assumed to unfold quicker at the interface and thus have a higher surface activity compared to more rigid proteins such as whey proteins. This model can still be found in current literature (Bergfreund, Bertsch, & Fischer, 2021; Maldonado-Valderrama et al., 2005; Martin, Grolle, Bos, Cohen Stuart, & van Vliet, 2002).

However, others showed that the unfolding (i.e., the molecular flexibility) is less important for the adsorption rate of proteins at interfaces as no noteworthy adsorption-induced change in the secondary structure of β -Lg occurs (Lad, Birembaut, Matthew, Frazier, & Green, 2006; Meinders & Jongh, 2002). Based on these, among others, results it was suspected that there must be an underlying cause other than protein unfolding that explains the differences in initial adsorption rate (Wierenga & Gruppen, 2010). In this regard, Wierenga, Meinders, Egmond, Voragen, and Jongh (2003) postulated the existence of an energy barrier to adsorption as it was shown that the initial rate of protein adsorption at the interface increases with increasing surface hydrophobicity. In addition to the impact of the surface hydrophobicity, the net charge of the proteins was shown to affect the initial adsorption process at the air/water interface (Wierenga & Gruppen, 2010). Thereby, approaching a zeta potential of ~ 0 , i.e., approaching the isoelectric point, resulted in an increased protein adsorption at the interface (Dombrowski, Gschwendtner, & Kulozik, 2017; Wierenga, Meinders, Egmond, Voragen, & Jongh, 2005). Based on these facts, Wierenga and Gruppen (2010) postulated a colloidal model in which diffusing proteins close to the interface either adsorb or diffuse back into the bulk without significant changes in their conformation. This is in contrast to the 'unfolding model' proposed by Graham and Phillips (1979), in which diffusing proteins adsorb with 100% efficiency and adopt a 'loop-train' structure.

In addition to the use of proteins in their native states, protein-based particles can be used to stabilize interfaces (Amagliani & Schmitt, 2017; Dickinson, 2017; Dombrowski et al., 2017; Sarkar & Dickinson, 2020; Schmitt et al., 2007). Protein-based particles consist of covalent and/ or non-covalent cross-linked protein monomers and have a deformable porous structure. In dependence of their size, these particles can be referred to as microgels (> 100 nm) or nanogels (≤ 100 nm) (Dickinson, 2015). As already discussed in Section 1.2, the structural and/or surface properties of heat-induced protein particles can differ from those of the native protein. In turn, the adsorption behavior can be distinctly different between native proteins and protein-based particles. The impact of changes in the physicochemical characteristics such as surface charge, surface hydrophobicity, degree of covalent cross-linking (as a measure for the particles' structural flexibility or deformability), and size on the adsorption behavior of proteins or protein-based particles are discussed in Section 1.4 in combination with foaming and emulsifying properties.

Methods to Characterize the Properties of Surface-Active Substances

Several methods such as Wilhelmy plate method, capillary rise method, bubble pressure method, drop volume method, spinning drop method, ring method according to Du Noüy, or pendant drop method exist for the determination of the static (i.e., surface tension in thermodynamic equilibrium independently of time) or dynamic (i.e., surface tension referred to a particular surface age) surface (gas/liquid) or interfacial (liquid/liquid) tension. In this work, the pendant drop method was used for evolution of surface (interfacial) tension. The method allows for the determination of the surface (interfacial) tension from the characteristics of the droplet profile. Thereby, a drop hangs from a cannula in a surrounding gaseous (liquid) phase (Fig. 1.9).

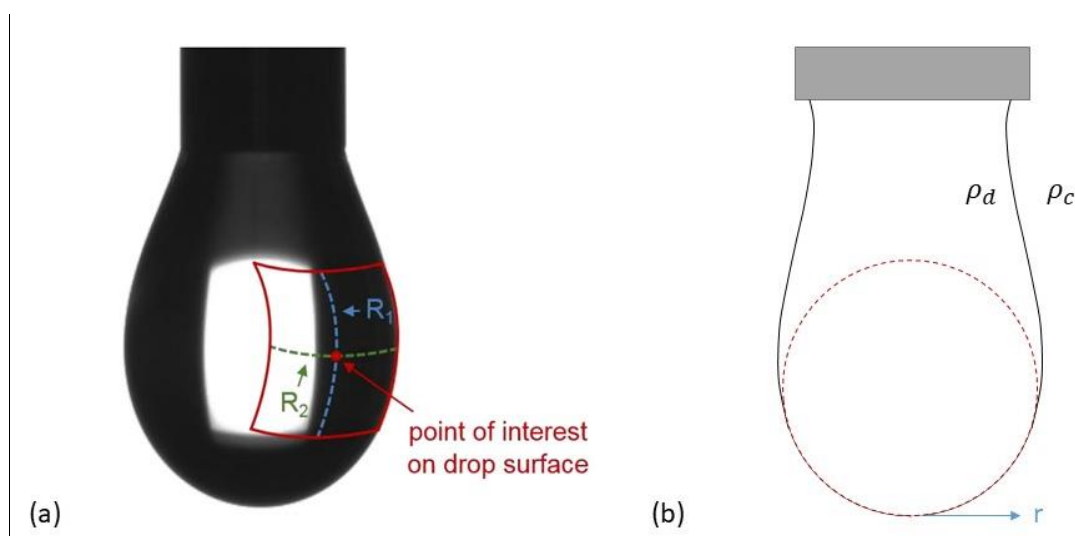


Fig. 1.9: A schematic representation of a pendant drop below a needle for surface (interfacial) tension estimation by means of pendant drop tensiometry. (a) The principal radii of curvature are indicated by R_1 and R_2 (adopted from Dombrowski (2017b)). (b) The density difference between the droplet and the continuous phase are indicated by ρ_d and ρ_c (modified according to Berry, Neeson, Dagastine, Chan, and Tabor (2015)).

In general, the surface (interfacial) tension can be estimated under consideration of the Young–Laplace equation (Eq. (1-10)) with the surface (interfacial) tension σ (γ), the principal radii of curvature R_1 and R_2 (Fig. 1.9 (a)), the Laplace pressure Δp ($\equiv p_{in} - p_{out}$) across the interface; the density difference $\Delta\rho = \rho_d - \rho_c$ between the droplet and the continuous phase (Fig. 1.9 (b)). This can be alternatively written in terms of a reference pressure p_0 at $z = 0$ and a hydrostatic pressure $\Delta\rho g z$ (Berry et al., 2015).

$$\sigma \cdot \left(\frac{1}{R_1} + \frac{1}{R_2} \right) = \Delta p \equiv \Delta p_0 - \Delta\rho g z \quad (1-10)$$

In this context it is important to note that the Young-Laplace equation can only be solved analytically when the droplet profile is a sphere. In consequence, the Young Laplace equation needs to be solved numerically in terms of pendant drop tensiometry as the shape of the drop results from the relationship between surface (interfacial)

tension and gravity (i.e., deviates from a sphere). In these cases, the surface (interfacial) tension can be obtained by the Bond number (Eq. (1-11)), which is a dimensionless quantity. If the Bond number of a pendant drop can be determined from the drop shape together with the drop radius (R_0 ; Fig. 1.9 (b)) at the apex with known density difference between the phases ($\Delta\rho$), the surface (interfacial) tension σ (γ) can be obtained by (Eq. (1-11)) (Berry et al., 2015).

$$Bo \equiv \frac{\Delta\rho g R_0^2}{\sigma} \quad (1-11)$$

Next to the evolution of the surface (interfacial) tension to describe the adsorption kinetics of proteins, the surface (interfacial) pressure π_σ (π_γ) as a function of time can be calculated (Eq. (1-12)) (Bergfreund, Bertsch, Kuster, & Fischer, 2018; Beverung, Radke, & Blanch, 1999; Dombrowski et al., 2016):

$$\pi_\sigma(t) = \sigma_0 - \sigma_t \quad (1-12)$$

with the surface (interfacial) tension of the pure solvent at the air/liquid (liquid/liquid) interface σ_0 (γ_0) and the time-dependent surface (interfacial) tension of the protein molecules within the solvent σ_t (γ_t).

After adsorption at the air/water (oil/water) interface, the adsorbed proteins have the ability to form an interfacial protein film via non-covalent or covalent interactions. The elastic and viscous properties of these films are often correlated with foam and emulsion stability (Bos & van Vliet, 2001; Dombrowski et al., 2016; Engelhardt et al., 2013). In general, the formed protein film subsequent to adsorption needs to withstand mechanical stress to prevent rupture and the consequent destabilization of foams and emulsions. Applying interfacial rheology to interfacial layers can give indirect information on the inter- and intramolecular interactions at interfaces and in consequence, on the elastic and viscous properties of the surface film (Krägel & Derkatch, 2010; Ravera, Loglio, & Kovalchuk, 2010). As interfacial rheology was not performed in this thesis, it will be addressed only briefly. Interfacial rheology is the study of the resistance of a surface film against mechanical stress. Generally, the formation of a stabile protein film at the interface, i.e., a film that resists mechanical stress, depends on the protein properties (e.g., surface hydrophobicity or charge) and their interactions as well as the type of interface (air/water or oil/water) (Dombrowski et al., 2016; Hinderink, Sagis, Schroën, & Berton-Carabin, 2020; Ulaganathan, Retzlaff, Won, Gochev, Gunes et al., 2017).

1.4 Foaming and Emulsifying Properties of Proteins and Protein-Based Particles

Foams and emulsions are dispersions of two different, immiscible phases. In the case of (liquid) foams, gas (e.g., air) is dispersed in a continuous liquid phase. In the case of emulsions both phases are liquid (e.g., water and oil) (Stubenrauch & Klitzing, 2003). In the following, the formation and the structure of foams and emulsions as well as the stabilization and destabilization mechanisms will be addressed first.

1.4.1 *Foams: Formation and Structure*

Large gas volumes dispersed in a comparatively small liquid volume are usually designated as foams even though foams can also consist of a solid instead of a liquid continuous phase. In foam preparation, a basic distinction is made between two methods: condensation and dispersion. The condensation method refers to the formation of gas bubbles by decreasing the external pressure, or by altering the temperature or as a result of chemical reactions. By contrast, the dispersion method refers to the direct injection of gas through capillaries or porous plates (sparging method) or by mechanical mixing of gas and liquid (whipping method) (Tadros, 2014). The sparging method is advantageous over other methods due to the possibility for in-situ foam characterization. Therefore, a sparging method was used in this work. In general, air was inserted through a porous frit into the stationary phase (becoming the continuous phase of the foam) within a glass column, which has a prism incorporated over the full length of the column. Thereby, the liquid and foam height can be monitored by measuring the light transmission through the glass column, as the liquid and the gas (above the foam) phases are light-permeable (Fig. 1.10 (a)).

The evolution of the foam structure is measured based on the principle of total reflection, whereby the prism integrated in the column allowed to generate 2-dimensional images of the foam structure. As can be seen in Fig. 1.10 (b), thin liquid films exist between the bubbles and the prism. The bubbles are pressed against the prism forming a gas-liquid interface parallel to the prism-liquid interface. Due to the fact that liquid and prism have similar refractive indices, light hitting the foam lamella is transmitted into the foam due to low diffraction. By contrast, liquid-gas interfaces exhibit different refractive indices and thus, light hitting the gas bubbles is totally reflected. Moreover, light needs to leave the prism below an angle of 90° to be detected by the camera. This is not the case for light coming from curved areas and being illuminated by LED (Oetjen, Bilke-Krause, Madani, & Willers, 2014; www.krüss.de, 2021).

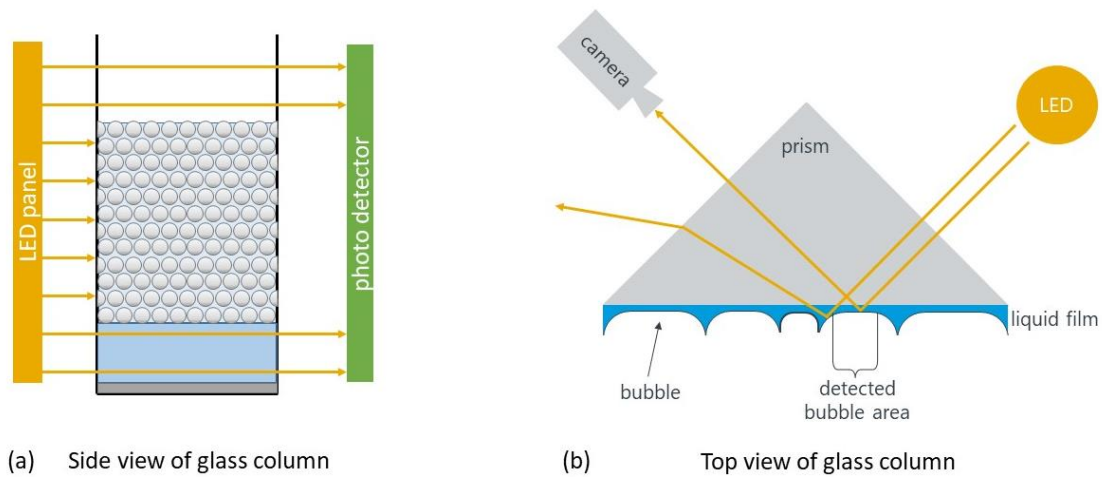


Fig. 1.10: Measurement principle of (a) foam height and (b) foam structure measurements (adopted from Winkler and Schörkl (2011), Oetjen et al. (2014), and (www.krüss.de, 2021)).

The shape of the gas bubbles varies in dependence of the gas volume fraction φ (Fig. 1.11), which is defined as the volume of dispersed phase divided by the total volume of the foam (McClements, 2005; Wilson, 1989). In the range of $0.52 < \varphi < 0.74$, bubbles exhibit a rather spherical shape, whereas for $\varphi > 0.74$, the shape is rather polyhedral (Wilson, 1989).

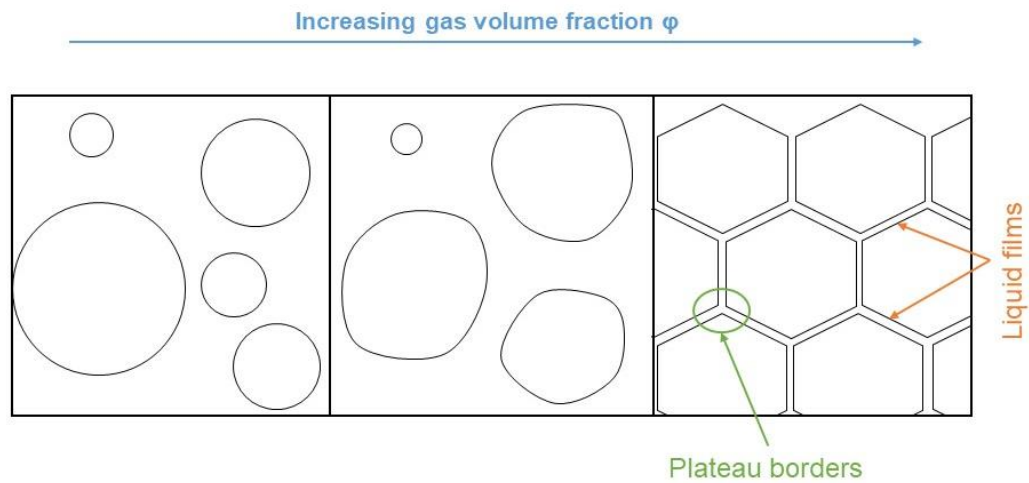


Fig. 1.11: Schematic representation of changes in the foam structure in dependency of the gas volume fraction φ (modified according to Wilson (1989)).

However, the bubble shape also varies in dependence of the foam height after foam formation. Due to the upflow of bubbles and drainage (downflow) of liquid, a rather polyhedral foam is formed on the top of the column (Fig. 1.12). In contrast, the bubbles are rather spherical in the bottom layers of the foam.

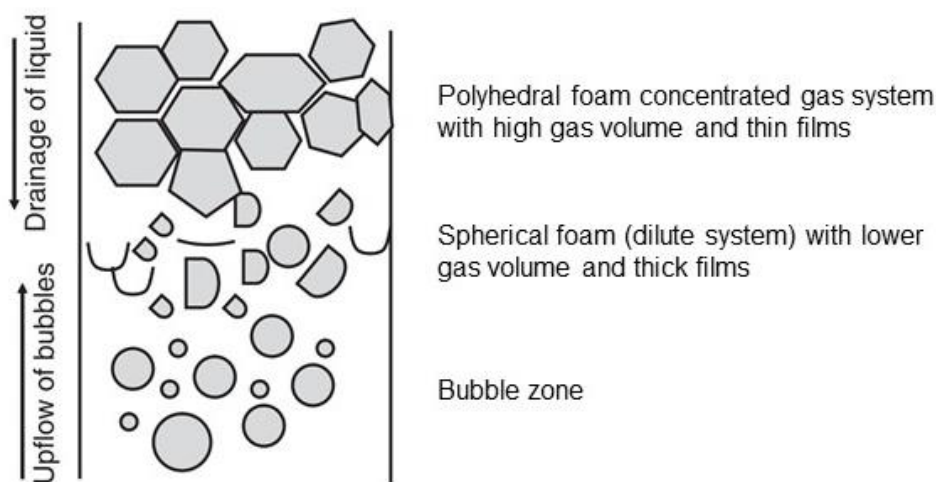


Fig. 1.12: Schematic representation of a foam structure in a foam column (modified according to Tadros (2014)).

Independently of their form, the bubbles are separated by thin liquid films (lamella) made of continuous phase (Schramm & Wassmuth, 1994). In the case of a polyhedral foam, three lamella meet each at angles of 120° . The respective meeting channel is referred to as plateau border (Fig. 1.11) (Schramm, 1994; Wilson, 1989). The thickness of the liquid films has a distinct impact on foam stability. This will be discussed in more detail later on.

1.4.2 Emulsions: Formation and Structure

Emulsions are disperse systems consisting of two or more immiscible liquids such as oil and water. Thereby, liquid droplets (dispersed phase) are dispersed in another liquid medium (continuous phase). Different types of emulsions can be distinguished by the composition of disperse and continuous phase. The most widespread ones are oil in water (o/w; oil represents the dispersed phase) and water in oil (w/o; water represents the dispersed phase) emulsions (Tadros, 2009). The concentration of droplets in an emulsion can be described by the disperse volume fraction φ , which is equal to the volume of dispersed phase divided by the total volume of the emulsion (McClements, 2005) (compare gas volume fraction with foams). Breaking up emulsion droplets to smaller ones requires an input of free energy to increase the thermodynamically unfavorable contact area between the immiscible liquids. In emulsion preparation, different methods such as static mixers and general stirrers, high-speed mixers such as the Ultra-Turrax, colloid mills and high-pressure homogenizers, and ultrasound generators can be used, resulting in differences in the emulsion formation process, e.g., the obtained oil droplet characteristics such as size. High-speed mixers are used most often for directly homogenizing oil and aqueous phases, i.e., to prepare a coarse emulsion.

In the food industry, high-pressure homogenization is the most common method for producing fine emulsions by reducing the droplet size of pre-existing emulsions. Due to this, this method was used in the present work. In brief, the coarse emulsion is

sucked in a chamber and subsequently forced through a narrow valve by a piston pump, whereby intense disruptive forces cause the larger droplets to brake down to smaller ones. In general, decreasing the gap size increases the pressure drop across the valve, which causes a greater degree of droplet disruption and thus, a smaller mean droplet diameter. The forces responsible for droplet disruption are dependent on the flow conditions, i.e., laminar, turbulent, or cavitation flow. However, the flow profile of the emulsion in close range to the gap is complex and often a combination of the different flow types. The tendency of an emulsion to flow laminar (i.e., $Re < \sim 1000$) or turbulent ($Re > \sim 2000$) can be characterized by the Reynolds number (Re ; Eq. (1-13)) (McClements, 2005).

$$Re = \frac{\text{inertial forces}}{\text{viscous forces}} = \frac{Lv\rho}{\eta} \quad (1-13)$$

Here, L is some characteristic length of the system (e.g., the diameter of a pipe or a droplet), v is the average fluid velocity, ρ is the density of the fluid, and η is the dynamic viscosity of the fluid. Due to the high speeds which can be reached in the gap, turbulent and cavitation flow can be considered as the main flow profiles. The phenomenon of cavitation may occur during high pressure homogenization.

In general, cavitation occurs when a flow is forced through a reduced cross-section, i.e., the flow velocity increases. According to the Bernoulli equation, the potential energy (pressure) is converted into kinetic energy. If the increase in kinetic energy is sufficiently high, the static pressure decreases below the vapor pressure. In consequence, the liquid spontaneously evaporates and forms bubbles. A subsequent decrease in the kinetic energy by enlarging the cross-section (i.e., the pressure increases as the kinetic energy is converted back to potential energy) leads to a sudden implosion of the cavitation bubbles. This effect can cause disruption of emulsion droplets (McClements, 2005).

1.4.3 Foam and Emulsion Stabilization

As already mentioned in Section 1.4.1, the liquid films, which separate neighboring bubbles (droplets), are important in terms of foam (and emulsion) stability. In foams (and emulsions), the pressure in the dispersed phase (P_d) is higher than the pressure in the surrounding liquid continuous phase (P_l). This pressure difference (ΔP) is given by the Laplace equation (Eq. (1-14):

$$\Delta P = P_d - P_l = P_c = \frac{2\sigma}{r} \quad (1-14)$$

with the capillary or Laplace pressure P_c , the surface (interfacial) tension of the continuous phase σ (γ), and the radius of the dispersed bubble (droplet) r (Stubenrauch & Klitzing, 2003). This pressure difference causes an unwanted thinning of the liquid films and consequently, destabilization by drainage as discussed in detail in Section 1.4.4. This phenomena can be prevented or diminished by interactions

between the protein-covered film surfaces (Stubenrauch & Klitzing, 2003). The disjoining pressure, which arises from the forces between the two protein-covered interfaces of the thin liquid film, counteracts the film thinning induced by the pressure difference (Section 1.4.4) (Damodaran, 2005; Stubenrauch & Klitzing, 2003). The disjoining pressure ($\Pi(h)$) can be defined as the sum of pressures resulting from intermolecular interactions between adsorbed surface active substances such as proteins (Eq. (1-15)). In this context, the most important ones are the repulsive electrostatic forces ($\Pi_{elec}(h)$), the repulsive steric forces ($\Pi_{steric}(h)$), and the attractive van der Waals forces ($\Pi_{vdW}(h)$). Following this, the disjoining pressure is negligible for clean (i.e., no adsorbed surface active substances) interfaces (Bergeron, 1999; Damodaran, 2005; Stubenrauch & Klitzing, 2003).

$$\Pi(h) = \Pi_{elec}(h) + \Pi_{vdW}(h) + \Pi_{steric}(h) + \dots \quad (1-15)$$

Note that the three main contributors on the disjoining pressure vary in dependence of the film thickness (h). As can be seen in Fig. 1.13, the disjoining pressure initially increases by decreasing film thickness. With further decreasing film thickness, the disjoining pressure decreases until either the film ruptures or the disjoining pressure increases again. (Damodaran, 2005; Stubenrauch & Klitzing, 2003). According to Damodaran (2005), this disjoining pressure increase at small film thickness originates from a developed osmotic pressure gradient. As neighboring interfaces approximate each other, the concentration of counter ions in the liquid film increases compared to that in the plateau region resulting in an osmotic pressure gradient. In addition, overlapping side chains of protein-covered surfaces contribute to the osmotic pressure (Damodaran, 2005). In consequence, foam destabilization in terms of foam drainage and further film thinning is diminished.

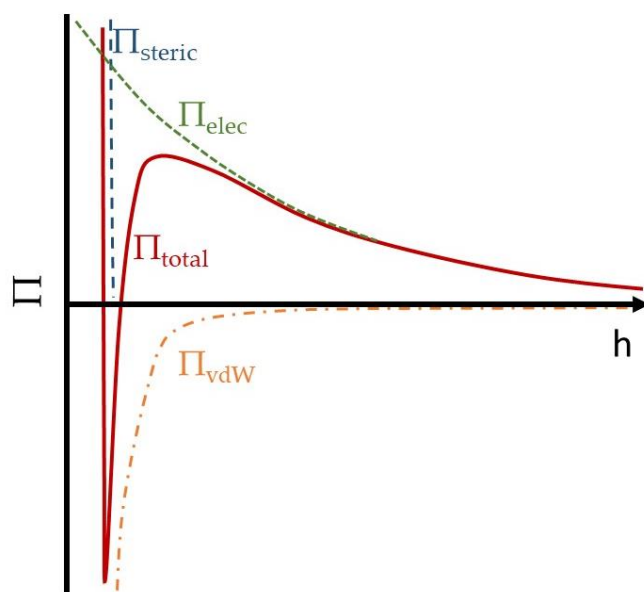


Fig. 1.13: Schematic representation of the disjoining pressure (Π) as a function of the thin film thickness (h) including the three main contributions namely (attractive) van der Waals forces (Π_{vdW}), (repulsive) electrostatic forces (Π_{elec}), and (repulsive) steric forces (Π_{steric}) on the disjoining pressure (Π_{total}). (modified according to Stubenrauch and Klitzing (2003)).

Besides that, the ability of adsorbed proteins at the interface to form viscoelastic surface films contributes to foam (and emulsion) stability. Due to the high concentration of protein after interfacial adsorption, aggregation and protein-protein interactions are favored, whereas film rupture during film stretching (e.g., due to drainage) diminishes (Bos & van Vliet, 2001; Dickinson, 1999; Dombrowski et al., 2016). In contrast to proteins, low molecular weight surfactants do not form a viscoelastic surface film due to the lack of intermolecular interactions. During film stretching, the surface tension in the stretched areas increases, i.e., a surface tension gradient arises. Thus, additional low molecular weight surfactants have to adsorb from the bulk phase at the interface to stabilize the surface film. Apart from that, the surfactants can also diffuse lateral along the surface film. This mechanism is referred to as 'Gibbs-Marangoni effect' (Walstra, 2003; Wilde, Mackie, Husband, Gunning, & Morris, 2004; Wilson, 1989). As the desorption energy of proteins is high compared to that of low molecular weight surfactants, their adsorption can be considered irreversible (Fainerman & Miller, 2005).

1.4.4 *Foam and Emulsion Destabilization Mechanisms*

The driving force for destabilization of foams and emulsions is the thermodynamically preferable decrease of the Gibbs' free energy by minimizing the contact area between the two immiscible phases (Walstra, 2003). Thereby, different physical destabilization mechanisms can occur depending on the type of disperse system. In terms of foams, disproportionation, foam drainage, and coalescence are the main destabilization mechanism, whereas creaming, aggregation, and coalescence are important in terms of emulsions (Damodaran, 2005).

Disproportionation

Disproportionation, also known as Ostwald ripening, is possible if the material of the dispersed phase (i.e., gas) is soluble in the continuous phase (i.e., water). In the case of polydisperse foams, disproportionation refers to the inter-bubble gas diffusion, i.e., diffusion of gas from smaller to larger bubbles. According to the Equation of Laplace (Eq. (1-14)), the pressure difference ΔP between the dispersed and the continuous phase increases with decreasing bubble radius. As the solubility of gas (m_A) in the continuous phase increases with increasing pressure (Henry's law; (1-13)), the higher pressure in the smaller bubbles results in a higher gas solubility in the continuous phase (near the bubbles) compared to the lower pressure in the larger bubbles. This relationship can be described by Eq. (1-16), where p_A is the partial pressure of component A in the gas phase, m_A its mol fraction in the liquid phase, and k_H the Henry constant, which depends for every component on the liquid phase and on the temperature. Along this solubility gradient, dissolved gas diffuses from the small to the large bubbles.

$$p_A = k_H m_A \quad (1-16)$$

Therefore, smaller bubbles shrink until they eventually disappear while larger bubbles expand (Damodaran, 2005; Walstra, 2003). Since food foams usually have a polydisperse bubble size distribution, disproportionation cannot be completely prevented. However, the elasticity of the surface layer is assumed to impact the shrinkage rate of the bubbles. According to Lucassen-Reynders (1981) disproportionation can be connected with the properties of the surface film. It was supposed that disproportionation can be stopped if the surface film is purely elastic and the surface dilatational elasticity is larger than half the surface tension (Dickinson, 1995). As already mentioned before, protein-covered surface films exhibit viscoelastic properties. This means, their behavior is not purely elastic and disproportionation is inevitable.

Foam Drainage

In terms of foam drainage, it needs to be distinguished between direct (gravitational drainage) and indirect (film/capillary drainage) foam drainage. Subsequent to foam formation (spherical bubbles), the (excess) liquid begins to flow (drain) into the plateau borders and then down from the upper to the lower foam layers due to gravity. As a consequence of the differences in the hydrostatic pressure at the bottom of the foam and the external pressure, the liquid drains off of the foam. However, due to the hydrostatically driven liquid drainage, bubbles become (eventually) more and more distorted forming a polyhedral foam with thin films (Fig. 1.12) (Tadros, 2014). Based on this structural change of the foam, the Laplace pressure (Eq. (1-14)) becomes increasingly important and the foam drainage transitions from direct to indirect drainage. Due to the concave curvature of the Plateau border, there is a negative Laplace pressure inside the Plateau border, i.e., the pressure in the plateau border is smaller than in the liquid films (Fig. 1.14).

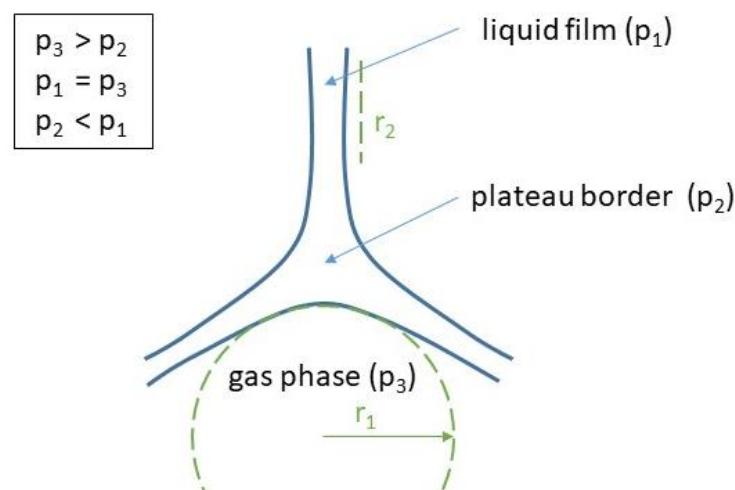


Fig. 1.14: Schematic representation of the pressure conditions within foam lamellae, leading to film drainage. r_1 and r_2 represent the radii of curvature. p_1 , p_2 , and p_3 represent the respective pressures. Modified according to Wilson (1989).

This negative pressure forces liquid from the films into the Plateau border leading to film thinning (Anazadehsayed, Rezaee, Naser, & Nguyen, 2018; Walstra, 2003;

Wilson, 1989). Consequently, foam destabilization is favored. The rate of film drainage (\dot{V}) can be calculated by Eq. (1-17):

$$\dot{V} = \frac{2 h^3 (P_c - \Pi)}{3 \eta r^2} \quad (1-17)$$

in which h is the liquid film thickness, η is the dynamic viscosity, r is the bubble radius, P_c is the capillary pressure, and Π the disjoining pressure. Due to the fact that the capillary pressure is always greater than the disjoining pressure in food foams, drainage cannot be prevented completely. However, an increase in viscosity or the disjoining pressure based on the properties of the surface film (e.g., colloidal interactions between the protein-covered surface films) can slow down the destabilization process. Additionally, an increase in viscoelasticity of the surface film or lamella blocking by particles stabilizes the foam (Damodaran, 2005; Denkov, Tcholakova, & Politova-Brinkova, 2020).

Coalescence

The term coalescence refers to fusion of two or more adjacent bubbles (creamed or flocculated droplets) into a larger one. This is caused by thinning and subsequent disruption of the liquid film between the bubbles (droplets). In general, the driving force for coalescence is the decrease in the Gibbs' free energy resulting from the reduction of the total surface area due to film rupture (Damodaran, 2005; Walstra, 2003). Thereby, two opposing effects determine whether the film ruptures and bubbles (droplets) merge. As already discussed before, the capillary pressure (Laplace pressure) causes drainage resulting in a thinning of the liquid films and consequently, an eventual collapse of the film and bubble (droplet) fusion. As a result, bubble size increases. By contrast, the disjoining pressure, i.e., colloidal interactions, contribute to film stability via repulsive forces between the (protein-) covered surface films, whereby drainage and thus, coalescence is slowed down (Damodaran, 2005; Stubenrauch & Klitzing, 2003).

Creaming

Creaming refers to the rise (i.e., against gravity) of oil droplets in an emulsion due to differences in the density of the dispersed and the continuous phase. For diluted emulsions with monodispersed oil droplets, the physical stability of the emulsion can be described in a simplified way by means of Stokes' law (Eq. (1-18)).

$$v = \frac{2 r^2 (\rho_d - \rho_c)}{9 \eta_c} g \quad (1-18)$$

Here, v is the creaming rate, r is the oil droplet radius, ρ_d is the density of the dispersed phase, ρ_c is the density of the continuous phase, η_c is the viscosity of the continuous phase, and g is the acceleration due to gravity. In this regard, the particle size plays an important role in terms of creaming. In general, the average oil droplet size decreases with an increase in energy input during emulsification and a decrease

in interfacial tension. In turn, the energy input can be influenced by the used emulsification technology, whereas the actual interfacial tension can be influenced by the concentration and activity of the used emulsifier (Damodaran, 2005).

Aggregation

Aggregation (or flocculation) refers to the loose association of (oil) droplets (without any change in primary droplet size) due to net attractive interactions. In general, emulsion stability in terms of aggregation depends on inter-droplet interactions. The most important non-covalent interactions are the attractive van der Waals forces, which contribute to aggregation, and the repulsive electrostatic and steric forces, which counteract aggregation. In general, the interaction potential is given by the sum of attractive and repulsive interactions (Damodaran, 2005; Dickinson, 2010). This means, the inter-droplet repulsion needs to overcome the combined effect of attractive van der Waals forces, gravity, convection, and Brownian motion to ensure the maintenance of a stable system (Dickinson, 2010). Fig. 1.15 schematically shows two possible generic curve progressions of the interaction potential (U) as a function of the surface-to-surface distance (d_{s-to-s}). The shape of the curve is dependent on the underlying nature and strength of the interaction force (F) between the droplet surfaces ($F = -dU(d_{s-to-s})/dd_{s-to-s}$). Curve progression I shows a positive or zero interaction potential, independently of the droplet distance. This means, the interaction force is negative or zero and in consequence, the system is stable. This could represent emulsion droplets stabilized by long-range electrostatic and/or steric repulsion (Dickinson, 2010). Electrostatic repulsion arises mainly from the charges on the stabilizing (protein) layer adsorbed at the droplet surface or the presence of electrical charges on the droplet surface. Increasing the ionic strength of the aqueous medium or decreasing the surface charge density decreases the interactions potential and thus, emulsion stability against aggregation (Dickinson, 2010).

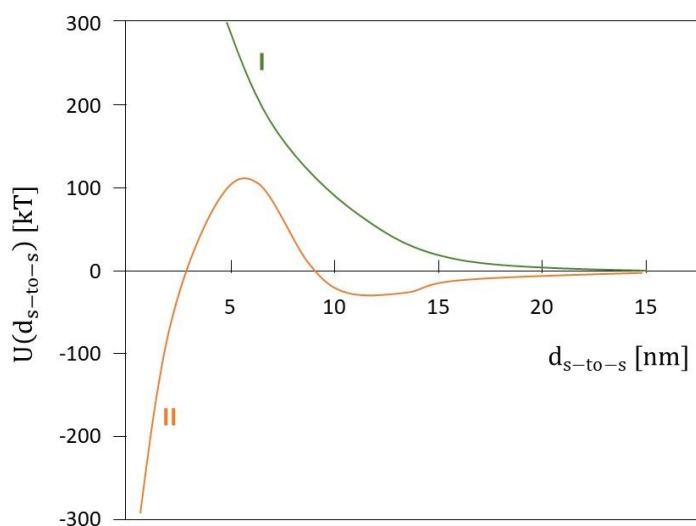


Fig. 1.15: Exemplary representation of the interaction potential between a pair of spherical emulsion droplets. The interaction potential ($U(d_{s-to-s})$) is plotted as a function of surface-to-surface distance (d_{s-to-s}). (I) corresponds to purely repulsive colloidal interactions. (II) corresponds to a DLVO-type interaction having a potential energy barrier more than sufficient to confer colloidal stability. Modified according to Dickinson (2010).

Curve progression II represents a situation in which the interaction potential is varies in dependence of the surface-to-surface distance. At close distances, the interactions potential is negative (i.e., attractive van der Waals interaction predominate), at medium distances it is positive (i.e., repulsive interaction predominate), and slightly negative or zero at larger distances (Dickinson, 2010).

1.4.5 *Factors Affecting the Interfacial, Foaming and Emulsifying Properties of Proteins*

The proteins interfacial, foaming and emulsifying behavior is affected by several factors. The most important ones in connection with this thesis (compare Section 3 to 6) are the type of interface (air/water or oil/water) and the type of oil in terms of emulsions as well as the protein concentration and the proteins structural properties.

Type of Interface

By comparing the adsorption behavior of proteins at air/water and oil/water interfaces, contradictory results can be found. Some authors reported on higher interfacial pressure values compared to the surface pressure values under equal conditions (Krägel et al., 2003; Ulaganathan, Retzlaff, Won, Gochev, Gunes et al., 2017; Won et al., 2017b). This was explained by strong interactions between the protein (β -Lg) and the oil molecules at the interface. Thereby, higher elasticity of the adsorbed protein film could be found for water/oil interfaces, which is in parallel with the higher interfacial pressure (Won et al., 2017a). By contrast, others reported lower interfacial pressure values and lower elasticity of the adsorbed protein film at the oil/water interface compared to the air/water interface by using WPI. The lower elasticity was explained by hindered inter-protein interactions due to the fact that the oil phase interacts with the hydrophobic parts of the proteins (Hinderink et al., 2020). Other studies reported no difference in the elasticity of the adsorbed β -Lg films at the air/water and oil/water interface (Williams & Prins, 1996). However, differences in the adsorption behavior and also in the elasticity of the protein films at air/water and oil/water interfaces are not surprising as the adsorption behavior of β -Lg at the oil/water interface is strongly influenced by the type of oil. According to literature, protein adsorption is slower at more polar oils, independent of the protein type. More polar oils interact stronger with the hydrophilic exterior of proteins, leading to decelerated protein unfolding, resulting in higher interfacial tension values and slower formation of viscoelastic networks (Bergfreund et al., 2018; Bergfreund et al., 2021). Consequently, comparison of results of different studies for air/water and oil/water interfaces can lead to contradictory results due to using different types of oil.

Protein Concentration

In general, an increasing bulk protein concentration increases the surface coverage (Γ) and accelerates the initial decrease in surface (interfacial) tension upon time, resulting in shorter initial lag times (Fig. 1.16) (Beverung et al., 1999; Gochev, Retzlaff, Aksenenko, Fainerman, & Miller, 2013; Kanthe, Tu, & Maldarelli, 2021; Krägel et al., 2003; Rodríguez Patino, Rodríguez Niño, & Sánchez, 1999; Tripp et al., 1995; Ulaganathan, Retzlaff, Won, Gochev, Gunes et al., 2017).

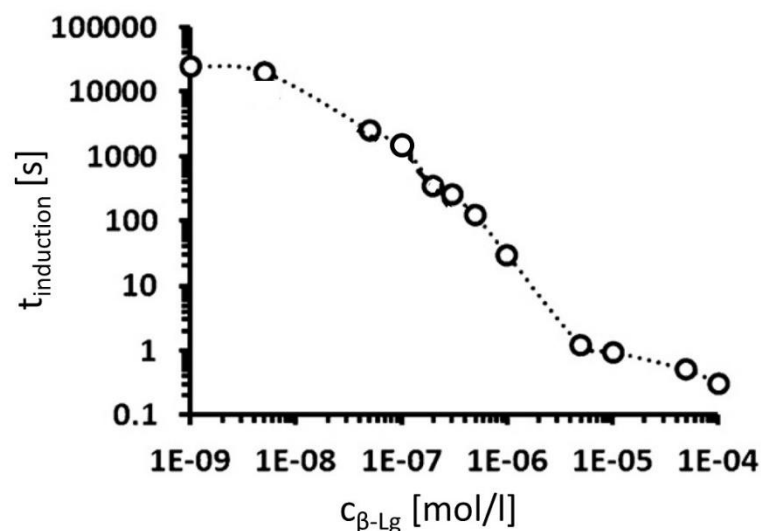


Fig. 1.16: Induction time ($t_{\text{induction}}$) as a function of the β -Lg concentration ($c_{\beta\text{-Lg}}$) (modified according to Gochev et al. (2013)). Induction time was determined by the onset of the measurable surface pressure.

The equilibrium (i.e., steady state) surface tension is reached, when the surface tension does not further decrease, i.e., reaches an equilibrium surface concentration (Tripp et al., 1995). The molar area per adsorbed molecule and the conformation of the adsorbed molecules are thereby dependent on the surface pressure and the surface coverage, respectively, as shown in Fig. 1.17. In general, at low surface pressure values, the adsorbed proteins occupy a larger molar area per molecule and vice versa. Following this, the thickness of the adsorbed layer increases with increasing protein concentration (Miller et al., 2000).

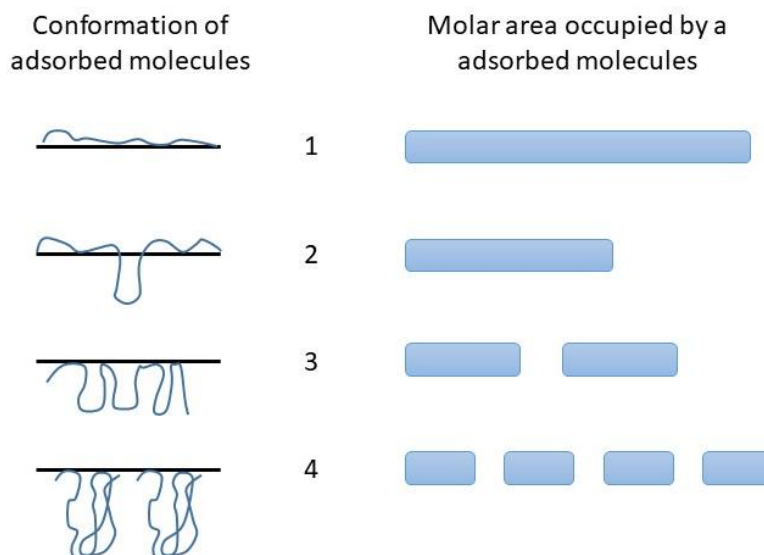


Fig. 1.17: Schematic representation of the conformational changes of adsorbed protein molecules and the molar area occupied by one adsorbed molecule according to Miller et al. (2000). The states 1-4 correspond to increasing surface pressure or surface coverage, i.e., decreasing average molar surface area.

With regard to the formation of emulsions and foams, the droplet/ bubble size was shown to depend on the protein concentration. Below a critical protein concentration (i.e., protein poor regime), the droplet size is equal to the minimal droplet size for which the complete interface can be covered with protein (Delahaije, Gruppen, Giuseppin, & Wierenga, 2015; Tcholakova, Denkov, Sidzhakova, Ivanov, & Campbell, 2003). Above a critical protein concentration (i.e., protein rich regime), the droplet size is affected by factors such as energy input and interfacial tension (Delahaije, Gruppen et al., 2015). A similar trend as observed for the formation of emulsions in dependence of the protein (β -Lg, whey proteins, and caseins) concentration was observed for foams. In the protein poor regime, bubble size decreases and foamability increases with increasing protein concentration whereas foamability and bubble size level off above a specific critical concentration. In terms of emulsion and foam stability, an increase in the protein concentration was shown to positively correlate with system stability (e.g., by preventing coalescence, flocculation or drainage) (Delahaije, Gruppen et al., 2015; Hebishy, Buffa, Guamis, Blasco-Moreno, & Trujillo, 2015; Lech, Delahaije, Meinders, Gruppen, & Wierenga, 2016; Marinova et al., 2009; Tcholakova et al., 2003).

Protein Structural Properties

Concluding from a multitude of studies, physicochemical properties of proteins including surface charge, surface hydrophobicity, structural flexibility (i.e., degree of disulfide cross-linking), as well as the protein size are known to influence the interfacial, foaming, and emulsifying properties next to environmental variables. The impact of the individual characteristics as well as their interrelation and the priority in terms of interfacial, foaming and emulsifying properties need to be known to draw conclusions regarding structure-function-relationships (compare Section 4 to 6).

According to the Stokes-Einstein equation (Eq. (1-19)) the conventional bulk diffusion coefficient (D_B) decreases with increasing **particle radius** (r). Here, k_B is the Boltzmann constant, T the absolute temperature, and η the solution's dynamic viscosity.

$$D_B = \frac{k_B T}{6 \pi \eta r} \quad (1-19)$$

Accordingly, the diffusion coefficient decreases with increasing protein particle **size**. The consequence thereof is a slower decrease in surface and interfacial tension (Dhayal et al., 2015; Murphy, Farkas, & Jones, 2016; Rullier, Novales, & Axelos, 2008). In this regard, Rullier et al. (2008) reported that for the initial stabilization of interfaces, a share of non-particulated proteins next to protein particles are necessary to produce stable foams. This effect becomes more pronounced with increasing particle size as the larger particles by themselves are not able to adsorb at the interface. Contrary to these observations, investigations on highly pure β -Lg particles showed that particles up to a size of 1 μm are able to directly adsorb at the air/water interface during its formation, i.e., no remaining non-particulated protein is required (Dombrowski et al., 2016;

Dombrowski, Gschwendtner, Saalfeld, & Kulozik, 2018). With regard to the foam stability, Dombrowski et al. (2016) reported that an increase in particle size correlates with an increasing stability to a certain extent. The difference between the findings shown above leads to the conclusion that the interaction of different physicochemical properties such as size, surface hydrophobicity, and zeta potential must to be more important with regard to surface activity and foam stability than the particle size per se. Similar conclusions can be drawn in connection with the stabilization of oil/water interfaces, at which the surface activity of whey proteins increased due to structural modifications upon heating at neutral pH, which caused the formation of particles (Zhou, Tobin, Drusch, & Hogan, 2021).

The protein particles' **zeta potential** is well accepted to play a key role in formation and stabilization of both foams and emulsions. A variation can be achieved via pH adjustment or salt-mediated charge screening. In general, lowering the surface charge, and consequently the zeta potential and electrostatic repulsion can be linked to an increase in the adsorption rate at the air/water and the oil/water interface (Dombrowski et al., 2017; Gochev, Retzlaff, Exerowa, & Miller, 2014; Wierenga et al., 2005; Won et al., 2017b). This can be referred to the reduced barrier to adsorption (Wierenga et al., 2005). In this context, it is important to note that the effect of the pH value on the surface charge and thus the surface activity can differ in dependence of the protein concentration. At a sufficiently high protein concentration ($> 10^{-6}$ mol L⁻¹), β -Lg is more surface active at pH 5 than at pH 7. In contrast to that, this effect cannot be observed at lower protein concentrations (Ulaganathan, Retzlaff, Won, Gochev, Gunes et al., 2017; Won et al., 2017b, 2017b). With regard to the foaming properties, an increase in foamability by decreasing the net zeta potential (i.e., decreasing the pH from 7 to 5) can be detected for native β -Lg and WPC as well as for nano-sized β -Lg particles. Further, the foamability was found to be positively linked to the rate of initial surface pressure increase (Dombrowski et al., 2017; Marinova et al., 2009). However, also results contradictory to the aforementioned ones can be found in literature. Marinova et al. (2009) reported that the foam formation was worst at a zeta potential of ~ 0 (i.e., pH around the isoelectric pH) when using the more flexible protein sodium caseinate. This difference to whey proteins was referred to differences in the proteins' structure (globular with the whey proteins and flexible with the sodium caseinate). With regard to foam stability, different stabilization mechanisms in connection with surface charge are discussed: (1) A decreasing net zeta potential can be related to the formation of thick surface layers whereby foam stability increases due to a higher mechanical barrier against surface film rupture (Engelhardt et al., 2013). Next to this, (2) the thickness of the liquid films between bubbles was shown to increase with increasing net zeta potential. Due to this, bubbles are kept at distance resulting in a higher foam stability (i.e., coalescence probability is reduced) (Gochev et al., 2014). In addition, (3) an increase in foam stability at a zeta potential of ~ 0 is often referred to lamellae blocking by self-aggregated proteins or particles leading to a reduction of gravitational liquid drainage (Rullier et al., 2008; Schmitt, Bovay, & Rouvet, 2014).

In terms of emulsions, a lower net zeta potential was shown to favor oil droplet flocculation and thus, to decrease emulsion stability (Delahaije, Hilgers, Wierenga, & Gruppen, 2017; Destribats, Rouvet, Gehin-Delval, Schmitt, & Binks, 2014; Sobhaninia, Nasirpour, Shahedi, & Golkar, 2017). However, as shown in connection with whey protein microgels, an increased creaming rate due to flocculation may not necessarily lead to coalescence of the oil droplets (Destribats, Rouvet et al., 2014). This may be due to a high elasticity of the surface films, which withstand the destabilizing processes (McClements & Jafari, 2018; Rühls, Scheuble, Windhab, Mezzenga, & Fischer, 2012).

Surface hydrophobicity is often mentioned in connection with foam and emulsion formation by affecting the protein adsorption at the interface (Wierenga et al., 2003). In general, a higher surface hydrophobicity is attributed to a faster diffusion to and adsorption at the interface resulting in higher foamability and emulsifying activity (Moro, Báez, Ballerini, Busti, & Delorenzi, 2013; Moro, Báez, Busti, Ballerini, & Delorenzi, 2011; Wierenga et al., 2003). However, the effect of the surface hydrophobicity differs in dependence of the type of interface showing lower importance with regard to the emulsion formation (Moro et al., 2013). In addition, other factors such as zeta potential and particle size are mentioned to balance out the specific effect of the surface hydrophobicity (Dombrowski et al., 2017). Next to the average surface hydrophobicity, the distribution of the hydrophobic patches at the surface is associated with the surface activity of proteins (Chen, Stricek, Gray, & Liu, 2017; Schmitt et al., 2021). Concluding from this, proteins of similar average surface hydrophobicity might have a differing surface activity. This is why the average surface hydrophobicity seems to be insufficient to completely describe surface activity of proteins.

The degree of disulfide **cross-linking**, i.e., the structural flexibility of proteins, is attributed to influence the foaming and emulsifying behavior of proteins. It is likely that instead of the conformational change due to adsorption at the interface (already discussed in Section 1.3.2 (Wierenga & Gruppen, 2010)) the particle-particle interactions at the interface after adsorption (e.g., surface dilatational properties) impact foam and emulsion stability (Dhayal et al., 2015; Kim, Cornec, & Narsimhan, 2005; Murphy, Zhu, Narsimhan, & Jones, 2018). According to Dhayal et al. (2015), the thickness of the adsorbed layer and also foam stability were found to be higher when using more strongly cross-linked particles.

Although a lot of studies investigated the impact of the different physicochemical properties on the interfacial as well as foaming and emulsifying properties of proteins and protein particles, still no clear correlation can be drawn regarding the specific impact of individual particle properties and their interplay.

2 Motivation and Objectives

Various physicochemical characteristics are referred to as important for the formation and stabilization of foams and emulsions by proteins and protein-based particles. In this regard, particle size, surface charge, surface hydrophobicity, and structural flexibility are among the most important mentioned in recent literature (Amagliani et al., 2021; Damodaran, 2005; Sarkar & Dickinson, 2020).

However, despite decades of research, it remains still unclear in which way the various characteristics of organic, protein-based particles are linked to their respective techno-functionality, i.e., which individual attributes or attribute interrelations are of influence for foam and emulsion formation and stabilization. First, this is due to the fact that most studies compared protein-based particles, which varied in more than one characteristic (e.g., size and surface charge). Consequently, it was not possible to assess the individual impact of the single characteristics. Second, different methods for the characterization of the particles as well as the formation and stabilization of foams and emulsions were used, whereby drawing a general consensus becomes even more complicated due to the lack of comparability. Third, the majority of the studies focused on the stabilization of air/water or oil/water interfaces. For this reason, it is difficult to assess whether the formation and stabilization of both types of interfaces require the same particle properties.

The hypothesis of this thesis is that structural attributes of organic (protein-based) particles are linked to their respective techno-functionality. Therefore, it was the objective to systematically study the correlation between individual protein particle characteristics and the particles' ability to form and stabilize foams as well as emulsions. Based on this, the priority and interrelations between the individual characteristics can be assessed to specifically design particles for different applications.

To verify the hypothesis, in a first step organic particles of defined properties need to be created. For this purpose, the whey protein β -Lactoglobulin (β -Lg) was chosen as a model system due to its well-characterized structure and its thermal aggregation behavior. Based on the current state of literature it was hypothesized that protein-based particles varying in only a single characteristic can be produced by heat-treatment by specific variation of environmental conditions (i.e., pH value and ionic strength).

To allow a meaningful comparison and to identify the decisive particle characteristics, availability of standardized bulk (e.g., protein concentration) and environmental (e.g., ionic strength) conditions is vital. Due to the differences in environmental conditions during the heat-induced generation of the protein particles, this prerequisite could not be met directly after heating, because some native proteins and salts remain in different extents. Therefore, a purification of the particles by isoelectric precipitation and centrifugation or membrane filtration in diafiltration mode was required before characterization of the particle properties.

The characterization of the protein-based particles included particle size, zeta potential, surface hydrophobicity, and the structural flexibility characterized by the degree of disulfide cross-linking. With regard to the latter, a specific RP-HPLC method based on literature should be adapted to quantify disulfide cross-links directly to overcome the disadvantages of, inter alia, a spectrophotometric method (e.g., Ellman's assay).

To understand how the individual particle characteristics affect the formation and stabilization of foams and emulsions, their adsorption behavior at the air/water and the oil/water interface should be studied by means of surface and interfacial tension measurements. In addition, macroscopic foam and emulsion properties such as the evolution of the bubble and oil droplet size upon time or the time-resolved foam height should be studied to determine foam and emulsion stability. Next to the protein-based particles, the characteristics and the techno-functionality of native (i.e., non-particulated) protein needs to be studied as this systems serves as a reference.

Overall, the goal of this study is to provide a deeper understanding of the stabilization mechanisms of foams and emulsions stabilized by proteins and protein-based particles. Additionally, the results could serve as guideline for the practical optimization of the use of proteins and protein-based particles.

3 RP-HPLC Method for Simultaneous Quantification of Free and Total Thiol Groups in Native and Heat Aggregated Whey Proteins¹

Summary and Contribution of the Doctoral Candidate Franziska Maria Hartinger (Name at Birth: Kurz)

Free thiol groups and/or oxidized disulfide bonds are included in many proteins such as whey or plant proteins. The degree of cross-linking of these thiol groups is thereby decisive for the proteins techno-functionality, e.g., by defining the protein's structural flexibility. Several methods to determine the formation of disulfide bonds and thus, the alteration of the structural flexibility during heat treatment of protein solutions (e.g., spectrophotometric Ellman's assay; semi-quantitative SDS-PAGE) are described in literature. However, none is suitable to quantify the concentration of disulfide bonds and free thiol groups of native and heat-particulated proteins upon processing accurately and efficiently. Thus, an improved method needed to be established, which is based on the findings of Hansen, Østergaard, Nørgaard, and Winther (2007), who used the thiol detecting reagent 4,4'-dithiodipyridine (DTDP) to quantify free thiol groups.

The major contributions of the doctoral candidate were as follows. First, literature was reviewed to gain information on which method might be feasible to accurately and efficiently determine the concentration of free thiols and disulfide bonds of native and heat-particulated proteins. Second, the buffer systems and the RP-HPLC method protocol used in the study of Hansen et al. (2007) were adapted by the doctoral candidate to ensure high reproducibility and high thiol recovery rates. Highly pure proteins containing (different) defined amounts of free thiols and disulfide bonds were used by the doctoral candidate to check plausibility and to verify the method. In a next step, heat-particulated proteins were investigated to further validate the method. Next to the design of the experiments, data acquisition and interpretation, and the method validation, the contributions of the doctoral candidate included writing and reviewing of the manuscript. The co-authors contributed to the execution of experiments, the discussion of results, and the revision of the manuscript.

¹ Original publication: Kurz, Franziska; Hengst, Claudia; Kulozik, Ulrich (2020) RP-HPLC method for simultaneous quantification of free and total thiol groups in native and heat aggregated whey proteins. *MethodsX*. doi: 10.1016/j.mex.2020.101112. Adapted original manuscript. Adaptions of the manuscript refer to enumeration type, citation style, spelling, notation of units, format, and merging all lists of references into one at the end of the dissertation.

Adapted Original Manuscript¹

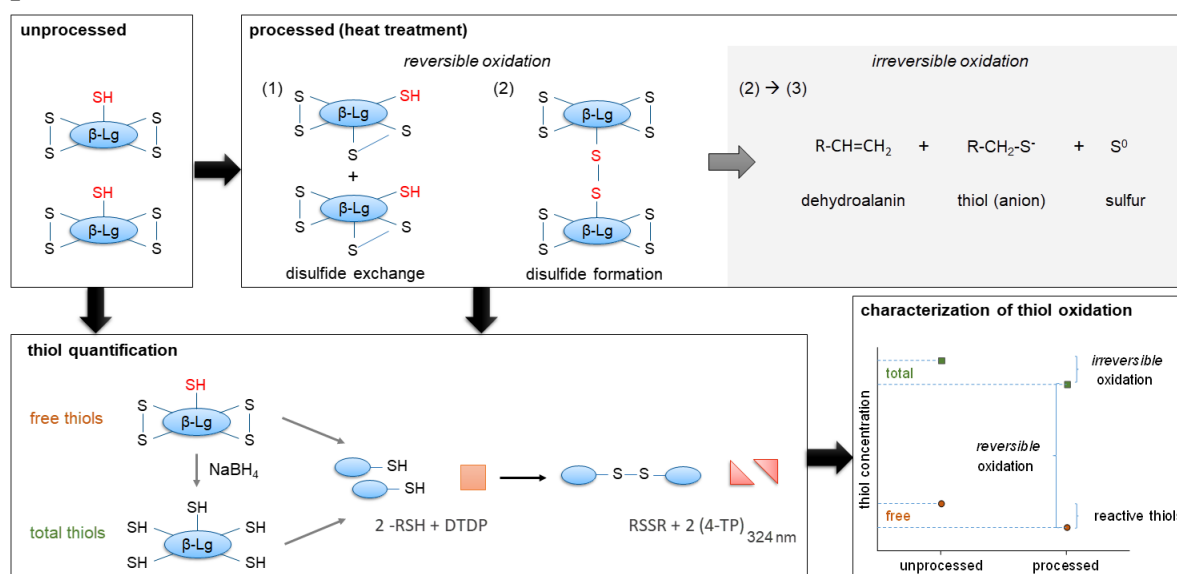
RP-HPLC method for simultaneous quantification of free and total thiol groups in native and heat aggregated whey proteins¹

Franziska Kurz*, Claudia Hengst, Ulrich Kulozik

Chair of Food and Bioprocess Engineering, Technical University of Munich, Freising, Germany

* Corresponding Author

Graphical Abstract



Abstract

Disulfide formation of whey proteins during heat treatment via thiol oxidation is important with regard to techno-functional properties. Due to the formation of other oxidation products than disulfides, the decrease in free thiol concentration is not proportional to the disulfide formation. Thus, in order to evaluate thiol reactivity and disulfide concentration both parameters are required. Currently applied methods focus mainly on the loss of free thiols using the spectrophotometric Ellman's assay. Next to that, we improved an existing RP-HPLC assay using the thiol reagent 4,4'-Dithiodipyridine (DTDP) to quantify free thiols as well as total (free thiols and disulfide bonds) thiols of native and heat treated whey proteins. Thereby, the sample preparation technique, the sample handling, and the analysis technique were optimized.

Thus, the paper provides a simple RP-HPLC method for quantification of thiol oxidation reactions to determine heat-induced changes in the structure of whey proteins. In addition, the method should be applicable to other protein system due to the method validation by proteins of different amounts of free and total thiols in their structure.

- Simple RP-HPLC method for quantification of free and total thiols using 4,4'-Dithiodipyridine (DTDP).
- High recovery rates for free and total thiols.
- High stability within 24 h.

Specification Table

Subject Area	Chemistry
More specific subject area	Thiol quantification
Method name	RP-HPLC method for simultaneous quantification of free and total thiol groups in native and heat aggregated whey proteins
Name and reference of original method	(Hansen et al., 2007) Hansen, R. E., Østergaard, H., Nørgaard, P., & Winther, J. R. (2007). Quantification of protein thiols and dithiols in the picomolar range using sodium borohydride and 4,4'-dithiodipyridine. <i>Anal. Biochem.</i> , 363(1), 77–82
Resource availability	<p>Reagents (Merck KGaA, Germany)</p> <ul style="list-style-type: none"> • Hydrochloric acid (37%) • d Ethylenediaminetetraacetic acid (EDTA) • Sodium hydroxide (NaOH) • Sodium borohydride (NaBH₄) • Guanidine hydrochloride (GdnHCl >99%) • Sodium phosphate dibasic (Na₂HPO₄) • Potassium phosphate monobasic (KH₂PO₄) • Tris(hydroxymethyl)aminomethane • 4,4'-Dithiodipyridine (98%) (DTDP) • 1-Octanol • L-Cysteine hydrochloride (anhydrous, ≥98%) <p>Materials</p> <ul style="list-style-type: none"> • Syringe filter RC-45/25 Chromafil Xtra, pore size 0.45 μm (Macherey-Nagel GmbH & Co. KG, Germany) <p>RP-HPLC</p> <ul style="list-style-type: none"> • 1100 series (Agilent Technologies Deutschland GmbH, Germany) • Zorbax 300SB-C18-3.5 μm 4.6 x 150mm (column) • Zorbax 300SB-C18-5 μm 4.6 x 12.5mm (precolumn) • Agilent ChemStation software (Rev. B.04.03[16])

3.1 Background Information

Cysteine residues in proteins occur as the free thiol group or the oxidized disulfide cross-links and are known to be decisive for techno-functionality, sensory, and nutritional quality (Calvo & La Hoz, 1992; Kleinzeller & Bronner, 1970). An important group of thiol-containing proteins are whey proteins, which are used in food structure design, e.g., in terms of creating gels stabilized by inter- and intramolecular disulfide crosslinks (Alting, Hamer, Kruif, Paques, & Visschers, 2003; Mulvihill & Donovan, 1987; Suttiprasit et al., 1992). The main whey proteins are β -Lactoglobulin (β -Lg) and α -Lactalbumin (α -La). α -La is absent of free thiol groups and contains four disulfide bonds (Permyakov & Berliner, 2000; Suttiprasit et al., 1992), whereas β -Lg holds one free thiol group and two disulfide bonds in its structure (Sawyer & Kontopidis, 2000; Suttiprasit et al., 1992). The free thiol group of β -Lg, which is not accessible in the native protein structure, needs to be exposed to induce thiol oxidation and thus, the formation of disulfide bonds. This exposure via an unfolding of the tertiary protein structure can be achieved by exceeding a critical temperature (dependent on the medium about 60 °C) (Tolkach & Kulozik, 2007). Then, the free thiol group either interacts with an existing disulfide bond by a disulfide exchange reaction or with another free thiol forming a disulfide bond (Havea, Singh, & Creamer, 2000; Hoffmann & van Mil, 1997; Visschers & Jongh, 2005). The latter results in a reduction of the amount of free thiol groups. The decrease in concentration of free thiols during processing, which is known as thiol reactivity, is thereby often used as an indicator to determine the formation of disulfide bonds. To monitor the decrease in free thiols, the spectrophotometric "Ellman's" assay is mainly used (Feng & Lee, 2016; Leeb et al., 2018; Schmitt et al., 2007). In brief, the sample is incubated with the thiol detecting reagent 5,5'-di-thiobis(2-nitrobenzoic acid) (DTNB), the so-called Ellman's reagent. Free thiol groups, but not thiols interconnected in disulfide bonds, react with DTNB, whereupon one equivalent of p-nitrothiophenol (NTP) per mol of free thiol groups is formed. As the NTP is detectable spectrophotometrically at 412 nm (molar extinction coefficient $\epsilon = 14,150 \text{ M}^{-1}\text{cm}^{-1}$ at pH 7.0) at a pH between 6.0 and 9.5, the concentration of free thiol groups can be quantified via the absorbance of the sample (Ellman, 1959; Hansen et al., 2007; Riddles, Blakeley, & Zerner, 1983).

It is important to note that this approach neglects that free thiols do not necessarily form new disulfide bonds upon oxidation but multiple other oxidation products can result from the oxidation of the free thiol group, e.g., dehydroalanine residues and lanthionine (Friedman, 1999; Klostermeyer & Reimerdes, 1977; Poole, 2015; Watanabe & Klostermeyer, 1976). This means, a decrease in the concentration of free thiols is not proportional to the increase in disulfide bonds. Thus, the final concentration of disulfide bonds cannot be calculated from the reduction in free thiol groups (thiol reactivity) during processing.

To identify the existence of disulfide bonds of native and heat treated whey proteins directly, the reducing and non-reducing SDS PAGE is performed most often. In this method, dithiothreitol (DTT) is used to reduce disulfide bonds before analysis. After

electrophoresis the proteins are stained and thus detectable by the performed bands (Hoffmann & van Mil, 1997). Thereby, it is important to note that this is a semi-quantitative method. As an alternative, spectrophotometric assays, i.e. Ellman, can also be used for quantification of reduced thiols. Thereby, the disadvantage of spectrophotometry in general is the interference by components absorbing at the same wavelength contributing to the background absorbance at a specific wavelength. In this regard, a RP-HPLC method should be more suitable to this problem due to the possibility of a peak separation. Chen, Zhao, Seefeldt, and Guan (2008) reported an HPLC assay based on the reaction of thiols with DTNB. Comparably to the Ellman's reagent, Hansen et al. (2007) reported also an RP-HPLC assay for quantification of free thiol groups and the total (free thiols and reduced disulfide bonds) amount of thiols of native proteins using the thiol detecting reagent 4,4'-Dithiodipyridine (DTDP) as can be seen in Fig. 3.1.

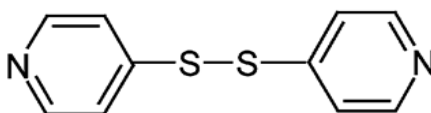


Fig. 3.1: Structural formula of 4,4'-Dithiodipyridine (DTDP) (adapted from Hansen et al. (2007)).

The reaction is thereby based on the stoichiometric conversion of DTDP to 4-thiopyridine (4-TP); absorbing at 324 nm (Grassetti & Murray, 1967). Compared to the Ellman's assay using DTNB, the DTDP assay has an increased sensitivity, due to the higher extinction coefficient of the reaction product 4-TP (ϵ : 21,400 M⁻¹cm⁻¹ at pH 7) compared to NTP (Riener, Kada, & Gruber, 2002). In addition, the extinction coefficient is stable in the pH range from 3 to 7 and thus enables the detection of 4-TP by RP-HPLC operating at acidic pH values (Hansen et al., 2007).

As a conclusion from the above, the purpose of this study was to establish a simple and accurate method to quantify the concentration of disulfide bonds as well as the concentration of the free thiol groups in native and heat-treated whey proteins to finally determine both, thiol reactivity and the amount of disulfide cross-linking.

Therefore, the method of Hansen et al. (2007) was used as a basis. For the detection of thiol groups, Hansen et al. (2007) incubated the sample in a buffer mixture consisting of the thiol detection reagent DTDP (0.36 mM), EDTA (0.2 mM) as a metal chelating agent, and the denaturation agent urea (6 M) to make the free thiol groups accessible to the reaction with DTDP. In addition, citrate (0.1 M) is used to adjust the pH to 4.5. After an incubation time of 30 min, DTDP is quantitatively converted to 4-TP, which is analyzed via RP-HPLC. A C-18 reversed-phase column was therefore operated isocratically with a 50 mM potassium acetate eluent at pH 4.0. Before determining the 4-TP concentration, a correction by the background signal (reagent blank in absence of protein) is required. Similar to the Ellman's reagent, DTDP cannot react with disulfide bonds. Thus, a cleavage of disulfide bonds by sodium borohydride (NaBH₄) is required to analyze the amount of total thiols (free thiols and thiols bond

in disulfide bonds). However, Hansen et al. (2007) only carried out the quantification of free thiol groups and the total amount of thiols of native proteins (lysozyme, bovine serum albumin (BSA), RNase A, carboxypeptidase Y, and papain) and did not investigate heat-induced thiol oxidation of whey proteins.

In this regard, several adaptations to their method are needed to quantify thiol reactivity and disulfide cross-linking between proteins upon processing accurately and efficiently. Therefore, in brief, we improved the method by optimization of the composition of the reaction buffer and the used eluent to enable a fast, separated, complete, and time independent (24 h) quantification of the reaction product 4-TP as shown in the method validation in detail. In addition, the demand of DTDP was adapted to the thiol content of the sample to reduce chemical consumption. Based on these changes, we provide a simple RP-HPLC method for quantification of free and total thiols of native and heat aggregated whey proteins using 4,4'-Dithiodipyridine (DTDP). Thus, thiol reactivity can be determined by quantification of the loss of free thiols during heat treatment. In addition, the amount of disulfide bonds can be calculated by subtraction of the concentration of free thiols from that of the total thiols before and after heat treatment. The amount of irreversible formed oxidation products during heat treatment can be calculated by subtracting the concentration of total thiols after heat treatment from that before heat treatment.

To verify the method, proteins of varying amounts of free and total thiols in their native structure were analyzed. In order to assess cross-linking in the samples, a heating step was applied to expose the free thiol group and thus, to enable thiol oxidation.

However, this method should be applicable to other thiol containing protein samples for thiol and disulfide quantification and will be a useful analytical method in the study of thiol reactivity, disulfide formation, and degradation during processing. A method for verifying the method's accuracy for other proteins will be provided in the section of method validation.

3.2 Method Protocol

3.2.1 Preparation and Storage of 40 mM 4,4'-dithiodipyridine Stock Solution

- No. 0: 40 mM 4,4'-Dithiodipyridine (DTDP) (Dissolve 0.40 mmol of DTDP in 80 μ L of 37% HCl and fill up to a total volume of 10 mL with deionized water)
- Store the solution in the dark and cold (4 °C).

3.2.2 Buffer and Sample Preparation for Free Thiols

3.2.2.1 Preparation of Buffer Solutions

- *No.1:* 20 mM EDTA stock solution (Dissolve 0.4 mmol of EDTA in 10 mL of deionized water and adjust to pH 7 by using 1 M NaOH. Fill up to a total volume of 20 mL by using deionized water.)
- *No. 2:* 100 mM potassium dihydrogen phosphate (Dissolve 10 mmol of KH_2PO_4 in deionized water to a total volume of 100 mL).
- *No. 3:* 100 mM sodium phosphate dibasic (Dissolve 10 mmol of Na_2HPO_4 in deionized water to a total volume of 100 mL.)
- *No. 4:* $\text{Na}_2\text{PO}_4/\text{KH}_2\text{PO}_4$ buffer (Mix buffer *No. 2* and *No. 3* in such ratio that the resulting pH is 5).
- *No. 5:* 6 M guanidine HCl/100 mM phosphate/0.2 mM EDTA buffer (Dissolve 600 mmol of GdnHCl up to 70 mL by using the KH_2PO_4 solution (*No. 2*). Add 1 mL of EDTA stock solution (*No. 1*). Add Na_2HPO_4 solution (*No. 3*) in small quantities until the pH value of the mixture is 5.0. Fill up to a total volume of 100 mL with buffer *No. 4*.)

3.2.2.2 Calculation of the Minimum Required Amount of 4,4'-dithiodipyridine (DTDP)

The minimum amount of DTDP, which has to be added to the sample, can be calculated by Eq. (3-1) with the expected concentration of free thiols $c_{\text{RSH expected}}$ referred to a sample volume of 500 μL and the concentration of DTDP in the stock solution $c_{\text{DTDP stock solution}}$ (*No. 0*). The value 0.6 is referred to the optimum required ratio of DTDP [μmol] to the expected thiols [μmol] in the sample solution.

$$V_{\text{DTDP stock solution}} [\mu\text{l}] = \frac{0.6 \cdot c_{\text{RSH expected}} [\mu\text{mol } \mu\text{L}^{-1}] \cdot 500 [\mu\text{L}]}{c_{\text{DTDP stock solution}} [\mu\text{mol } \mu\text{L}^{-1}]} \quad (3-1)$$

The theoretical concentration of free thiols per protein-sample solution $c_{\text{RSH expected}}$ can be calculated as shown in Eq. (3-2). c_i refers to the concentration of the respective protein i in a mixture of m proteins, its molecular mass M_i , and its amount n_i of free thiols. The respective molecular mass is calculated based on the amino acid composition of the respective protein.

$$c_{\text{RSH expected}} [\text{mol } \text{L}^{-1}] = \sum_{i=1}^m \frac{c_i [\text{g } \text{L}^{-1}]}{M_i [\text{g } \text{mol}^{-1}]} \cdot n_i \quad (3-2)$$

3.2.2.3 Sample Preparation

- Transfer 1500 μL guanidine-phosphate buffer including EDTA (*No. 5*) into a reaction tube.

- Add 500 μ L sample solution and mix.
- Add the calculated amount of DTDP stock solution (compare Eq. (3-1) and shake.

Note: Short-time light exposure (outside of an amber HPLC vial) won't affect the results.

- Wait 10 min until the reaction is completed.
- Check for pH 5.

Note: The absorption coefficient of 4-TP is constant within the pH value of 3-7. If pH value is not 5, an adjustment of the pH has to be done by buffer No. 2 or No. 3. The dilution of the sample by adjusting the buffer has to be considered.

- Transfer an aliquot of the solution into an amber HPLC vial.
- Determination of total thiol concentration by RP-HPLC by monitoring 4-thiopyridine (4-TP) at a wavelength of 324 nm (refer to Section 3.2.4)

3.2.3 *Buffer and Sample Preparation for Free Thiols and Disulfide Bonds (Total Thiols)*

Note: In contrast to Section 3.2.2, the total amount of thiols (free thiols and thiols of disulfide bonds) is analyzed with this method. Therefore, an additional disulfide bonds cleavage step has to be carried out to cleave the disulfide bonds).

3.2.3.1 *Buffer Preparation*

- No. 1: (Section 3.2.2): 20 mM EDTA stock solution (Dissolve 0.40 mmol of EDTA in 10 mL of deionized water and adjust to pH 7 by using 1 M NaOH. Fill up to a total volume of 20 mL by using deionized water.)
- No. 6: 750 mM potassium dihydrogen phosphate (Dissolve 75.0 mmol of KH_2PO_4 in deionized water to a total volume of 100 mL.)
- No. 7: 750 mM sodium phosphate dibasic (Dissolve 75.2 mmol of Na_2HPO_4 in deionized water to a total volume of 100 mL.)
- No. 8: $\text{Na}_2\text{PO}_4/\text{KH}_2\text{PO}_4$ buffer (Mix buffer No. 6 and No. 7 in such ratio that the resulting pH is 5).
- No. 9: 6 M guanidine HCl /750mM phosphate/0.31mM EDTA buffer (Dissolve 600 mmol of GdnHCl up to 70 mL by using the prepared KH_2PO_4 stock solution (No. 6). Add 1.55 mL of EDTA stock solution (No. 1). Add Na_2HPO_4 solution (No. 7) in small quantities until the pH value of the mixture is 5.0. Fill up to a total volume of 100 mL with buffer No. 8.)

3.2.3.2 *Preparation of Solutions for the Reduction of the Disulfide Bonds*

- No. 10: 6 M guanidine HCl/ 0.5 M Tris (hydroxyl-methyl) amino-methane solution (Dissolve 50 mmol of Tris (hydroxyl-methyl-) amino-methane and 600 mmol of GdnHCl in deionized water to a total volume of 100 mL.)

- *No. 11*: Prepare a solution of 30% (w/v) sodium borohydride (NaBH₄) using 1 M NaOH (Dissolve 40 mmol of sodium borohydride in 5 mL of 1 M NaOH).

3.2.3.3 Calculation of 4,4'-dithiodipyridine (DTDP)

The minimum amount of DTDP, which has to be added to the sample, can be calculated by Eq. (3-3) with the concentration of all thiols $c_{total\ thiols\ expected}$ referred to a sample volume of 1,000 μL and the concentration of DTDP in the stock solution $c_{DTDP\ stock\ solution}$ (*No. 0*). The value 0.6 is referred to the optimum required ratio of DTDP [μmol] to the expected thiols [μmol] in the sample solution.

$$V_{DTDP\ stock\ solution} [\mu\text{L}] = \frac{0.6 \cdot c_{total\ thiols\ expected} [\mu\text{mol}\ \mu\text{L}^{-1}] \cdot 1000 [\mu\text{L}]}{c_{DTDP\ stock\ solution} [\mu\text{mol}\ \mu\text{L}^{-1}]} \quad (3-3)$$

The theoretical concentration total thiols per protein-sample solution $c_{thiol\ expected}$ can be calculated as shown in Eq. (3-4). c_i refers to the concentration of the respective protein i in a mixture of m proteins, its molecular mass M_i , and its amount n_i of total thiols after reduction by sodium borohydride (NaBH₄). The respective molecular mass is calculated based on the amino acid composition of the respective protein.

$$c_{total\ thiols\ expected} [\text{mol}\ \text{L}^{-1}] = \sum_{i=1}^m \frac{c_i [\text{g}\ \text{L}^{-1}]}{M_i [\text{g}\ \text{mol}^{-1}]} \cdot n_i \quad (3-4)$$

3.2.3.4 Sample Preparation

- Add 1000 μL of sample solution to 770 μL Tris-guanidine solution (*No. 10*) and mix.
- Add 230 μL of freshly prepared sodium borohydride (*No. 11*) and mix.
- Put 50 μL of 1-octanol on top.

Note: The 1-octanol prevents foaming due to hydrogen formation.

- Incubate the mixture at 65 °C for 60 min.
- Quench the reaction by addition of 400 μL of 5 M HCl. To do so, penetrate the 1-octanol layer and mix with the pipette.

Note: NaBH₄ is completely removed by acidification (Hansen et al., 2007; Hansen & Winther, 2009).

- Wait for 10 min until the reaction is completed.
- Add calculated amount of DTDP (compare Eq. (3-3)) and mix.
- Wait for 10 min until the reaction is completed.
- Filter the solution with a RC extra 0.45 μm syringe filter.
- Transfer 500 μL of the filtrate into an amber HPLC vial and add 1000 μL of guanidine-phosphate buffer (*No. 9*). Close the vial and mix well.
- Determination of total thiol concentration by RP-HPLC.

3.2.4 Calibration and Analysis of Thiols by RP-HPLC

- *No. 12*: Prepare a 10 mM L-cysteine hydrochloride monohydrate stock solution (Dissolve 1 mmol of L-cysteine hydrochloride monohydrate in deionized water up to 100 mL.) for preparation of calibration standards.
- Dilute the stock solution *No. 12* to 5.0, 2.5, 1.0, and 0.5 mM with deionized water.
- Transfer 1850 μL guanidine phosphate buffer (*No. 5*) into reaction tubes and add 100 μL of each cysteine solution and 50 μL DTDP stock solution (*No. 0*) into each tube.
- Wait for 10 min until the reaction is completed.
- Transfer 1000 μL of the standard mixtures into amber HPLC vials.

Analyze the standards by RP-HPLC using an Agilent 1100 Series (Agilent Technologies Inc., Santa Clara, CA, USA) fitted with a Zorbax 300SB-C18-3.5 μm 4.6 x 150 mm column and a Zorbax 300SB-C18-5 μm 4.6 x 12.5 mm precolumn. Set the injection volume to 20 μL and the column oven temperature to 40 $^{\circ}\text{C}$. Gradient elution is performed according Tab. 3-1 at a flow rate of 1 mL min^{-1} . A Diode-array-detector operating at 324 nm is used to monitor the absorption of the reaction product 4-thiopyridine (4-TP). The total duration of the analysis is 10 min. The peak areas are integrated by using the Agilent ChemStation software (Rev. B.04.03 [16]). The standards of L-cysteine hydrochloride monohydrate are used to obtain a reference curve as shown in Fig. 3.2. It can be seen that the peak area is proportional to the 4-TP concentration ($R^2 = 0.99991$).

The analysis of the sample solutions is carried out accordingly. The amount of 4-TP in the sample is correlated to the peak area via the correlation function (Fig. 3.2).

Tab. 3-1: Gradient used for elution of 4-TP. Solvent A 100% gradient grade water containing 0.2% (v/v) trifluoroacetic acid (TFA); Solvent B 100% gradient grade acetonitrile (ACN) containing 0.2% (v/v) TFA.

time	solvent A	solvent B	flow
min	%	%	mL min^{-1}
0.0	98.5	1.5	1.0
1.5	98.5	1.5	1.0
6.0	94.0	6.0	1.0
6.5	0.0	100.0	1.0
7.0	0.0	100.0	1.0
8.0	98.5	1.5	1.0
10.0	98.5	1.5	1.0

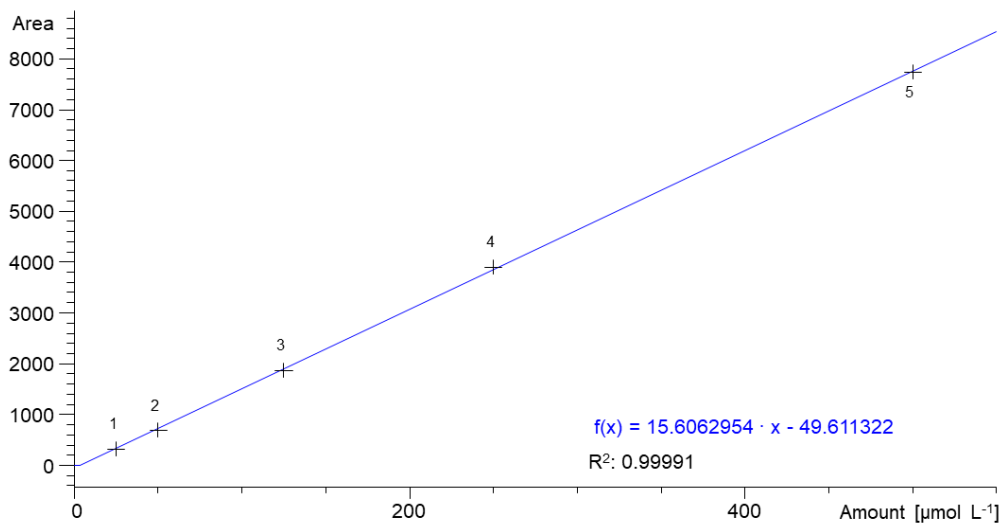


Fig. 3.2: Peak area as a function of the amount of 4-TP in the cysteine standard solutions.

3.2.5 Calculation of Parameters for Characterization of Thiol-Disulfide Reactions During Processing

The quantified concentration of free (C_{RSH}) and total (C_{total}) thiols of unprocessed and processed proteins by using the described method can be used to calculate important parameters for characterization of thiol-disulfide reactions during processing.

The concentration of reactive thiols $C_{reactive\ thiols}$ can be quantified by the decrease in concentration of free thiols before and after processing according to Eq. (3-5).

$$C_{reactive\ thiols} [\mu\text{mol}_{SH} g_{protein}^{-1}] = (C_{RSH\ unprocessed} - C_{RSH\ processed}) \quad (3-5)$$

In addition, the amount of irreversible formed oxidation products during heat treatment can be calculated by subtracting the concentration of total thiols after processing from that before processing (Eq. (3-6)).

$$C_{irreversible\ oxidation} [\mu\text{mol}_{SH} g_{protein}^{-1}] = (C_{total\ thiols\ unprocessed} - C_{total\ thiols\ processed}) \quad (3-6)$$

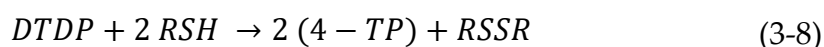
The knowledge on the concentration of free and total thiols before and after heat treatment is important for the calculation of the concentration of the disulfide bonds C_{RSSR} before and after processing. The concentration of disulfide bonds after heat treatment is influenced by the thiol reactivity but also by degradation of disulfide bonds. This is considered by using Eq. (3-7). The concentration of finally existing disulfide bonds (C_{RSSR}) is thereby an important information for the investigation of

thiol-related protein aggregate properties such as the molecular flexibility in the context of stabilization of interfaces, e.g. adsorption and anchoring at interfaces (Damodaran, 2005).

$$c_{RSSR} [\mu\text{mol}_{SH} g_{protein}^{-1}] = (c_{total\ thiols} - c_{RSH}) \quad (3-7)$$

3.3 Method Validation

The quantification of free thiols (RSH) by RP-HPLC is based on the detection of 4-TP (324 nm). Free thiols react with DTDP to 4-TP and a disulfide bond (RSSR) as follows (3-8) (Grassetti & Murray, 1967).



To validate the method, the following protein powders were used:

- β -Lactoglobulin (β -Lg) A, β -Lactoglobulin B prepared from milk of cows homozygous for the A or B variant by skimming and production of whey protein isolates by membrane filtration (micro- and ultrafiltration in diafiltration mode) and subsequent isolation of β -Lg A and B, respectively, according to the method of Toro et al. (Toro-Sierra, Tolkach, & Kulozik, 2013) (>99%, RP-HPLC)
- α -Lactalbumin (α -La) from bovine milk ($\geq 85\%$ (polyacrylamide gel electrophoresis (PAGE)), Merck KGaA, Germany)
- Albumin from bovine serum (BSA) ($\geq 98\%$ (agarose gel electrophoresis, Merck KGaA, Germany)
- Patatin purified from a commercial potato protein isolate powder (Solanic 200) with a high content of Patatin (AVEBE, The Netherlands) by preparative size exclusion chromatography using a Superdex 200 pg 26/600 (GE Healthcare, Germany) (>95% (PAGE))

3.3.1 Buffer Composition

For the analysis of free thiol groups, their accessibility is required to enable the reaction with DTDP, i.e., a complete unfolding of the proteins is decisive. According to the literature, guanidine HCl (GdnHCl) as an protein unfolding reagent is generally 1.5 to 2.5 times more effective per mole than urea (Greene & Pace, 1974; Pace, 1986; Pace & Marshall, 1980). This is probably of minor importance with native protein samples of small size as used by Hansen et al. (2007). However, aggregated gel-like structures are more resistant to dissolving and unfolding compared to native proteins. According to Dümpler et al. (Dümpler, Wohlschläger, & Kulozik, 2017), a buffer containing 6 M GdnHCl is capable of completely unfolding native milk proteins as well as heat denatured milk proteins in gel-like structures within a maximum time of

30 min. Since the method should be capable for unfolding of highly denatured and aggregated structures completely and within appropriate time, GdnHCl was chosen as denaturation reagent in contrast to urea used in the preceding method by Hansen et al. (Hansen et al., 2007). Therefore, it has to be tested whether the use of GdnHCl has a negative effect on the elution or the unfolding capacity and thus, the thiol recovery, respectively (Section 3.3.3 and 3.3.5).

In order to provide an optimum peak separation (e.g. 4-TP, DTDP, protein) as well as to remove all materials from the column to improve the operation time of the reversed-phase C-18 column, a gradient elution using acetonitrile/water mixtures was applied as recommended for RP-HPLC columns instead of 50 mM potassium acetate eluent used by Hansen et al. (2007).

To investigate the influence of GdnHCl and the acetonitrile/water mixture on the elution, a buffer system containing GdnHCl (6 M) as a denaturation agent, EDTA, the thiol reagent DTDP, and β -Lg as a thiol containing sample to release 4-TP was prepared. The pH was adjusted to 5 using citrate. Thus, except for the GdnHCl, the buffer components were the same as used by Hansen et al. (2007). The chromatogram of the GdnHCl-buffer system at a wavelength of 210 and 324 nm is shown in Fig. 3.3.

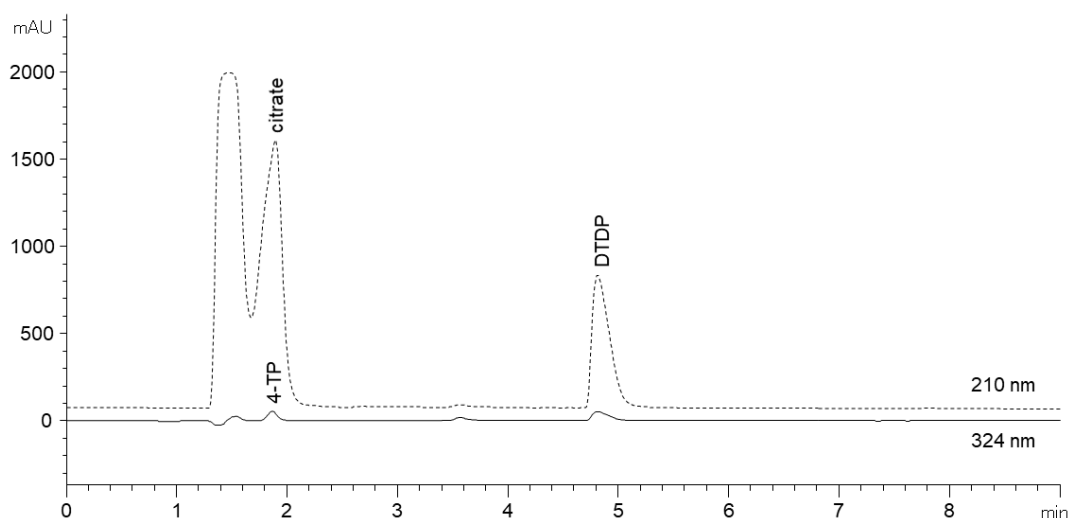


Fig. 3.3: Chromatogram of a buffer system (GdnHCl, EDTA, and DTDP) containing citrate (pH 5) and 4-TP released by β -Lg at a wavelength of 210 (dashed line) and 324 nm (solid line).

It can be seen that citrate and the reaction product 4-TP exhibit the same retention time. Thus, the binding capacity of 4-TP on the column is interfered by citrate and this leads to peak deformation (chromatogram not shown) and consequently to limited quantification of 4-TP. Resulting from these findings, citrate was substituted by Na_2HPO_4 and KH_2PO_4 to adjust the buffer pH to 5. The sample preparation and analysis was performed as described in the Section 3.2. As can be seen in Fig. 3.4, no overlaying peaks can be observed at neither wavelength (solid line). The buffer blank (without protein) only exhibit the solvent peak (1 min) and thus, no interference by the blank is detectable (data not shown). In addition, the chromatogram of the buffer blank

solution containing citrate is shown (dashed line). Thereby, the overlaying of the citrate peak over the 4-TP peak at 210 nm (and 324 nm) is quite clear to see (Fig. 3.4). Thus, using the modified buffer system containing GdnHCl, Na₂HPO₄, and KH₂PO₄ no interference on the elution can be detected.

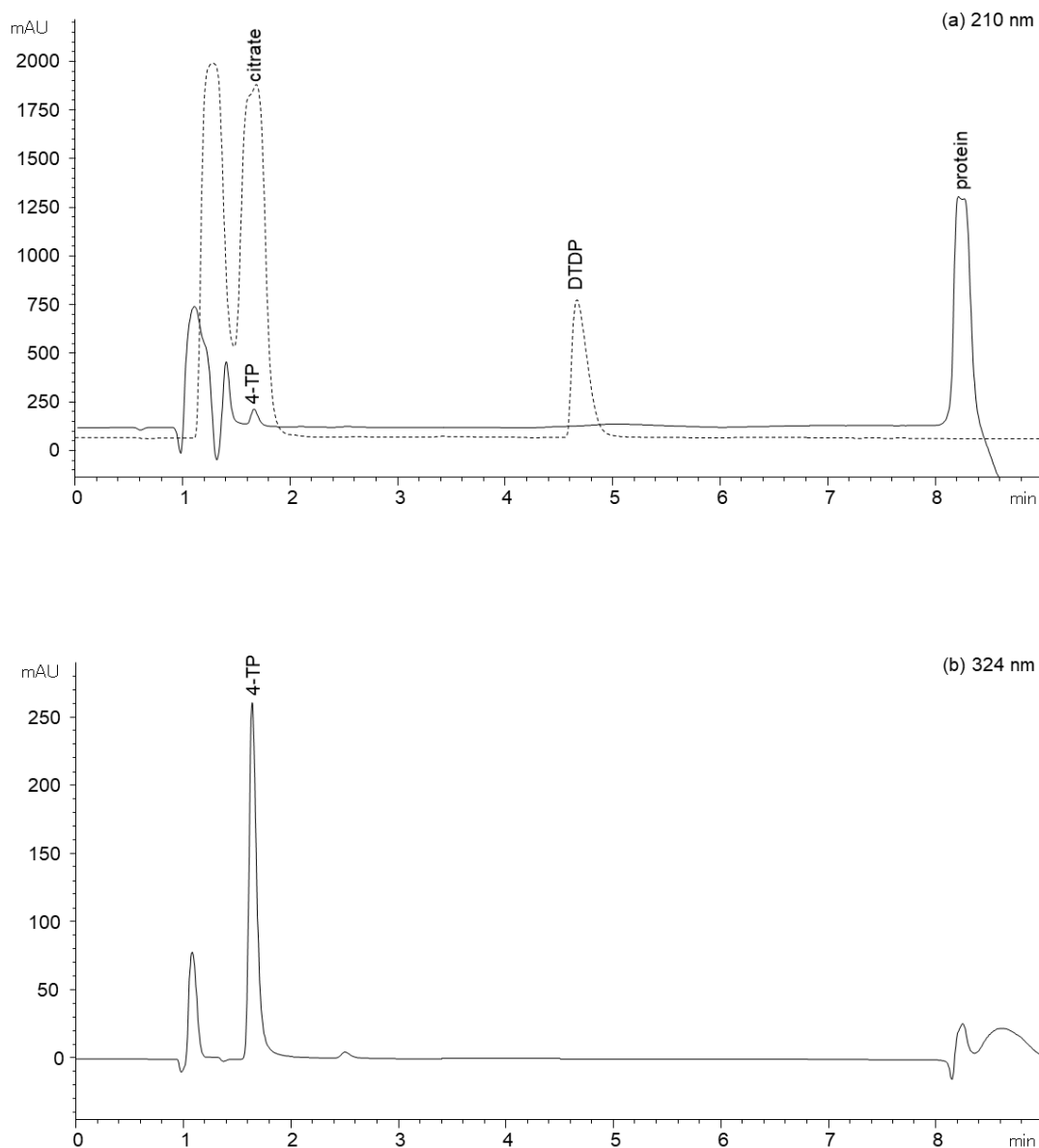


Fig. 3.4: Chromatograms for quantification of 4-TP at a wavelength of 210 (a) and 324 nm (b) using a reaction buffer consisting of GdnHCl, EDTA, DTDP, Na₂HPO₄, KH₂PO₄, and β -Lg to release 4-TP (solid line). As a guide to the eyes, the chromatogram of the GdnHCl, EDTA, DTDP, and citrate buffer (dashed line) is shown.

Apart from peak overlaying, the elution of all retained materials is important with regard to the column operation time. As can be seen in Fig. 3.4 a all adsorbing buffer components (DTDP, 4-TP, and protein) are eluted of the column by using the acetonitrile/water mixtures as an eluent. In consequence, an accumulation of buffer

components on the column as well as a carryover of ingredients to the next run can be avoided. Thus, the used buffer-eluent combination ensures a high peak quality and a long column operation time.

The applicability of GdnHCl as an unfolding agent with regard to its effect on thiol accessibility of native and heat-aggregated proteins is shown in Section 3.3.3 (native) and 3.3.5 (aggregated proteins).

3.3.2 DTDP Concentration

Next to complete unfolding, a sufficient concentration of DTDP is required in order to quantify all free thiols. To avoid excess reagent consumption as well as to ensure quantitative detection of all existing thiols, the minimum required DTDP concentration has to be investigated. The concentration is thereby dependent on the amount of accessible thiols of the sample solution.

According to the reaction equation of DTDP (Eq. (3-8)), 1 mol DTDP reacts with 2 mol of free thiols forming 2 mol of 4-TP (Grassetti & Murray, 1967). Thus, at least a ratio of 1 mol DTDP to 2 mol accessible thiols (RSH) is required to ensure complete quantification. The theoretical concentration of accessible thiols (free or total thiols) per protein-sample solution $c_{\text{thiol expected}}$ can be calculated according to Eq. (3-2) or (3-4), respectively.

Consequently, the minimum required amount of DTDP is depending on the thiol content of the sample. In order to check whether a stoichiometric concentration of DTDP is capable to determine the total amount of free thiols, a β -Lg (A+B) solution (c_{protein} : 9 g L⁻¹) was investigated. Thus, the theoretical concentration of free and total thiols was calculated according to Eq. (3-2) and (3-4). As both β -Lg A and B contain one free thiol group and five thiols in total and have a molecular weight (M_w) of 18.3 kg mol⁻¹ (Suttiprasit et al., 1992), the expected concentration of free thiols was 492 $\mu\text{mol L}^{-1}$ (0.246 μmol per 500 μL) and 2459 $\mu\text{mol L}^{-1}$ (2.459 μmol per 1000 μL) for total thiols.

According to the reaction Eq.(3-8), the minimum ratio of DTDP (μmol) to expected thiols ($\mu\text{mol}_{\text{thiols expected}}$) is 0.5. Therefore, samples of different DTDP/thiols_{expected} ratios of 0.5 to 1.6 were prepared and analyzed as described in the Section 3.2. The chromatograms are shown in Fig. 3.5. It can be seen, that similar 4-TP peak areas (percentage variation_{peak area}: <5% for free thiols and <0.3% for total thiols) occur for free as well as for total thiols, independently of the investigated DTDP/thiols_{expected} ratio. Thus, an excess concentration of DTDP did not result in a change in 4-TP concentration and thus in constant thiol concentration.

Apart from that, the concentration of 4-TP in the sample blanks (without protein) using also different amounts of DTDP (0.13 to 0.40 μmol or 1.24 to 4.00 μmol , respectively) was investigated. Due to the lack of proteins, the amount of 4-TP was expected to be zero. The concentration of 4-TP in the samples was below the detection limit of quantification for free thiols (area of 11.68) and total thiols (area of 26.69) independently of the added amount of DTDP. Therefore, a compensation of background absorbance is not necessary in that case.

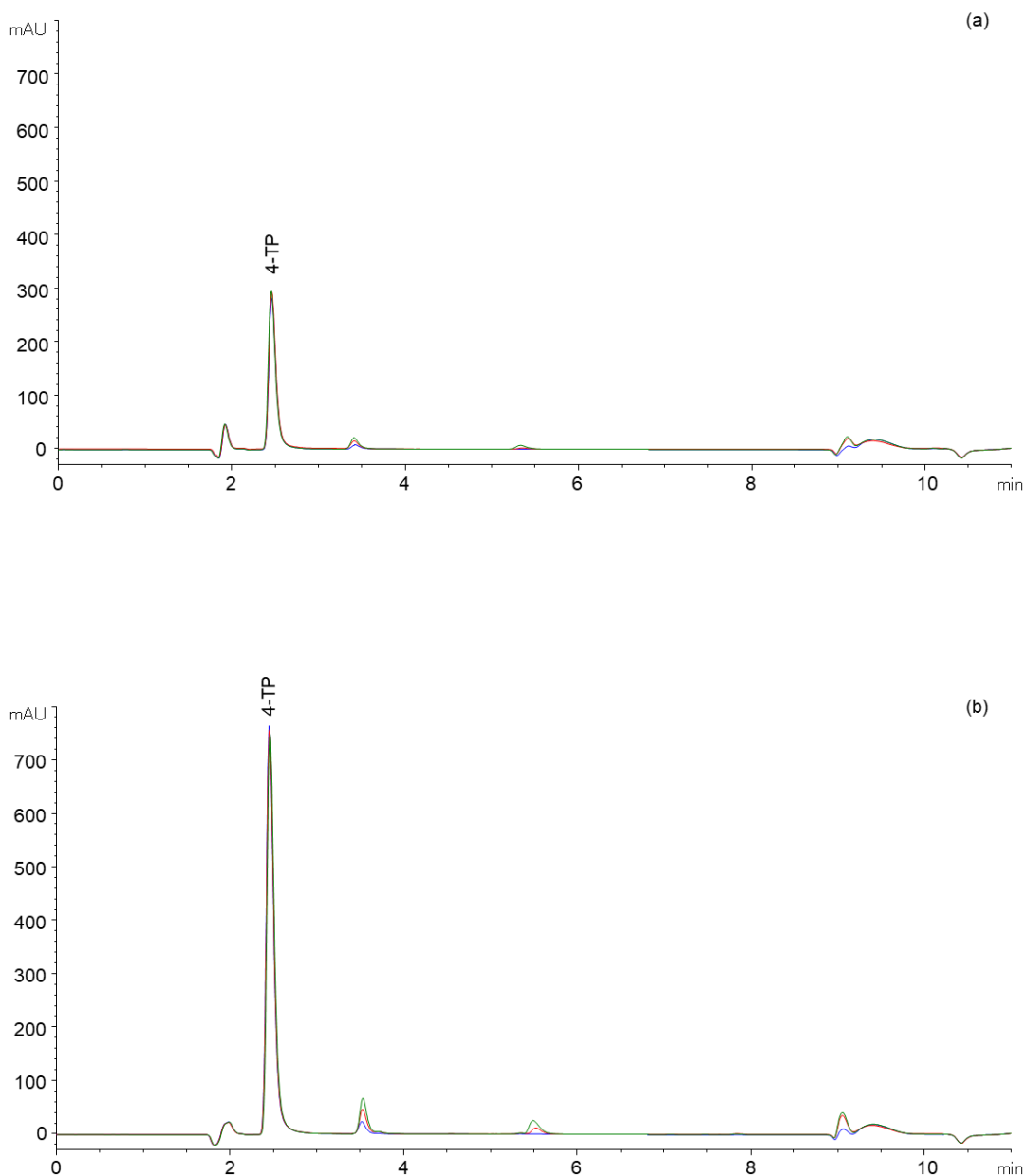


Fig. 3.5: Chromatograms of β -Lg solutions (9 g L^{-1}) for quantification of free (a) and total (b) thiols as a function of the DTDP [μmol]/thiol_{expected} [μmol] concentration ratio (0.5/1 (blue), 1.1/1 (red), 1.6/1 (green)).

Concluding from the above, a DTDP/thiol_{expected} ratio of 0.6 is recommended. In their method, Hansen et al. (2007) used a constant concentration of 0.36 mM DTDP with more than 10 molar excess of 4-DTDP over thiol.

In addition, the unfolding capacity of GdnHCl as well as the stability of 4-TP in the solution after reaction is essential for sample handling. Therefore, we investigated, whether a time-related change in the concentration of 4-TP was observable. To do so, the measured absorbance at 324 nm of all samples directly after preparation was

compared to the absorbance of the same sample measured after 24 h (data not shown). Thereby, only a slight difference (< 1%) in the quantified 4-TP concentration within 24 h was detected. Consequently, GdnHCl is efficient to unfold native proteins within 10 min. In addition, at ambient temperature, 4-TP is stable for 24 h.

To conclude, within 24 h the detected concentration of 4-TP is independent of the DTDP/ thiols_{expected} ratio as long as this ratio exceeds 0.5. However, this has to be verified for each new sample system.

3.3.3 Recovery Rates

As shown above, the DTDP/thiols_{expected} ratio did not affect the 4-TP absorbance. However, in order to further establish the method, proteins of varying amounts of free thiols and disulfide bonds per molecule in their native structure were chosen for validation. Therefore, the recovery rates (Eq. (3-9)) for free and total thiols, were calculated.

In detail, appropriate amounts of powder of the following proteins (Tab. 3-2) were dissolved in deionized water to a protein concentration of 9 g L⁻¹ each (7.5 g L⁻¹ Patatin) and stirred for 12 h at 4 °C to ensure complete hydration.

This was followed by calculation of the expected free and total thiol concentration on the basis of Eq. (3-2) and (3-4). As shown in Tab. 3-2, the whey proteins β -Lactoglobulin (β -Lg), genetic variants A and B, and bovine serum albumin (BSA) include one free thiol group and two (β -Lg) or 17 (BSA) disulfide bonds in their native structure (Sawyer & Kontopidis, 2000; Suttiprasit et al., 1992). In contrast, α -Lactalbumin (α -La) is absent of a free thiol group and exhibits four disulfide bonds (Permyakov & Berliner, 2000; Suttiprasit et al., 1992) whereas the potato protein Patatin includes one free thiol group and is absent of disulfide bonds (Delahaije, Wierenga et al., 2015).

$$\text{Recovery rate [\%]} = \frac{\text{thiols quantified (RP-HPLC)}}{\text{thiols expected}} \cdot 100\% \quad (3-9)$$

The calculated recovery rates for each protein solution is shown in Tab. 3-2. It can be seen that high recovery rates of more than 94% for free thiols and for total thiols can be found with BSA as an exception. It has to be noted that the nativity of the β -Lg powder was 94% determined by RP-HPLC according to the method of Toro-Sierra et al. (Toro-Sierra et al., 2013) and Dimpler et al. (Dimpler et al., 2017), whereas the nativity of the BSA and the α -La powder was unknown. As protein denaturation during powder production can cause irreversible thiol oxidation lower values of free and total thiols might occur. This accounts for the deviation of expected recovery value of 100% and thus, the quantification accuracy is acceptable. In addition, the recovery rates of the free thiol group of Patatin for both sample preparation ways (free and total thiols) shows high and similar values. Thus, the method shows high accuracy regardless of the preparation way.

Tab. 3-2: Recovery rates for free and total thiols of different whey proteins (Delahaije, Wierenga et al., 2015; Suttiprasit et al., 1992).

protein	M _w	RSH _{expected}	recovery _{0h}	total _{expected}	recovery _{0h}
-	g mol ⁻¹	RSH molecule ⁻¹	%	RSH molecule ⁻¹	%
β-Lg A+B	18,320	1	95.12 ± 2.07	5	96.31 ± 5.88
BSA	66,267	1	*1	35	86.27 ± 0.82
α-La	14,161	0	*2	8	98.65 ± 0.18
Patatin	40,009	1	94.27 ± 1.89	1	94.43 ± 1.06

*1 not determined due to missing information regarding powder nativity; *2 below detection limit

As already shown in Section 3.3.2, the 4-TP also shows a high stability within 24 h for BSA and α-La. The deviation in detected thiols is thereby < 2%. Thus, the reaction can be performed after 10 min until 24 h after sample preparation. In addition, it can be concluded, that GdnHCl is an effective unfolding reagent due to the high and time independent recovery rate for free and total thiols of all investigated proteins.

3.3.4 Reproducibility of the Method

To validate the reproducibility of the method a whey protein mixture (ideal whey), containing different proteins of variable amounts of free and total thiols, was used. The reproducibility was assessed as follows: An ideal whey was produced by pH 4.6 precipitation of fresh raw milk and subsequent filtration using a 0.45 μm filter to separate caseins and whey proteins contained in the filtrate. The whey protein composition and concentration was analyzed according to Dumpler et al. (Dumpler et al., 2017). Based on this, the concentration of free and total thiols of the whey, consisting of β-Lg (A+B), α-La, BSA, lactoferrin (17 disulfide bonds; M_w 82,400 g mol⁻¹ (Levay & Viljoen, 1995; Pierce et al., 1991)), and immunoglobulin G (16 disulfide bonds, M_{w IgG2} 150,000 g mol⁻¹ (Butler, 1969)) was calculated according to Eq. (3-2) and (3-4). The recovery rates (Eq. (3-9)) were 82.11% ± 1.65% for the free thiols and 101.88% ± 1.67 for total thiols. The results for the 24 h analysis showed a deviation of less than 1.5%, for concentrations of both, free and total thiols.

Thus, the results clearly show that the method can also be used for mixtures of thiol containing proteins.

3.3.5 Thiol Reactivity and Disulfide Formation/ Degradation during Heat Treatment

Thiol-disulfide exchange reactions of whey proteins mainly occur due to heat treatment. Thus, next to the quantification of free and total thiols of proteins in their native states, heat-treated whey proteins were investigated to further validate the method and to determine thiol reactivity and disulfide formation during processing.

To do so, a β-Lg solution (C_{protein} 8.8 ± 0.5 g L⁻¹, pH 6.8) was heat treated at 80 °C for 90 min to expose the free thiol group and thus inducing thiol-disulfide exchange

reactions. In addition, the ionic strength was increased up to 40 mM by NaCl to increase the denaturation velocity.

Tab. 3-3 shows the quantified thiol concentrations as well as the calculated concentrations for irreversible oxidation, reactive thiols, and disulfide concentration before and after processing according to Eq. (3-5) - (3-7). Thereby, a decrease in free thiol concentration of $23.10 \pm 3.18 \mu\text{mol}_{\text{SH}} \text{g}_{\text{protein}}^{-1}$ can be determined due to heat treatment. This corresponds an increase in thiol reactivity ($C_{\text{reactive thiols}}$) of $23.1 \pm 3.2 \mu\text{mol}_{\text{SH}} \text{g}_{\text{protein}}^{-1}$. These results are in accordance with those found by Leeb et al. (Leeb et al., 2018) for heat treated β -Lg using the spectrophotometric Ellman's assay.

Tab. 3-3: Concentration of free and total thiols before and after heat treatment (80 °C/90 min) of a β -Lg solution (pH 6.8, 40 mM NaCl) as well as calculated amounts of irreversible oxidation products, reactive thiols and disulfide concentration.

process	$C_{\text{free RSH}}$	C_{total}	$C_{\text{irreversible oxidation}}$	$C_{\text{reactive thiols}}$	C_{RSSR}
-	$\mu\text{mol}_{\text{SH}} \text{g}_{\text{protein}}^{-1}$	$\mu\text{mol}_{\text{SH}} \text{g}_{\text{protein}}^{-1}$	$\mu\text{mol}_{\text{SH}} \text{g}_{\text{protein}}^{-1}$	$\mu\text{mol}_{\text{SH}} \text{g}_{\text{protein}}^{-1}$	$\mu\text{mol}_{\text{SH}} \text{g}_{\text{protein}}^{-1}$
unheated	53.40 ± 1.69	265.83 ± 14.07	28.35 ± 6.59	23.1 ± 3.2	212.43 ± 12.39
heated	30.30 ± 3.04	229.91 ± 1.41			199.61 ± 1.64

However, the concentration of total thiols decreased by $28.35 \pm 6.59 \mu\text{mol}_{\text{SH}} \text{g}_{\text{protein}}^{-1}$ after heat treatment. This difference in total thiol concentration indicates the formation of irreversible oxidation products which cannot be reduced using NaBH_4 . An insufficient reaction time can be excluded due to the slight deviation (<5%) of thiol content within 24 h (data not shown). Regarding to the literature, degradation of disulfide bonds due to desulfuration (β -elimination) can occur during heat treatment, leading to the formation of dehydroalanine and persulfide. Further reactions between dehydroalanine and thiols result in the formation of irreversible oxidation products (Friedman, 1999), which are not detectable by 4-TP due to lacking reduction. According to Klostermeyer et al. (Klostermeyer & Reimerdes, 1977) and Watanabe et al. (Watanabe & Klostermeyer, 1976), heat treatment of β -Lg solutions mainly results in the loss of sulfur due to the formation of dehydroalanine and further reaction products. Thereby, the extent of the loss of sulfur is increased at alkaline heating pH (Klostermeyer & Reimerdes, 1977; Watanabe & Klostermeyer, 1977). Thus, to further confirm the formation of irreversible oxidation products and to validate the method, solutions of β -Lg (A+B) (9 g L^{-1} , 60 mM NaCl) were heated (80 °C, 90 min) at pH 6.8 and 8.5, accompanied by quantification of total thiols before and after heat treatment. The concentration of irreversible oxidation products ($C_{\text{irreversible oxidation}}$) was calculated by subtraction of the total thiol amount after heat treatment from that before heat treatment according to Eq. (3-6). Thereby, an increase in the concentration of irreversible oxidation from 33.3 ± 8.1 (pH 6.8) to $56.6 \pm 0.5 \mu\text{mol}_{\text{SH}} \text{g}_{\text{protein}}^{-1}$ (pH 8.5) products can be determined with increasing heating pH. Thus, the amount of detectable total thiols is decreased.

To sum up, the developed method has the advantage to quantify both, concentration of free thiols and disulfide bonds. This is important to describe free thiol oxidation due to the lacking proportionality of the increase in disulfide formation and the decrease in free thiol concentration during heat treatment. The described method can therefore be used for a separated consideration of thiol reactivity (Eq. (3-5), formation of irreversible oxidation products (Eq. (3-6)), and the presence of disulfide bonds (Eq. (3-7)) during processing of proteins. Using the presented method, thiol oxidation reactions of whey proteins are determined more accurately as compared to the commonly used application of the Ellman's assay for determination of thiol reactivity and the semi-quantitative PAGE for disulfide formation. The knowledge on the concentration of existing disulfide bonds before and after processing is thereby crucial regarding the characterization of disulfide induced changes in molecular flexibility.

In addition, the described method should be applicable for other protein systems than whey proteins. However, the method has to be verified for each new sample system.

Acknowledgements

We gratefully thank Hermine Roßgoderer, Vera Reitberger, Christina Dörmeier, Daniel Saalfeld, Joseph Dümpler, and Martin Hartinger for their support during the development of the method. David Andlinger is acknowledged for preparation of the Patatin.

This IGF Project of the FEI (AiF 18621 N) was supported via AiF within the program for promoting the Industrial Collective Research (IGF) of the German Ministry of Economic Affairs and Energy (BMWi), based on a resolution of the German Parliament.

Declaration of Competing Interest

The authors declare that they have no known competing financial interests or personal relationships that could have appeared to influence the work reported in this paper.

4 Correlation between Physico-Chemical Characteristics of Particulated β -Lactoglobulin and Its Behavior at Air/Water and Oil/Water Interfaces²

Summary and Contribution of the Doctoral Candidate Franziska Maria Hartinger (Name at Birth: Kurz)

Protein-based particles are known to efficiently stabilize foams and emulsions. In this context, the individual particle properties such as size, surface charge, and structural flexibility are known to influence the stability of the different systems. However, the priority of the individual particle characteristics and their interrelations have not yet been fully elucidated with regard to the formation and stabilization of foams and emulsions. In this context, most studies focused on air/water or oil/water interfaces. Thus, it remains unclear, whether correlations found for foams can be transferred to emulsions. Moreover, many studies varied more than one particle characteristic at a time, whereby no clear conclusions regarding the impact of the individual protein particle properties on the techno-functionality can be drawn.

Therefore, the main goal of this study was the controlled generation of protein-based particles with one physicochemical characteristic varying at a time to unravel the correlation between individual particle characteristics and their ability to stabilize air/water and oil/water interfaces.

It could be shown that foam and emulsion stability are not linked to the same particle characteristics. While a low cross-linking degree was found to enhance foam stability, emulsion stability decreased due to oil droplet aggregation. With regard to the initial interfacial adsorption behavior, the degree of disulfide cross-linking was observed to be unimportant. In this context, it could be shown that a decreasing zeta potential has a positive effect on the adsorption behavior at both types of interfaces, rather independently of the particle size. The impact of the zeta potential was investigated by variation of pH value. This study helps to understand correlations between structural and techno-functional properties and thus, to draw generalized conclusion regarding the stabilization of foams and emulsion.

The doctoral candidate designed the experiments after critically reviewing the literature. Furthermore, the doctoral candidate carried out experimental work, data analysis, interpretation, and plotting. The doctoral candidate mainly wrote the original manuscript and revised the manuscript. The co-authors contributed to the

² Original publication: Kurz, Franziska; Reitberger, Vera; Hengst, Claudia; Bilke-Krause, Christine; Kulozik, Ulrich; Dombrowski, Jannika (2021) Correlation between Physico-Chemical Characteristics of Particulated β -Lactoglobulin and Its Behavior at Air/Water and Oil/Water Interfaces Foods. doi: 10.3390/foods10061426. Adapted original manuscript. Adaptions of the manuscript refer to enumeration type, citation style, spelling, notation of units, format, and merging all lists of references into one at the end of the dissertation.

conceptualization, the execution of experiments, the validation of results and formal analysis, the discussion of results, and the revision of the manuscript.

Adapted Original Manuscript²

Correlation between Physico-Chemical Characteristics of Particulated β -Lactoglobulin and Its Behavior at Air/Water and Oil/Water Interfaces²

Franziska Kurz^{1,*}, Vera Reitberger¹, Claudia Hengst¹, Christine Bilke-Krause², Ulrich Kulozik¹ and Jannika Dombrowski^{1,3}

¹ Chair of Food and Bioprocess Engineering, TUM School of Life Sciences, Technical University of Munich, Weihenstephaner Berg 1, 85354 Freising, Germany; franziska.kurz@tum.de (F.K.), vera.reitberger@mytum.de (V.R.), claudia.hengst@tum.de (C.H.), ulrich.kulozik@tum.de (U.K.)

² Krüss GmbH, Borsteler Chaussee 85, 22453 Hamburg, Germany; c.bilke-krause@kruss.de (C.B.)

³ Nestlé Research, Société des Produits Nestlé SA, Route du Jorat 57, 1000 Lausanne 26, Switzerland ; Jannika.Dombrowski@rd.nestle.com (J.D.)

* Correspondence: franziska.kurz@tum.de

Abstract

It is widely accepted that protein-based particles can efficiently stabilize foams and emulsions. However, it is not fully elucidated which particle properties are decisive for the stabilization of air/water and oil/water interfaces. To unravel this correlation selected properties of nano-sized soluble β -lactoglobulin particles were changed one at a time. Therefore, particles of (1) variable size but similar zeta potential and degree of cross-linking and (2) similar size but different further properties were produced by heat treatment under specific combination of pH-value and NaCl concentration and then analyzed for their interfacial behavior as well as foaming and emulsifying properties.

On the one hand, it was found that the initial phase of protein adsorption at both the air/water and the oil/water interface was mainly influenced by the zeta potential, independent of the particle size. On the other hand, foam stability as resolved from the time-dependent evolution of mean bubble area negatively correlated with disulfide cross-linking, whereas emulsion stability in terms of oil droplet flocculation showed a positive correlation with disulfide cross-linking. In addition, flocculation was more pronounced for larger particles. Concluding from this, foam and emulsion stability are not linked to the same particle properties and thus, explanatory approaches cannot be used interchangeably.

Keywords: β -lactoglobulin; thermal aggregation; particle size; zeta potential; cross-linking degree; interfacial properties; foam; emulsion

4.1 Introduction

Protein particles have attracted considerable attention during the last few years, particularly in the context of stabilizing foams and emulsions as they are deemed to provide high product stability and offer novel opportunities for the food industry (Amagliani & Schmitt, 2017; Dickinson, 2017; Sarkar & Dickinson, 2020). However, based on the current state of the literature, the correlation between specific particle properties and high foam as well as emulsion stability has still not been fully elucidated, i.e., knowledge of decisive particle properties for different applications as well as interface types is lacking. In this regard, a mechanistic understanding of how those particles act at both air/water and oil/water interfaces is crucial for their design and applicability. Due to the deformable and porous structure of protein particles, a transfer of the classical contact angle-based 'Pickering concept' is not considered reasonable (Dickinson, 2015; Pickering, 1907; Schmidt et al., 2011). Thus, to better understand and explain their functionality in contrast to inorganic particles or to proteins in their native state, in depth knowledge about their behavior at air/water and oil/water interfaces is required.

According to the literature, several physicochemical characteristics are referred to as being important for the formation and stabilization of protein-based foams and emulsions. These include the proteins' particle size, degree of (intramolecular) cross-linking, surface charge (zeta potential), and surface hydrophobicity (Amagliani & Schmitt, 2017; Dickinson, 2017; Sarkar & Dickinson, 2020; Shi, Feng, Wang, & Adhikari, 2020). However, there is no consensus on their prioritization as well as specific relevance for protein particle-based foams or emulsions.

Whey proteins, have often been used as a model system to produce (heat-induced) protein-based particles and to evaluate their behavior at air/water or oil/water interfaces, as described in detail in the following.

Concluding from a multitude of foam-related studies it is generally recognized that protein diffusion to the interface and thus foamability decreases with increasing particle size (Dhayal et al., 2015; Dombrowski et al., 2016; Rullier et al., 2008). However, the lowering of the protein particles' surface charge (zeta potential) via pH adjustment or salt-mediated charge screening leading to a reduced electrostatic barrier of adsorption as well as an increase in surface hydrophobicity seems to be even more important in view of foamability than particle size (Dombrowski et al., 2017; Moro et al., 2011; Schmitt et al., 2007; Schmitt et al., 2014). By contrast, foam stability seems to positively correlate with particle size and negatively correlate with zeta potential (Dombrowski et al., 2016; Schmitt et al., 2007; Schmitt et al., 2014). By contrast, Lazidis et al. (2016) reported contradicting findings regarding the influence of the zeta potential. Moreover, the degree of cross-linking (i.e., the structural flexibility) is known to influence foam stability (Dhayal et al., 2015; Kim et al., 2005; Schmitt et al., 2007). Regarding the degree of cross-linking, however, the drawing of generalized conclusions is quite difficult. This is due to the variety of cross-linking techniques used

in different studies such as heat-induced or enzymatic cross-linking as well as the lack of a common definition of the 'degree of cross-linking' (Dhayal, Gruppen, Vries, & Wierenga, 2014; Kim et al., 2005; Moro et al., 2011; Schmitt et al., 2007).

In terms of emulsions or oil/water interfaces, similar factors are described to affect their formation and stabilization (Destribats, Rouvet et al., 2014; Moro et al., 2013; Murphy et al., 2016; Murphy et al., 2018; Sobhaninia et al., 2017; Wu et al., 2015; Zhou, Sala, & Sagis, 2020). However, in contrast to foams, oil droplet flocculation and thus emulsion stability was found to be negatively affected by the screening of the particles' zeta potential (Destribats, Rouvet et al., 2014; Sobhaninia et al., 2017). Surface hydrophobicity seems to be decisive in terms of the emulsifying activity, however, the effect was less pronounced compared to its impact on foamability (Moro et al., 2013).

Overall, this shows that the interrelation and priority of the different particle physicochemical properties in terms of foam and emulsion formation as well as stabilization are still not fully elucidated. This can be explained as follows: First, many studies varied more than one particle characteristic at a time (e.g., particle size and zeta potential or particle size and surface hydrophobicity), wherefore it is difficult to assess their respective specificity. Second, most studies focused on either air/water or oil/water interfaces and used different particle formation as well as characterization methods.

Therefore, to approach this knowledge gap, the objective of this work was (i) the controlled production of protein-based particles with one physicochemical property changed at a time to (ii) unravel the correlation between particle characteristics and their behavior at the air/water and the oil/water interface. For this, the main whey protein β -lactoglobulin (β -Lg) was used, because its structure is well-characterized and its aggregation behavior can be influenced in a targeted manner (Nicolai et al., 2011; Nicolai & Durand, 2013; Tolkach & Kulozik, 2007). In detail, particles of (1) variable size but similar zeta potential and degree of cross-linking and (2) similar size but different further physicochemical properties were produced by heat treatment of β -Lg solutions (i.e., $c = 10 \text{ g L}^{-1}$, $80 \text{ }^\circ\text{C}/90 \text{ min}$) at different pH values (i.e., 5.8 to 8.5) and in the presence of NaCl at various molarities (i.e., 0-60 mM). The obtained β -Lg particles were then analyzed for their interfacial behavior as well as foaming and emulsifying properties. Particle purity in terms of the absence of remaining native β -Lg molecules and NaCl was achieved by an isoelectric precipitation in combination with a centrifugal separation and subsequent re-dissolution of the particle pellet.

Following this, conclusions regarding a correlation between specific physicochemical particle properties and the surface/interfacial behavior as well as foam/emulsion stabilization capability shall be drawn. Moreover, this was supposed to provide some general conclusions guiding the practical optimization of the stability of foams and emulsions stabilized by protein-based particles.

4.2 Materials and Methods

4.2.1 Materials

Bovine β -lactoglobulin (β -Lg) (A and B) was purified from whey protein isolate (WPI 895, Fonterra Co-operative Group, Auckland, New Zealand) by selective thermal aggregation with subsequent microfiltration/ultrafiltration and spray drying as described in detail by Toro-Sierra et al. (2013). The obtained powder had a total protein content of > 99% on a dry matter basis (Vario MAX cube, Elementar Analysensysteme GmbH, Langenselbold, Germany; RP-HPLC), whereby > 99% was β -Lg. Native β -Lg represented > 86% of the total protein as determined by RP-HPLC (Toro-Sierra et al., 2013). Lactose (HPLC) and salts (Na, K, Ca) (ELEX 6361, Eppendorf AG, Hamburg, Germany) concentration were < 0.05% and 0.7%, respectively.

4.2.2 Production of β -Lactoglobulin Particles by Thermal Treatment and Particle Concentration

β -Lg powder was dissolved in deionized water (Millipore Corporation, Bedford, MA, USA) or in NaCl solutions of different molarities (20 or 60 mM) (Merck KGaA, Darmstadt, Germany) to a total protein content of 10 g L⁻¹. For the determination of protein content during particle production and purification a method according to Dumas was used (Elementar Analysensysteme GmbH, Hanau, Germany). The solutions were stirred for 12 h at 4 °C to ensure complete hydration.

4.2.2.1 Production of β -Lactoglobulin Particles by Thermal Treatment

Prior to heat treatment, the solutions were tempered to 20 °C and the pH was adjusted to 5.8, 6.2, 6.8, 7.6 or 8.5 with 1 M HCl (Merck KGaA, Darmstadt, Germany) or 1 M NaOH (Merck KGaA, Darmstadt, Germany). The formation of β -Lg particles was conducted at a temperature of 80 °C for a heat holding time of 90 min using a thermostatically controlled water bath. The solutions were stirred during heating and their temperature was monitored by a sensor connected to an Almemo 2590-4AS (Ahlborn Mess-und Regelungstechnik, Holzkirchen, Germany). The denaturation was stopped by cooling the solutions to 20 °C in ice water.

4.2.2.2 Determination of the Concentration of Particles after Heat Treatment

Due to the dependence of β -Lg's denaturation reaction rate constant on the pH value and salt concentration during heating, a native fraction of β -Lg molecules could remain in the particle solution after heat treatment. In order to determine the residual native β -Lg, the denatured proteins (i.e., the protein particles) were precipitated at pH 4.6 as described by Toro-Sierra et al. (2013). The native and the denatured proteins were separated by using a syringe filter (pore size 0.45 μ m, Chromafil Xtra RC-45/25, Macherey-Nagel GmbH & Co. KG, Düren, Germany). The protein content of the native fraction, i.e., the filtrate, was determined by reversed phase high performance liquid chromatography (RP-HPLC, Agilent 1100 Series Chromatograph, Agilent Technologies Inc., Santa Clara, CA, USA) as reported by Dumpler et al. (2017). For this,

200 μL of the solution were dissolved in 800 μL guanidine buffer and left for 30 min at room temperature to ensure complete solubilization (i.e., denaturation and cleavage of disulfide bonds) of the protein molecules (Dumpler et al., 2017). The total protein content, native and denatured, was determined accordingly, however, no precipitation step at pH 4.6 was conducted.

The degree of denaturation (DD) was calculated by the following equation (Eq. (4-1)).

$$DD (\%) = \left(1 - \frac{C_t}{C_0}\right) * 100\% \quad (4-1)$$

C_t is the native β -Lg concentration in a pH 4.6 precipitated sample, whereas C_0 is the native β -Lg concentration in the unheated solution.

Particle Purification

In order to exclude the influence of remaining native β -Lg molecules as well as the NaCl on the interfacial investigations, a purification step was necessary, in some cases, to obtain a purified ($DD \geq 96\%$, conductivity (κ) $< 1 \text{ mS cm}^{-1}$) particle solution. Therefore, a concentration-purification step based on an isoelectric precipitation was performed after heat treatment in order to reduce the content of remaining native protein and NaCl (Dannenbergs & Kessler, 1988). The pH of the heated protein solution was adjusted to 4.6. Consequently, the denatured protein particles precipitated, whereas the native proteins as well as the salt remained soluble. To accelerate the separation process, the samples were centrifuged at $500 \cdot g$ for 15 min at $20 \text{ }^\circ\text{C}$ (38.5 g sample solution per centrifuge tube) using the Multifuge 1S-R (Thermo Fisher Scientific, Waltham, MA, USA). The supernatant was discarded and the particle pellet was re-dissolved in deionized water. The volume of deionized water was chosen to achieve a total protein concentration of about 1.0% (Elementar Analysensysteme GmbH, Hanau, Germany). In addition, 1 M NaOH was added to adjust the pH to 6.8. After at least 2 hours ($\sim 12 \text{ h}$: pH 5.8/0 mM; pH 6.2/0 mM, and pH 8.5/60 mM) of gentle shaking, the concentration-purification step was repeated until a DD of $\geq 96\%$ (monitored by RP-HPLC) and a conductivity (κ) $< 1 \text{ mS cm}^{-1}$ (S47 - SevenMulti™, Mettler-Toledo AG, Schwerzenbach, Switzerland) was achieved. Subsequently, the total protein concentration of the purified particles (i.e., pH 6.8, DD of $\geq 96\%$, κ $< 1 \text{ mS cm}^{-1}$) was adjusted to 8.2 g L^{-1} by using deionized water.

All experiments were carried out at a temperature of $20 \text{ }^\circ\text{C}$ using a protein concentration of 8.2 g L^{-1} (determined by RP-HPLC) and a pH of 6.8. Apart from that, the solutions with particles produced at pH 5.8 (0 mM) and at pH 6.2 (0 mM) were additionally investigated at pH values of 6.2 and 6.3, respectively.

4.2.3 Quantification of Protein Thiols and Disulfide Bonds

In order to determine the concentration of thiols, which are part of disulfide bonds, the concentration of free and total (free thiols and thiols associated in disulfide bonds) thiols was quantified by RP-HPLC using the thiol reagent 4,4'-Dithiodipyridine (DTDP) as described by Kurz, Hengst, and Kulozik (2020). In brief, free thiols (and reduced disulfide bonds) react with DTDP forming 4-Thiopyridine (4-TP), which absorbs at 324 nm in the pH range from 3-7. Therefore, the concentration of thiols associated in disulfide bonds c_{RSSR} can be calculated by the difference between the concentration of free thiols and total thiols. In order to determine the degree of disulfide cross-linking and thus the structural flexibility, the change in the concentration of disulfide bonds due to processing was used according to the following equation (Eq. (4-2)).

$$\begin{aligned} & \text{degree of disulfide cross - linking (\%)} \\ & = \frac{c_{RSSR \beta-Lg \text{ aggregates}}}{c_{RSSR \text{ untreated } \beta-Lg}} \cdot 100\% \end{aligned} \quad (4-2)$$

4.2.4 Particle Size and Zeta Potential Measurements

The volume-based particle size distributions as well as the median volume-based particle size ($d_{50.3}$) were measured by dynamic light scattering using a Zetasizer Nano ZS (Malvern Panalytical GmbH, Kassel, Germany). Samples were measured in 173° backscatter mode 10 times for 1 min after an equilibration time of 2 min. The refractive index (RI) used for calculation was set to 1.344. Results of the particle size measurements are means of two samples of at least two individual experiments.

The zeta potential of the unheated and purified protein solutions was measured by a Zetasizer Nano ZS System (Malvern Panalytical GmbH, Kassel, Germany). The measurement consisted of two runs. The obtained electrophoretic mobility was converted to the zeta potential by the Zetasizer Software 7.13 (Malvern Panalytical GmbH, Kassel, Germany). Results of the zeta potential measurements are means of at least two individual experiments with three samples each.

4.2.5 Viscosity Measurements

Viscosity of the purified solutions was determined on the Modular Compact Rheometer MCR 302 (Anton Paar GmbH, Graz, Austria) using a double gap geometry (DG 26.7, Anton Paar GmbH, Graz, Austria). The used procedure included an increasing shear rate ramp from 0.1 to 100 s^{-1} followed by a decreasing ramp from 100 to 0.1 s^{-1} . For data analysis and calculation of the dynamic viscosity the software RheoPlus and RheoCompass 1.22 were used. Thereby, all samples showed Newtonian behavior. Results of the measurements are means of at least two individual experiments.

4.2.6 *Surface and Interfacial Tension*

The surface tension (σ) at the air/water interface as well as the interfacial tension (γ) at the oil/water interface were measured by the pendant drop method using the Drop Shape Analyzer DSA 100 (Krüss GmbH, Hamburg, Germany) equipped with a pendant drop module (Krüss GmbH, Hamburg, Germany). A drop containing the purified particle solutions was formed automatically at the tip of a cannula of a syringe into either air or a cuvette containing 100% caprylic acid (Primal State Performance GmbH, Berlin, Germany). Caprylic acid was used due to its negligible surface activity compared to vegetable oil (data not shown). The change in the bubble radius and shape was recorded for a time period of 3600 s. The surface tension and the interfacial tension were calculated by the Young-Laplace-Fitting using the Advance software (Krüss GmbH, Hamburg, Germany). Therefore, the needle diameter and the densities of air or oil and the water phase were considered for the calculation. Results of the surface/ interfacial measurements are means of at least two individual experiments. In order to better compare the interfacial properties of the specific particles at the air/water and oil/water interface the surface pressure ($\pi_\sigma(t)$) and the interfacial pressure ($\pi_\gamma(t)$) were calculated additionally as follows (Eq. (4-3) and (4-4), respectively).

$$\pi_\sigma(t)(mN m^{-1}) = \sigma_0 - \sigma(t) \quad (4-3)$$

$$\pi_\gamma(t)(mN m^{-1}) = \gamma_0 - \gamma(t) \quad (4-4)$$

Here, σ_0 (γ_0) is the surface tension (interfacial tension) of deionized water and $\sigma(t)$ ($\gamma(t)$) is the time-dependent surface tension (interfacial tension) of the β -Lg particle sample solutions.

4.2.7 *Foaming and Characterization of Foam Stability*

Foams were prepared by air sparging (foam height = 180 mm, $\dot{V} = 0.2$ L) through a porous frit (pore size 9-16 μm) into the β -Lg particle solution ($V = 50$ mL, $c = 8.2$ g L⁻¹) by using the Dynamic Foam Analyzer DFA100 (Krüss GmbH, Hamburg, Germany). The pH values of the respective β -Lg solutions were kept at 6.8. Apart from that, the solution with particles produced at pH 5.8 (0 mM) was additionally investigated at a pH value of 6.2. The evolution of the bubble area distribution was recorded over a time period of 3600 s by the attached Foam Structure Module (DFA100FSM, Krüss GmbH, Hamburg, Germany). The camera was thereby located at a column height of 65 mm. Thereof, the mean bubble area was determined by using the software Advance (Krüss GmbH, Hamburg, Germany). The obtained mean bubble area (A) in dependence of time (t) was used to describe and compare the structural decay behavior of the different foams. According to Schmitt et al. (2007) the number of air bubbles within a foam can be characterized by an exponential foam decay, revealing an increase in the air bubble area during coarsening. The plotting of the air bubble area against time thereby allows for the estimation of the coarsening exponent α . Therefore, a power-

law fit of the experimental data according to $A \sim t^\alpha$ was performed ($t_{>50s}$ > air sparging for foam formation) to evaluate the foam bubble stabilization behavior.

Results of the foaming experiments are means of at least two individual experiments. Details about the measuring principle are described by Oetjen et al. (2014).

4.2.8 Emulsification and Measurement of Oil Droplet Size

Oil-in-water emulsions (10/90 (w/w)) with sunflower oil (THOMY, Nestlé Deutschland AG, Neuss, Germany) and β -Lg particles ($c = 8.2 \text{ g L}^{-1}$) in the aqueous phase were produced by high pressure homogenization (APV 1000, SPX Corporation, Inc., Soborg, Denmark) at 300 bar. The pH values of the respective β -Lg solutions were kept at 6.8 prior to adding the oil. Apart from that, the solutions with particles produced at pH 5.8 (0 mM) was additionally investigated at a pH value of 6.2. A pre-mix was produced by diluting the oil in the protein-water phase under stirring at 300 rpm followed by stirring at 6000 rpm for 60 s using an ultra turrax (ULTRA-TURRAX® T 25 digital (S25N), IKA®-Werke GmbH & Co. KG, Staufen, Germany). Thereof, the measurements of the particle size distribution and the median volume based particle size ($d_{50.3}$) as well as the surface weighted mean ($d_{3.2}$) of the freshly prepared emulsions were carried out with the Mastersizer 2000 with a Hydro 2000 unit (Malvern Panalytical GmbH, Kassel, Germany). In order to determine the emulsion stability, the flocculation factor (ff) was used as calculated according to the following equation (Eq. (4-5)).

$$\text{flocculation factor } (-) = \frac{d_{50.3} (\text{without SDS})}{d_{50.3} (\text{with SDS})} \quad (4-5)$$

Therefore, 1 mL of the emulsion sample was mixed with 9 mL of 0.5% sodium dodecyl sulfate (SDS) solution and measured as described before. Results of the oil droplet measurements are means of at least two individual experiments.

4.3 Results and Discussion

4.3.1 Preparation and Structural Characterization of β -Lg Particles

The variation of the pH value and the NaCl concentration during heat treatment of the β -Lg solutions allowed for the formation of soluble (not sedimenting) particles of different size and degree of denaturation (i.e. remaining native protein after heat treatment) as can be seen in Tab. 4-1.

Tab. 4-1: Median particle size ($d_{50.3}$) and degree of denaturation (DD) in dependence of heating pH and NaCl concentration of heat-treated (80 °C/ 90 min) β -Lg solutions (10 g L⁻¹) (*n.d.* not determined).

pH (-)	NaCl (mM)	$d_{50.3}$ (nm)	DD (%)
5.8	0	80 ± 3	88 ± 1
6.2	0	41 ± 9	82 ± 1
6.8	0	20 ± 1	81 ± 1
7.6	0	<i>n.d.</i>	<i>n.d.</i>
8.5	0	3 ± 1	69 ± 4
5.8	20	495 ± 72	96 ± 1
6.8	20	23 ± 1	96 ± 1
8.5	20	6 ± 1	83 ± 1
5.8	60	> 1000 ^c	<i>n.d.</i>
6.2	60	189 ± 19	> 96
6.8	60	28 ± 4	> 96
7.6	60	28 ± 1	> 96
8.5	60	25 ± 1	96 ± 1

Thereby, all samples had monodisperse size distributions except for two pH-NaCl-combinations (i.e., pH 5.8/ 60 mM NaCl and pH 6.2/ 60 mM NaCl), which showed a polydisperse distribution (data not shown). Generally, particle size increased with decreasing pH. This can be attributed to the reduced range of electrostatic interactions between protein molecules upon approaching the isoelectric point (IEP) of the native β -Lg ($d_{50.3}$ 4 nm), which is around 5.1 (Dombrowski et al., 2016; Engelhardt et al., 2013). In consequence, hydrophobic interactions become more dominant leading to an increased aggregation tendency. In addition, the presence of ions leads to less pronounced repulsive forces and in consequence to an increased aggregation probability of β -Lg. Thereby, the effective range of electrostatic forces decreases with increasing concentration of ions (Fig. 4.1). Therefore, increasing the concentration of NaCl at constant pH caused a slight increase in particle size.

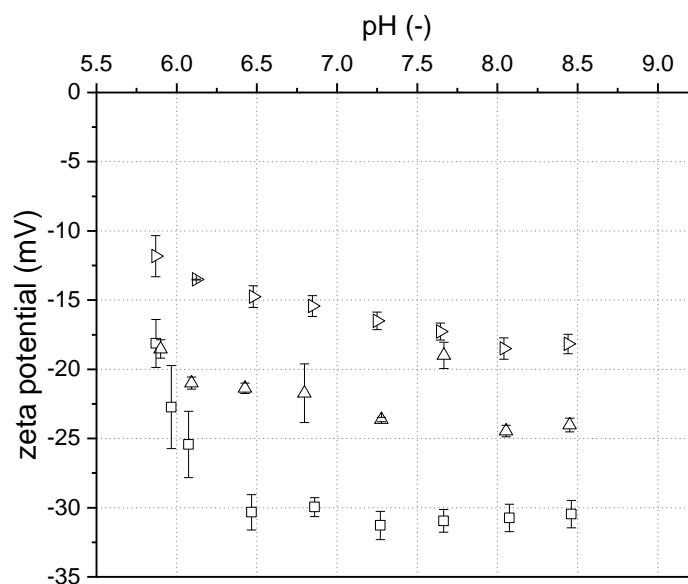


Fig. 4.1: Zeta potential of native β -Lg solutions ($c = 10 \text{ g L}^{-1}$) as a function of the pH at varying NaCl concentrations (\square 0, \triangle 20, and \triangleright 60 mM) before heat treatment. Error bars indicate standard deviation.

Besides the particle size, the reaction rate constant k for particle formation depends on the pH value. As a result, the concentration of remaining native protein after heat treatment varies (Leeb et al., 2018; Tolkach & Kulozik, 2005). Heat treatment of the different β -Lg solutions therefore did not always result in a full denaturation as can be seen from the values of the degree of denaturation (DD), which varied from 69 to > 96% (Tab. 4-1). Thus, in order to exclude the influence of remaining native protein as well as NaCl on interfacial and foaming/ emulsifying properties, the remaining native molecules in the heat-treated samples were removed by purification steps until the degree of denaturation DD and the electric conductivity κ reached $\geq 96\%$ and $< 1 \text{ mS cm}^{-1}$, respectively. Thereby, particles of different size clusters could be produced (Tab. 4-2), which allowed for the investigation of particle size-related techno-functional properties (i.e., foaming and emulsification). It is important to note that resuspending the pellets of samples heat-treated at pH 6.2, 6.8, and 7.6 in presence of 60 mM NaCl did not result in the formation of separated particles after purification. This may be due to incomplete resolubilization based on reinforced attractive interactions. Thus, the purification method using centrifugation and resuspension was not suitable to process these particles. These samples were therefore excluded from further investigations. The size of the other particles was not changed markedly by purification with exception of the ones produced at pH 5.8. The size distributions of the purified particles are shown in the Appendix A (Fig. 4.8). As summarized in Tab. 4-2, the purified particles were also analyzed for their zeta potential as well as their disulfide cross-linking degree. An increase in the degree of cross-linking corresponded to an increase in disulfide cross-links (i.e., a decrease in the particle structural flexibility). It can be deduced that particles of a similar size range ($\sim 22 \text{ nm}$) (pH 6.8/ 0 mM NaCl, pH 6.8/ 20 mM NaCl, and pH 8.5/ 60 mM NaCl) and zeta potential ($\sim -30 \text{ mV}$) but different degrees of disulfide cross-linking were produced.

Tab. 4-2: Characteristics (median particle size ($d_{50.3}$), poly dispersity index (PDI), degree of cross-linking (DC), and zeta potential (ZP)) and interfacial properties (surface (π_{σ}) and interfacial pressure (π_{γ}) after 5 and 3550 s) of purified ($DD \geq 96\%$ and $\kappa < 1 \text{ mS cm}^{-1}$) β -Lg particles formed by heat treatment (80 °C/ 90 min) under variation of pH and NaCl.

formation		icon	purified particle characteristics					interfacial properties			
pH	NaCl		pH	$d_{50.3}$	PDI	DC	ZP	$\pi_{\sigma 5s}$	$\pi_{\sigma 3550s}$	$\pi_{\gamma 5s}$	$\pi_{\gamma 3550s}$
(-)	(mV)		(-)	(nm)	(-)	(%)	(mV)	(mN m ⁻¹)	(mN m ⁻¹)	(mN m ⁻¹)	(mN m ⁻¹)
5.8	0	●	6.8	120 ± 14	0.19 ± 0.02	104 ± 0.1	-38 ± 1.1	10.4 ± 0.3	22.8 ± 0.2	5.2 ± 0.1	10.4 ± 0.4
5.8	0	○	6.2	119 ± 10	0.19 ± 0.01	104 ± 0.1	-30 ± 0.7	15.8 ± 1.3	24.3 ± 0.5	8.4 ± 0.4	12.2 ± 0.5
6.2	0	◀	6.8	44 ± 9	0.19 ± 0.02	106 ± 4.3	-35 ± 1.7	13.7 ± 0.9	21.6 ± 0.3	7.2 ± 0.1	10.6 ± 0.1
6.2	0	◁	6.3	40 ± 7	0.19 ± 0.02	106 ± 4.3	-29 ± 0.4	15.4 ± 0.1	23.0 ± 0.4	8.8 ± 0.8	11.8 ± 0.5
6.8	0	◆	6.8	20 ± 1	0.26 ± 0.00	109 ± 1.0	-31 ± 0.2	15.0 ± 0.1	21.6 ± 0.1	8.3 ± 0.1	11.1 ± 0.1
8.5	0	■	6.8	3 ± 1	0.64 ± 0.11	120 ± 6.5	-30 ± 0.5	16.2 ± 0.2	21.4 ± 0.2	9.3 ± 0.3	11.5 ± 0.3
6.8	20	▼	6.8	22 ± 1	0.47 ± 0.02	85 ± 1.1	-29 ± 1.3	14.1 ± 0.6	22.9 ± 0.9	7.3 ± 0.2	10.9 ± 0.1
8.5	60	▲	6.8	22 ± 2	0.41 ± 0.04	92 ± 3.2	-29 ± 2.2	15.9 ± 1.0	23.1 ± 0.6	9.3 ± 0.1	11.7 ± 0.1

In addition, the pH value of the particles with a given median diameter of 44 and 120 nm was changed to modify the zeta potential. Due to this, the investigation of the influence of different particle sizes (3, ~ 22, ~ 42, ~ 120 nm) independent of the zeta potential (~ -30 mV) was possible. Therefore, the zeta potential of these particles was adjusted to ~ -30 mV corresponding to pH 6.2 and 6.3, respectively (Fig. 4.9). Thereby, no significant effect of pH adjustment on the particle size distributions was observed (Tab. 4-2). Furthermore, it can be assumed that the degree of cross-linking does not change due to the change in pH value after heat treatment, since, e.g., a certain temperature increase is necessary to induce the reactivity of the free thiol group (Hoffmann & van Mil, 1999).

In addition, the dynamic viscosity of the samples ranged between 1.10 (heating pH 5.8) and 1.39 mPas (heating pH 8.5), whereby the differences were not significant. This allows for the exclusion of viscosity effects with regard to both interfacial adsorption and foam destabilization (e.g., foam drainage).

To sum up, the applied method allowed for the production of purified β -Lg particles with variable physicochemical properties (i.e., size, zeta potential, and degree of disulfide cross-linking) as summarized in Tab. 4-2. Therewith, the specific relevance of these properties for the particles' interfacial properties, considering both the air/water and the oil/water interface, could be assessed.

4.3.2 β -Lg Particles at the Air/Water Interface: Interfacial Properties and Foam Structure Dynamics

4.3.2.1 Interfacial Properties

In order to investigate the interfacial behavior of specific particle physicochemical properties (i.e., particle size, zeta potential, and degree of cross-linking (Tab. 4-2), the evolution of surface tension in dependence of the particles' physiochemical characteristics during a period of 3600 s was determined. In general, all particles reduced the surface tension from 72 to around 50 mN m^{-1} as can be seen in Fig. 4.2 a-c. The respective insets in the Fig. 4.2 a-c highlight the initial decrease in the surface tension.

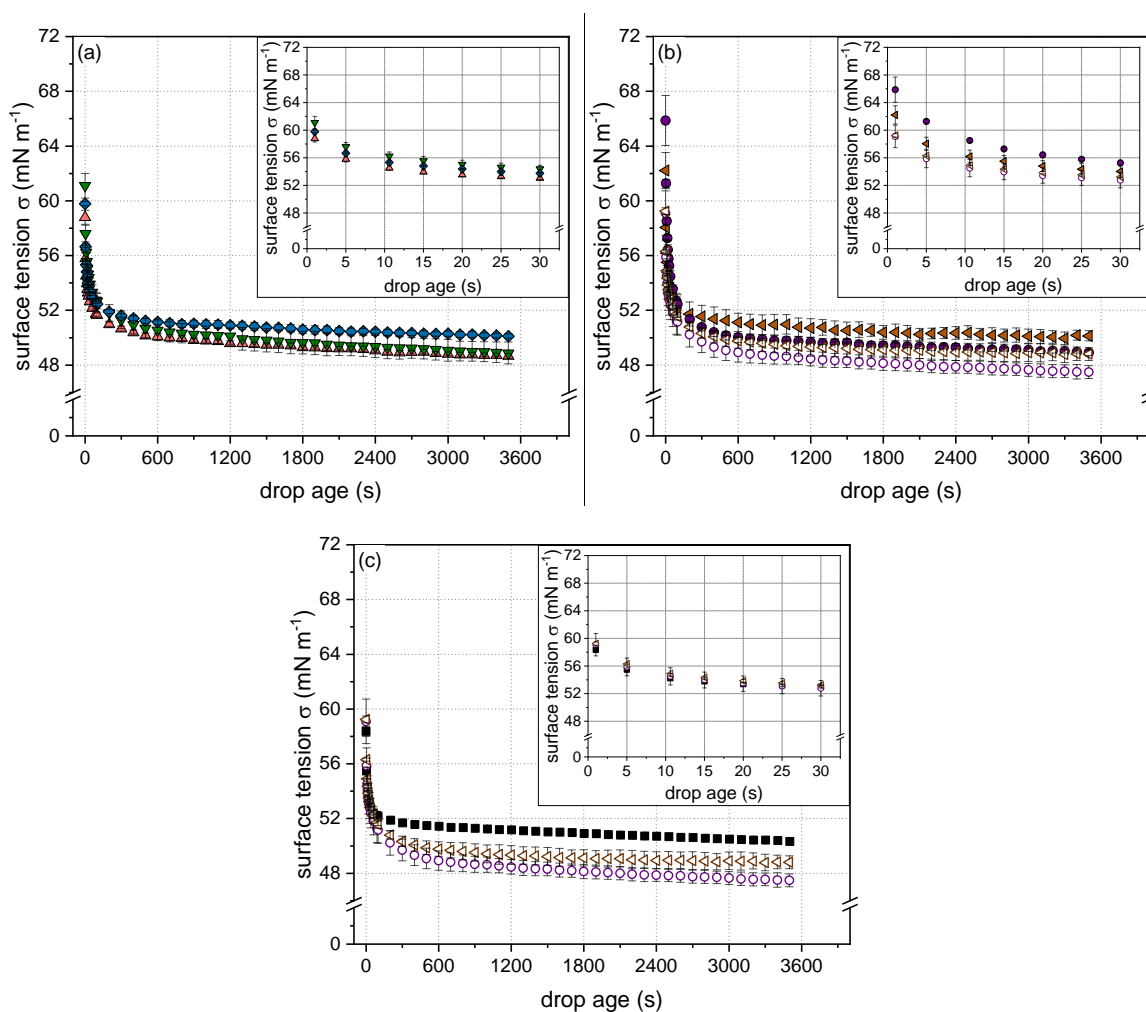


Fig. 4.2: Evolution of surface tension (σ) in dependence of time as a function of the β -Lg particle ($c = 8.2 \text{ g L}^{-1}$) physicochemical properties: (a) varying degree of cross-linking (\blacktriangledown 85, \blacktriangle 92, and \blacklozenge 109%) but similar size ($\sim 22 \text{ nm}$) and similar zeta potential ($\sim -30 \text{ mV}$); (b) varying net zeta potential (\bullet -38 and \circ -30 mV or \blacktriangleleft -35 and \triangleleft -29 mV , respectively) but similar size ($\bullet/\circ \sim 120$ and $\blacktriangleleft/\triangleleft \sim 42 \text{ nm}$, respectively) and similar degree of cross-linking ($\sim 105\%$); (c) varying particle size (\blacksquare 3, \triangleleft 40, and \circ 119 nm) and degree of cross-linking (\blacksquare 120 and $\triangleleft/\circ \sim 105\%$) but a similar zeta potential of $\sim -30 \text{ mV}$. Error bars indicate standard deviation.

(a) Surface tension as a function of degree of cross-linking

Fig. 4.2 a shows the evolution of the surface tension for particles of similar size (~ 22 nm) and zeta potential (~ -30 mV) but different degree of disulfide cross-linking (85, 92, and 109%). According to literature, the cross-linking degree, i.e., the molecular flexibility is important in terms of rearrangement at the interface. Thus, it plays a role at longer time scales rather than in the initial phase of adsorption. Similar conclusions were drawn by Dhayal et al. (2015) using enzymatic cross-linked α -lactalbumin particles. Hence, as expected, no specific effect of the degree of cross-linking during the initial phase ($t < 5$ s) of adsorption was observed. For longer time scales, it appeared that dependent on the cross-linking degree, the surface tension reduction varied among the samples. Thereby, the decrease of surface tension was found to be more pronounced for particles with a lower ($< 100\%$) cross-linking degree. Due to the greater reduction of surface tension of the less cross-linked particles subsequent to the initial phase, the curve corresponding to the particles of the lowest cross-linking degree and the curve corresponding to the particles of the highest cross-linking degree crossed each other (in the time range of $20 \leq t < 2000$ s). The effect became most evident for $t > 2000$ s, however, it was not significant ($p > 0.05$; one way ANOVA analysis with Tukey post-hoc test performed by Origin Lab 2018). Nonetheless, the results shown in Fig. 4.2 a indicate a more pronounced rearrangement of less-cross-linked particles at the air/water interface.

(b) Surface tension as a function of zeta potential and particle size

Fig. 4.2 b shows the surface tension as a function of time for particles of two size classes (~ 42 and ~ 120 nm) with different zeta potentials respectively (~ 42 nm: -35 and -30 mV; ~ 120 nm: -38 and -30 mV) (Tab. 4-2). The degree of cross-linking of the particles was similar ($\sim 105\%$). Comparing the particles of similar size but different zeta potential (filled and non-filled symbols), a stronger initial decrease in surface tension (i.e., in the range of $t < 5$ s) can be detected with decreasing zeta potential. As it has been shown for proteins in general, an energetic barrier must be overcome to allow for adsorption at the air/water interface (Dombrowski et al., 2017; Wierenga et al., 2005). This adsorption barrier can be reduced by decreasing the zeta potential of a particle, resulting in a higher adsorption speed (Dombrowski et al., 2017; Engelhardt et al., 2013; Ulaganathan, Retzlaff, Won, Gochev, Gehin-Delval et al., 2017).

Comparing the particles of different size (~ 42 and ~ 120 nm) but similar zeta potential (-30 mV) (non-filled symbols), no significant difference in their potential to reduce surface tension could be detected ($t < 3000$ s). A decrease in particle size is in general associated with a stronger decrease of the initial surface tension (Dhayal et al., 2015; Rullier et al., 2008; Schmitt et al., 2007). However, according to the obtained results, the particle size was clearly less important than the zeta potential in terms of adsorption at the interface. However, particle size could become more evident as an influential factor at greater differences in size and lower particle concentrations.

Interestingly, towards longer time scales ($t > 100$ s), the rate of surface tension reduction was higher for the larger particles (~ 120 nm) than for the smaller ones (~ 42 nm) despite the similarities in zeta potential (~ -30 mV) and cross-linking degree ($\sim 105\%$). The same trend could be detected at higher net zeta potentials. It has to be noted that although particles exhibited a similar degree of cross-linking (Tab. 4-2), they might have differed in their disulfide bond distribution. Due to the influence of the pH value and the heating conditions (temperature and time) on the reactivity of the free thiol group and thus, the formation of disulfide cross-links (Leeb et al., 2018), inhomogeneous distributions of disulfide bonds within the particle can occur. This aspect in turn can affect the rearrangement of the particles after adsorption at the interface (Destribats et al., 2011; Destribats, Eyharts et al., 2014). Thereof, the detected differences in the surface tension reduction at longer time scales are likely to be due to the differences in the distribution of the disulfide cross-links within the particles limiting the interfacial rearrangement based on the distribution of the cross-links.

(c) Surface tension as a function of particle size and degree of cross-linking

In order to unravel the effect of the particle size itself, Fig. 4.2 c shows the time-dependent evolution of the surface tension for particles differing in size (3, 40, and 119 nm) but having a similar zeta potential of ~ -30 mV (Tab. 4-2). In accordance with the results shown before, no significant influence of the particle size on the initial surface tension reduction could be detected despite the greater magnitudes of size. Thus, the decrease in zeta potential appeared to balance out the decelerated diffusion rate related to an increasing particle size in the investigated particle size range.

However, at longer time scales ($t > 100$ s) the smallest particles exhibited higher surface tension values compared to the larger ones. This can be related to the higher degree of cross-linking of the smallest particles (120%) compared to the larger ones ($\sim 105\%$) (Tab. 4-2) and thus, to a less effective rearrangement at the air/water interface as stated above.

4.3.2.2 *Foam Stability*

In order to investigate the influence of specific particle physicochemical properties (i.e., particle size, zeta potential, and degree of cross-linking (Tab. 4-2) decoupled from each other on air bubble stability, the mean bubble area (A) as a function of time (t) was analyzed. The obtained data were used to calculate the coarsening factor (α) according to $A \sim t^\alpha$ as described by Schmitt et al. (2007). The results are displayed in Fig. 4.3 a-c.

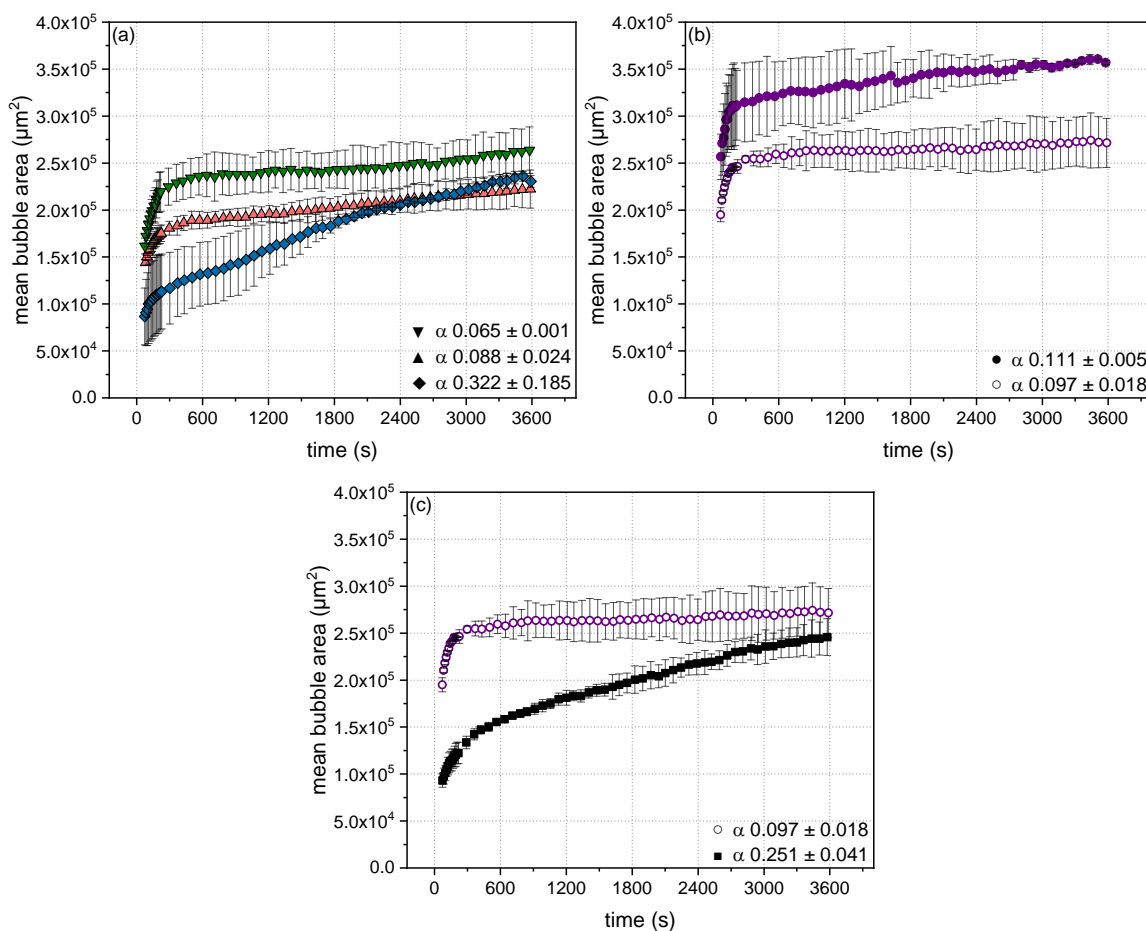


Fig. 4.3: Evolution of the mean bubble area in dependence of time as a function of the β -Lg particle ($c = 8.2 \text{ g L}^{-1}$) physicochemical properties: (a) varying degree of cross-linking (∇ 85, \triangle 92, and \diamond 109%) but similar size ($\sim 22 \text{ nm}$) and similar zeta potential ($\sim -30 \text{ mV}$); (b) varying zeta potential (\bullet -38 and \circ -30 mV) but similar size ($\sim 120 \text{ nm}$) and similar degree of cross-linking (104%); (c) varying size (\blacksquare 3 and \circ 119 nm) and degree of cross-linking (\blacksquare 120 and \circ 104%) but similar zeta potential ($\sim -30 \text{ mV}$) including the coarsening factor α . Error bars indicate standard deviation.

(a) Surface tension as a function of degree of cross-linking

Fig. 4.3 a shows the time-dependent evolution of the mean bubble area for β -Lg particles of similar size ($\sim 22 \text{ nm}$) and similar zeta potential ($\sim -30 \text{ mV}$) but variable degrees of disulfide cross-linking (Tab. 4-2). As can be seen, the mean bubble area rapidly increased within the first 500 s , whereby the foams formed by particles with the highest degree of cross-linking (109%) exhibited the smallest mean bubble area.

However, for measurement times longer than 500 s, the mean bubble area of foams from particles with a high degree of cross-linking (109%) continued to increase more strongly (almost linear) as compared to foams stabilized by particles having a lower degree of cross-linking (< 100%). As a result, bubble coalescence was mitigated by decreasing the particles' cross-linking degree as reflected in the decreasing coarsening factor (α) values. In turn, this means that those foams had higher stability. Potentially, this increase in stability could be due to network formation of the less cross-linked particles within the interfacial film subsequent to the adsorption and rearrangement at the interface resulting in an increase in the elasticity of the formed surface film and, thereby, a higher resistance against destabilization (Kim et al., 2005; Picard et al., 2017). Besides, a lower cross-linking degree is assumed to promote the formation of regular and, thus, high packed interfacial layers at high particle concentrations at the interface or at late adsorption stages, thereby increasing the foam stability (Picard et al., 2017; Pinaud et al., 2014).

(b) Mean bubble area as a function of zeta potential

When comparing the foaming behavior of particles of similar size (~ 120 nm) and disulfide cross-linking (104%) but different zeta potential (-30 and -38 mV), it appeared that a decrease in zeta potential resulted in the formation of smaller air bubbles after foaming (< 100 s) (Fig. 4.3 b). This can be explained by the faster initial surface tension decrease (Fig. 4.2 b) due to the reduction of the electrostatic barrier of adsorption (Wierenga et al., 2005). The evolution of the mean bubble area in dependence of time generally showed a high bubble stability as can be seen by the rather constant mean bubble area up to 3600 s. However, the effect was slightly more pronounced for the particles exhibiting a lower zeta potential.

(c) Mean bubble area as a function of particle size and degree of cross-linking

As can be seen in Fig. 4.3 c, particle size had a clear effect on the initial mean bubble area and its evolution over time. At a similar zeta potential of ~ -30 mV, the smallest particles (3 nm) resulted in the formation of air bubbles of half the area of those from the largest particles (119 nm) directly after foaming. However, beginning at about 250 s after foam formation, the larger particles kept the bubble area rather constant (α : 0.097), whereas the mean bubble area of foams from smaller particles continued to increase (α : 0.251). Thus, the smaller ones were able to occupy the air/water interface faster, but they were not able to lastingly stabilize the bubbles. The enhanced foam stability in the presence of larger particles could be due to a blocking of the foam lamellae by non-adsorbed particles resulting in a decreased drainage and, thus, keeping the bubbles apart from each other (Lazidis et al., 2016; Schmitt et al., 2014). In addition, a lower cross-linking degree of the larger particles (119 nm) compared to the smaller ones (3 nm) allowed for a better rearrangement at the air/water interface and thus, the formation of more cohesive films based on more pronounced particle-particle interaction imparting higher foam stability (Dombrowski et al., 2016).

As can be seen in Fig. 4.4, an increase in the coarsening factor α (i.e. a lower bubble stability) was found to correlate with an increase in the cross-linking degree, whereby a variation of the particle size only showed minor effects. In contrast, the zeta potential had no distinct effect on the foam stability, but was related to the initial rate of particle adsorption at the air/water interface (Fig. 4.2).

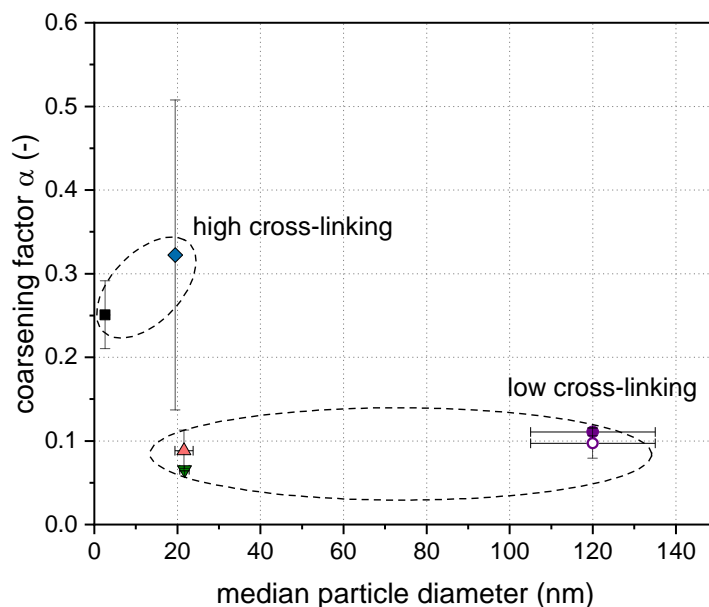


Fig. 4.4: Coarsening factor α in dependence of the median particle size as a function of the cross-linking degree (\blacktriangledown 85, \blacktriangle 92, \bullet / \circ 104, \blacklozenge 109, and \blacksquare 120; $C_{\text{particles}}$: 8.2 g L^{-1}). Error bars indicate standard deviation.

4.3.3 β -Lg Particles at the Oil/Water Interface: Interfacial Properties and Emulsion Stabilization

4.3.3.1 Interfacial Properties

Besides the air/water interface, the particles' behavior at the oil/water interface was investigated. Fig. 4.5 a-c show the evolution of the interfacial tension as a function of the particles' physicochemical properties (i.e., particle size, zeta potential, and degree of cross-linking (Tab. 4-2), whereby the respective insets highlight the initial interfacial tension decrease. As can be seen, all particles reduced the oil/water interfacial tension from 24 to around 12-15 mN m^{-1} .

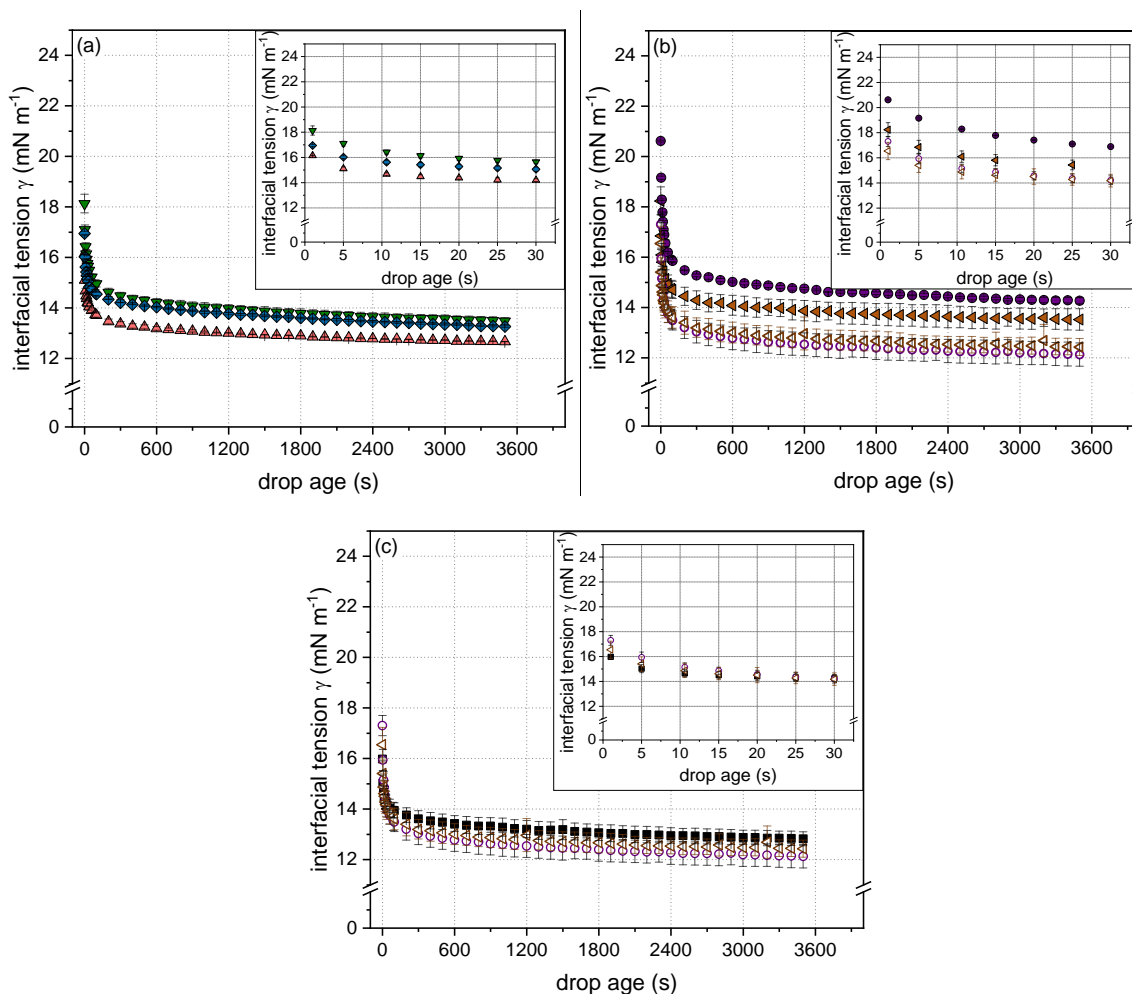


Fig. 4.5: Evolution of interfacial tension (γ) in dependence of time as a function of the β -Lg particle ($c = 8.2 \text{ g L}^{-1}$) physicochemical properties: (a) varying degree of cross-linking (\blacktriangledown 85, \blacktriangle 92, and \blacklozenge 109%) but similar size ($\sim 22 \text{ nm}$) and similar zeta potential ($\sim -30 \text{ mV}$); (b) varying net zeta potential (\bullet -38 and \circ -30 mV or \blacktriangleleft -35 and \triangleleft -29 mV , respectively) but similar size ($\bullet/\circ \sim 120$ and $\blacktriangleleft/\triangleleft \sim 42 \text{ nm}$, respectively) and similar degree of cross-linking ($\sim 105\%$); (c) varying particle size (\blacksquare 3, \triangleleft 40, and \circ 119 nm) and degree of cross-linking (\blacksquare 120 and \triangleleft $\sim 105\%$) but a similar zeta potential of $\sim -30 \text{ mV}$. Error bars indicate standard deviation.

(a) Interfacial tension as a function of degree of cross-linking

At the oil/water interface, no clear influence of the degree of covalent cross-linking (85, 92, and 109%) on the reduction in interfacial tension could be determined for particles of similar size ($\sim 22 \text{ nm}$) and zeta potential ($\sim -30 \text{ mV}$) during a time range of 3600 s Fig. 4.5 a). The curve corresponding to the most cross-linked particles (109%) was initially between those of lower cross-linking degree, whereas for longer adsorption times, the curves approached each other. However, a crossing over of the curves may occur at longer time scales, due to the less intense reduction in interfacial tension of the more cross-linked particles (109%) after the initial phase compared to the least cross-linked ones (85%). This could indicate a limited rearrangement at the

interface due to the increased number of cross-links (Buchcic, Tromp, Meinders, & Cohen Stuart, 2017; Picard et al., 2017).

(b) Interfacial tension as a function of zeta potential and particle size

As can be seen in Fig. 4.5 b, lowering the zeta potential from -38 to -30 mV or from -35 to -30 mV for particles with ~ 120 and ~ 42 nm, respectively, with similar cross-linking degrees of $\sim 105\%$ resulted in a significantly stronger decrease in the interfacial tension during 3600 s. This increased reduction rate can be explained by a reduction in the energy barrier of adsorption by decreasing the particles' zeta potential (Wierenga et al., 2005). Comparing the particles of different sizes but similar zeta potential (-30 mV) (non-filled symbols) no significant difference in their interfacial behavior could be detected during measurement time of 3600 s. However, the influence of particle size in terms of diffusion might become more evident for particles of a larger magnitude of size.

Similar to the results on surface activity (Section 4.3.2.1), the results shown clearly demonstrate the relevance of the zeta potential in terms of the interfacial activity of β -Lg particles.

(c) Surface tension as a function of particle size and degree of cross-linking

In order to separate the influence of particle size from the effect of zeta potential, Fig. 4.5 c shows the interfacial behavior of particles of different sizes (3, 40, and 119 nm) but similar zeta potential of ~ -30 mV. As can be seen, smaller-sized particles showed a faster initial reduction in the interfacial tension than larger ones, whereby the effect was only significant for the particles of 3 and 119 nm. This can be explained by the higher diffusion coefficient of the smaller particles and thus, the faster diffusion to and adsorption at the oil/water interface. Similar results were shown in previous studies (Jung, Gunes, & Mezzenga, 2010; Murphy et al., 2016). However, this difference disappeared for adsorption times > 20 s as can be seen by the less intense reduction in interfacial tension of the smallest particles compared to the larger ones. In this regard, it is important to mention that the smallest particles exhibited a much higher cross-linking degree (120%) compared to the larger ones ($\sim 105\%$). Thus, due to the enhanced ability of the less cross-linked particles to rearrange at the oil/water interface (Buchcic et al., 2017), a more pronounced reduction in interfacial tension was achieved.

To conclude, the zeta potential seems to be most decisive in view of reducing the interfacial tension. Nevertheless, a decrease in particle size at a similar zeta potential resulted in a faster reduction in the initial interfacial tension and thus, a faster adsorption at the interface. In terms of the influence of the cross-linking degree, no significant effect could be detected during the measurement time up to 3600 s.

4.3.3.2 *Emulsion Stability*

Besides measuring interfacial tension, oil-in-water emulsions were prepared to evaluate the significance of specific particle properties, i.e., size, zeta potential, and degree of cross-linking. The concentration used for emulsion preparation was

assumed to completely cover the oil droplet surface as an increase in β -Lg concentration ($\geq 5 \text{ g L}^{-1}$) did not result in a decrease in oil droplet size (results not shown). This also implies that the presence of non-adsorbed protein in the bulk phase can be assumed.

In general, an increase in particle size (3, 22, and 120 nm) with the zeta potential set to $\sim -30 \text{ mV}$ led to an increase in the oil droplet size (Fig. 4.6 a). Similar results were reported by others (e.g., (Murphy et al., 2018; Sobhaninia et al., 2017)). However, differences in oil droplet size stabilized by particles of similar size (~ 22 or $\sim 120 \text{ nm}$) could also be determined. Thus, further particle properties (i.e., zeta potential and structural flexibility) might influence the oil droplet size. Thereby, decreasing the particles' ($\sim 120 \text{ nm}$) zeta potential from -38 to -30 mV resulted in the formation of smaller oil droplets (Fig. 4.6 a). Unlike expected, lower cross-linking degrees of particles of similar size ($\sim 22 \text{ nm}$) and zeta potential ($\sim -30 \text{ mV}$) from 109 to 92% resulted in higher oil droplet sizes, whereby particles of high cross-linking degrees ($\geq 109\%$) and different sizes (3 and $\sim 22 \text{ nm}$) resulted in the formation of oil droplets of similar size.

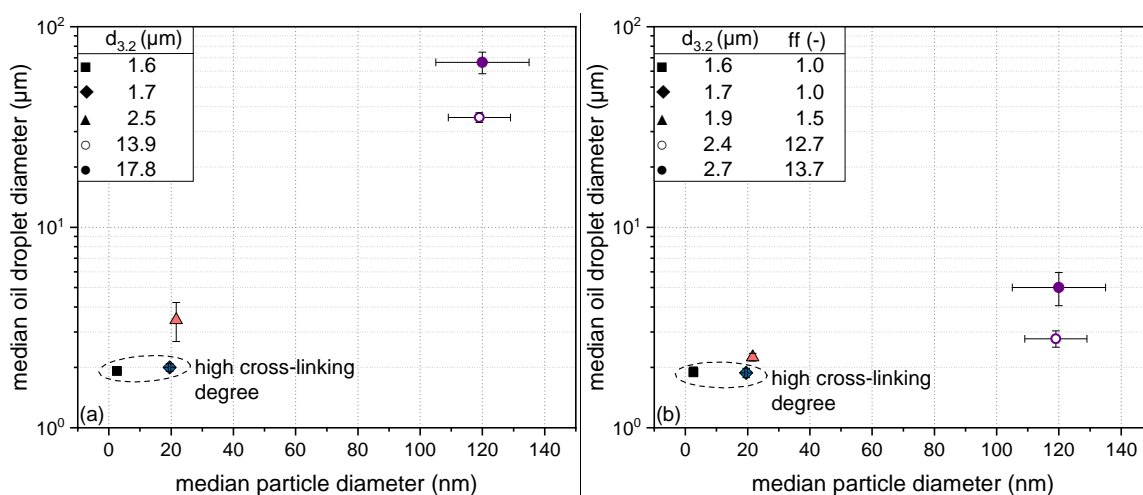


Fig. 4.6: Median oil droplet diameter (and surface weighted mean ($d_{3,2}$)) in dependence of the median particle diameter (a) without the addition of sodium dodecyl sulfate (SDS) and (b) with the addition of SDS and including the flocculation factor (ff) using a particle concentration of 8.2 g L^{-1} (degree of disulfide cross-linking/zeta potential: \blacktriangle 92%/ -29 mV , \circ 104%/ -30 mV , \bullet 104%/ -38 mV , \blacklozenge 109%/ -31 mV , and \blacksquare 120%/ -30 mV). Error bars indicate standard deviation.

As the degree of particle cross-linking affects particle-particle interactions (Murphy et al., 2018), it was assumed that this could also have an impact on oil droplet aggregation. Therefore, the flocculation factor (ff) was calculated according to Eq.(4-5). This allowed us to determine the degree of oil droplet aggregation as well as the actual oil droplet size.

In general, the flocculation factor increases with the tendency of oil droplets to aggregate (Demetriades & McClements, 2000). In this regard, sodium dodecyl sulfate (SDS) was used to disaggregate flocculated oil droplets by increasing the electrostatic

repulsion between oil droplets. As can be seen in Fig. 4.6 (b), the addition of SDS resulted in a significant reduction in the oil droplet size in emulsions stabilized by particles of lower cross-linking degree ($< 104\%$). Furthermore, the effect of SDS was more pronounced for the larger protein particles (~ 120 nm). By contrast, rather rigid particles (cross-linking degree $> 104\%$) were not affected by the addition of SDS independent of their size (i.e., 3 and ~ 22 nm).

An influence of the viscosity of the continuous phase on emulsion stability (i.e., creaming rate) can be excluded as no significant differences in terms of dynamic viscosity of the samples were detected. However, the viscosity may become important by using particles much larger than reported in this study as well as by using higher oil contents (Hebishy, Zamora, Buffa, Blasco-Moreno, & Trujillo, 2017; Sobhaninia et al., 2017).

4.3.4 Comparison of the Properties of β -Lg Particles at the Air/Water and the Oil/Water Interfaces

In order to compare the interfacial properties of the specific particles at the air/water and oil/water interface, the surface pressure ($\pi_\sigma(t)$) and the interfacial pressure ($\pi_\gamma(t)$) were calculated according to Eq. (4-3) and (4-4). The respective results are shown exemplarily in Fig. 4.7 (a), (b) As can be seen, surface pressure was found to increase faster and to higher values compared to interfacial pressure in the present set of experiments. This could be related to a lower adsorption barrier and higher packing density of particles at the air/water interface. However, contrary results were found in the literature (Hinderink et al., 2020; Krägel et al., 2003). In this regard, it is important to mention that the interfacial rearrangement at the oil/water interface is additionally influenced by the type of oil used (Bergfreund et al., 2018).

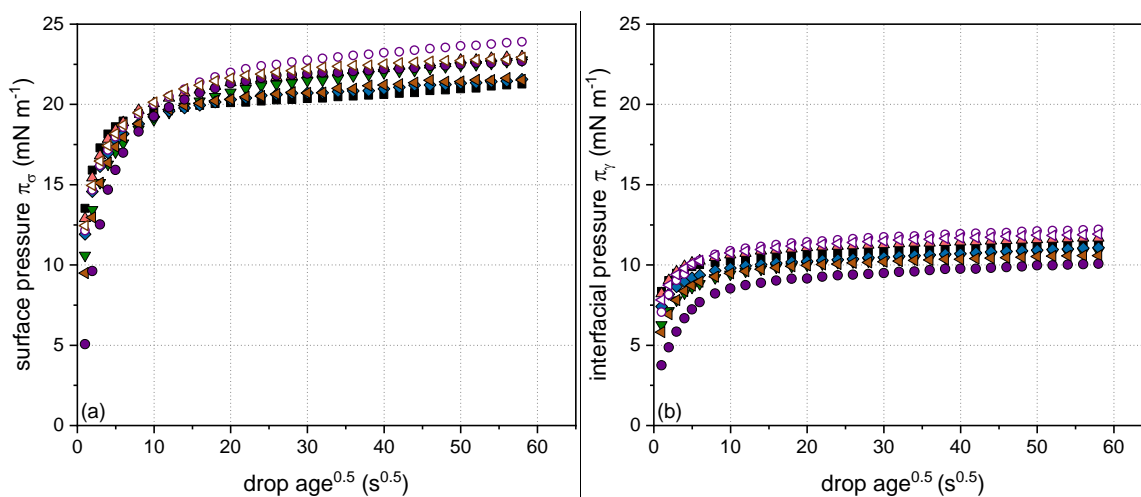


Fig. 4.7: Evolution of (a) surface pressure π_σ at the air/water interface and (b) interfacial pressure π_γ at the oil/water interface as a function of the particle properties using a particle concentration of 8.2 g L^{-1} (median particle size: ■ 3, ◆ 20, ▼ 22, ▲ 22, ◁ 40, ◀ 44, ○ 119, and ● 120 nm). For further interpretation of the symbols, the reader is referred to Tab. 4-2.

In order to highlight the influence of the particle properties in the initial ($t = 5$ s) and final ($t = 3550$ s) measurement time regime, the surface pressure ($\pi_{\sigma}(t)$) and the interfacial pressure ($\pi_{\gamma}(t)$) values after 5 and 3550 s are included in Tab. 4-2 next to the particles' physicochemical properties. Thereby, a decrease in zeta potential from -35 and -38 mV, respectively, to ~ -30 mV for particles of ~ 42 and ~ 120 nm was observed to be decisive in terms of fast adsorption at both types of interface. By contrast, an increase in particle size up to ~ 120 nm at a similar zeta potential of ~ -30 mV was less important for both systems. A decreasing cross-linking degree was found to differently impact the surface and interfacial pressure. Whereas a decrease in the cross-linking degree increased the surface pressure at longer time scales ($t = 3550$ s), no significant effect on the interfacial pressure could be detected over the whole measurement duration of 3600 s. This could be an indication that particle rearrangement at oil/water interfaces requires a longer time than at the air/water interface.

Regarding the particles' physicochemical properties being relevant for foam and emulsion stabilization, an increase in particle size as well as a decrease in cross-linking degree were found to lead to an increased foam bubble stability (Fig. 4.3), whereas emulsion stability decreased (Fig. 4.6). In order to explain this difference, it is important to note that the produced foams and emulsions differed in their characteristics. Emulsification was performed by high pressure homogenization, wherefore oil droplet stabilization was based on convective transport rather than diffusion. This high energy input combined with an oil-to-protein ratio close to 10:1 allowed for achieving relatively small oil droplet sizes ($<5 \mu\text{m}$) (Hebisy et al., 2015; Hebisy et al., 2017). Compared to that, foams were produced by air sparging. Thereby, air bubbles are formed and detached from the porous frit mainly based on the equilibrium of surface tension force and buoyancy force (Bals & Kulozik, 2003). Due to the inherent structure of the porous frit, instantaneous bubble coalescence cannot be avoided. Additionally, with the time of sparging, a foam column is formed, which is very prone to gravitational drainage, also promoting bubble coalescence, which is the main foam destabilization mechanism. Overall, combined with an air-to-protein ratio of 90:1 this leads to the formation of comparatively large air bubbles ($> 100 \mu\text{m}$).

Hence, for the foams, it could be assumed that the high stability observed for large particles with low cross-linking degree, on the one hand, was due to the formation of cohesive surface films based on particle-particle interactions (adsorbed particles) (Dombrowski et al., 2016; Kim et al., 2005). On the other hand, non-adsorbed particles might have contributed to foam stability by means of the blocking of lamellae leading to a reduction in drainage and, therewith, less coalescence (Lazidis et al., 2016).

For emulsions, however, it was supposed that more pronounced inter-particle-interactions occurring at lower cross-linking degrees triggered the formation of oil droplet aggregates. Unlike for foams, aggregation rather than coalescence is the main destabilization mechanism for emulsions. Resulting from the oil droplet aggregation,

oil-enriched and oil-depleted areas were formed (data not shown). In this context, it is to mention that at a high oil volume fraction (i.e., $\geq 74\%$), oil droplet cluster formation would lead to an increased stability (e.g., increase in viscosity), whereas for foams, a high air volume fraction rather provokes an opposite effect (Fuhrmann, Sala, Stieger, & Scholten, 2019; Shi et al., 2020).

4.4 Conclusion

In this study, we aimed to assess the specific role of particle size, zeta potential, and cross-linking degree of purified β -Lg particles decoupled from each other in the stabilization of air/water and oil/water interfaces. This was supposed to allow to (i) determine and evaluate the influence of individual particle properties under the exclusion of overlapping effects and (ii) to compare the behavior of standardized particles at different types of interfaces. With regard to the particles' behavior at both, the air/water and the oil/water interface, zeta potential was found to be decisive during the initial adsorption regime, i.e., a fast increase in the initial surface/ interfacial pressure was linked to reduced zeta potential. Unlike expected, at constant zeta potential, particle size did not distinctly affect the initial adsorption regime. In terms of foam and emulsion stabilization, the degree of cross-linking was found to be key, whereby contradictory effects were observed for the two systems. While an increased flexibility resulted in an increased foam stability, emulsion stability was decreased due to oil droplet aggregation.

Overall, it can be concluded that a specific type of protein particle has a different impact on stabilizing foams compared to emulsions, wherefore explanatory approaches cannot be used interchangeably. Nonetheless, the systematic investigation of the stabilization of air/water and oil/water interfaces offers a particle 'toolbox' which opens new opportunities to precisely design particles for specific applications, e.g., the stabilization of air/water and oil/water interfaces.

Author Contributions

Conceptualization, F.K. and J.D.; methodology, F.K.; validation, F.K., V.R. and C.H.; formal analysis, F.K., V.R. and C.H.; investigation, F.K., V.R. and C.H.; resources, U.K.; data curation, F.K., V.R. and C.H.; writing—original draft preparation, F.K.; writing—review and editing, F.K., J.D., U.K., C.B.-K., V.R. and C.H.; visualization, F.K.; supervision, U.K.; project administration, F.K. and U.K.; funding acquisition, U.K.; software, F.K. All authors have read and agreed to the published version of the manuscript.

Funding

This IGF Project of the FEI (AiF 18621 N) was supported via AiF within the program for promoting the Industrial Collective Research (IGF) of the German Ministry of

Economic Affairs and Energy (BMWi), based on a resolution of the German Parliament.

Institutional Review Board Statement

This study does not involve humans or animals.

Informed Consent Statement

This study does not involve humans or animals.

Data Availability Statement

No data supporting material is available.

Acknowledgements

We gratefully thank Hermine Roßgoderer and Christina Kiener for their assistance during the experiments. Martin Hartinger and Joseph Dumpler are thanked for helpful discussions.

Conflicts of Interest:

The authors declare no conflict of interest.

4.5 Appendix A

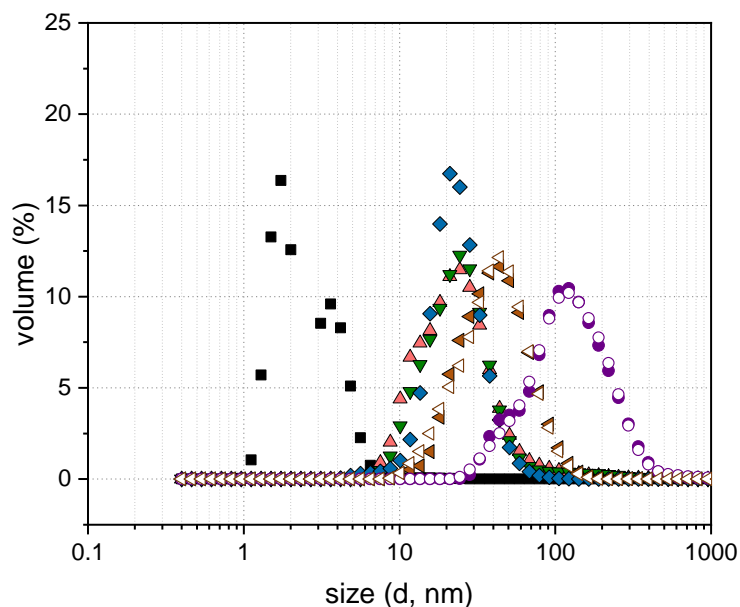


Fig. 4.8: Particle size distribution curves of β -Lg particles ($c = 8.2 \text{ g L}^{-1}$, pH 6.8) after purification (heating conditions (pH/ NaCl): ■ pH 8.5/ 0 mM, ◆ pH 6.8/ 0 mM, ▲ pH 6.2/ 0 mM, ● pH 5.8/ 0 mM, ▼ pH 6.8/ 20 mM, and ▲ pH 8.5/ 60 mM). Non-filled symbols indicate an additional variation in the pH value (i.e., pH \neq 6.8) after purification (◁ pH 6.2/ 0 mM (pH 6.3) and ○ 5.8/ 0 mM (pH 6.2).

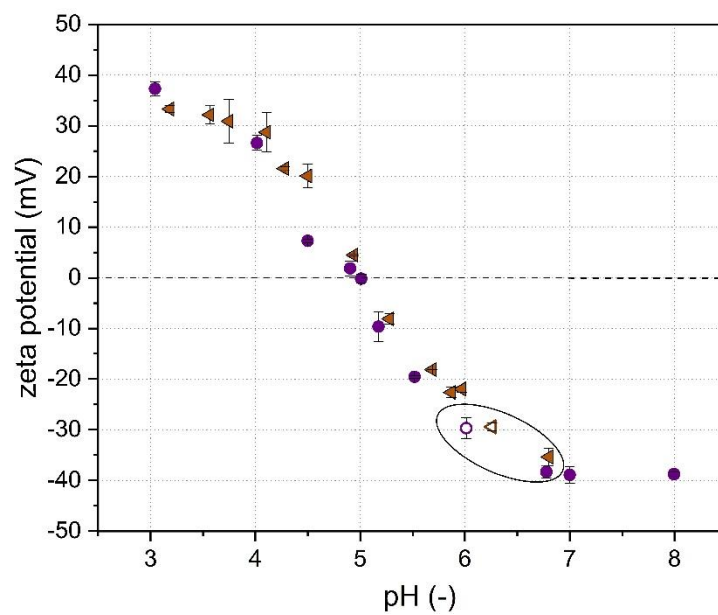


Fig. 4.9: Zeta potential of purified β -Lg particles ($c = 8.2 \text{ g L}^{-1}$) obtained at different heating pH values (\bullet pH 5.8, \blacktriangle pH 6.2) as a function of the pH. Error bars indicate standard deviation.

5 Technofunctionality of β -Lg and β -Lg Nanosized Particles at Air/Water and Oil/Water Interfaces as a Function of Structural and Surface Characteristics³

Summary and Contribution of the Doctoral Candidate Franziska Maria Hartinger (Name at Birth: Kurz)

The stability of foams and emulsions stabilized by native and particulated protein depends on various factors including the proteins structural properties such as size, surface hydrophobicity, and charge. However, no clear correlations regarding their respective impact can be drawn. Besides, different types of interfaces, i.e., air/water or oil/water, were shown to require different protein characteristics to achieve a high stability. Thus, transferability of results of the different systems is rather difficult.

Nevertheless, a lower surface hydrophobicity resulted in a decreased adsorption rate at both interfaces and in a lower stability. With foams, an increasing particle size was shown to enhance foam stability, while the non-particulated protein had the lowest stabilization potential. Apart from that, the effect of impurities being present in oil was assessed. It was observed that the oil type was less important with regard to the emulsion stability, despite significant differences in the interfacial activity.

The doctoral candidate planned and validated the experiments and developed the experimental concept. Data acquisition, analysis, interpretation, curation, and plotting were carried by the doctoral candidate. The doctoral candidate mainly wrote and revised the manuscript. The co-authors contributed to the execution of experiments, the discussion of results, and the revision of the manuscript.

³ Original publication: Kurz, Franziska; Dombrowski, Jannika; Matyssek, Andreas; Hartinger, Martin; Kulozik Ulrich (2021) Technofunctionality of β -Lg and β -Lg Nanosized Particles at Air/Water and Oil/Water Interfaces as a Function of Structural and Surface Characteristics. ACS Food Science & Technology. doi: 10.1021/acsfoodscitech.1c00337. Adapted original manuscript. Adaptions of the manuscript refer to enumeration type, citation style, spelling, notation of units, format, and merging all lists of references into one at the end of the dissertation. Permission for the reuse of the article is granted by ACS.

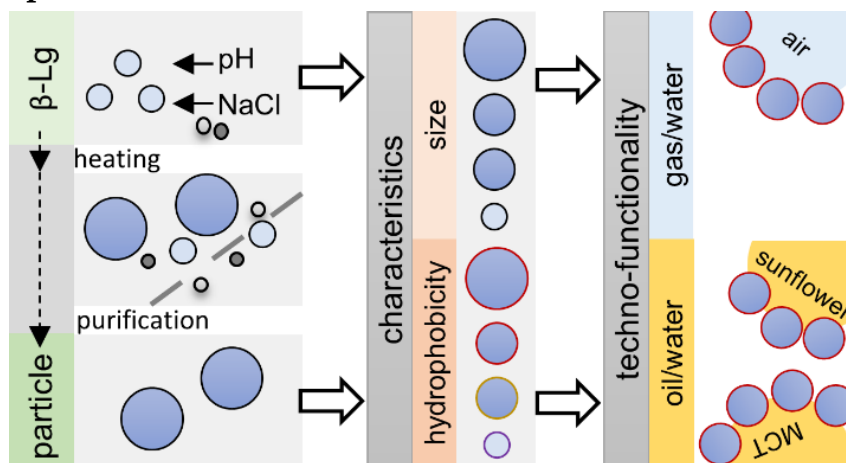
Adapted Original Manuscript³

Technofunctionality of β -Lg and β -Lg Nanosized Particles at Air/Water and Oil/Water Interfaces as a Function of Structural and Surface Characteristics

Franziska Kurz,* Jannika Dombrowski, Andreas Matyssek, Martin Hartinger, and Ulrich Kulozik

* Corresponding Author

Graphical Abstract



Abstract

Different perspectives exist on how particle properties and continuous and dispersed phase characteristics affect the formation and stabilization of foams and emulsions. Therefore, β -Lg particles of varying size or surface hydrophobicity were produced and analyzed for their interfacial behavior, foaming, and emulsifying properties using different types of oil (medium-chain triglycerides (MCTs) and sunflower (SF) oil). At a fixed particle size, an increased surface hydrophobicity resulted in a decreased initial activity at both air/water and oil/water interfaces as well as in lower foam and emulsion stabilities. This indicates that the distribution of the hydrophobic patches is more decisive than the absolute surface hydrophobicity. At a fixed surface hydrophobicity, the initial foam bubble size increased with increasing particle size, while, unexpectedly, foam stability also increased. In the case of emulsions, the oil type did not affect emulsion stability despite a higher interfacial activity at the MCT/water compared to that at the SF/water interface.

Keywords: β -lactoglobulin, surface hydrophobicity, interfacial properties, foaming properties, emulsification properties, oil type

5.1 Introduction

Stabilization of air/water (a/w) and oil/water (o/w) interfaces requires surface-active components such as proteins. Thereby, the foam and emulsion stability depends on various factors. These include not only the individual protein's characteristics such as size, structural flexibility, zeta potential, and surface hydrophobicity but also their interplay (Dombrowski et al., 2016; Dombrowski et al., 2017; Kurz, Reitberger et al., 2021; Moro et al., 2013). Regarding the whey proteins, their specific properties can be altered by thermal treatment or pH variation, for example, resulting in an increased surface activity and higher foam stability (Dombrowski et al., 2016; Dombrowski et al., 2017; Nicolai & Durand, 2013). Thereby, the low diffusion rate resulting from an increased particle size was shown to be compensated by an increased surface hydrophobicity or lower zeta potential (Dombrowski et al., 2016; Dombrowski et al., 2017; Kurz, Reitberger et al., 2021). Overall, however, the specific role of certain protein characteristics such as surface hydrophobicity is still discussed controversially in the literature. While some authors (Li et al., 2018; Moro et al., 2011; Moro et al., 2013; Wierenga et al., 2003) reported an increase in surface activity and improved foaming and emulsifying properties with increasing surface hydrophobicity, contradictory results were reported by other works (Chen et al., 2017; Sorgentini & Wagner, 2002). This discrepancy originates from the fact that several particle properties such as size and surface hydrophobicity are often changed at the same time so that it is difficult to draw conclusions about their individual specific impact on foam and emulsion characteristics.

Besides, different types of interfaces (i.e., a/w or o/w) require different protein properties to ensure high foam and emulsion stability, respectively. Kurz, Reitberger et al. (2021) reported that β -Lg particles of large size (120 nm) and high structural flexibility (i.e., a low content of intraparticle disulfide cross-links) were able to effectively stabilize foams, whereas emulsion stability was impaired. It is so far not clear whether, or how, surface hydrophobicity affects the interfacial behavior at different types of interfaces.

In the case of o/w interfaces, the oil type also has an impact on the evolution of the interfacial tension due to different impurities of minor components and thus influences the emulsification process (Bergfreund et al., 2018; Dopierala et al., 2011; Gmach, Bertsch, Bilke-Krause, & Kulozik, 2019; Gomes, Costa, & Cunha, 2018). Due to their different sources and production processes, oils often differ in their composition and purity. As a consequence, surface-active components (e.g., monoglycerides, vitamins) can be contained in the oil, which, in turn, could affect the interfacial properties and emulsion stability (Al-Malah, 2000; Andrade & Corredig, 2016; Cong, Zhang, Liu, & Huang, 2020; Gmach et al., 2019; Gomes et al., 2018; Gu, Campbell, & Euston, 2009). While Al-Malah (2000) found no correlation between the oil type and the stability of bovine serum albumin-stabilized emulsions (homogenization at 18 600 rpm for 1.5 min), Gmach et al. (2019) reported differences for an egg yolk (granule)-based emulsion (colloid mill at 6000 rpm). To the best of our knowledge, little is known

about the impact of different types of oils on the emulsifying properties of β -Lg particle-stabilized emulsions produced by high-pressure homogenization.

Overall, the state of knowledge described above shows that the interplay of the different factors has an impact on the interfacial behavior of proteins and thus on foam and emulsion stability. However, the respective impact of protein structural characteristics at different types of interfaces on the functionality of protein (β -Lg) particles is still not fully elucidated. Therefore, to approach this knowledge gap, the objective of this study was to evaluate the impact of (i) protein characteristics, which includes the generation of particles of (1) different sizes but similar exposed surface hydrophobicity, zeta potential, and degree of cross-linking and (2) particles of differently exposed surface hydrophobicity but equal size, zeta potential, and degree of cross-linking, and (ii) type of interface (a/w and o/w) on the surface activity and formation and stabilization of foams and emulsions. The production of these defined particles can be achieved by targeting the unfolding and aggregation reaction of the native protein toward specific properties by varying the processing and/or environmental conditions. As shown by Schmitt et al. (2007) a stepwise decrease of the heating pH in increments of 0.2 from 7 to 6 (0 mM NaCl) resulted in an increasing particle size while surface hydrophobicity was the highest at pH 6.4. An increase in the NaCl concentration additionally increased the particle size while surface hydrophobicity decreased. Concluding from many studies (Andlinger, Röscheisen, Hengst, & Kulozik, 2021; Dombrowski et al., 2016; Dombrowski et al., 2017; Donato et al., 2009; Schmitt et al., 2007), a specific combination of pH and salt concentration during thermal-induced particulation allows the particle properties to be controlled in terms of size, reactivity of the free thiol group, and surface hydrophobicity. A change in the pH following particulation allows the zeta potential to be changed subsequently (Dombrowski et al., 2017). In addition, (iii) the effect of the type of oil was examined on interfacial and emulsion characteristics. The following approach was chosen: β -lactoglobulin (β -Lg) particles were generated by thermal treatment (80 ° C/90 min) of native β -Lg solutions (0 or 60 mM NaCl) under variation of pH (5.8, 6.8, or 8.5). To exclude the impact of remaining native β -Lg and NaCl on the surface activity, membrane filtration in diafiltration mode was performed to avoid problems related to isoelectric precipitation, as shown in our previous study (Kurz, Reitberger et al., 2021). pH adjustment to a fixed value after purification allowed us to exclude the effect of the zeta potential and thus the specific investigation of particle size and surface hydrophobicity on the stabilization of air/water and oil/water interfaces using sunflower (SF) oil and medium-chain triglycerides (MCTs) in comparison to unaggregated β -Lg.

5.2 Materials and Methods

5.2.1 *Materials*

Purification of bovine β -Lg from whey protein isolate (WPI 895, Fonterra Cooperative Group, Auckland, New Zealand) was done by selective thermal aggregation with subsequent micro/ultra filtration and spray drying according to Toro-Sierra et al. (2013). On a dry matter basis, the obtained powder had a total protein content of > 99% (Vario MAX cube, Elementar Analysensysteme GmbH, Langenselbold, Germany; RP-HPLC), whereby >99% thereof was β -Lg. Native β -Lg represented > 86% of the total protein as determined by reversed-phase high-performance liquid chromatography (RP-HPLC, Agilent 1100 Series Chromatograph, Agilent Technologies Inc., Santa Clara, CA, USA) (Toro-Sierra et al., 2013). Lactose (HPLC) and salt (Na, K, Ca) (ELEX 6361, Eppendorf AG, Hamburg, Germany) concentrations were < 0.05 and 0.7%, respectively.

5.2.2 *β -Lg Particle Preparation*

β -Lg powder was dissolved in deionized water (Millipore Corporation, Bedford, MA, USA) or in 60 mM NaCl (Merck KGaA, Darmstadt, Germany) solutions to a total protein content of 8.5 g L⁻¹. The solutions were stirred for at least 12 h at 4 ° C to ensure complete hydration. The protein content was determined by RP-HPLC according to Dimpler et al. (2017). In brief, 200 μ L of the protein solution was dissolved in 800 μ L of guanidine buffer and left for 30 min to ensure complete solubilization of the protein, i.e., denaturation and cleavage of disulfide bonds. Subsequently, the protein content was quantified by reversed-phase high-performance liquid chromatography (RP-HPLC, Agilent 1100 Series Chromatograph, Agilent Technologies Inc., Santa Clara, CA, USA). The injection volume was set according to the protein content of the sample to a value between 10 and 80 μ L.

Prior to further processing, the solutions were tempered to 20 ° C and pH was adjusted to either 5.8, 6.8, or 8.5 with 1 M HCl or 1 M NaOH (Merck KGaA, Darmstadt, Germany). This was done to produce β -Lg particles of different size and exposed surface hydrophobicity during subsequent heating (Dombrowski et al., 2016; Kurz, Reitberger et al., 2021). For the particulation, 4.5 L of the respective β -Lg solution was heated in batch mode at 80 ° C for 90 min using a double-jacketed stainless steel vessel (V = 8 L) in combination with a thermostatically controlled water bath (Thermo Scientific ARCTIC A25, Fisher Scientific GmbH, Germany). The vessel was closed with a lid to minimize water loss by evaporation. A target temperature of 80 ° C was reached after 15 min; the holding time before starting the cooling step was 90 min. The temperature was monitored by a thermometer (Testo 108, Testo SE & Co. KGaA, Germany). The heat-induced denaturation was stopped by cooling the solution to 20 ° C within 15 min. During the heating/cooling process, the solution was continuously stirred (125 rpm) to ensure ideal mixing and to avoid spatial temperature profiles.

To assess the denaturation process, the content of native proteins before and after heating (as well as after purification) was determined according to Toro-Sierra et al. (2013). For this, the denatured (particulated) proteins were precipitated at pH 4.6. Afterward, the native (filtrate) and the denatured proteins were separated by using a syringe filter (pore size 0.45 μ m, Chromafil Xtra RC-45/25, Macherey-Nagel GmbH & Co. KG, Düren, Germany). The content of native proteins was determined by RP-HPLC, as described above. On this basis, the degree of denaturation (DD) was calculated according to Eq. (5-1).

$$DD = \left(1 - \frac{C_t}{C_0}\right) \times 100\% \quad (5-1)$$

C_t is the native β -Lg concentration in a pH 4.6 precipitated heated sample, whereas C_0 is the native β -Lg concentration in the unheated solution.

Thereby, full denaturation (DD > 96%) was achieved for the particles (median volume-based particle size ($d_{50.3}$) of \sim 25 nm) heated at pH 6.8 and 8.5 in the presence of 60 mM NaCl, while a certain amount of native protein (\sim 10%) was retained after heat-induced particulation at pH 5.8 (deionized water) ($d_{50.3} \sim$ 70 nm). To obtain particle dispersions with a maximum DD (> 96%) and a constant NaCl concentration of 10 mM, a purification based on membrane filtration in diafiltration mode was performed.

5.2.3 Purification of the β -Lg Particles by Membrane Filtration in Diafiltration Mode

Purification, i.e., reduction of the content of the remaining native protein (heating conditions: pH 5.8, deionized water) or NaCl (heating conditions: pH 6.8 or 8.5, 60 mM NaCl), of the heat-induced β -Lg particles of different sizes was done by membrane filtration in diafiltration (DF) mode. In brief, the remaining native proteins or NaCl (60 mM) are convectively transported by the solvent through the membrane (nominal cutoff: 300 and 10 kDa, respectively; Pall, Port Washington, WI, USA), whereas the particulated β -Lg is retained and accumulates in the retentate. As soon as 500 mL of permeate was produced from the 4.0 L of feed solution, the same amount of DF medium (500 mL of 10 mM NaCl) was added to the feed tank to replace the permeate and wash out the remaining native proteins or NaCl. In total, this step was repeated 16 times until the content of the remaining native protein in the retentate was <4% or a NaCl content of 10 mM was reached. Thereby, the electrical conductivity (κ) (Seven Multi, Mettler-Toledo GmbH, Gießen, Germany) and the concentration of Na^+ (ELEX 6361, Eppendorf AG, Hamburg, Germany) in the retentate and permeate served as a control for the NaCl reduction. HPLC analysis was used to monitor the reduction of native β -Lg. Afterward, 500 mL of permeate was produced to concentrate the particle dispersion.

After the purification by membrane filtration, the pH of the particle dispersions was adjusted to obtain a zeta potential of -28 mV. This value was reached at pH 6.2 (20 ° C) for the particles heated at pH 5.8 in deionized water, whereas the rest of the particle

dispersions needed to be adjusted to pH 6.8. Finally, the protein concentration of all samples was adjusted to 8.2 g L⁻¹ using a 10 mM NaCl solution. This means each subsequent experiment was carried out at a temperature of 20 ° C, 10 mM NaCl, and a protein concentration of 8.2 g L⁻¹ unless mentioned otherwise.

An untreated solution of β -Lg powder in 10 mM NaCl (pH adjusted to 6.8) served as a reference.

5.2.4 Particle Size

For the determination of volume-based particle size distributions and the median volume-based particle size ($d_{50.3}$) by dynamic light scattering, a Zetasizer Nano ZS (Malvern Panalytical GmbH, Kassel, Germany) was used. Samples (unheated, heated, and purified) were measured in a 173 ° backscatter mode 10 times for 1 min after an equilibration time of 2 min. The used refractive index (RI) for calculation was set to 1.344. Results of the particle size measurements are the means of two samples of at least two individual experiments.

5.2.5 Zeta Potential

The zeta potential measurement of the native β -Lg and purified particle dispersions in dependence of the pH was conducted by an MPT-2 Autotitrator (Malvern Panalytical GmbH, Kassel, Germany) in combination with the Zetasizer Nano ZS System (Malvern Panalytical GmbH, Kassel, Germany). Therefore, the pH value was automatically decreased from 7.0 to 3.0 (increment: 0.2, precision: 0.1) using 0.1 and 1 M HCl and 0.1 M NaOH. The obtained electrophoretic mobility at each pH value was converted to the zeta potential by the Zetasizer Software 7.13 (Malvern Panalytical GmbH, Kassel, Germany). Results of the zeta potential measurements are means of two individual samples and two individual trials.

5.2.6 Degree of Disulfide Cross-Linking

The degree of disulfide cross-linking (DC) of the β -Lg particles after heat treatment was calculated by the change in the concentration of thiols associated with disulfide bonds (C_{RSSR}) due to heating according to the following Equation (Eq. (5-2)), as described by Kurz et al. (2020). For quantification, the thiol reagent 4,4'-dithiodipyridine (DTDP) was used.

$$DC = \frac{C_{RSSR \beta-Lg \text{ particles}}}{C_{RSSR \text{ unheated } \beta-Lg}} \quad (5-2)$$

The degree of disulfide cross-linking of the heat-induced protein particles refers to the degree of disulfide cross-linking of the native β -Lg solution; its value was set to 1.0. Results are means of two individual samples and two independent trials.

5.2.7 *Hydrophobicity of the Particle Surface*

The exposed surface hydrophobicity was determined by fluorescence spectroscopy (Tecan Group Ltd., Männedorf, Switzerland) using a 1.41 mM N,N-dimethyl-6-propionyl-2-naphthylamine (PRODAN) solution dissolved in methanol, as described by Andlinger et al. (2021). In brief, the native β -Lg and heat-induced β -Lg particles were diluted to 1 g L⁻¹ using a 100 mM phosphate buffer pH 7. Amounts of 0, 5, 10, 15, 20, 25, 30, 40, and 50 μ L of the PRODAN solution were added to each 1000 μ L of the diluted solution. After mixing, 100 μ L of each sample was transferred to a black 96-well plate and incubated for 30 min in the dark. After incubation, the solutions were excited at 365 nm in a Tecan Spark microplate reader (Tecan Group Ltd., Männedorf, Switzerland) and the emission spectra between 400 and 650 nm were recorded. A plot of the fluorescence intensity at 440 nm versus the amount of PRODAN yields a linear correlation up to \sim 25 μ L. The linear region up to 20 μ L was fitted by linear regression; the slope of the graph represents the surface hydrophobicity. The relative exposed surface hydrophobicity (S_0) of the protein particles refers to the surface hydrophobicity of the native β -Lg solution, whose value was set to 1.0. Results of the measurements are means of two samples of two individual experiments.

5.2.8 *Viscosity*

Determination of the viscosity of the native and purified samples was carried out with the Modular Compact Rheometer MCR 302 (Anton Paar GmbH, Graz, Austria) using a double gap geometry (DG 26.7, Anton Paar GmbH, Graz, Austria). Therefore, an increasing shear rate ramp from 0.1 to 100 s⁻¹ was applied followed by a decreasing ramp from 100 to 0.1 s⁻¹. For data analysis and calculation of the dynamic viscosity, the software RheoCompass 1.22 was used. All samples showed Newtonian behavior. Results of the measurements are means of two individual experiments.

5.2.9 *Surface and Interfacial Tension*

Determination of the surface ($\sigma(t)$) as well as interfacial tension ($\gamma(t)$) by the pendant drop method was performed with the Drop Shape Analyzer (DSA 100 R, Krüss GmbH, Hamburg, Germany) for a time period of 3600 s, as described by Kurz, Reitberger et al. (2021). For determination of the interfacial tension, a commercially available sunflower (SF) oil (THOMY, Nestlé Deutschland AG, Neuss, Germany) or medium-chain triglycerides (MCTs; 70% caprylic acid (C8) and 30% capric acid (C10), Primal State Performance GmbH, Berlin, Germany) were used. The densities of the protein dispersions and the oils were determined by DMA 4100 M (Anton Paar GmbH, Graz, Austria) at 20 °C and were considered for the calculation of the surface and interfacial tension.

Based on this, the surface pressure ($\pi_\sigma(t)$) and the interfacial pressure ($\pi_\gamma(t)$) were calculated as follows (Eqs. (5-3) and (5-4))

$$\pi_\sigma(t) = \sigma_0(t) - \sigma_t(t) \quad (5-3)$$

$$\pi_{\gamma}(t) = \gamma_0(t) - \gamma_t(t) \quad (5-4)$$

where $\sigma_0(t)$ ($\gamma_0(t)$) is the time-dependent surface tension (interfacial tension (MCT and SF, respectively)) of deionized water and $\sigma_t(t)$ ($\gamma_t(t)$) is the time-dependent surface (interfacial) tension of the β -Lg (native and particulated, respectively). To better compare the interfacial properties of the specific proteins at the SF/water and MCT/water interfaces, the normalized interfacial pressure (π^*) was calculated according to Bergfreund et al. (2021) as follows (Eq. (5-5))

$$\pi^* = \frac{\pi_{\gamma}(t)}{\pi_{\sigma}(t)} \quad (5-5)$$

Results are means of two individual experiments.

5.2.10 Foam Formation and Stability

Investigation of the foam formation and decay was performed using the Dynamic Foam Analyzer DFA100 (Krüss GmbH, Hamburg, Germany), as described by Kurz, Reitberger et al. (2021). The evolution of the foam stability was recorded over a time period of 5400 s. The obtained data were used to calculate the foamability (FA; Eq. (5-6)), the normalized foam stability (FS; Eq. (5-7)), and the normalized foam drainage (FD) after 5 min (Eq. (5-8))

$$FA = \frac{V_{foam,t=50s}}{V_{liquid,initial}} \times 100\% \quad (5-6)$$

$$FS_{t=x} = \frac{h_{foam,t=x}}{h_{foam,t=0}} \times 100\% \quad (5-7)$$

$$FS_{5\ min} = \frac{V_{liquid,t=5min} - V_{liquid,t=0}}{V_{liquid,initial} - V_{liquid,t=0}} \quad (5-8)$$

where $V_{foam,t=50s}$ is the generated foam volume after 50 s of air sparging in the respective protein solutions and $V_{liquid,initial} = 50$ mL. $h_{foam,t=0}$ is the foam height after foaming. Foaming was stopped upon reaching a total (liquid and foam) height of 180 mm. $h_{foam,t=x}$ is the remaining foam height after x min. $V_{liquid,t=0}$ is the remaining liquid volume directly after air sparging. $V_{liquid,t=5\ min}$ is the actual volume of liquid underneath the foam at a time of 5 min of decay.

The bubble size distribution at a column height of 65 mm was recorded over a time period of 5400 s using the Foam Structure Module (DFA100FSM, Krüss GmbH, Hamburg, Germany). Thereof, two-dimensional pictures of the foam structure were taken, including information about the Sauter, surface weighted mean diameter ($d_{3,2}$). A detailed description of the measurement principle is given by Oetjen et al. (2014). Results of the foaming experiments are means of at least two individual experiments.

5.2.11 *Emulsion Formation and Stability*

Oil-in-water emulsions (10/90 (v/v)) with an 8.2 g L⁻¹ protein content in the aqueous phase and either sunflower (SF) oil or medium-chain triglycerides (MCTs) were produced by high-pressure homogenization (APV 1000, SPX Corporation, Inc., Soborg, Denmark) at 300 bar. A premix was obtained by adding the oil to the protein–water phase and subsequent stirring (6000 rpm, 90 s; ULTRA-TURRAX T25 digital (S25N), IKA Werke GmbH & Co. KG, Staufen, Germany). The measurements of the oil droplet size distribution, the median volume-based oil droplet size ($d_{50.3}$), and the Sauter, surface weighted mean diameter ($d_{3.2}$) of the prepared emulsions were carried out after 0, 1, and 7 days with the Mastersizer 2000 with a Hydro 2000 unit (stirrer speed: 1750 rpm; dispersant refractive index: 1.33; Fraunhofer; Malvern Panalytical GmbH, Kassel, Germany). Results of the oil droplet measurements are means of two individual experiments. In addition, homogenization (300 bar) of the pure particle solutions after heat treatment had a negligible impact on the median particle diameter of the β -Lg particles (data not shown).

5.2.12 *Statistical Analysis*

To test whether particle size and surface hydrophobicity have a statistically significant influence on the interfacial activity, foam, and emulsion properties, independent t-tests were performed (OriginPro 2018b, two sampled t-test, one-tailed, assuming equal variances in the respective data sets). The level of significance was set to a p-value of 0.1.

5.3 **Results and Discussion**

5.3.1 *β -Lg Particle Generation, Purification, and Characterization.*

According to our previous study (Kurz, Reitberger et al., 2021), the thermal treatment of β -Lg as a function of pH and NaCl concentration in combination with a purification step allows for the formation of highly pure, soluble, nanosized particles with defined zeta potential and degree of disulfide cross-linking. With regard to particle purification aiming at removing the remaining native protein and NaCl, different options can be applied: isoelectric precipitation or membrane filtration. As shown in our previous study (Kurz, Reitberger et al., 2021), isoelectric precipitation may entail certain limitations related to incomplete resolubilization of the particle pellet. Therefore, membrane filtration in diafiltration mode was used in this study. As shown in Tab. 5-1, based on the variables chosen (i.e., heating pH and NaCl concentration), particles of (1) different sizes but similar surface hydrophobicity, zeta potential, and degree of cross-linking and (2) different surface hydrophobicity but similar size, zeta potential, and degree of cross-linking were produced. The size of the particles was in the range of ~ 23 or 70 nm, with both having a low disulfide cross-linking degree of ~ 1 and a zeta potential of ~ -28 mV. The latter was achieved by pH adjustment after purification and thus allowed to neglect the effect of zeta potential on further investigations. The defined differences and similarities in the particles' surface

hydrophobicity (~ 2.0 or 3.2) next to their size allowed for the specific and separate investigation of the influence of particle size and surface hydrophobicity on the interfacial properties of the β -Lg particles. In addition, native β -Lg served as a reference. The particle size distribution curves of native and particulated β -Lg are exemplarily shown in the Supporting Information (Fig. 5.6).

Tab. 5-1: Median Particle Diameter ($d_{50.3}$), Surface Hydrophobicity (S_0), Degree of Disulfide Cross-Linking (DC), and Zeta Potential (ZP) for Heat-Particulated β -Lg as a Function of the Heating pH and NaCl Concentration. pH_p and κ_p Display the Adjusted pH and Electrical Conductivity (κ) after Purification. The Number of Replicates (n) was ≥ 2 .

sample	heating		purification		characteristics			
	pH	NaCl	pH_p	κ_p	$d_{50.3}$	S_0	DC	ZP ^a
-	-	mM	-	$mS\ cm^{-1}$	nm	-	-	mV
particulated	5.8	0	6.2	1	69.0 ± 5.7	1.8 ± 0.2	1.08 ± 0.02	-28.3 ± 0.9
particulated	6.8	60	6.8	1	25.5 ± 0.8	3.2 ± 0.2	0.87 ± 0.02	-28.2 ± 1.8
particulated	8.5	60	6.8	1	21.2 ± 0.9	2.0 ± 0.2	0.82 ± 0.04	-26.8 ± 0.1
native	-	-	6.8	1	4.6 ± 0.1	1.0	1.00	-28.5 ± 1.9

^a The zeta potential was measured at pH_p .

The dynamic viscosity of the samples ranged between 1.3 and 1.6 mPa s. No significant changes were detectable. Thus, an impact of solution viscosity on interfacial and foaming/emulsifying properties was excluded.

5.3.2 Behavior of β -Lg Particles at the Air/Water and Oil/Water (MCT and SF) Interface

For the characterization of the impact of size and surface hydrophobicity on the evolution of surface and interfacial tension, β -Lg particles and native β -Lg of similar zeta potential and low cross-linking degree were used (Tab. 5-1). For all samples, a fast initial decrease of surface and interfacial tension followed by a flattening of the slope by approximation to the final values was detected.

5.3.2.1 Air/Water Interface

As can be seen in Fig. 5.1, both native β -Lg and the β -Lg particles were able to effectively lower the surface tension from ~ 72 to $\sim 49\ mN\ m^{-1}$.

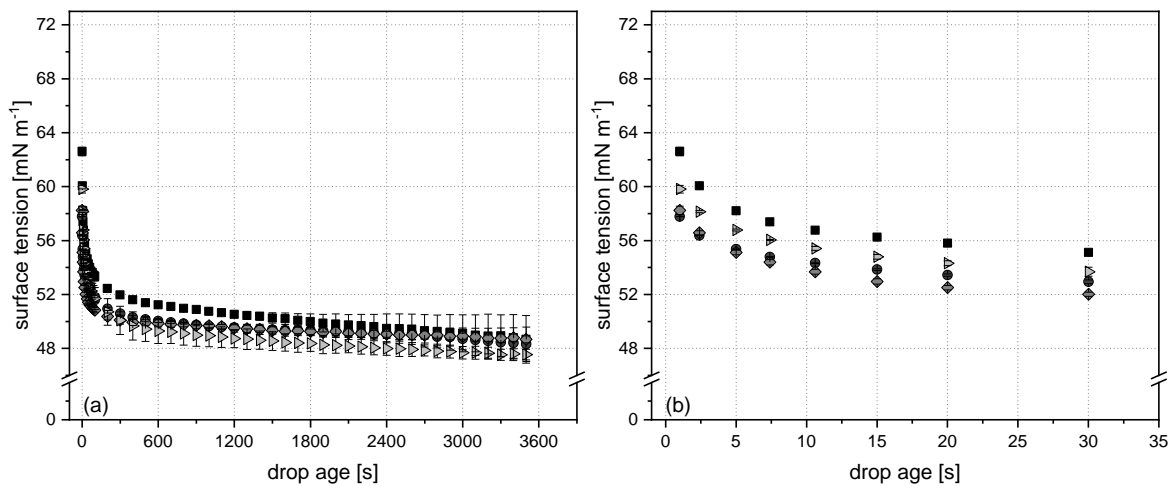


Fig. 5.1: (a) Time-dependent evolution of surface tension for native (\blacklozenge $d_{50.3}/S_0$: 5 nm/1.0) and particulated β -Lg of similar zeta potential (-28 mV) and low cross-linking degree (~ 1) as a function of size ($d_{50.3}$) and surface hydrophobicity (S_0) ($d_{50.3}/S_0$: \blacktriangleright 69 nm/1.8; \blacksquare 26 nm/3.2, and \bullet 21 nm/2.0). Panel (b) highlights the initial surface tension decrease. Error bars indicate the standard deviation. The number of replicates was 2.

Nonetheless, certain differences could be detected. An increase in surface hydrophobicity from 1 (native β -Lg: 5 nm) up to ~ 2 (particulated β -Lg: 21 nm) (see Tab. 5-1) resulted in a similar reduction of the surface tension during the initial ($t < 10$ s) regime (Fig. 5.1), i.e., no significant difference could be detected ($p > 0.1$). This indicates that the increase in particle size was compensated by the concurrent increase in surface hydrophobicity. However, a further increase in size to 69 nm while maintaining a similar surface hydrophobicity of ~ 2 resulted in a greater surface tension during the initial regime ($p < 0.05$) indicating a particle size-induced deceleration of diffusion. In contrast, at longer time scales ($t > 10$ s), the curves corresponding to the particles of similar hydrophobicity but different sizes converged, whereby no significant differences could be determined during a measurement time of 3600 s ($p > 0.1$). Interestingly, a further increase in the particles' surface hydrophobicity from 2 up to 3 while maintaining particle size at ~ 23 nm resulted in a lower reduction of the surface tension up to a time of 1500 s ($p < 0.1$ at $t = 1500$ s). According to the literature, an increase in particle size was shown to result in a greater surface tension at early time (Dhayal et al., 2015; Rullier et al., 2008).

However, it is important to note that more than one parameter was changed at a time (e.g., size, surface hydrophobicity, and zeta potential), so no clear conclusion can be drawn from these studies regarding the impact of individual factors. Therefore, the strategy used in this study, i.e., the variation of one parameter at a time, allows for a more specific investigation of the impact of particle size and surface hydrophobicity. Using chemical modification to increase the surface hydrophobicity while maintaining the surface charge, an increase in the exposed hydrophobicity was shown to result in accelerated adsorption kinetics (Wierenga et al., 2003). However, in contrast to these findings for caprylated ovalbumin (Wierenga et al., 2003), our findings support the hypothesis that an increase in surface hydrophobicity does not necessarily increase

surface activity. Therefore, we postulate that local surface hydrophobicity differences are more decisive than surface hydrophobicity per se as the hydrophobic patches are assumed to be distributed nonuniformly due to the heat-induced particulation method. Similar results were reported, and comparable conclusions were drawn in a review on plant proteins (Schmitt et al., 2021). During heat-induced particulation, native β -Lg unfolds resulting in an exposure of its hydrophobic core, buried inside of its globular structure (Tolkach & Kulozik, 2007). Thereby, the distribution of the exposed hydrophobic patches may be random at the particles' surface. As a result, local hydrophobicity differences may exist at the particle surface resulting in an increased surface activity despite a lower net surface hydrophobicity. Similar results of an increased surface activity at low surface hydrophobicity were shown for soy proteins (Sorgentini & Wagner, 2002). Another explanation could be that an intermediate surface hydrophobicity may exhibit a higher stabilizing potential compared to higher or lower values, as shown by Chen et al. (2017) for stabilized oil/water interfaces. Relating to our results, an increase in surface hydrophobicity for particles of a similar size of ~ 23 nm seemed to exceed the "surface activity optimum", beyond which the surface activity decreased. Also, the distribution of the hydrophobic residues can be assumed to be irregular and could thus be responsible for the increased surface activity of the particles exhibiting the lower surface hydrophobicity. To clarify this, a direct method for determining the local distribution of hydrophobic patches at the particles' surface would be required. The detected similarities in the surface tension values at longer time scales may be due to the high structural flexibility of the particles based on the low degree of cross-linking resulting in a high structural rearrangement at the interface (Kurz, Reitberger et al., 2021).

5.3.2.2 *Oil/Water Interface*

The MCT/water interface showed a nearly constant interfacial tension (~ 23.5 mN m⁻¹) over time, whereas the SF/water interface showed a decreasing value from ~ 25 to ~ 17 mN m⁻¹, as can be seen in Fig. 5.2. These differences can be attributed to differences in the oil composition such as the presence of surface-active compounds (e.g., fat-soluble vitamins (tocopherols)) and unsaturated fatty acids of higher fatty acid chain length (C18:2) in SF compared to the rather pure MCT, which primarily contains saturated C8 and C10 fatty acids (Cong et al., 2020; Dopierala et al., 2011; Ho & Chow, 2000; Wang, Sun, Wei, & Pu, 2018).

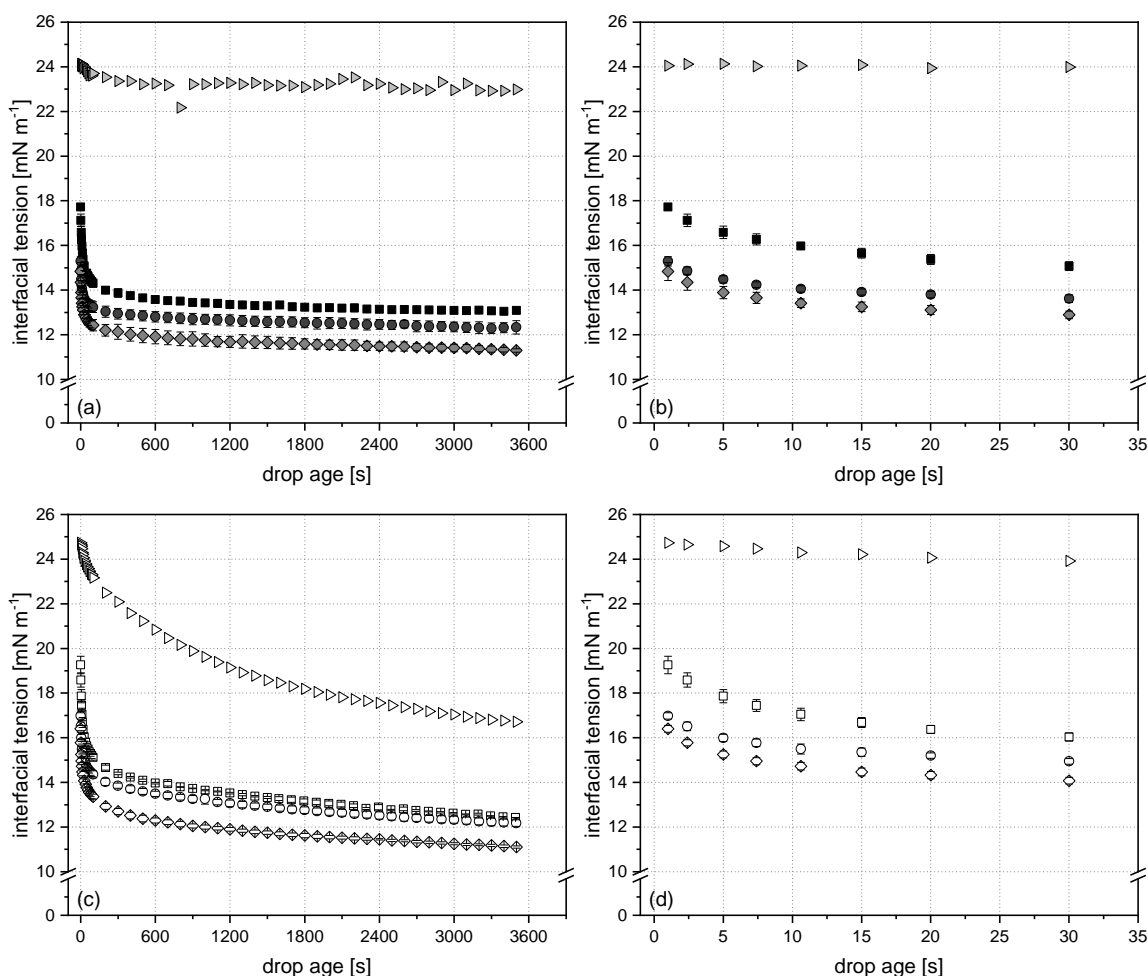


Fig. 5.2: Time-dependent evolution of interfacial tension at the (a, b) MCT/water and (c, d) sunflower oil/water interface of native (\blacklozenge/\lozenge $d_{50.3}/S_0$: 5 nm/1.0) and particulated β -Lg of similar zeta potential (-28 mV) and low cross-linking degree (~ 1) as a function of size ($d_{50.3}$) and surface hydrophobicity (S_0) ($d_{50.3}/S_0$: \blacksquare/\square 26 nm/3.2, and \bullet/\circ 21 nm/2.0). $\blacktriangleright/\triangleright$ represents the bare oil/water interfacial tension. Panels (b) and (d) highlight the initial interfacial tension decrease. Error bars indicate the standard deviation. The number of replicates was 2.

The impact of native and particulated β -Lg of different sizes and surface hydrophobicity on the evolution of the interfacial tension for SF/water and MCT/water interfaces can be seen in Fig. 5.2. Fig. 5.2 b, d highlights the initial interfacial tension decrease. Similar trends corresponding to those at the air/water interface were found. In detail, the slowest initial reduction of interfacial tension was detected for the particles with the highest surface hydrophobicity (~ 3) followed by the particles of lower surface hydrophobicity, independently of the type of oil ($p < 0.05$ at $t = 5$ s). The interfacial tension decreased fastest for the native protein ($p < 0.1$ at $t = 5$ s). In this case, a faster reduction of the interfacial tension with increasing surface hydrophobicity was expected (Kato & Nakai, 1980). As already discussed for a/w interfaces, a distribution of hydrophobic patches at the interface or the exceeding of a “surface activity optimum” could be the reason for this deviant behavior. At longer time scales ($t > 10$ s), the interfacial tension reduction was most pronounced for the native β -Lg ($p < 0.05$ at $t = 3550$ s), whereby the curves of the particles converged.

To compare the initial protein adsorption for the different types of oil, the normalized interfacial pressure π^* was calculated as proposed by Bergfreund et al. (2021). As can be seen in Fig. 5.3, the normalized interfacial pressure of the respective proteins is significantly higher ($p < 0.05$ at $t = 5$ s) at the MCT/water interface compared to that at the SF/water interface, indicating a higher interfacial activity. This may be due to the increased content of surface-active components in SF adsorbing at the interface from the oil side. As a result, protein adsorption from the aqueous side may be less effective or in a secondary adsorbed layer resulting in a slower normalized interfacial pressure increase. Similar findings were reported by Gmach et al. (2019) who investigated the impact of oil type on the interfacial behavior of egg yolk granules. The diffusion constant for granules decreased with increasing content of surface-active components.

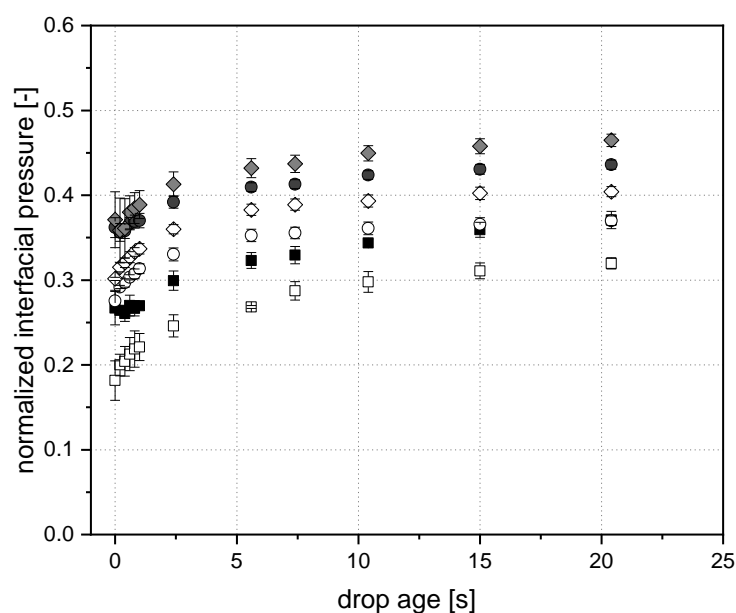


Fig. 5.3: Time-dependent evolution of the normalized interfacial pressure at the MCT/water (filled symbols) and SF/water interface (non-filled symbols) for native (\blacklozenge/\lozenge $d_{50.3}/S_0$: 5 nm/1.0) and particulated β -Lg of similar zeta potential (-28 mV) and low cross-linking degree as a function of size ($d_{50.3}$) and surface hydrophobicity (S_0) ($d_{50.3}/S_0$: \blacksquare/\square 26 nm/3.2, and \bullet/\circ 21 nm/2.0). Error bars indicate the standard deviation. The number of replicates was 2.

5.3.3 β -Lg Particles: Foaming and Emulsifying Properties

5.3.3.1 Foaming Properties

With regard to the formation and stability of foams, differences were observable from the modulation of size and surface hydrophobicity. While the values for foamability (FA) and foam/liquid drainage ($FD_{5\min}$) were in a similar range, differences were found for foam stability ($FS_{90\min}$) (Tab. 5-2).

Tab. 5-2: Foamability (FA) after 50 s, foam stability after 90 min (FS_{90min}), and foam drainage after 5 min (FD_{5min}) of native and particulated β -Lg formed by heat treatment under variation of pH value and NaCl concentration as a function of protein size ($d_{50.3}$) and surface hydrophobicity (S_0) (n_{foam} 2 or 3).

sample	$d_{50.3}$	S_0	FA	FS_{90min}	FD_{5min}
-	nm	-	%	%	%
particulated	69	1.8	367.0 ± 0.2	84.9 ± 1.7	48 ± 0.1
particulated	26	3.2	366.9 ± 1.3	70.1 ± 0.9	46 ± 6
particulated	21	2.0	379.3 ± 0.2	77.0 ± 8.1	55 ± 9
native	5	1.0	364.8 ± 2.8	37.2 ± 10.8	52 ± 0.4

^a Number of replicates (n)

Besides the foam formation, the time-dependent evolution of the foam stability was investigated. For native β -Lg, the foam height decreased constantly from $t > 20$ min resulting in a foam stability of 37% after 90 min. In contrast, particulation resulted in a significant increase in foam stability ($p < 0.05$ at $t = 90$ min) (Fig. 5.4).

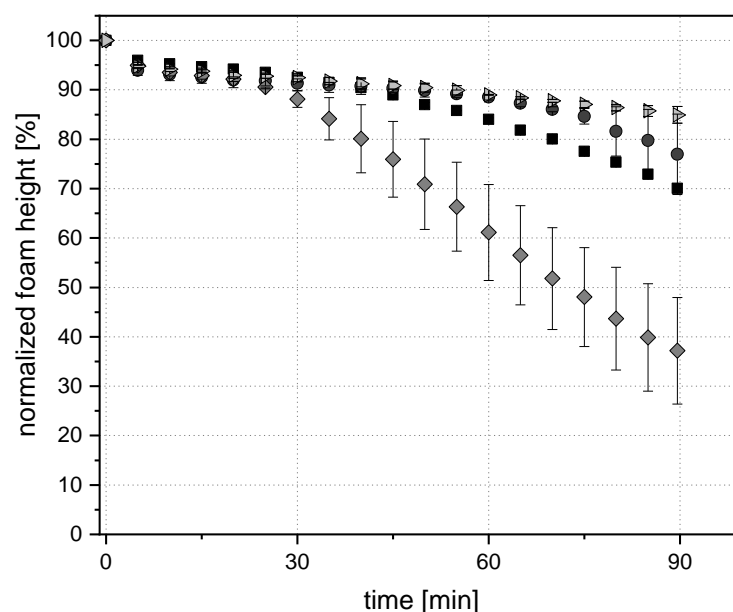


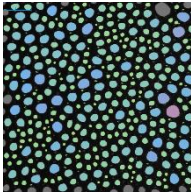
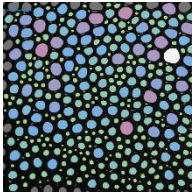
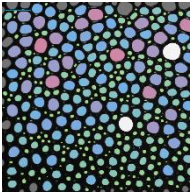
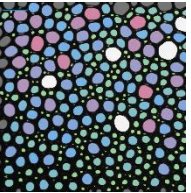
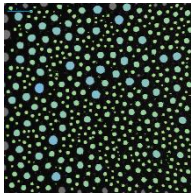
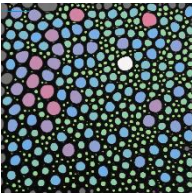
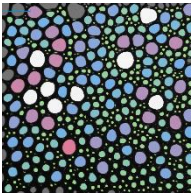
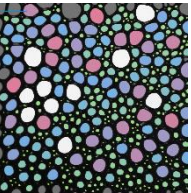
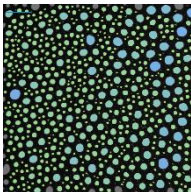
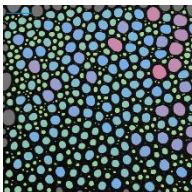
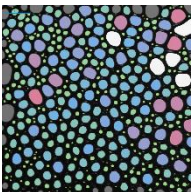
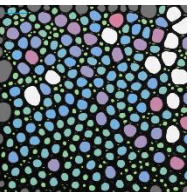
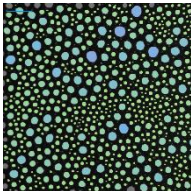
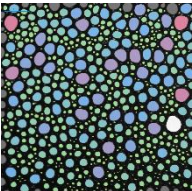
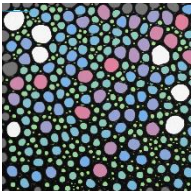
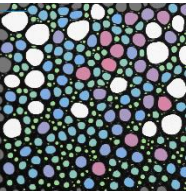
Fig. 5.4: Time-dependent evolution of normalized foam height for native (\blacklozenge $d_{50.3}/S_0$: 5 nm/ 1.0) and particulated β -Lg of similar zeta potential and cross-linking degree as a function of size ($d_{50.3}$) and surface hydrophobicity (S_0) ($d_{50.3}/S_0$: \blacktriangleright 69 nm/1.8; \blacksquare 26 nm/3.2, and \bullet 21 nm/2.0). Error bars indicate standard deviation. The number of replicates was 2.

The highest foam stability (85%) was determined for the large particles (69 nm) exhibiting a surface hydrophobicity of ~ 2 . A particle size of ~ 23 nm while maintaining a surface hydrophobicity of ~ 2 resulted in a decreased stability for $t > 75$ min. However, this effect was not yet significant ($p > 0.1$). An increase in surface hydrophobicity while maintaining the particle size of ~ 23 nm had no additional positive effect on foam stability, i.e., foam stability decreased more strongly for

$t > 45$ min ($p < 0.1$ at $45 < t < 80$ min). However, longer measurement times are likely to result in greater differences. As foam stabilization by particles is often related to lamellae blocking, i.e., leading to a reduction of liquid drainage (Moro et al., 2011; Rullier et al., 2008; Schmitt et al., 2014), the drainage behavior of native and particulated proteins was analyzed. Drainage causes thinning of the liquid films and in consequence, coalescence due to film rupture (Damodaran, 2005). As can be seen in Tab. 5-2, no clear correlation can be drawn between the percentage of drainage 5 min after foaming and the particle size, i.e., the drainage values did not differ significantly between the samples of different sizes ($p > 0.1$). About 50% of the liquid was still present in the foam after 5 min, whereby the liquid incorporated in the foams was similar for all investigated samples, with the exception of foams produced from particles produced at pH 8.5 ($d_{50.3}$: 26 nm/ S_0 : 3.2). This indicates that lamellae blocking due to the increased size of the particles as compared to the native protein does not seem to be the main stabilization mechanism. Rather, other structural characteristics may be of higher significance.

Accordingly, the time-dependent increase in the bubble size was found to be linked to foam stability. These observations are depicted exemplarily in Tab. 5-3, including images of the different foam structures in dependence of time (0, 30, 60, and 90 min after foam preparation) and the Sauter, surface weighted mean diameter ($d_{3.2}$). The lower increase in bubble size with increasing particle size can be explained by the formation of surface films exhibiting a higher elasticity due to the particles' higher structural flexibility (i.e., the distribution of disulfide bonds) and the formation of thicker adsorbed layers resulting in an effective steric barrier against bubble coalescence (Dhayan et al., 2015; Dombrowski et al., 2017).

Tab. 5-3: Changes in foam structure and the Sauter, surface weighted bubble mean diameter ($d_{3,2}$) in dependence of time as a function of protein/particle size ($d_{50,3}$) and exposed surface hydrophobicity (S_0) of native and heat-induced β -Lg particles.

sample	$d_{50,3}$	S_0	time			
			0	30	60	90
-	nm	-	min			
▶ particulated	69	1.8				
			$d_{3,2}$: 604 μm		$d_{3,2}$: 784 μm	
■ particulated	26	3.2				
			$d_{3,2}$: 458 μm		$d_{3,2}$: 828 μm	
● particulated	21	2.0				
			$d_{3,2}$: 446 μm		$d_{3,2}$: 804 μm	
◆ native	5	1.0				
			$d_{3,2}$: 432 μm		$d_{3,2}$: 942 μm	

5.3.3.2 Emulsifying Properties

The oil-in-water emulsions (10/90 v/v) were prepared with SF oil and MCT using β -Lg particles with different surface hydrophobicity but similar size (~ 23 nm), as well as with smaller-sized native β -Lg (Tab. 5-1). As shown in our previous study (Kurcz, Reitberger et al., 2021), the particles of large size and low degree of disulfide cross-linking purified by isoelectric precipitation showed a low emulsion stability due to oil droplet aggregation under similar conditions (pH 6.2; 10/90 (o/w); SF). Therefore, the particles of a size of 69 nm and low cross-linking degree were excluded from this investigation. The resulting oil droplet size distributions are shown exemplarily in Fig.

5.5. The median volume-based droplet diameter ($d_{50.3}$) and the Sauter, surface weighted mean diameter ($d_{3.2}$) are given in Tab. 5-4.

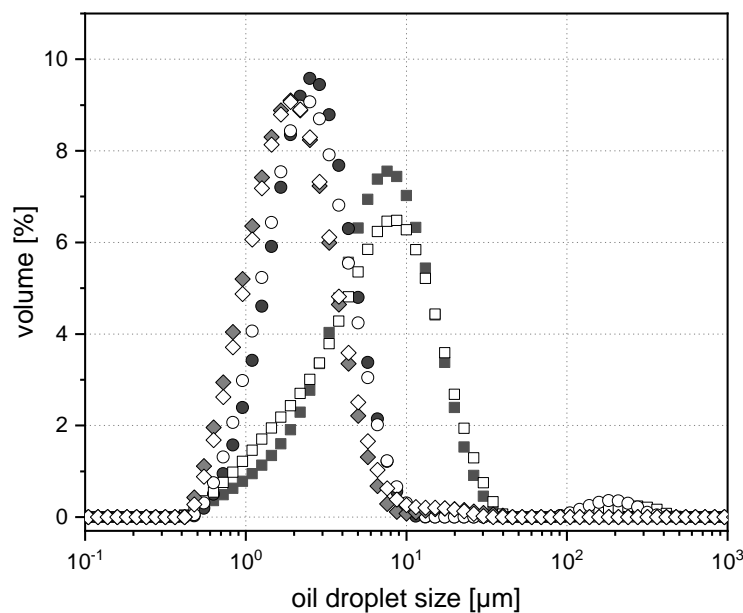


Fig. 5.5: Oil droplet size distribution curves for native (\blacklozenge/\lozenge $d_{50.3}/S_0$: 5 nm/1.0) and particulated β -Lg of similar zeta potential and cross-linking degree as a function of size ($d_{50.3}$) and surface hydrophobicity (S_0) ($d_{50.3}/S_0$: \blacksquare/\square 26 nm/3.2, and \bullet/\circ 21 nm/2.0). For emulsification, medium chain triglycerides (MCT; filled symbols) or sunflower oil (SF; nonfilled symbols) was used. The number of replicates was 2.

As can be seen in Fig. 5.5, oil droplets of $\sim 2 \mu\text{m}$ were formed using native β -Lg ($d_{50.3}$: 5 nm, S_0 : 1) and the particles with a surface hydrophobicity of ~ 2 , independently of the oil type. However, the droplets ($d_{3.2}$) stabilized by the native protein are slightly smaller ($p < 0.1$). An increase in the particles' surface hydrophobicity from 2 to 3 resulted in an increase in the oil droplet size ($d_{3.2}$) from 2.0 to 4.2 μm (MCT; $p < 0.1$) and 2.3 to 3.8 μm (SF; $p < 0.1$). This indicates a lower emulsifying activity with increasing surface hydrophobicity, which can be positively linked to the initial normalized interfacial pressure increase (Fig. 5.3). Similar results were reported by Moro et al. (2013) showing that longer β -Lg heat treatment times (85 °C/15 min, $c = 5.5\%$ (w/v)) and thus a higher surface hydrophobicity resulted in the formation of oil droplets of larger size, whereas no effect was detectable at shorter heating times. In this context, Chen et al. (2017) showed that an intermediate particle hydrophobicity of bitumen froth dominated the particles' behavior at o/w interfaces, whereas a higher or lower particle hydrophobicity had a rather destabilizing potential. This indicates the importance of the content and the distribution of hydrophobic patches at the particles' surface, which, however, cannot be directly measured yet.

However, despite the faster increase in the normalized interfacial pressure at the MCT/water compared to that at the SF/water interface, no significant differences in the resulting oil droplet size were detected ($p > 0.1$). Thereof, it can be concluded that the oil type has less influence on the oil droplet size when using high-pressure homogenization for emulsification, especially at low oil volume fractions (10% v/v).

This may be due to the fact that homogenization occurs within milliseconds and is based on convective transport rather than on diffusion.

With respect to emulsion stability, no significant increase in the oil droplet size ($d_{3.2}$) during a storage time of 7 days could be detected ($p > 0.1$). This indicates that the oil droplets are stabilized by cohesive protein films, whereby coalescence can be prevented.

Tab. 5-4: Median oil droplet size ($d_{50.3}$) and Sauter, surface weighted mean ($d_{3.2}$) of oil droplets stabilized by native or particulated β -Lg of defined size ($d_{50.3}$) and surface hydrophobicity (S_0) in dependence of the oil type (medium chain triglycerides (MCT) or sunflower oil (SF)) and storage time ($n^a = 2$).

oil	time d	sample ($d_{50.3}$ / S_0)					
		particulated (26 / 3.2) (■/□)		particulated (21 / 1.8) (●/○)		native: (5 / 2.0) (◆/◇)	
		oil droplet size		oil droplet size		oil droplet size	
		$d_{50.3}$ (μm)	$d_{3.2}$ (μm)	$d_{50.3}$ (μm)	$d_{3.2}$ (μm)	$d_{50.3}$ (μm)	$d_{3.2}$ (μm)
MCT	0	6.6 ± 2.5	4.2 ± 1.2	2.4 ± 0.3	2.0 ± 0.3	1.7 ± 0.1	1.5 ± 0.0
SF	0	6.9 ± 3.5	3.8 ± 1.2	2.3 ± 0.0	1.9 ± 0.0	1.8 ± 0.1	1.6 ± 0.1
MCT	7	6.2 ± 1.8	4.0 ± 0.8	2.4 ± 0.3	2.1 ± 0.2	1.7 ± 0.0	1.6 ± 0.0
SF	7	6.1 ± 3.4	3.3 ± 1.0	2.3 ± 0.0	1.9 ± 0.0	1.8 ± 0.1	1.6 ± 0.1

^a Number of replicates (n)

Overall, the results showed the respective impact of (i) protein structural characteristics, (ii) interface type (a/w or o/w), and (iii) oil type on the functionality of β -Lg particles. This study extends the understanding of protein adsorption at a/w and o/w interfaces as well as stabilization of foams and emulsions to better predict and understand the underlying mechanisms.

Associated Content – Supporting Information

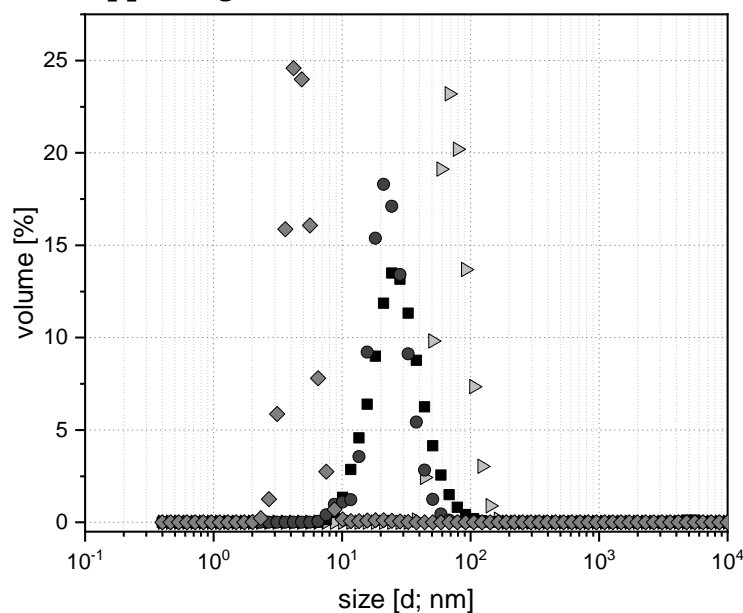


Fig. 5.6: Particle size distribution curves of native and heat-induced β -Lg particles under variation of heating pH and NaCl concentration.

Author Information

Corresponding Author

Franziska Kurz – Chair of Food and Bioprocess Engineering, TUM School of Life Sciences, Technical University of Munich, 85354 Freising, Germany; Email: franziska.kurz@tum.de

Authors

Jannika Dombrowski – Chair of Food and Bioprocess Engineering, TUM School of Life Sciences, Technical University of Munich, 85354 Freising, Germany; Nestlé Research, Société des Produits Nestlé SA, 1000 Lausanne 26, Switzerland

Andreas Matyssek – Chair of Food and Bioprocess Engineering, TUM School of Life Sciences, Technical University of Munich, 85354 Freising, Germany

Martin Hartinger – Chair of Food and Bioprocess Engineering, TUM School of Life Sciences, Technical University of Munich, 85354 Freising, Germany

Ulrich Kulozik – Chair of Food and Bioprocess Engineering, TUM School of Life Sciences, Technical University of Munich, 85354 Freising, Germany

Author Contributions

Conceptualization, methodology, validation, formal analysis, data curation, writing-original draft preparation, visualization, and software, F.K.; investigation, F.K., M.H., and A.M.; resources, supervision, and funding acquisition, U.K.; writing-review and editing, F.K., J.D., U.K., A.M., and M.H.; and project administration, F.K. and U.K. All authors have read and agreed to the published version of the manuscript.

Funding

This IGF Project of the FEI (AiF 18621 N) was supported via AiF within the program for promoting the Industrial Collective Research (IGF) of the German Ministry of Economic Affairs and Energy (BMWi) based on a resolution of the German Parliament.

Notes

The authors declare no competing financial interest. This article does not contain any studies with human or animal subjects performed by any of the authors.

Acknowledgements

The authors gratefully thank Hermine Roßgoderer and Claudia Hengst for their assistance during the experiments. In addition, the authors would also like to thank Joseph Dumpler and Hannes Petermeier for the helpful discussions.

Abbreviations

β -Lg	β -Lactoglobulin
a/w	air/water
o/w	oil/water
MCT	medium-chain triglycerides
SF	sunflower oil
DD	degree of denaturation
DF	diafiltration
κ	electrical conductivity
S_0	surface hydrophobicity
DC	degree of disulfide cross-linking
ZP	zeta potential
c	concentration
t	time
$\sigma_0(t)$	surface tension of deionized water
$\gamma_0(t)$	interfacial tension of deionized water
$\sigma_i(t)$	surface tension
$\gamma_i(t)$	interfacial tension
$\pi_\sigma(t)$	surface pressure
$\pi_\gamma(t)$	interfacial pressure
π^*	normalized interfacial pressure
$d_{50.3}$	median volume based size
$d_{3.2}$	the Sauter, surface weighted mean
FA	foamability
FS	normalized foam stability
FD	normalized foam drainage

6 Impact of the pH Value on the Techno-Functionality of Native and Particulated β -Lg

6.1 Introduction

Whey proteins are suitable for the formation and stabilization of foams due to their pronounced surface activity. However, despite long-lasting research on the techno-functionality of whey proteins, several issues still remain unclear. This is due to the high structural complexity of the proteins as well as the complexity of the underlying mechanisms during the generation and stabilization of interfaces. Next to the proteins in their native state, protein-based particles have attracted interest in connection with stabilizing foams (Amagliani & Schmitt, 2017; Dickinson, 2017; Dombrowski, 2017a; Lam, Velikov, & Velev, 2014; Schmitt et al., 2007). By altering the native proteins' physicochemical properties such as size, surface hydrophobicity, surface charge, and degree of disulfide cross-linking, their techno-functionality can be enhanced (Dombrowski et al., 2016; Dombrowski et al., 2017; Moro et al., 2011; Schmitt et al., 2007). However, a major challenge is the definition of decisive protein and protein particle characteristics as well as their interrelations with regard to good foaming properties. This is based on the fact that prior studies varied more than one characteristic at a time and thus, the individual properties could not be assessed independently (Dombrowski et al., 2016; Rullier et al., 2008; Schmitt et al., 2007). Therefore, to better understand and explain the foaming properties of native (i.e., non-particulated) and particulated proteins, knowledge about their behavior at the air/water interface as a function of their individual characteristics is required.

According to literature, the protein size as well as the zeta potential are often mentioned as most important with regard to their effect on the functionality (Dombrowski et al., 2016; Dombrowski et al., 2017; Engelhardt et al., 2013; Gochev et al., 2014; Rullier et al., 2008).

With regard to the impact of the size, an increase in particle size is generally associated with a slower diffusion to the interface (Rullier et al., 2008). However, with regard to foams, different effects have been reported. While Rullier et al. (2008) reported that the effectiveness of foam stabilization decreased with increasing protein particle size (due to the lacking ability to adsorb at the interface), Dombrowski et al. (2016) reported increasing foam stability with increasing particle size up to 1 μm . Dombrowski et al. (2016) justified the differences in the findings of the two studies by the presence of further differences in the particle characteristics, however, they did not finally clarify the impact of the individual characteristics.

Besides size, the zeta potential was shown to be decisive for the techno-functionality of proteins and protein-based particles (Dombrowski et al., 2017). In general, reducing the effective net charge of proteins by approaching the isoelectric pH or increasing the

ionic strength by addition of salt reduces the repulsive electrostatic forces between the proteins, favoring attractive interactions (e.g., hydrophobic bonds). Lowering the surface charge (i.e., zeta potential) and thus, the electrostatic repulsion is thereby linked to an increase of the adsorption rate due to the reduced barrier to adsorption (Wierenga et al., 2005) and foamability is thus enhanced. In addition, thicker adsorbed layers of higher elasticity are formed at the interface by decreasing the net zeta potential contributing to surface film stability and thus, bubble stability against coalescence (Engelhardt et al., 2013). However, also contrary results are reported, where a net zeta potential > 0 , i.e. a certain amount of charges, contributes to foam stability by keeping the bubbles at distance. This can be referred to thicker liquid films due to an increasing disjoining pressure (Eq. (1-15)) by increasing pH (pH $>$ isoelectric pH) (Gochev et al., 2014).

It becomes clear that the formation and stabilization of foams is a complex research field. To unravel and prioritize the effect of individual protein characteristics (i.e., size and zeta potential) as well as their interrelation on the foaming properties, native β -Lg and β -Lg particles of different size were investigated. The β -Lg particles were produced by heat-treatment (80 °C, 90 min) of native β -Lg solutions ($c = 8.2 \text{ g L}^{-1}$, deionized water) at pH 5.8. In order to investigate the impact of the zeta potential, the zeta potential of the native and particulated β -Lg was varied. Following this, the impact of the size and the zeta potential as well as their interrelation on the interfacial adsorption and foaming behavior was assessed.

6.2 Material and Methods

6.2.1 Materials

Highly pure bovine β -Lactoglobulin (β -Lg) (genetic variants A and B) was obtained from whey protein Isolate (WPI; Fonterra Co-operative Group, Auckland, New Zealand) via selective thermal aggregation in combination with filtration and subsequent spray drying according to Toro-Sierra et al. (2013). The produced powder had a total protein content of > 99% on a dry matter basis (Vario MAX cube, Elementar Analysensysteme GmbH, Langenselbold, Germany; RP-HPLC). Thereof, > 99% was β -Lg, whereby native β -Lg represented > 86% of the total protein as determined by RP-HPLC (Toro-Sierra et al. 2013). Lactose (HPLC) and salts (Na, K, Ca) (ELEX 6361, Eppendorf AG, Hamburg, Germany) concentrations were <0.05% and 0.7%, respectively.

6.2.2 Native (Non-Particulated) β -Lg Solutions

β -Lg powder was dissolved in 10 mM NaCl (Merck KGaA, Darmstadt, Germany) solutions to a total protein content of 8.5 g L⁻¹ and were stirred for at least 12 h at 4 °C. The protein content was determined by RP-HPLC according to Dimpler et al. (2017). A brief description of the sample preparation and measurement method is given in Kurz, Dombrowski, Matyssek, Hartinger, and Kulozik (2021).

In order to investigate the impact of the pH value on the foaming and emulsifying properties, the pH value of the protein solutions were adjusted to pH 5.6, 6.2, and 6.8 (20 °C) with 1 M HCl or 1 M NaOH (Merck KGaA, Darmstadt, Germany). Finally, the total protein concentration of all samples was adjusted to 8.2 g L⁻¹ using a 10 mM NaCl concentration.

6.2.3 β -Lg Particle Preparation and Purification

β -Lg powder was dissolved in deionized water (Millipore Corporation, Bedford, MA, USA) to a total protein content of 8.5 g L⁻¹ and the solution was stirred for at least 12 h at 4 °C. The protein content was determined as described above. Prior to thermal-induced particulation (80 °C/ 90 min), the pH value of the protein solution was adjusted to pH 5.8 (20 °C) with 1 M HCl (Merck KGaA, Darmstadt, Germany). The particulation and the subsequent purification to reduce the content of remaining native β -Lg (< 4%) after heat-treatment were performed as given Kurz, Dombrowski et al. (2021).

Subsequently, the pH values of particulated β -Lg dispersions was adjusted to pH 5.6, 6.2, and 6.8 with 1 M HCl (20 °C). Finally, the total protein concentration of all samples was adjusted to 8.2 g L⁻¹ using a 10 mM NaCl concentration.

Unless indicated otherwise, the following experiments were conducted at a total protein concentration of 8.2 g L⁻¹, an electric conductivity of 1 mS cm⁻¹ and a temperature of 20 °C.

6.2.4 *Particle Size and Zeta Potential*

The volume-based size distributions of non-particulated and particulated β -Lg as well as the median volume-based particle size ($d_{50.3}$) were determined by dynamic light scattering (Zetasizer Nano ZS, Malvern Panalytical GmbH, Kassel, Germany). The respective samples were measured in backscatter mode (173°) 10 times for 1 min. The used refractive index (RI) for calculation was set to 1.344. Results of the particle size measurements are the means of two samples of at least two individual experiments.

The zeta potential of the respective samples in dependence of the pH value was conducted using a MPT-2 Autotitrator (Malvern Panalytical GmbH, Kassel, Germany) in combination with the Zetasizer Nano ZS System as given by Kurz, Dombrowski et al. (2021). Results of the particle size measurements are the means of at least two individual experiments.

6.2.5 *Viscosity*

The dynamic viscosity of the non-particulated and particulated β -Lg as a function of the pH was carried out with the Modular Compact Rheometer MCR 302 (Anton Paar GmbH, Graz, Austria) using a double gap geometry (DG 26.7, Anton Paar GmbH, Graz, Austria). The measurement method and analysis is given in Kurz, Dombrowski et al. (2021). All samples showed Newtonian behavior (i.e., values < 2 mPas). Results of the measurements are means of two individual experiments.

6.2.6 *Surface Tension*

Surface tension ($\sigma(t)$) over time ($t = 3600$ s) was determined by the pendant drop method using the Drop Shape Analyzer (DSA 100 R, Krüss GmbH, Hamburg, Germany) as described by Kurz, Reitberger et al. (2021).

6.2.7 *Foam Formation and Stability*

Investigation of the foam formation and decay was performed using the Dynamic Foam Analyzer DFA100 (Krüss GmbH, Hamburg, Germany), as described in detail by Kurz, Reitberger et al. (2021). The evolution of the mean bubble area and the foam stability was recorded over a time period of 5400 s. Based on the evolution of the mean bubble area (A) in dependence of time (t), the coarsening factor α was estimated via a power law fit of the experimental data according to $A \sim t^\alpha$ ($t > 50$ s $>$ air sparging for foam formation) as stated by Schmitt et al. (2007). The obtained coarsening factor allows to evaluate the foam bubble stabilization behavior.

6.3 Results and Discussion

According to Kurz, Dombrowski et al. (2021), heat-treatment (80 °C, 90 min) of native β -Lg solutions (pH 5.8, deionized water) results in the formation of β -Lg particles with a median particle diameter of 69 nm. During purification (i.e., reducing the content of remaining native protein) subsequent to heating, no significant changes in the particle size could be detected as shown by Kurz, Dombrowski et al. (2021).

For the evaluation of the effect of surface charge (i.e., zeta potential) on the surface and foaming properties of native (non-particulated) and particulated β -Lg, zeta potential measurements were performed in dependence of the pH value. The results are shown in Fig. 6.1 (a), indicating a decrease in zeta potential by approaching the isoelectric pH of β -Lg of ~ 5 . The increased net zeta potential of the particles at high pH values (i.e., pH 6-7) compared to the native β -Lg can be referred to structural modifications due to the exposure of interior groups during heat treatment (Tolkach, 2007). In this context, the median particle diameter ($d_{50,3}$; Tab. 6-1) of both native and particulated β -Lg increased by decreasing the pH from 6.8 to 5.6 as exemplarily shown in Fig. 6.1 (b). The increased size can be referred to self-aggregation induced by net charge reduction, i.e., reduced electrostatic repulsion, due to the decrease in pH.

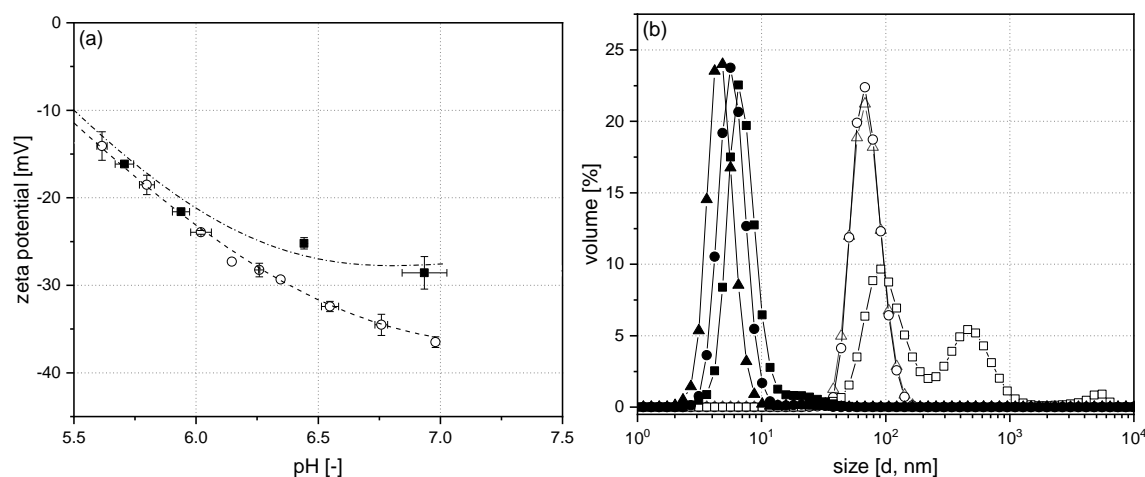


Fig. 6.1: (a) Zeta potential and (b) particle size distribution of native (black-filled symbols) and particulated (non-filled symbols) β -Lg as a function of the pH. Lines are guides to the eyes. In (b), triangle up indicates pH 6.8, circle pH 6.2, square pH 5.6. (Symbols \blacktriangle and \circ : data from Kurz, Dombrowski et al. (2021)).

6.3.1 Interfacial Properties

In order to investigate the impact of the zeta potential on the interfacial behavior of native and particulated β -Lg, the evolution of the dynamic surface tension over time was recorded across a period of 3600 s. In general, a rapid decrease in the surface tension within the first 300 s followed by a slower decrease and a levelling off can be observed (Fig. 6.2). The initial ($t = 5$ s) and final ($t = 3550$ s) surface tension values were generally found to decrease faster and to lower values by decreasing the pH from 6.8 to 5.6. As it was already indicated by Wierenga et al. (2005), approaching the isoelectric

pH, i.e., decreasing the net zeta potential, results in a decreasing energy barrier to adsorption by which the adsorption rate increases.

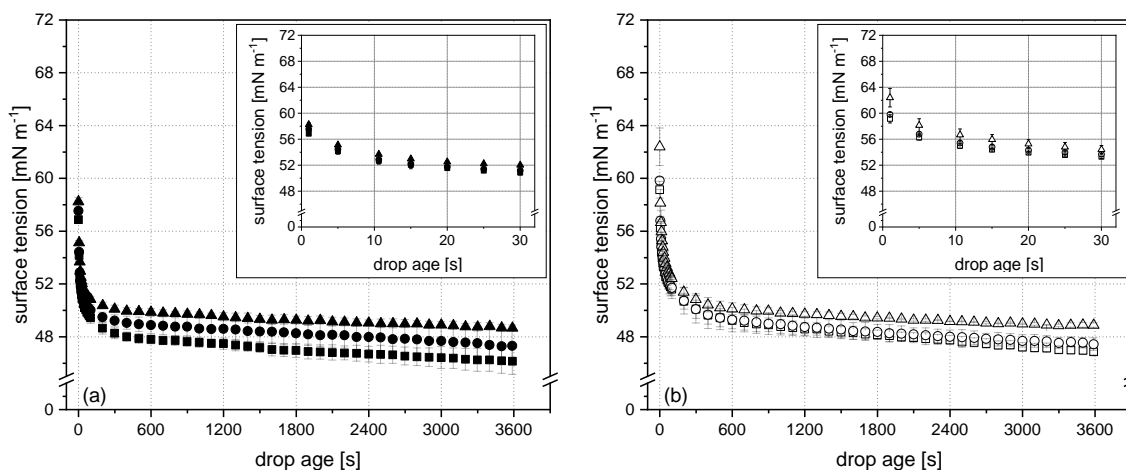


Fig. 6.2: Time-dependent evolution of the surface tension for (a) native and (b) particulated β -Lg as a function of the pH (triangle up indicates pH 6.8, circle pH 6.2, square pH 5.6). (Symbols \blacktriangle and \circ : data from Kurz, Dombrowski et al. (2021)).

Comparing the surface tension of the different systems, a faster initial decrease for the pure native β -Lg solution compared to the particle suspension can be detected at all investigated pH levels. This is likely caused by two overlapping effects: On the one hand, the increased particle size leads to a deceleration of the diffusion velocity and thus, a slower interfacial adsorption (Rullier et al., 2008). On the other hand, the net zeta potential at pH 6.8 and 6.2 was higher for the particles compared to the non-particulated β -Lg, which, in turn, increases the barrier to adsorption (Wierenga et al., 2005).

In order to investigate the individual impact of the particle size independently of the zeta potential, the native and the particulated β -Lg were compared at similar zeta potential (i.e., ~ -30 mV (pH 6.8 (native) and 6.2 (particulated)) and ~ -14 mV (both pH 5.6) with regard to their surface activity. Therefrom, it becomes clear that an increase in particle size at similar zeta potential results in a reduced adsorption behavior (Tab. 6-1).

With regard to the interrelation of size and zeta potential it can be concluded from the above that a particle-size decelerated adsorption rate can be compensated by reducing the net zeta potential.

Tab. 6-1: Characteristics (median particle size ($d_{50.3}$), initial ($t = 5$ s; σ_{5s}) and final ($t = 3550$ s; σ_{3550s}) surface tension) as well as foam stabilization behavior (coarsening factor ($\alpha_{t=90min}$)) of native and particulated β -Lg as a function of the pH value.

sample	pH	$d_{50.3}$	σ_{5s}	σ_{3550s}	$\alpha_{t=90min}$
	(-)	(nm)	(mN m ⁻¹)	(mN m ⁻¹)	(-)
native	6.8 ^a	4.6 ± 0.1 ^a	55.1 ± 0.2 ^a	48.7 ± 0.3 ^a	0.29 ± 0.12
	6.2	5.7 ± 0.4	54.4 ± 0.7	47.3 ± 1.2	0.25 ± 0.08
	5.6	6.9 ± 0.2	54.2 ± 0.4	46.2 ± 1.0	0.10 ± 0.02
particle	6.8	69.0 ± 5.7	58.1 ± 1.0	48.9 ± 0.1	0.07 ± 0.04
	6.2 ^a	69.0 ± 3.3 ^a	56.8 ± 0.1 ^a	47.5 ± 0.4 ^a	0.07 ± 0.04
	5.6	259 ± 225 ^b	56.3 ± 0.4	46.9 ± 0.2	0.03 ± 0.02

^aData from Kurz, Dombrowski et al. (2021)

^bBimodal particle size distribution

6.3.2 Foaming Properties

Regarding foam formation, clear differences resulted from using native or particulated β -Lg. Thereby, independently of the pH value, small initial mean bubble areas in a range of $\sim 1 \times 10^5 \mu\text{m}^2$ were formed by using native β -Lg as a stabilizer (Fig. 6.3). The smallest mean bubble area was detected for native β -Lg with pH 5.6. This can be linked to the high surface activity at low net zeta potentials. In terms of particulated β -Lg, the initial mean bubble area was found to be significantly higher ($\sim 1.75 \times 10^5 \mu\text{m}^2$) compared to the native one. As the initial mean bubble area is related to the initial surface tension, i.e., a faster adsorption rate results in smaller bubbles as can be seen in Fig. 6.3.

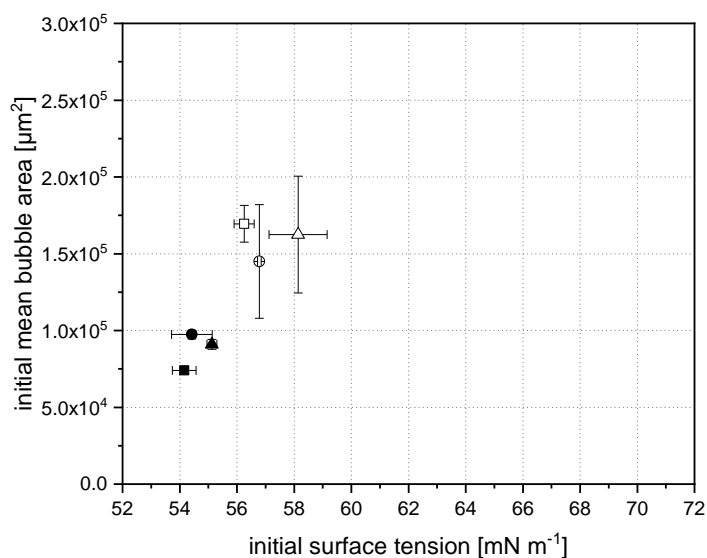


Fig. 6.3: Initial ($t = 5$ s) mean bubble area as a function of the initial surface tension for native (filled symbols) and particulated (non-filled symbols) β -Lg at variable pH values (triangle up indicates pH 6.8, circle pH 6.2, square pH 5.6). (Symbols \blacktriangle and \circ : data from Kurz, Dombrowski et al. (2021)).

However, despite the fact of smaller initial bubbles, i.e., a higher interfacial activity, the mean bubble area increased more strongly for the foams stabilized by native β -Lg (smaller initial bubble area) during the measurement time of 5400 s (Fig. 6.4 (a)) compared to foams stabilized by β -Lg particles (Fig. 6.4 (b)).

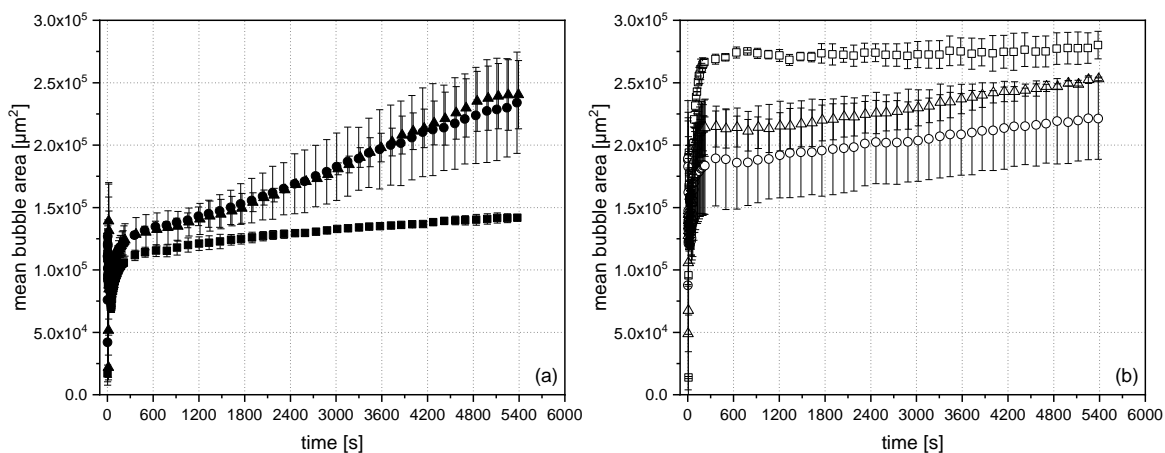


Fig. 6.4: Time-dependent evolution of the mean bubble area for (a) native and (b) particulated β -Lg as a function of the pH (triangle up indicates pH 6.8, circle pH 6.2, square pH 5.6).

A measure for the stability of foams is the coarsening factor α , which was determined by a power law fit ($A \sim t^\alpha$) of the experimental data (i.e., mean bubble area in dependence of time) as stated by Schmitt et al. (2007). In this regard, a higher coarsening factor correlates with a lower stability of the respective foam. The coarsening factors (α) for foams stabilized by native β -Lg were found to decrease from 0.29 to 0.10 with decreasing the pH from 6.8 to 5.6 (Fig. 6.5). The increasing stability with decreasing pH and thus, decreasing net zeta potential is most likely to be explained by the formation of closely-packed, thick adsorbed films of high elasticity. These films are known to be formed at pH values around the isoelectric pH due to reduced repulsive interactions between the proteins (Dombrowski et al., 2017; Engelhardt et al., 2013).

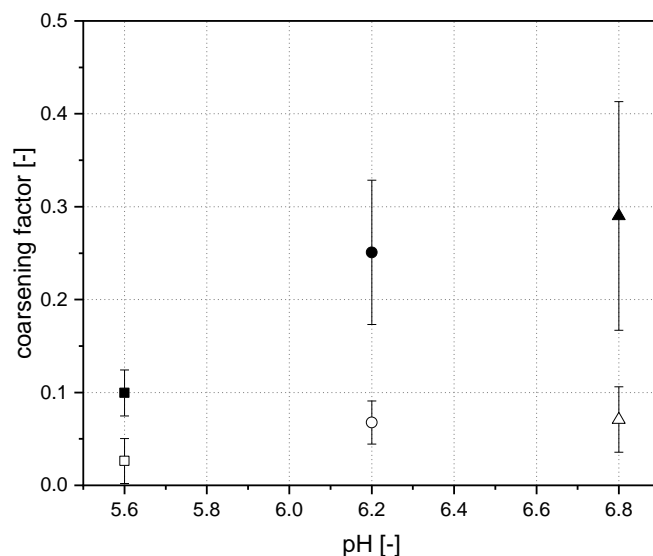


Fig. 6.5: Coarsening factor α as a function of the foaming pH for native (filled symbols) and particulated (non-filled symbols) β -Lg.

Regarding the effect of β -Lg particles, foam destabilization by coarsening was generally less pronounced for the initially larger-sized bubbles (Fig. 6.4 (b)). As shown in Fig. 6.5, this results in significantly lower coarsening factors of 0.15 (pH 6.8) to 0.07 (pH 5.6). This indicates the importance of the protein size in connection with foam stability. The findings are in accordance with Dhayal et al. (2015), who reported that the thickness of the adsorbed protein layer at the interface as well as the thickness of the liquid films between the bubbles increase with increasing protein particle size resulting in an enhanced foam stability. In this context, Gochev et al. (2014) showed that the thickness of the liquid films also increases with increasing net zeta potential using native β -Lg as a model system.

Concluding from the above, increasing particle size while maintaining a similar zeta potential increases foam stability. With regard to the impact of the zeta potential, differences in dependence of the size could be detected. While a decreasing net zeta potential resulted in an increasing stability for foams stabilized by native β -Lg, no significant effect could be detected for foams stabilized by particulated β -Lg. This indicates that not a single characteristic is decisive but rather an interrelation of protein size and zeta potential with regard to foam stability.

7 Overall Discussion and Main Findings

The physicochemical properties of proteins and protein particles including surface charge, surface hydrophobicity, structural flexibility, and also the particle size are known to influence their interfacial behavior as well as their techno-functionality in terms of stabilizing foams and emulsions (Damodaran, 2005). However, identifying and prioritizing the effects of the different properties is still complex. This is mainly due to the fact that during particulation several protein properties (e.g., size and surface charge) are varied simultaneously. This renders it difficult to assess the surface activity and the respective impact on foam and emulsion formation and stabilization due to overlapping mechanisms. Therefore, it was the objective of this study to modify the native β -Lg structural properties in such a way that particles of defined physicochemical properties are obtained. To achieve this goal, native β -Lg was heated under variation of pH value and NaCl concentration to induce structural modifications. By this, a process platform (“tool box”) is created, which allows for the selection of particles that differ only in a single property (e.g., size or surface charge). This bottom-up strategy opens new ways for

- prioritizing the different physicochemical properties in terms of their effect on surface activity and foam and emulsion formation and stabilization,
- clarifying the interplay of individual properties.

Various characteristics of proteins and protein-based particles have been discussed regarding their ability to stabilize interfaces, i.e., to define their techno-functionality in foam and emulsion systems.

7.1 β -Lg Particles: Generation and Purification

The major goal of this study was to assess the influence of individual particle properties as well as their interrelations on their techno-functionality. Since thermally induced particulation results in a variety of simultaneous and consecutive reactions (Dombrowski et al., 2016; Schmitt et al., 2007), a precise “design” of particles with defined properties is complex. In this regard, the influence of the environmental conditions pH and ionic strength (via addition of NaCl) during heating on the particle characteristics was assessed first. In order to form soluble (i.e., non-sedimenting) protein particles, the protein concentration was set at a value of 8.5 g L⁻¹ as higher protein concentrations would result in insoluble gels or flocculated particles (Hoffmann et al., 1997).

7.1.1 *Impact of pH Value and Ionic Strength Upon Heating on the Resulting β -Lg Particles Characteristics*

It was observed that a decrease in the **pH** from 8.5 to 5.8 during heating, i.e., approaching the isoelectric point of β -Lg (~ pH 5), resulted in an increasing particle size. This can be attributed to a reduced extent of electrostatic repulsive forces between the molecules, which favor aggregation reactions. Apart from the effect on the particle

size, decreasing the heating pH from 8.5 to 5.8 (without NaCl addition) resulted in the formation of less disulfide cross-linked particles (Kurz, Reitberger et al., 2021). This is due to the reduced accessibility of the free thiol group and the protonation of the thiol group with decreasing the heating pH from 8.5 to 5.8, resulting in reduced rates of polymerization via thiol-disulfide-exchange reactions or thiol-thiol-reactions (compare Section 1.2.3) (Hoffmann & van Mil, 1997; McSwiney et al., 1994; Tanford et al., 1959). The consequence is that the cross-linking within particles transforms from rather covalent at elevated pH values to rather non-covalent at pH values closer to the isoelectric point. In this context it is to note, that the decrease in the concentration of free thiols may not be proportional to the increase in disulfide bonds. This is because multiple chemical degradation products can result from the oxidation of the free thiol group or the formation of dehydroalanine by degradation of disulfide bonds. This effect becomes more pronounced by increasing the pH value to the alkaline range (Klostermeyer & Reimerdes, 1977; Poole, 2015; Watanabe & Klostermeyer, 1976). Due to this, the concentration of disulfide bonds was determined using a RP-HPLC method (Kurz et al., 2020) and used as a basis for calculating the degree of disulfide cross-links (Section 4.2.3) in this thesis.

As indicated above, the electrostatic repulsive force has a major effect on the intermolecular interactions and thus, on the resulting particle properties. Next to charge reduction by approaching the isoelectric point, charge shielding can be utilized. By increasing the **ionic strength** (e.g., by addition of NaCl, as executed in this study), the range of electrostatic repulsive forces is reduced (i.e., the molecules can approach each other more closely) and thus, hydrophobic interactions can become dominant. In general, heat treatment was found to result in a two to three-fold increase in surface hydrophobicity compared to the native β -Lg (Kurz, Dombrowski et al., 2021). Consequently, an increase in the concentration of NaCl resulted in the formation of larger, less disulfide cross-linked particles (Kurz, Reitberger et al., 2021).

This shows that the effects of pH and ionic strength can modulate or intensify themselves. As summarized in Fig. 7.1, a pH close to the isoelectric point and a high ionic strength during heating induce large non-covalently bound particles, whereas a pH far from the isoelectric point and a low ionic strength result in significantly smaller particles mainly cross-linked via disulfide bonds. The harmonization of both environmental variables allowed for the production of defined particle properties.

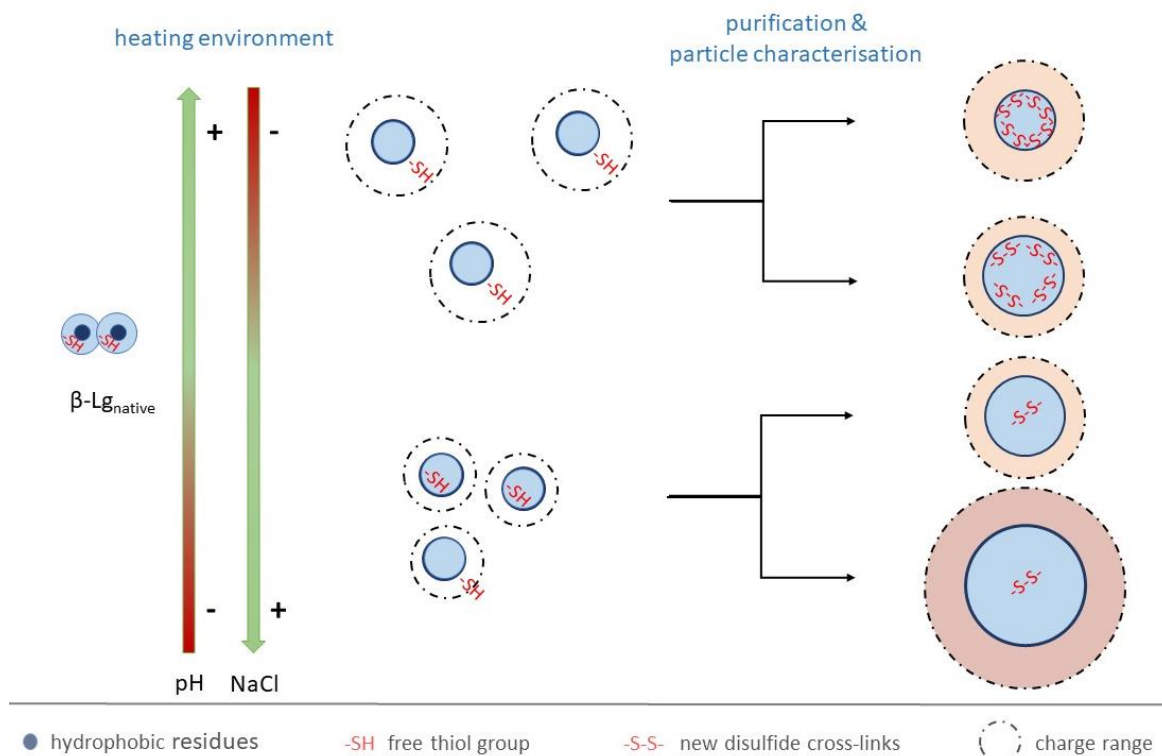


Fig. 7.1: Schematic representation of the impact of varying heating environments on the resulting β -Lg particle characteristics based on the results from Kurz et al. (2020), Kurz, Reitberger et al. (2021), and Kurz, Dombrowski et al. (2021).

The formation and stabilization of foams and emulsions are both decisively dependent on the medium composition. Therefore, the availability of standardized bulk (e.g., protein concentration) and environmental (e.g., ionic strength) conditions are vital for the investigation on the correlation between protein particle structural attributes and their techno-functionality. However, due to the selected environmental conditions, native β -Lg or salt residues remain in dependence of the heating environment (Kurz, Dombrowski et al., 2021; Kurz, Reitberger et al., 2021). Thus, a purification step was required to maintain standardized conditions by reducing the content of interfering “impurities” in the form of non-particulated protein and salts. For this task, two different purification approaches were investigated:

- isoelectric precipitation (laboratory scale) - purification based on solubility properties of the formed protein particles (Kurz, Reitberger et al., 2021)
- membrane filtration in diafiltration mode (pilot scale) - purification based on the particle size (Kurz, Dombrowski et al., 2021)

7.1.2 Comparison of Purification Methods

The purification methods mentioned above provide specific advantages. The method based on **isoelectric precipitation** can be used for small sample quantities on a laboratory scale and the separation works independently of size differences between native β -Lg molecules and β -Lg particles. However, this purification method was not suitable for all particles. By adjusting the pH to 4.6, i.e., approaching the isoelectric point of the particles, the electrostatic repulsion between the particles becomes

negligible. This step is needed to make the protein particles charge neutral and insoluble, whereas the native protein remains soluble (Toro-Sierra et al., 2013). In the subsequent sedimentation step, the particles are strongly concentrated and dewatered in the pellet. Consequently, the protein particles approach each other closely and can form attractive particle-particle interactions (e.g., hydrophobic interactions). In this regard, resolubilization (i.e., protein-solvent interactions) of the particle pellet was found to be limited despite an increase in pH up to 6.8 and thus, the enhanced repulsive electrostatic particle-particle interactions. In general, this effect becomes more relevant with particles generated in a condition of reduced electrostatic repulsion between the proteins (i.e., reduced net surface charge by approaching the isoelectric pH or charge screening due to electrolytes) (Kurz, Reitberger et al., 2021).

When comparing the zeta potential (ZP) and surface hydrophobicity (R_0) of different particles and the non-particulated β -Lg (Tab. 7-1) it becomes clear that the resolubilization is markedly reduced above a certain surface hydrophobicity value. Concluding from this, an increase in surface hydrophobicity may potentially enhance attractive particle interactions and in consequence, lead to the domination of particle-particle interactions over particle-solvent interactions, whereby the isoelectric purification method is limited to particles with a low surface hydrophobicity.

Tab. 7-1: Resolubilization ability of precipitated native (non-particulated) and particulated β -Lg as a function of their respective zeta potential (ZP; at pH 6.8) and surface hydrophobicity (R_0).

sample	native	particulated	particulated	particulated
heating environment	-	5.8/0	6.8/60	8.5/60
pH/NaCl				
ZP_{pH 6.8}				
[mV]	-29 ± 1.9^b	-38 ± 1.1^a	-28 ± 1.8^b	-29 ± 2.2^a
R_0				
[-]	1 ^b	1.8 ± 0.2^b	3.2 ± 0.2^b	2.0 ± 0.2^b
resolubilization	good	good	inferior	good

^a Data from Kurz, Reitberger et al. (2021)

^b Data from Kurz, Dombrowski et al. (2021)

In contrast to that, particle interactions based on significantly increased concentration is no issue with the purification by **membrane filtration**, as diafiltration medium (10 mM NaCl) is added to maintain a constant particle concentration. Following this, the particles do not come in close contact to form attractive hydrophobic particle-particle interactions. Furthermore, repulsive particle-particle interactions keep the particles at a distance as the pH value is not changed (i.e., the pH is not set to 4.6) during the purification by membrane filtration. Thus, with the filtration in diafiltration mode, the initial particle properties are preserved more accurately than with isoelectric precipitation. In some cases (e.g., particles exhibiting high surface hydrophobicity) it was only possible to obtain purified particles with the membrane filtration approach (Kurz, Dombrowski et al., 2021). However, a

considerable difference in size between the protein particles and impurities is a prerequisite for the applicability of membrane filtration in diafiltration mode to separate native β -Lg from particulated β -Lg.

A comparison of the effect of the purification method on the techno-functionality will be discussed in Section 7.2.5.

7.2 Influence of Specific Particle Characteristics on the Techno-Functional Properties of β -Lg and β -Lg Particles at the Air/Water Interface

Foam stability is often linked to the proteins' structural properties, i.e., size, zeta potential, surface hydrophobicity, and degree of disulfide cross-linking. However, for attaining high foam stability, different aspects need to be considered. First, proteins need to adsorb at the air/water interface to reduce the surface tension and thus, to enable foam formation. Second, the formed bubbles need to be stabilized in long term by reducing drainage, bubble coalescence, and disproportionation.

Thus, in order to understand the formation of stable foams, the impact of the individual protein characteristics on the

- adsorption behavior at the interface,
- foam formation,
- foam stabilization

need to be investigated. By this, decisive protein characteristics can be determined, which allow to provide conclusions on the optimization of the formation and stabilization of foams stabilized by proteins and protein-based particles.

7.2.1 *Understanding Protein Adsorption at the Air/Water Interface*

As adsorption at the air/water interface is a prerequisite for the formation of foams, the specific impact of the zeta potential, size, molecular flexibility (i.e., the degree of disulfide cross-linking), and the surface hydrophobicity of native and particulated β -Lg on the evolution of the surface tension needs to be considered first.

The **zeta potential** (i.e., the charge effective range) is known to have a major impact on the interfacial adsorption behavior of proteins. According to Wierenga et al. (2005), decreasing the proteins net charge and thus the zeta potential enhances the initial adsorption rate by reducing the energy barrier to adsorption. In the context of this thesis, a variation of the zeta potential by means of variation of the pH provided a powerful tool to vary the amount of charges and thus, the charge effective range. In this regard, decreasing the net zeta potential of native and particulated β -Lg was shown to decrease the initial surface tension more rapidly (Section 6; (Kurz, Reitberger et al., 2021)) compared to higher net zeta potentials. However, as can be seen in Fig. 7.2, significant differences can be detected with regard to the initial adsorption behavior when comparing particles of similar zeta potential in the range of ~ -30 to -28 mV. This indicates the importance of further protein properties next to the zeta potential. Therefore, to clarify this interrelation of different effects in more detail, the

zeta potential of the different samples was held constant (~ -30 to ~ -28 mV) in the following.

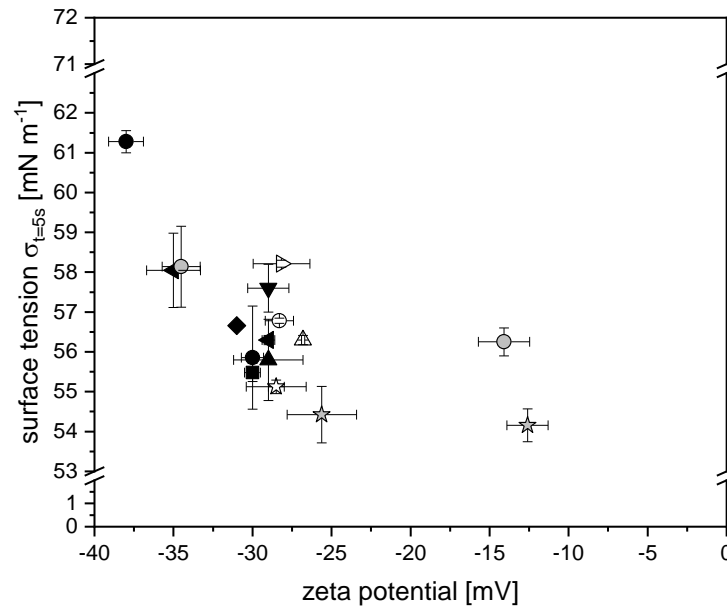


Fig. 7.2: Initial ($t = 5$ s) surface tension ($\sigma_{t=5s}$) of native (star symbol) and particulated β -Lg in dependence of the zeta potential. (Symbols: black-filled: data from Kurz, Reitberger et al. (2021), non-filled: data from Kurz, Dombrowski et al. (2021), gray-filled: data from Section 6).

According to the Stokes-Einstein equation (Eq. (1-19)), the conventional bulk diffusion coefficients (D_B) decrease with increasing **particle radius** (r). Accordingly, in the case of diffusion-based processes, smaller-sized particles should consequently decrease the initial surface tension faster compared to larger ones, as smaller particles will diffuse to the interface more rapidly. This diffusion-based process can be reproduced by using the pendant drop tensiometry for determination of the surface tension. In order to investigate the specific impact of the particle size on the evolution of the surface tension in more detail, native (~ 5 nm) and particulated β -Lg of varying size (up to 120 nm) but similar zeta potential (~ -30 to ~ -28 mV) were compared (Kurz, Dombrowski et al., 2021; Kurz, Reitberger et al., 2021). However, against expectation, no direct correlation between the particle size and the initial surface tension values could be observed, despite significant differences in the size as can be seen in Fig. 7.3. Even when comparing particles of a similar size range of ~ 20 nm significant differences in the initial ($t = 5$ s) surface tension values were detected (Kurz, Dombrowski et al., 2021; Kurz, Reitberger et al., 2021).

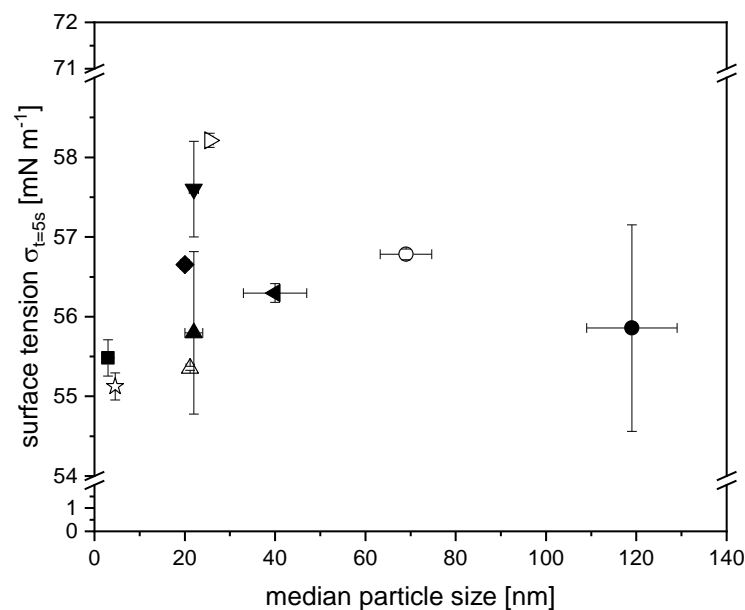


Fig. 7.3: Initial ($t = 5$ s) surface tension ($\sigma_{t=5s}$) of native (star symbol) and particulated β -Lg in dependence of the median particle size at constant zeta potential (~ -30 to ~ -28 mV). (Symbols: black-filled: data from Kurz, Reitberger et al. (2021), non-filled: data from Kurz, Dombrowski et al. (2021)).

Concluding from this, further particle characteristics may balance out the negative effect of an increased particle size on the initial surface tension decrease. In this context, molecular flexibility as well as surface hydrophobicity are emphasized as important factors. Thus, the additional impact of these properties needed to be investigated. During heat-induced particulation, the exposure of the free thiol group is strongly dependent on the heating pH (Hoffmann & van Mil, 1997; Kurz et al., 2020; Leeb et al., 2018). Based on the extent of this exposure, the formation of covalent inter-protein cross-linking becomes more or less intense. This causes the indirect correlation between **structural flexibility** and the number of newly formed **disulfide cross-links**.

According to literature, a high molecular flexibility, i.e., the proteins ability to structural adaptations during adsorption at the interface, is often linked to an increased initial rate of adsorption due to an accelerated interfacial unfolding of the protein (Graham & Phillips, 1979; Martin et al., 2002; Townsend & Nakai, 1983). Therefore, particles of similar size (~ 20 nm) and zeta potential but different degrees of disulfide cross-linking, i.e., different structural flexibility, were compared. However, no correlation between structural flexibility in terms of lower cross-linking degrees and the initial surface tension decrease could be observed (Kurz, Reitberger et al., 2021). This is in accordance with more recent studies, which question the molecular flexibility to be a crucial factor with regard to the initial adsorption behavior of proteins to the interfaces (Wierenga & Gruppen, 2010).

Instead, the **surface hydrophobicity** seems to be more important during the initial regime. According to many studies, an increased surface hydrophobicity resulting from heat-treatment or caprylation is linked to a higher adsorption rate and, moreover, may compensate the particle-size dependent deceleration of the adsorption rate

(Dombrowski et al., 2016; Dombrowski et al., 2017; Kato & Nakai, 1980; Wierenga et al., 2003). In this thesis, no clear correlation between initial surface tension decrease and surface hydrophobicity increase from 1 (native β -Lg) up to 3 (particulated β -Lg) could be observed (Kurz, Dombrowski et al., 2021). Comparing particles of similar surface hydrophobicity (~ 2), cross-linking degree, and zeta potential but different size (20 or 70 nm), a slower decrease in initial surface tension could be detected for the larger particles. This indicates that the particle size has a distinct effect on the adsorption rate (Kurz, Dombrowski et al., 2021).

However, comparing particles of different surface hydrophobicity (2 or 3; *ceteris paribus*) with regard to their interfacial activity, a higher surface hydrophobicity was not reflected in a more rapid decrease in surface tension (Kurz, Dombrowski et al., 2021). This latter finding was surprising, as it seems contradictory to literature (Wierenga et al., 2003). However, it is important to mention that the aforementioned surface hydrophobicity measured in this study refers to the average surface hydrophobicity. During heat-induced particulation, the hydrophobic core of β -Lg becomes exposed resulting in a twofold to threefold increase in average surface hydrophobicity compared to the native protein (Kurz, Dombrowski et al., 2021; Schmitt et al., 2007; Tolkach & Kulozik, 2007). However, as the exposure of the hydrophobic residues of β -Lg is most likely at random, local hydrophobicity differences evolve at the surface. Due to this, it is hypothesized that the distribution of the hydrophobic patches at the surface needs to be considered in addition to the average surface hydrophobicity to clarify the role of the surface hydrophobicity on foams. Similar observations and conclusion were drawn in connection with plant proteins (Schmitt et al., 2021).

Based on the results shown above, the zeta potential seems to be a factor of priority in combination with surface hydrophobicity and size. This indicates that not a single particle property is decisive but rather the interplay of the individual protein particle characteristics. The structural flexibility by means of the degree of disulfide cross-links seems to be unimportant during the initial regime of adsorption. It is to note that the average surface hydrophobicity is indicated to have limited validity and thus, does not provide conclusive clarification. To clarify this, a direct method for determining the local distribution of hydrophobic patches at the particles' surface would be required.

7.2.2 *Understanding Foam Formation*

As mentioned before, protein adsorption at the interface is a prerequisite for foam formation. Thereof, the assumption arises that the protein adsorption at the interface and foam formation can be linked to the same protein characteristics. In general, the foaming process can be described by different parameters such as the mean bubble area directly after foaming or the achieved foam volume and foam height after a specific foaming time, respectively. To clarify the influence of the protein particles' structural properties on the foam characteristics, the initial ($t = 5$ s) surface tension was correlated with the initial mean bubble area after foaming. As can be seen in Fig. 7.4, a faster initial adsorption behavior (i.e., a lower surface tension value) can be linked to

a lower initial mean bubble area. This indicates that the observed correlations between the protein characteristics and the initial surface tension reduction can be transferred to the foam formation. This means, the initial surface tension decrease can be used as an indicator for the initial bubble size.

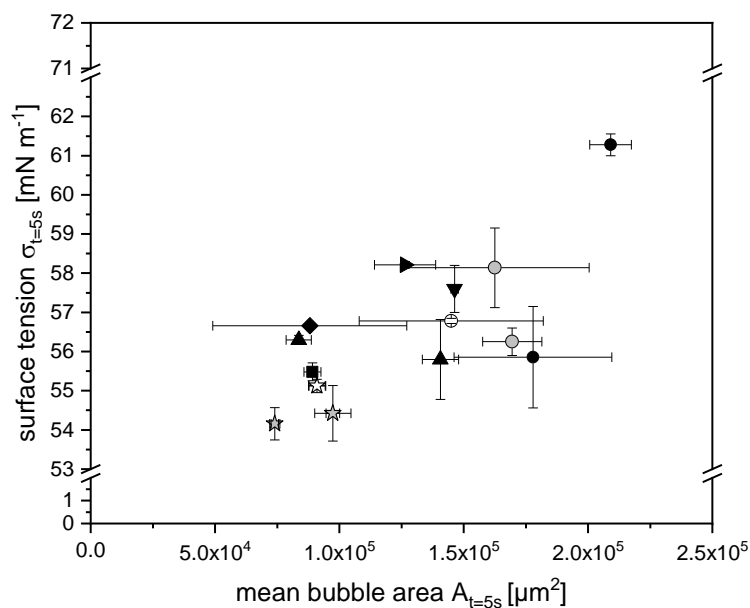


Fig. 7.4: Initial ($t = 5$ s) mean bubble area ($A_{t=5s}$) of native (star symbol) and particulated β -Lg as a function of the initial surface tension ($\sigma_{t=5s}$). (Symbols: black-filled: data from Kurz, Reitberger et al. (2021), non-filled: data from Kurz, Dombrowski et al. (2021), gray-filled: data from Section 6).

7.2.3 Understanding Foam Stabilization

Foam stabilization refers to the ability of a protein or protein particle to stabilize the formed foam bubbles after foaming. In this context, the question arises whether foam stability and foam formation are linked to the same protein characteristics. Therefore, the impact of the protein and protein-particle characteristics on the foam stability needed to be investigated in the first step. In this thesis, foam stability refers to the alteration of the foam height and/or the mean bubble area after foam formation upon time. Based on the experimental data of the mean bubble area as a function of time, the coarsening factor (α) as a measure for bubble coarsening and thus, foam stability was determined. As the decrease in the number of air bubbles within a foam can be described by an exponential decay, a power law fit ($A \sim t^\alpha$) of the experimental data was performed according to Schmitt et al. (2007) to evaluate foam bubble stability.

The **zeta potential** is known to influence the electrostatic protein-protein interactions and thus, is assumed to influence foam stability (Dombrowski et al., 2017). Therefore, the impact of the zeta potential of native (~ 5 nm) and particulated (~ 70 nm) β -Lg on the foam stability was investigated. In order to adapt the zeta potential, the pH of the respective protein solutions was varied between pH 6.8 and 5.6. In general, lower pH values (i.e., lower net zeta potential) were shown to lower the coarsening factor (i.e., increasing the foam stability) for both native and particulated β -Lg stabilized foams compared to higher pH values. However, generally, lower coarsening

factors could be detected for the particulated β -Lg ranging from 0.07 (pH 6.8) to 0.03 (pH 5.6) compared to the native one (0.29 (pH 6.8) to 0.10 (pH 5.6)) (Section 6).

In this context, two different stabilization mechanisms need to be considered. On the one hand, the increasing foam stability with decreasing zeta potential (Section 6) may be linked to the formation of an effective steric barrier to adsorption due to the formation of thick, closely packed, and flexible adsorbed layers (Dombrowski et al., 2017; Engelhardt et al., 2013). On the other hand, the overall high foam stabilities found for β -Lg particles even at high zeta potentials (Section 6 (Kurz, Reitberger et al., 2021)) may be linked to the formation of thicker adsorbed layers and thicker liquid films. Referring to the latter one, an increase in the electrostatic repulsions between the particles may contribute to the disjoining pressure and thus, enhance foam stability by keeping the bubbles at distance (Gochev et al., 2014). In addition, an increase in particle size was shown to enhance both the thickness of the liquid films and the thickness of the adsorbed layer (Dhayal et al., 2015).

This indicates the **particle size** as an important factor contributing to foam stability. However, in the context of particle-stabilized foams, different stabilization mechanisms are discussed. On the basis of inorganic particles, the particle size and the contact angle were reported to be the main contributors to foam stability as summarized in the 'Pickering concept' (Section 1) (Pickering, 1907). In this regard, it is important to note that this concept is not applicable to deformable and porous particles such as protein-based particles (Schmidt et al., 2011). Thus, other stabilization theories need to be considered in connection with protein-particle stabilized foams. On the one hand, stabilization is often related to lamellae blocking by the particles, i.e., reducing liquid drainage and thus, reducing film thinning and the subsequent coalescence (Moro et al., 2011; Rullier et al., 2008; Schmitt et al., 2014). In this regard, the drainage behavior of foams stabilized by protein particles of similar zeta potential (~ -30 to ~ -27 mV), but different size ranging from 5 nm (native β -Lg) up to 70 nm were compared. However, no clear correlation could be drawn between the percentage of drainage after 5 min and the particle size. Consequently, foam stabilization due to size-based lamellae blocking seems to be less important with protein-based particles (Kurz, Dombrowski et al., 2021). This indicates that other structural characteristics may be of higher significance than size alone.

In this regard, the degree of **disulfide cross-linking** as a measure for **structural flexibility** was hypothesized to be an important factor. Due to enhanced particle-particle interactions within the surface film formed by less cross-linked particles, an increasing surface film elasticity and thus, a higher foam stability were assumed. In this context, the coarsening factors ($t = 60$ min) of particulated β -Lg of different degrees of disulfide cross-linking were compared by keeping the other properties constant (Kurz, Reitberger et al., 2021). By doing so, significant differences in the coarsening factors ranging between 0.32 and 0.07 could be detected. This assumption is supported by the lower final ($t = 3600$ s) surface tension values of the less cross-linked particles, which may be related to a structural rearrangement after adsorption

leading to lower coarsening factors ($t = 60$ min) as can be seen in Fig. 7.7 (Kurz, Reitberger et al., 2021). This is in accordance with the results shown by Dombrowski (2017b), who observed a positive correlation between foam stability and surface dilatational elasticity, i.e., particle-particle interactions. Besides, particle-particle interactions between neighboring bubbles via non-adsorbed particles or narrow distances may be possible as a consequence of low cross-linking degrees, contributing to foam stability by formation of a stable three-dimensionally foam structure. Concluding from these results, structural characteristics, i.e., the combination of disulfide cross-linking and particle size, may be the main contributor to foam stability rather than size-based lamellae blocking (Kurz, Dombrowski et al., 2021).

With regard to the average **surface hydrophobicity**, no significant impact on the foam stability could be detected. In this context, even local surface hydrophobicity differences can be assumed to be unimportant (Kurz, Dombrowski et al., 2021).

Based on these results, some general conclusions guiding the practical optimization of the stability of foams stabilized by non-particulated and particulated proteins can be provided as schematically summarized in Fig. 7.5. First, a high structural flexibility (i.e., a low degree of disulfide cross-linking) and an increasing particle size were shown to be primarily decisive in terms of foam stability. In addition, a decreasing net zeta potential has a positive effect on foam stability. However, this effect is more pronounced with smaller-sized proteins. The average surface hydrophobicity was found to be less important with regard to foam stability. In this regard, even local surface hydrophobicity differences can be assumed to be unimportant.

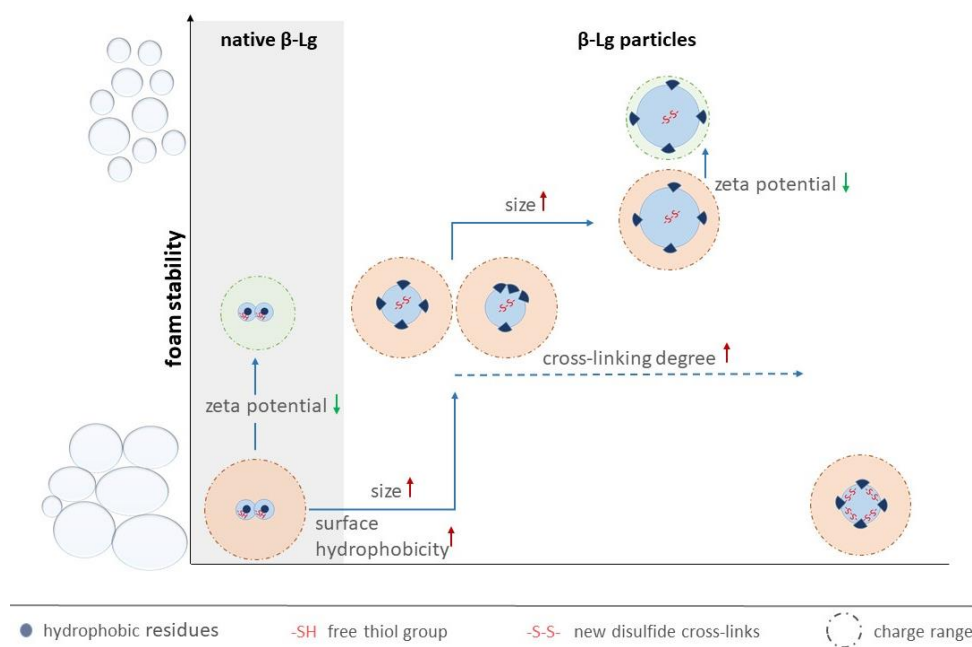


Fig. 7.5: Schematic representation of the impact of protein (particle) size, zeta potential (i.e., charge effective range), and content of disulfide cross-links on the foam stability based on the results from Kurz, Reitberger et al. (2021), Kurz, Dombrowski et al. (2021), Kurz et al. (2020), and Section 6.

7.2.4 Correlation between Interfacial and Foaming Properties

In the previous Sections (7.2.1 to 7.2.3), the influence of individual protein and protein particle characteristics on their interfacial as well as foam formation and stabilization behavior was investigated. In order to assess, whether interfacial and foaming properties are affected in the same way by the individual characteristics, correlations between interfacial and foaming properties were investigated.

As shown in Section 7.2.2, a fast initial surface tension reduction is reflected in a small initial mean bubble area, i.e., high foamability. However, a small initial mean bubble area ($A_{t=5s}$) and thus, a fast initial interfacial adsorption did not correlate with a low coarsening factor ($t = 60$ min), i.e., high foam stability, as can be seen in Fig. 7.6 (Kurz, Dombrowski et al., 2021; Kurz, Reitberger et al., 2021) Section 6). Thus, a fast diffusion to and adsorption at the interface were found to be not primarily decisive in terms of foam stability.

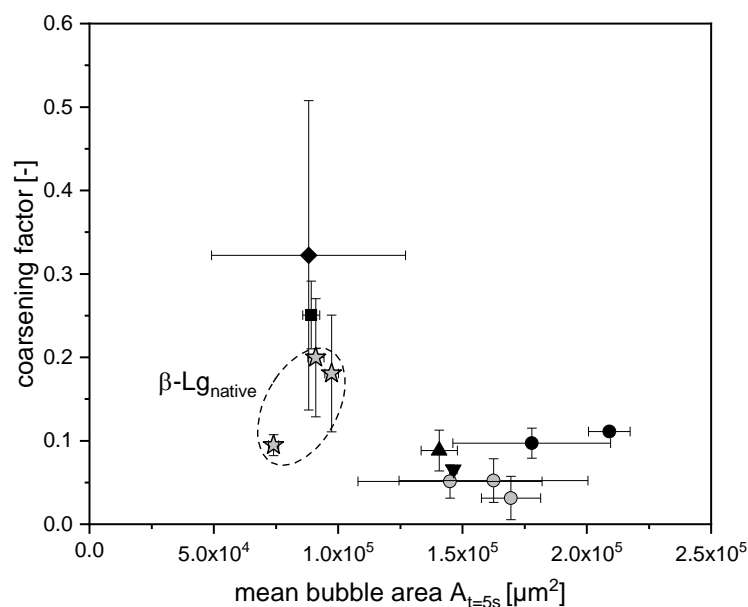


Fig. 7.6: Bubble coarsening factor of native (star symbol) and particulated β -Lg as a function of the mean bubble area ($A_{t=5s}$). (Symbols: black-filled: data from Kurz, Reitberger et al. (2021), gray-filled: based on data from Section 6 and Kurz, Dombrowski et al. (2021)). The reference time for determining the coarsening factor was 60 min.

This indicates differences in the impact and priority of the individual structural properties, i.e., size, zeta potential, degree of cross-linking, and surface hydrophobicity, on the interfacial and foaming properties. In this regard, a decreasing net zeta potential generally promotes the diffusion to and adsorption at the interface as well as foam formation and stabilization. An increasing structural flexibility (i.e., a lower cross-linking degree) results in an increasing foam stability, while the initial adsorption behavior and thus, the foam formation properties are not influenced. However, at longer measurement times, the final ($t = 3600$ s) surface tension values were found to decrease more strongly with increasing structural flexibility (Kurz, Reitberger et al., 2021). This can be linked to a more pronounced structural rearrangement after adsorption. This in turn resulted in lower coarsening factors

($t = 60$ min) as can be seen in Fig. 7.7 (Kurz, Reitberger et al., 2021). Following this, the final surface tension values are influenced by the structural flexibility. Thus, within certain limits, the final surface tension values can be correlated with foam stability.

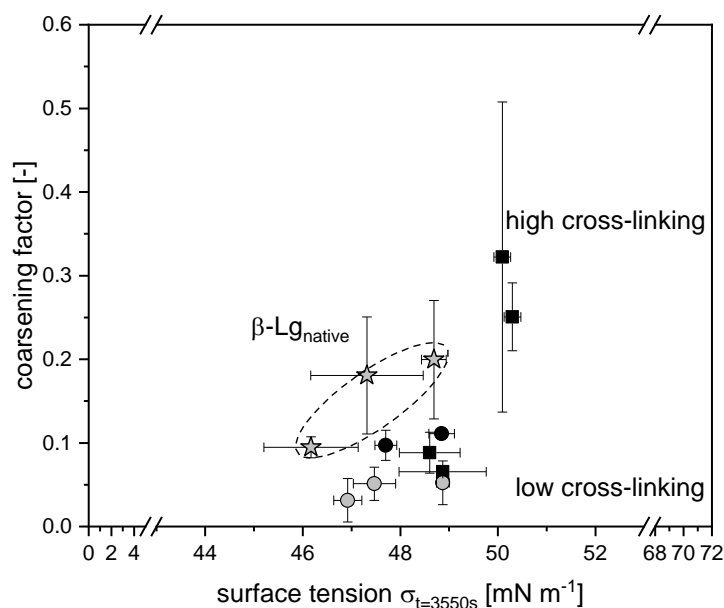


Fig. 7.7: Bubble coarsening factor of native (star symbol) and particulated β -Lg as a function of the final ($t = 3550$ s) surface tension values. (Symbols: black-filled: data from Kurz, Reitberger et al. (2021), gray-filled: based on data from Section 6 and Kurz, Dombrowski et al. (2021)). The reference time for determining the coarsening factor was 60 min.

The surface hydrophobicity was found to behave in the opposite way, i.e., it was not decisive with regard to foam stabilization but the initial surface tension reduction was influenced. However, the distribution of the hydrophobic patches at the surface seems to be more crucial than the average surface hydrophobicity. The particle size was found to be decisive for both foaming and interfacial properties, whereby contrary effects were observed. While the diffusion to and adsorption at the interface tends to be enhanced with decreasing particle size, foam stability appears to decrease.

The results of this thesis show that unfavorable protein particle characteristics can be balanced out by distinctly modulating other particle characteristics within certain limits. This means that not a single property alone is decisive but rather the interaction of the individual properties.

7.2.5 Comparison of Techno-Functionality as Affected by the Purification Method

Different purification methods (i.e., isoelectric precipitation or membrane filtration (Section 7.1)) were used for particle purification within the different data sets (Kurz, Dombrowski et al., 2021; Kurz, Reitberger et al., 2021; Section 6). Thus, in order to assess whether an influence of the purification method exists, the particles were compared in terms of significant differences in their functionality in dependence of the purification method (p -value = 0.05, two sampled t -test, one-tailed, assuming equal variances in the respective data sets, OriginPro 2018b). The results are shown in Tab. 7-2. In this context, negligible ($t < 0.05$) differences in the initial ($t = 5$ s) and final

($t = 3550$ s) surface pressure values as well as in the foam stability (i.e., coarsening factor (α) and foam stability after 60 min) could be detected. Based on these results, it was assumed that the purification methods can be applied interchangeably without changing the functionality of the particles.

Tab. 7-2: Physiochemical (median particle diameter ($d_{50.3}$), interfacial (surface (π_6) and interfacial pressure (π_γ)), foaming (coarsening factor (α) foam stability ($FS_{60\text{min}}$) and emulsifying characteristics (median oil droplet size ($d_{50.3\text{SF}}$)) of heat-induced β -Lg particles under variation of heating pH and NaCl concentration as a function of the purification method (isoelectric precipitation (IE-P) and membrane filtration in diafiltration mode (DF)).

heating	pH 5.8 / 0 mM NaCl		pH 8.5 / 60 mM NaCl	
method	IE-P	DF	IE-P	DF
$d_{50.3, \text{ heated}}$ (nm)	80 ± 3^a	70 ± 3	25 ± 1^a	25 ± 1
$d_{50.3, \text{ purified}}$ (nm)	119 ± 10^a	69 ± 6^b	22 ± 2^a	21 ± 1^b
$ZP_{\text{pH } 6.8}$ mV	-38 ± 1.1^a	-36 ± 1.2^b	-29 ± 2.2^a	-26.8 ± 0.1^b
a/w	pH 6.2		pH 6.8	
$\pi_{\sigma 5s}$ (mN m ⁻¹)	15.8 ± 1.3^a	14.9 ± 0.1^b	15.9 ± 1^a	16.3 ± 0.0^b
$\pi_{\sigma 3550s}$ (mN m ⁻¹)	24.3 ± 0.5^a	23.2 ± 0.4^b	23.1 ± 0.6^a	23.4 ± 1.3^b
$\alpha_{t=60 \text{ min}}$ (-)	0.097 ± 0.018^a	0.051 ± 0.020^c	n.d.	n.d.
$\alpha_{t=90 \text{ min}}$ (-)	n.d.	0.068 ± 0.023^c	n.d.	n.d.
$FS_{60\text{min}}$ (%)	n.d.	n.d.	88.9 ± 5.6^d	88.6 ± 0.6^b

n.d. not determined

^a Data from Kurz, Reitberger et al. (2021)

^b Data from Kurz, Dombrowski et al. (2021)

^c Based on data from Section 6

^d Data not shown

7.3 Transferability of Results from Air/Water to Oil/Water Interfaces

Apart from foams, emulsions are another group of thermodynamically instable food matrices. In the case of o/w interfaces, the oil type also has an impact on the interfacial characteristics due to different impurities of minor components and/or differences in the hydrophobicity and thus influences the emulsification process (Bergfreund et al., 2018; Bergfreund et al., 2021; Dopierala et al., 2011; Gmach et al., 2019; Gomes et al., 2018). The question arises, whether emulsion and foam formation as well as stabilization can be linked to the same particle properties, and therefore, whether the explanatory approaches found for air/water can be directly transferred to oil/water interfaces.

Interfacial Behavior

In general, the adsorption behavior of non-particulated and particulated β -Lg at the oil/water interface determined by means of the initial ($t = 5$ s) interfacial tension reduction can be linked to the same protein characteristics as for the air/water interface (Kurz, Dombrowski et al., 2021; Kurz, Reitberger et al., 2021). In brief, decreasing the net zeta potential was found to fasten the adsorption at both types of interface. By contrast, a decreasing particle size (at a constant zeta potential) was less important for both systems. As with foams, the distribution of hydrophobic residues on the surface of proteins appears to be more important than the average surface hydrophobicity for diffusion to and adsorption at the oil/water interface. A decreasing cross-linking degree was found to be unimportant during the initial regime of interfacial adsorption. However, at longer measurement times ($t = 3550$ s), lower cross-linking degrees decreased the surface tension more strongly than higher ones, whereas no significant effect on the interfacial tension could be detected over the whole measurement duration. This could be an indication that particle rearrangement at the oil/water interface requires a longer time than at the air/water interface. Concluding from these results, the interfacial behavior at the air/water and oil/water interface can be generally linked to the same particle properties.

By directly comparing the interfacial properties of the specific protein particles by the evolution of the surface and interfacial pressure (Eq. (4-3) and Eq. (4-4)), the surface pressure was found to increase faster and to higher values compared to the interfacial pressure (Kurz, Reitberger et al., 2021). This may indicate a lower barrier of adsorption and a higher protein packing density at the air/water compared to the oil/water interface. However, different results can be found in the literature, i.e., showing a higher pressure at the oil/water interface or the air/water interface (Hinderink et al., 2020; Krägel et al., 2003).

However, it is important to mention that the oil type also has an impact on the evolution of the interfacial tension and thus, the interfacial rearrangement at the oil/water interface (Bergfreund et al., 2018; Dopierala et al., 2011; Gmach et al., 2019; Gomes et al., 2018). This can be referred to differences in the fatty acid chain length, the degree of saturation, and/or impurities such as monoacylglycerides resulting from the oil production process. In order to clarify the impact of the oil type, the evolution

of the interfacial tension was investigated for a commercial sunflower (SF) oil and medium chain triglycerides (MCTs)). While the MCT/water interface showed a nearly constant interfacial tension, the value decreased for SF/water interface upon time. This indicates the presence of surface-active molecules in the SF oil. Investigating the interfacial behavior of native and particulated β -Lg at the different types of oil, significantly higher normalized interfacial pressures (Eq. (5-5)) could be detected for the MCTs. This indicates that the surface-active components adsorb at the interface from the oil side. Consequently, protein adsorption from the aqueous side is a less effective or in a secondary layer (Kurz, Dombrowski et al., 2021).

Foaming and Emulsifying Properties

In general, foam and emulsion stability can be linked to different parameters. In the context of this thesis, foam stability was referred to the evolution of the normalized foam height or the mean bubble area over time. Related to the latter one, the coarsening factor was determined (Section 4.2.7). For emulsion stability, the oil droplet size immediately after emulsification was used as an indicator. In addition, oil droplet aggregation (Section 4.2.8) or coagulation (Section 5.2.11) were considered as stability criteria.

In the context of physicochemical properties being relevant in terms of foam and emulsion stabilization, differences were detected. While an increase in particle size and a decreasing cross-linking degree can be positively correlated with foam stability, emulsion stability (i.e., oil droplet size) was reduced. This indicates that foam and emulsion stability can not be linked to the same particle properties (Kurz, Reitberger et al., 2021). However, the foam and emulsion characteristics (i.e., disperse volume fraction φ of air or oil and the disperse volume to protein ratio) need to be considered additionally in order to explain the observed differences. While the disperse volume fraction was 0.1 and the oil-to-protein ratio close to 10:1 in terms of emulsions, the air content was much higher in terms of foams with a value of 0.9 and an air-to-protein ratio close to 90:1. In consequence, larger-sized air bubbles ($> 100\mu\text{m}$) of high packing density compared to smaller-sized oil droplets ($< 5\mu\text{m}$) were formed (Kurz, Dombrowski et al., 2021; Kurz, Reitberger et al., 2021). The high disperse volume fraction in terms of foams may lead to the formation of closely packed systems, which enables the formation of a three-dimensional network between adsorbed particles at the interface and non-adsorbed particles in the continuous phase resulting in an increased stability. This network formation is favored by less cross-linked particles. In the case of emulsions with a low disperse volume fraction as used in this study, network formation between oil droplets favors creaming. In consequence, an increase in the disperse volume fraction of emulsions may also contribute to network formation and thus, to higher emulsion stability against creaming.

As a second point, the foam and emulsion formation process, i.e., the transport mechanisms for surface active material to the interface need to be considered. While foams were prepared by air sparging, which mainly results in diffusive transport to the interface, emulsions were produced by high pressure homogenization, which

mainly results in convective transport of particles towards the interface. However, no significant impact of the oil type on the emulsion stability could be detected (Kurz, Dombrowski et al., 2021).

Concluding from these results, explanatory approaches for stabilizing foams and emulsions cannot be used interchangeably. In addition, factors others than the proteins' physicochemical characteristics such as the disperse volume fraction and the foaming/ emulsification process need to be considered. However, the results found in this thesis provide some general conclusions guiding the practical optimization of the stability of foams and emulsions stabilized by non-particulated and particulated proteins.

8 Appendix

Peer Reviewed Publications (included in this thesis)

Kurz, F.; Hengst, C.; Kulozik, U. (2020): RP-HPLC method for simultaneous quantification of free and total thiol groups in native and heat aggregated whey proteins. *MethodsX*. 7: 101112.

Kurz, F.; Reitberger, V.; Hengst, C.; Bilke-Krause, C.; Kulozik, U.; Dombrowski, J. (2021): Correlation between Physico-Chemical Characteristics of Particulated β -Lactoglobulin and Its Behavior at Air/Water and Oil/Water Interfaces. *Foods (Basel, Switzerland)*. 10 (6): 1426.

Kurz, F.; Dombrowski, J.; Matyssek, A.; Hartinger, M.; Kulozik, U. (2021): Technofunctionality of β -Lg and β -Lg Nanosized Particles at Air/Water and Oil/Water Interfaces as a Function of Structural and Surface Characteristics. *ACS Food Science & Technology*.

Peer Reviewed Publications (not included in this thesis)

Hartinger, M.; Napiwotzki, J.; Schmid, E.-M.; Hoffmann, D.; Kurz, F.; Kulozik, U. (2020a): Influence of Spacer Design and Module Geometry on the Filtration Performance during Skim Milk Microfiltration with Flat Sheet and Spiral-Wound Membranes. *Membranes*. 10 (4).

Hartinger, M.; Napiwotzki, J.; Schmid, E.-M.; Kurz, F.; Kulozik, U. (2020b): Semi-quantitative, spatially resolved analysis of protein deposit layers on membrane surfaces. *MethodsX*. 7: 100780.

Non Reviewed Publications

Kurz, F. (2017): Stabilisierung von Emulsionen durch proteinbasierte Partikel. Jahresbericht 2016 der milchwissenschaftlichen Forschung am „Zentralinstitut für Ernährungs- und Lebensmittelforschung Weihenstephan (ZIEL)“ und am „Wissenschaftszentrum Weihenstephan (WZW)“. ISBN: 978-3-939182-93-1.

Kurz, F. (2018): Stabilisierung von Emulsionen durch proteinbasierte Partikel. Jahresbericht 2017 der milchwissenschaftlichen Forschung am „Zentralinstitut für Ernährungs- und Lebensmittelforschung Weihenstephan (ZIEL)“ und am „Wissenschaftszentrum Weihenstephan (WZW)“. ISBN: 978-3-947492-00-8.

Kurz, F. (2019): Herstellung, Charakterisierung und Emulgierereigenschaften proteinbasierter Partikel. Jahresbericht 2018 der milchwissenschaftlichen Forschung am „Zentralinstitut für Ernährungs- und Lebensmittelforschung Weihenstephan (ZIEL)“ und am „Wissenschaftszentrum Weihenstephan (WZW)“. ISBN: 978-3-947492-10-7.

Kurz, F.; Engel, J. (2020): Schäumungseigenschaften von Eigelbfraktionen. Jahresbericht 2019 der milchwissenschaftlichen Forschung am „Zentralinstitut für Ernährungs- und Lebensmittelforschung Weihenstephan (ZIEL)“ und am „Wissenschaftszentrum Weihenstephan (WZW)“. ISBN: 978-3-947492-16-9.

Kurz, F.; Hengst, C. (2021): Bestimmung von freien Thiolgruppen mittels einer neuen RP-HPLC-Methode. Jahresbericht 2020 der milchwissenschaftlichen Forschung am „Zentralinstitut für Ernährungs- und Lebensmittelforschung Weihenstephan (ZIEL)“ und am „Wissenschaftszentrum Weihenstephan (WZW)“. ISBN: 978-3-947492-20-6.

Oral and Poster Presentations

Kurz, F.; Kulozik, U. (2017). Poster presentation: Stabilisierung von Emulsionen durch proteinbasierte Partikel. Jahrestreffen der ProcessNet-Fachgruppe Lebensmittelverfahrenstechnik, Bruchsal, Februar 2017.

Kurz, F.; Kulozik, U. (2018). Oral presentation: Stabilisierung von Emulsionen und Schäumen durch Molkenproteinpartikel. Weihenstephaner Milchwirtschaftliche Herbsttagung, Freising, Germany, October 2018.

Kurz, F.; Kulozik, U. (2019). Oral presentation: A novel mechanistic understanding for the stabilization of emulsions and foams by native or aggregated whey proteins. International Congress on Engineering and Food ICEF13, Melbourne, Australia, September 2019.

9 References

- Al-Malah, K. (2000). Emulsifying properties of BSA in different vegetable oil emulsions using conductivity technique. *Food Hydrocolloids*, *14*(5), 485–490. [https://doi.org/10.1016/S0268-005X\(00\)00028-X](https://doi.org/10.1016/S0268-005X(00)00028-X)
- Alting, A. C., Hamer, R. J., Kruif, C. G. de, Paques, M., & Visschers, R. W. (2003). Number of thiol groups rather than the size of the aggregates determines the hardness of cold set whey protein gels. *Food Hydrocolloids*, *17*(4), 469–479. [https://doi.org/10.1016/S0268-005X\(03\)00023-7](https://doi.org/10.1016/S0268-005X(03)00023-7)
- Amagliani, L., & Schmitt, C. (2017). Globular plant protein aggregates for stabilization of food foams and emulsions. *Trends in Food Science & Technology*, *67*, 248–259. <https://doi.org/10.1016/j.tifs.2017.07.013>
- Amagliani, L., Silva, J. V.C., Saffon, M., & Dombrowski, J. (2021). On the foaming properties of plant proteins: Current status and future opportunities. *Trends in Food Science & Technology*, *118*(4), 261–272. <https://doi.org/10.1016/j.tifs.2021.10.001>
- Anazadehsayed, A., Rezaee, N., Naser, J., & Nguyen, A. V. (2018). A review of aqueous foam in microscale. *Advances in Colloid and Interface Science*, *256*, 203–229. <https://doi.org/10.1016/j.cis.2018.04.004>
- Andlinger, D. J., Röscheisen, P., Hengst, C., & Kulozik, U. (2021). Influence of pH, Temperature and Protease Inhibitors on Kinetics and Mechanism of Thermally Induced Aggregation of Potato Proteins. *Foods (Basel, Switzerland)*, *10*(4). <https://doi.org/10.3390/foods10040796>
- Andrade, J., & Corredig, M. (2016). Vitamin D3 and phytosterols affect the properties of polyglycerol polyricinoleate (PGPR) and protein interfaces. *Food Hydrocolloids*, *54*(1), 278–283. <https://doi.org/10.1016/j.foodhyd.2015.10.001>
- Bals, A., & Kulozik, U. (2003). Effect of pre-heating on the foaming properties of whey protein isolate using a membrane foaming apparatus. *International Dairy Journal*, *13*(11), 903–908. [https://doi.org/10.1016/S0958-6946\(03\)00111-0](https://doi.org/10.1016/S0958-6946(03)00111-0)
- Berg, J. M., Tymoczko, J. L., Stryer, L., & Gatto, G. J. (2014). *Biochemie* (7. Auflage, korrigierter Nachdruck). *Lehrbuch*. Berlin, Heidelberg: Springer Spektrum.
- Bergeron, V. (1999). Forces and structure in thin liquid soap films. *Journal of Physics: Condensed Matter*, *11*(19), R215–R238. <https://doi.org/10.1088/0953-8984/11/19/201>
- Bergfreund, J., Bertsch, P., & Fischer, P. (2021). Adsorption of proteins to fluid interfaces: Role of the hydrophobic subphase. *Journal of Colloid and Interface Science*, *584*, 411–417. <https://doi.org/10.1016/j.jcis.2020.09.118>
- Bergfreund, J., Bertsch, P., Kuster, S., & Fischer, P. (2018). Effect of Oil Hydrophobicity on the Adsorption and Rheology of β -Lactoglobulin at Oil-Water Interfaces. *Langmuir : the ACS Journal of Surfaces and Colloids*, *34*(16), 4929–4936. <https://doi.org/10.1021/acs.langmuir.8b00458>
- Berry, J. D., Neeson, M. J., Dagastine, R. R., Chan, D. Y. C., & Tabor, R. F. (2015). Measurement of surface and interfacial tension using pendant drop tensiometry.

- Journal of Colloid and Interface Science*, 454, 226–237.
<https://doi.org/10.1016/j.jcis.2015.05.012>
- Berton-Carabin, C. C., & Schroen, K. (2015). Pickering emulsions for food applications: background, trends, and challenges. *Annual Review of Food Science and Technology*, 6, 263–297. <https://doi.org/10.1146/annurev-food-081114-110822>
- Beverung, C. J., Radke, C. J., & Blanch, H. W. (1999). Protein adsorption at the oil/water interface: Characterization of adsorption kinetics by dynamic interfacial tension measurements. *Biophysical Chemistry*, 81(1), 59–80.
[https://doi.org/10.1016/S0301-4622\(99\)00082-4](https://doi.org/10.1016/S0301-4622(99)00082-4)
- Binks, B. P. (2002). Particles as surfactants—similarities and differences. *Current Opinion in Colloid & Interface Science*, 7(1-2), 21–41. [https://doi.org/10.1016/S1359-0294\(02\)00008-0](https://doi.org/10.1016/S1359-0294(02)00008-0)
- Bos, A. M., & van Vliet, T. (2001). Interfacial rheological properties of adsorbed protein layers and surfactants: A review. *Advances in colloid and interface science*, 91(3), 437–471. [https://doi.org/10.1016/S0001-8686\(00\)00077-4](https://doi.org/10.1016/S0001-8686(00)00077-4)
- Boye, J. I., Aksay, S., Roufik, S., Ribéreau, S., Mondor, M., Farnworth, E., & Rajamohamed, S. H. (2010). Comparison of the functional properties of pea, chickpea and lentil protein concentrates processed using ultrafiltration and isoelectric precipitation techniques. *Food Research International*, 43(2), 537–546.
<https://doi.org/10.1016/j.foodres.2009.07.021>
- Buchcic, C., Tromp, R. H., Meinders, M. B. J., & Cohen Stuart, M. A. (2017). Harnessing the advantages of hard and soft colloids by the use of core-shell particles as interfacial stabilizers. *Soft Matter*, 13(7), 1326–1334.
<https://doi.org/10.1039/C6SM02159J>
- Butler, J. E. (1969). Bovine Immunoglobulins: A Review. *Journal of Dairy Science*, 52(12), 1895–1909. [https://doi.org/10.3168/jds.S0022-0302\(69\)86871-2](https://doi.org/10.3168/jds.S0022-0302(69)86871-2)
- Calvo, M. M., & La Hoz, L. de (1992). Flavour of heated milks. A review. *International Dairy Journal*, 2(2), 69–81. [https://doi.org/10.1016/0958-6946\(92\)90001-3](https://doi.org/10.1016/0958-6946(92)90001-3)
- Cheison, S. C., Lai, M.-Y., Leeb, E., & Kulozik, U. (2011). Hydrolysis of β -lactoglobulin by trypsin under acidic pH and analysis of the hydrolysates with MALDI-TOF-MS/MS. *Food chemistry*, 125(4), 1241–1248.
<https://doi.org/10.1016/j.foodchem.2010.10.042>
- Chen, Q., Stricek, I., Gray, M. R., & Liu, Q. (2017). Influence of hydrophobicity distribution of particle mixtures on emulsion stabilization. *Journal of Colloid and Interface Science*, 491, 179–189. <https://doi.org/10.1016/j.jcis.2016.12.045>
- Chen, W., Zhao, Y., Seefeldt, T., & Guan, X. (2008). Determination of thiols and disulfides via HPLC quantification of 5-thio-2-nitrobenzoic acid. *Journal of Pharmaceutical and Biomedical Analysis*, 48(5), 1375–1380.
<https://doi.org/10.1016/j.jpba.2008.08.033>

- Cong, Y., Zhang, W., Liu, C., & Huang, F. (2020). Composition and Oil-Water Interfacial Tension Studies in Different Vegetable Oils. *Food Biophysics*, 15(2), 229–239. <https://doi.org/10.1007/s11483-019-09617-8>
- Damodaran, S. (2005). Protein Stabilization of Emulsions and Foams. *Journal of food science*, 70(3), R54-R66. <https://doi.org/10.1111/j.1365-2621.2005.tb07150.x>
- Dannenbergh, F., & Kessler, H.-G. (1988). Reaction Kinetics of the Denaturation of Whey Proteins in Milk. *Journal of food science*, 53(1), 258–263. <https://doi.org/10.1111/j.1365-2621.1988.tb10223.x>
- Delahaije, R. J. B. M., Gruppen, H., Giuseppin, M. L. F., & Wierenga, P. A. (2015). Towards predicting the stability of protein-stabilized emulsions. *Advances in Colloid and Interface Science*, 219, 1–9. <https://doi.org/10.1016/j.cis.2015.01.008>
- Delahaije, R. J. B. M., Wierenga, P. A., Giuseppin, M. L. F., & Gruppen, H. (2015). Comparison of heat-induced aggregation of globular proteins. *Journal of Agricultural and Food Chemistry*, 63(21), 5257–5265. <https://doi.org/10.1021/acs.jafc.5b00927>
- Delahaije, R. J.B.M., Hilgers, R. J., Wierenga, P. A., & Gruppen, H. (2017). Relative contributions of charge and surface coverage on pH-induced flocculation of protein-stabilized emulsions. *Colloids and Surfaces A: Physicochemical and Engineering Aspects*, 521, 153–160. <https://doi.org/10.1016/j.colsurfa.2016.10.043>
- Demetriades, K., & McClements, D. J. (2000). Influence of sodium dodecyl sulfate on the physicochemical properties of whey protein-stabilized emulsions. *Colloids and Surfaces A: Physicochemical and Engineering Aspects*, 161(3), 391–400. [https://doi.org/10.1016/S0927-7757\(99\)00210-1](https://doi.org/10.1016/S0927-7757(99)00210-1)
- Denkov, N., Tcholakova, S., & Politova-Brinkova, N. (2020). Physicochemical control of foam properties. *Current Opinion in Colloid & Interface Science*, 50, 101376. <https://doi.org/10.1016/j.cocis.2020.08.001>
- Destribats, M., Eyharts, M., Lapeyre, V., Sellier, E., Varga, I., Ravaine, V., & Schmitt, V. (2014). Impact of pNIPAM microgel size on its ability to stabilize Pickering emulsions. *Langmuir : the ACS Journal of Surfaces and Colloids*, 30(7), 1768–1777. <https://doi.org/10.1021/la4044396>
- Destribats, M., Lapeyre, V., Wolfs, M., Sellier, E., Leal-Calderon, F., Ravaine, V., & Schmitt, V. (2011). Soft microgels as Pickering emulsion stabilisers: Role of particle deformability. *Soft matter*, 7(17), 7689. <https://doi.org/10.1039/C1SM05240C>
- Destribats, M., Rouvet, M., Gehin-Delval, C., Schmitt, C., & Binks, B. P. (2014). Emulsions stabilised by whey protein microgel particles: towards food-grade Pickering emulsions. *Soft Matter*, 10(36), 6941–6954. <https://doi.org/10.1039/C4SM00179F>
- Dhayal, S. K., Delahaije, R. J. B. M., Vries, R. J. de, Gruppen, H., & Wierenga, P. A. (2015). Enzymatic cross-linking of α -lactalbumin to produce nanoparticles with increased foam stability. *Soft Matter*, 11(40), 7888–7898. <https://doi.org/10.1039/c5sm01112d>

- Dhayal, S. K., Gruppen, H., Vries, R. de, & Wierenga, P. A. (2014). Controlled formation of protein nanoparticles by enzymatic cross-linking of α -lactalbumin with horseradish peroxidase. *Food Hydrocolloids*, 36(16), 53–59. <https://doi.org/10.1016/j.foodhyd.2013.09.003>
- Dickinson, E. (Ed.) (1995). *Food macromolecules and colloids: [the proceedings of a conference organized by the Food Chemistry Group of The Royal Society of Chemistry, held at ENSBANA, Université de Bourgogne, Dijon, France on 23 - 25 March 1994]. Special publication / Royal Society of Chemistry: Vol. 156.* Cambridge.
- Dickinson, E. (1999). Adsorbed protein layers at fluid interfaces: Interactions, structure and surface rheology. *Colloids and Surfaces B: Biointerfaces*, 15(2), 161–176. [https://doi.org/10.1016/S0927-7765\(99\)00042-9](https://doi.org/10.1016/S0927-7765(99)00042-9)
- Dickinson, E. (Ed.) (2005). *Food emulsions and foams: Based on the proceedings of an International Symposium organised by the Food Chemistry Group of The Royal Society of Chemistry at Leeds from 24th to 26th March 1986. Woodhead Publishing Series in Food Science, Technology and Nutrition.* Cambridge, England: Woodhead Publishing. Retrieved from <http://search.ebscohost.com/login.aspx?direct=true&scope=site&db=nlebk&db=nlabk&AN=689099>
- Dickinson, E. (2010). Flocculation of protein-stabilized oil-in-water emulsions. *Colloids and Surfaces. B, Biointerfaces*, 81(1), 130–140. <https://doi.org/10.1016/j.colsurfb.2010.06.033>
- Dickinson, E. (2012). Use of nanoparticles and microparticles in the formation and stabilization of food emulsions. *Trends in Food Science & Technology*, 24(1), 4–12. <https://doi.org/10.1016/j.tifs.2011.09.006>
- Dickinson, E. (2015). Microgels — An alternative colloidal ingredient for stabilization of food emulsions. *Trends in Food Science & Technology*, 43(2), 178–188. <https://doi.org/10.1016/j.tifs.2015.02.006>
- Dickinson, E. (2017). Biopolymer-based particles as stabilizing agents for emulsions and foams. *Food Hydrocolloids*, 68, 219–231. <https://doi.org/10.1016/j.foodhyd.2016.06.024>
- Dombrowski, J., Gschwendtner, M., & Kulozik, U. (2017). Evaluation of structural characteristics determining surface and foaming properties of β -lactoglobulin aggregates. *Colloids and Surfaces A: Physicochemical and Engineering Aspects*, 516, 286–295. <https://doi.org/10.1016/j.colsurfa.2016.12.045>
- Dombrowski, J. (2017a). *Structural characterization of milk protein-stabilized foams: A multiscale approach.* Technische Universität München.
- Dombrowski, J. (2017b). *Structural characterization of milk protein-stabilized foams: A multiscale approach (Dissertation).* Technische Universität München.
- Dombrowski, J., Gschwendtner, M., Saalfeld, D., & Kulozik, U. (2018). Salt-dependent interaction behavior of β -Lactoglobulin molecules in relation to their

- surface and foaming properties. *Colloids and Surfaces A: Physicochemical and Engineering Aspects*, 558, 455–462. <https://doi.org/10.1016/j.colsurfa.2018.09.015>
- Dombrowski, J., Johler, F., Warncke, M., & Kulozik, U. (2016). Correlation between bulk characteristics of aggregated β -lactoglobulin and its surface and foaming properties. *Food Hydrocolloids*, 61, 318–328. <https://doi.org/10.1016/j.foodhyd.2016.05.027>
- Donato, L., Schmitt, C., Bovetto, L., & Rouvet, M. (2009). Mechanism of formation of stable heat-induced β -lactoglobulin microgels. *International Dairy Journal*, 19(5), 295–306. <https://doi.org/10.1016/j.idairyj.2008.11.005>
- Dopierala, K., Javadi, A., Krägel, J., Schano, K.-H., Kalogianni, E. P., Leser, M. E., & Miller, R. (2011). Dynamic interfacial tensions of dietary oils. *Colloids and Surfaces A: Physicochemical and Engineering Aspects*, 382(1-3), 261–265. <https://doi.org/10.1016/j.colsurfa.2010.11.027>
- Dumpler, J., Wohlschläger, H., & Kulozik, U. (2017). Dissociation and coagulation of caseins and whey proteins in concentrated skim milk heated by direct steam injection. *Dairy Science & Technology*, 96(6), 807–826. <https://doi.org/10.1007/s13594-016-0304-3>
- Ellman, G. L. (1959). Tissue sulfhydryl groups. *Archives of Biochemistry and Biophysics*, 82(1), 70–77. [https://doi.org/10.1016/0003-9861\(59\)90090-6](https://doi.org/10.1016/0003-9861(59)90090-6)
- Engelhardt, K., Lexis, M., Gochev, G., Konnerth, C., Miller, R., Willenbacher, N., . . . Braunschweig, B. (2013). pH effects on the molecular structure of β -lactoglobulin modified air-water interfaces and its impact on foam rheology. *Langmuir: the ACS Journal of Surfaces and Colloids*, 29(37), 11646–11655. <https://doi.org/10.1021/la402729g>
- Fainerman, V. B., & Miller, R. (2005). Equilibrium and Dynamic Characteristics of Protein Adsorption Layers at Gas-Liquid Interfaces: Theoretical and Experimental Data. *Colloid Journal*, 67(4), 393–404. <https://doi.org/10.1007/s10595-005-0110-8>
- Feng, Y., & Lee, Y. (2016). Surface modification of zein colloidal particles with sodium caseinate to stabilize oil-in-water pickering emulsion. *Food Hydrocolloids*, 56, 292–302. <https://doi.org/10.1016/j.foodhyd.2015.12.030>
- Fox, P. F., & McSweeney, P. L. H. (1998). *Dairy chemistry and biochemistry* (1. ed.). London: Blackie Acad. & Professional.
- Friedman, M. (1999). Lysinoalanine in food and in antimicrobial proteins. *Advances in Experimental Medicine and Biology*, 459, 145–159. https://doi.org/10.1007/978-1-4615-4853-9_10
- Fuhrmann, P. L., Sala, G., Stieger, M., & Scholten, E. (2019). Clustering of oil droplets in o/w emulsions: Controlling cluster size and interaction strength. *Food Research International (Ottawa, Ont.)*, 122, 537–547. <https://doi.org/10.1016/j.foodres.2019.04.027>
- Gibbs (Ed.) (1961). *The scientific papers of J. Willard Gibbs. 1: Thermodynamics*. New York: Dover Publ.

- Gmach, O., Bertsch, A., Bilke-Krause, C., & Kulozik, U. (2019). Impact of oil type and pH value on oil-in-water emulsions stabilized by egg yolk granules. *Colloids and Surfaces A: Physicochemical and Engineering Aspects*, 581, 123788. <https://doi.org/10.1016/j.colsurfa.2019.123788>
- Gochev, G., Retzlaff, I., Aksenenko, E. V., Fainerman, V. B., & Miller, R. (2013). Adsorption isotherm and equation of state for β -Lactoglobulin layers at the air/water surface. *Colloids and Surfaces A: Physicochemical and Engineering Aspects*, 422, 33–38. <https://doi.org/10.1016/j.colsurfa.2013.01.008>
- Gochev, G., Retzlaff, I., Exerowa, D., & Miller, R. (2014). Electrostatic stabilization of foam films from β -lactoglobulin solutions. *Colloids and Surfaces A: Physicochemical and Engineering Aspects*, 460, 272–279. <https://doi.org/10.1016/j.colsurfa.2013.12.037>
- Gomes, A., Costa, A. L. R., & Cunha, R. L. (2018). Impact of oil type and WPI/Tween 80 ratio at the oil-water interface: Adsorption, interfacial rheology and emulsion features. *Colloids and Surfaces B: Biointerfaces*, 164, 272–280. <https://doi.org/10.1016/j.colsurfb.2018.01.032>
- Graham, D.E., & Phillips, M.C. (1979). Proteins at liquid interfaces: Kinetics of Adsorption and Surface Denaturation. *Journal of colloid and interface science*, 70(3), 403–414. [https://doi.org/10.1016/0021-9797\(79\)90048-1](https://doi.org/10.1016/0021-9797(79)90048-1)
- Grassetti, D. R., & Murray, J. F. (1967). Determination of sulfhydryl groups with 2,2' - or 4,4' -dithiodipyridine. *Archives of Biochemistry and Biophysics*, 119, 41–49. [https://doi.org/10.1016/0003-9861\(67\)90426-2](https://doi.org/10.1016/0003-9861(67)90426-2)
- Greene, R. F., & Pace, C. N. (1974). Urea and guanidine hydrochloride denaturation of ribonuclease, lysozyme, alpha-chymotrypsin, and beta-lactoglobulin. *The Journal of Biological Chemistry*, 249(17), 5388–5393.
- Griko, Y. V., & Remeta, D. P. (1999). Energetics of solvent and ligand-induced conformational changes in alpha-lactalbumin. *Protein Science : a Publication of the Protein Society*, 8(3), 554–561. <https://doi.org/10.1110/ps.8.3.554>
- Gu, X., Campbell, L. J., & Euston, S. R. (2009). Effects of different oils on the properties of soy protein isolate emulsions and gels. *Food Research International*, 42(8), 925–932. <https://doi.org/10.1016/j.foodres.2009.04.015>
- Hansen, R. E., Østergaard, H., Nørgaard, P., & Winther, J. R. (2007). Quantification of protein thiols and dithiols in the picomolar range using sodium borohydride and 4,4'-dithiodipyridine. *Analytical Biochemistry*, 363(1), 77–82. <https://doi.org/10.1016/j.ab.2007.01.002>
- Hansen, R. E., & Winther, J. R. (2009). An introduction to methods for analyzing thiols and disulfides: Reactions, reagents, and practical considerations. *Analytical Biochemistry*, 394(2), 147–158. <https://doi.org/10.1016/j.ab.2009.07.051>
- Hartinger, M., & Kulozik, U. (2020). Milk protein fractionation by spiral-wound microfiltration membranes in diafiltration mode - Influence of feed protein concentration and composition on the filtration performance. *International Dairy Journal*, 102, 104606. <https://doi.org/10.1016/j.idairyj.2019.104606>

- Havea, P., Singh, H., & Creamer, L. K. (2000). Formation of new protein structures in heated mixtures of BSA and alpha-lactalbumin. *Journal of Agricultural and Food Chemistry*, 48(5), 1548–1556. <https://doi.org/10.1021/jf990736j>
- Havea, P., Carr, A. J., & Creamer, L. K. (2004). The roles of disulphide and non-covalent bonding in the functional properties of heat-induced whey protein gels. *Journal of Dairy Research*, 71(3), 330–339. <https://doi.org/10.1017/s002202990400024x>
- Hebishy, E., Buffa, M., Guamis, B., Blasco-Moreno, A., & Trujillo, A.-J. (2015). Physical and oxidative stability of whey protein oil-in-water emulsions produced by conventional and ultra high-pressure homogenization: Effects of pressure and protein concentration on emulsion characteristics. *Innovative Food Science & Emerging Technologies*, 32, 79–90. <https://doi.org/10.1016/j.ifset.2015.09.013>
- Hebishy, E., Zamora, A., Buffa, M., Blasco-Moreno, A., & Trujillo, A.-J. (2017). Characterization of Whey Protein Oil-In-Water Emulsions with Different Oil Concentrations Stabilized by Ultra-High Pressure Homogenization. *Processes*, 5(4), 6. <https://doi.org/10.3390/pr5010006>
- Hendrix, T., Griko, Y. V., & Privalov, P. L. (2000). A calorimetric study of the influence of calcium on the stability of bovine α -lactalbumin. *Biophysical Chemistry*, 84(1), 27–34. [https://doi.org/10.1016/s0301-4622\(99\)00140-4](https://doi.org/10.1016/s0301-4622(99)00140-4)
- Hinderink, E. B. A., Sagis, L., Schroën, K., & Berton-Carabin, C. C. (2020). Behavior of plant-dairy protein blends at air-water and oil-water interfaces. *Colloids and Surfaces. B, Biointerfaces*, 192, 111015. <https://doi.org/10.1016/j.colsurfb.2020.111015>
- Ho, C. C., & Chow, M. C. (2000). The effect of the refining process on the interfacial properties of palm oil. *Journal of the American Oil Chemists' Society*, 77(2), 191–199. <https://doi.org/10.1007/s11746-000-0031-7>
- Hoffmann, M. A. M., Roefs, S. P. F. M., Verheul, M., van Mil, P. J. J. M., & Kruif, K. G. de (1996). Aggregation of β -lactoglobulin studied by in situ light scattering. *Journal of Dairy Research*, 63(3), 423–440. <https://doi.org/10.1017/S0022029900031939>
- Hoffmann, M. A. M., Sala, G., Olieman, C., & Kruif, K. G. de (1997). Molecular Mass Distributions of Heat-Induced β -Lactoglobulin Aggregates. *Journal of Agricultural and Food Chemistry*, 45(8), 2949–2957. <https://doi.org/10.1021/jf9700788>
- Hoffmann, M. A. M., & van Mil, P. J. J. M. (1997). Heat-Induced Aggregation of β -Lactoglobulin: Role of the Free Thiol Group and Disulfide Bonds. *Journal of Agricultural and Food Chemistry*, 45(8), 2942–2948. <https://doi.org/10.1021/jf960789q>
- Hoffmann, M. A. M., & van Mil, P. J. J. M. (1999). Heat-Induced Aggregation of β -Lactoglobulin as a Function of pH. *Journal of Agricultural and Food Chemistry*, 47(5), 1898–1905. <https://doi.org/10.1021/jf980886e>
- Hussain, R., Gaiani, C., Jeandel, C., Ghanbaja, J., & Scher, J. (2012). Combined effect of heat treatment and ionic strength on the functionality of whey proteins. *Journal of Dairy Science*, 95(11), 6260–6273. <https://doi.org/10.3168/jds.2012-5416>
- Iametti, S., Cairoli, S., Gregori, B. de, & Bonomi, F. (1995). Modifications of High-Order Structures upon Heating of β -Lactoglobulin: Dependence on the Protein

- Concentration. *Journal of Agricultural and Food Chemistry*, 43(1), 53–58.
<https://doi.org/10.1021/jf00049a011>
- Jung, J.-M., Gunes, D. Z., & Mezzenga, R. (2010). Interfacial activity and interfacial shear rheology of native β -lactoglobulin monomers and their heat-induced fibers. *Langmuir : the ACS Journal of Surfaces and Colloids*, 26(19), 15366–15375.
<https://doi.org/10.1021/la102721m>
- Kanthe, A. D., Tu, R., & Maldarelli, C. (2021). *Protein Adsorption at a Gas-Aqueous Interface* (Protein Instability at Interfaces During Drug Product Development): Springer International Publishing.
- Kaptay, G. (2006). On the equation of the maximum capillary pressure induced by solid particles to stabilize emulsions and foams and on the emulsion stability diagrams. *Colloids and Surfaces A: Physicochemical and Engineering Aspects*, 282–283, 387–401. <https://doi.org/10.1016/j.colsurfa.2005.12.021>
- Kato, A., & Nakai, S. (1980). Hydrophobicity determined by a fluorescence probe method and its correlation with surface properties of proteins. *Biochimica et Biophysica Acta (BBA) - Protein Structure*, 624(1), 13–20. [https://doi.org/10.1016/0005-2795\(80\)90220-2](https://doi.org/10.1016/0005-2795(80)90220-2)
- Kim, D. A., Cornec, M., & Narsimhan, G. (2005). Effect of thermal treatment on interfacial properties of beta-lactoglobulin. *Journal of Colloid and Interface Science*, 285(1), 100–109. <https://doi.org/10.1016/j.jcis.2004.10.044>
- Kleinzeller, A., & Bronner, F. (Eds.) (1970). *Current topics in membranes and transport. Current Topics in Membranes and Transport: vol. 1*. New York: Academic Press.
- Klostermeyer, H., & Reimerdes, E. H. (1977). Heat induced crosslinks in milk proteins and consequences for the milk system. *Advances in Experimental Medicine and Biology*, 86B, 263–275. https://doi.org/10.1007/978-1-4757-9113-6_18
- Kontopidis, G., Holt, C., & Sawyer, L. (2004). Invited Review: B-Lactoglobulin: Binding Properties, Structure, and Function. *Journal of Dairy Science*, 87(4), 785–796. [https://doi.org/10.3168/jds.S0022-0302\(04\)73222-1](https://doi.org/10.3168/jds.S0022-0302(04)73222-1)
- Krägel, J., O'Neill, M., Makievski, A. V., Michel, M., Leser, M. E., & Miller, R. (2003). Dynamics of mixed protein–surfactant layers adsorbed at the water/air and water/oil interface. *Colloids and Surfaces B: Biointerfaces*, 31(1-4), 107–114. [https://doi.org/10.1016/S0927-7765\(03\)00047-X](https://doi.org/10.1016/S0927-7765(03)00047-X)
- Krägel, J., & Derkatch, S. R. (2010). Interfacial shear rheology. *Current Opinion in Colloid & Interface Science*, 15(4), 246–255. <https://doi.org/10.1016/j.cocis.2010.02.001>
- Kurz, F., Dombrowski, J., Matyssek, A., Hartinger, M., & Kulozik, U. (2021). Technofunctionality of β -Lg and β -Lg Nanosized Particles at Air/Water and Oil/Water Interfaces as a Function of Structural and Surface Characteristics. *ACS Food Science & Technology*. Advance online publication. <https://doi.org/10.1021/acscfoodscitech.1c00337>

- Kurz, F., Hengst, C., & Kulozik, U. (2020). RP-HPLC method for simultaneous quantification of free and total thiol groups in native and heat aggregated whey proteins. *MethodsX*, 7, 101112. <https://doi.org/10.1016/j.mex.2020.101112>
- Kurz, F., Reitberger, V., Hengst, C., Bilke-Krause, C., Kulozik, U., & Dombrowski, J. (2021). Correlation between Physico-Chemical Characteristics of Particulated β -Lactoglobulin and Its Behavior at Air/Water and Oil/Water Interfaces. *Foods (Basel, Switzerland)*, 10(6), 1426. <https://doi.org/10.3390/foods10061426>
- La Fuente, M. A. de, Singh, H., & Hemar, Y. (2002). Recent advances in the characterisation of heat-induced aggregates and intermediates of whey proteins. *Trends in Food Science & Technology*, 13(8), 262–274. [https://doi.org/10.1016/S0924-2244\(02\)00133-4](https://doi.org/10.1016/S0924-2244(02)00133-4)
- Lad, M. D., Birembaut, F., Matthew, J. M., Frazier, R. A., & Green, R. J. (2006). The adsorbed conformation of globular proteins at the air/water interface. *Physical Chemistry Chemical Physics*, 8(18), 2179–2186. <https://doi.org/10.1039/B515934B>
- Lam, S., Velikov, K. P., & Velev, O. D. (2014). Pickering stabilization of foams and emulsions with particles of biological origin. *Current Opinion in Colloid & Interface Science*, 19(5), 490–500. <https://doi.org/10.1016/j.cocis.2014.07.003>
- Lazidis, A., Hancocks, R. D., Spyropoulos, F., Kreuß, M., Berrocal, R., & Norton, I. T. (2016). Whey protein fluid gels for the stabilisation of foams. *Food Hydrocolloids*, 53, 209–217. <https://doi.org/10.1016/j.foodhyd.2015.02.022>
- Lech, F. J., Delahaije, R. J.B.M., Meinders, M. B.J., Gruppen, H., & Wierenga, P. A. (2016). Identification of critical concentrations determining foam ability and stability of β -lactoglobulin. *Food Hydrocolloids*, 57(22), 46–54. <https://doi.org/10.1016/j.foodhyd.2016.01.005>
- Leeb, E., Haller, N., & Kulozik, U. (2018). Effect of pH on the reaction mechanism of thermal denaturation and aggregation of bovine β -lactoglobulin. *International Dairy Journal*, 78, 103–111. <https://doi.org/10.1016/j.idairyj.2017.09.006>
- Levay, P. F., & Viljoen, M. (1995). Lactoferrin: a general review. *Haematologica*, 80(3), 252–267.
- Li, T., Wang, C., Li, T., Ma, L., Sun, D., Hou, J., & Jiang, Z. (2018). Surface Hydrophobicity and Functional Properties of Citric Acid Cross-Linked Whey Protein Isolate: The Impact of pH and Concentration of Citric Acid. *Molecules (Basel, Switzerland)*, 23(9). <https://doi.org/10.3390/molecules23092383>
- Lucassen-Reynders, E. H. (1981). *Anionic surfactants: Physical chemistry of surfactant action. Surfactant science series: Vol. 11*. New York: Dekker.
- Maldonado-Valderrama, J., Fainerman, V. B., Aksenenko, E., Jose Gálvez-Ruiz, M., Cabrerizo-Vílchez, M. A., & Miller, R. (2005). Dynamics of protein adsorption at the oil–water interface: comparison with a theoretical model. *Colloids and Surfaces A: Physicochemical and Engineering Aspects*, 261(1-3), 85–92. <https://doi.org/10.1016/j.colsurfa.2004.10.131>

- Marinova, K. G., Basheva, E. S., Nenova, B., Temelska, M., Mirarefi, A. Y., Campbell, B., & Ivanov, I. B. (2009). Physico-chemical factors controlling the foamability and foam stability of milk proteins: Sodium caseinate and whey protein concentrates. *Food Hydrocolloids*, 23(7), 1864–1876. <https://doi.org/10.1016/j.foodhyd.2009.03.003>
- Martin, A. H., Grolle, K., Bos, M. A., Cohen Stuart, M. A., & van Vliet, T. (2002). Network forming properties of various proteins adsorbed at the air/water interface in relation to foam stability. *Journal of Colloid and Interface Science*, 254(1), 175–183. <https://doi.org/10.1006/jcis.2002.8592>
- McClements, D. J. (2005). *Food emulsions: Principles, practices, and techniques* (2. ed.). CRC series in contemporary food science. Boca Raton, Fla.: CRC Press. Retrieved from <http://www.loc.gov/catdir/enhancements/fy0646/2004054209-d.html>
- McClements, D. J. (2012). Nanoemulsions versus microemulsions: Terminology, differences, and similarities. *Soft matter*, 8(6), 1719–1729. <https://doi.org/10.1039/C2SM06903B>
- McClements, D. J., & Jafari, S. M. (2018). Improving emulsion formation, stability and performance using mixed emulsifiers: A review. *Advances in Colloid and Interface Science*, 251, 55–79. <https://doi.org/10.1016/j.cis.2017.12.001>
- McSwiney, M., Singh, H., & Campanella, O. H. (1994). Thermal aggregation and gelation of bovine β -lactoglobulin. *Food Hydrocolloids*, 8(5), 441–453. [https://doi.org/10.1016/S0268-005X\(09\)80087-8](https://doi.org/10.1016/S0268-005X(09)80087-8)
- Meinders, M. B. J., & Jongh, H. H. J. de (2002). Limited conformational change of beta-lactoglobulin when adsorbed at the air-water interface. *Biopolymers*, 67(4-5), 319–322. <https://doi.org/10.1002/bip.10115>
- Miller, R., Fainerman, V. B., Makievski, A. V., Krägel, J., Grigoriev, D. O., Kazakov, V. N., & Sinyachenko, O. V. (2000). Dynamics of protein and mixed protein/surfactant adsorption layers at the water/fluid interface. *Advances in colloid and interface science*, 86(1-2), 39–82. [https://doi.org/10.1016/S0001-8686\(00\)00032-4](https://doi.org/10.1016/S0001-8686(00)00032-4)
- Monahan, F. J., German, J. B., & Kinsella, J. E. (1995). Effect of pH and temperature on protein unfolding and thiol/disulfide interchange reactions during heat-induced gelation of whey proteins. *Journal of Agricultural and Food Chemistry*, 43(1), 46–52. <https://doi.org/10.1021/jf00049a010>
- Moro, A., Gatti, C., & Delorenzi, N. (2001). Hydrophobicity of whey protein concentrates measured by fluorescence quenching and its relation with surface functional properties. *Journal of Agricultural and Food Chemistry*, 49(10), 4784–4789. <https://doi.org/10.1021/jf001132e>
- Moro, A., Báez, G. D., Ballerini, G. A., Busti, P. A., & Delorenzi, N. J. (2013). Emulsifying and foaming properties of β -lactoglobulin modified by heat treatment. *Food Research International*, 51(1), 1–7. <https://doi.org/10.1016/j.foodres.2012.11.011>

- Moro, A., Báez, G. D., Busti, P. A., Ballerini, G. A., & Delorenzi, N. J. (2011). Effects of heat-treated β -lactoglobulin and its aggregates on foaming properties. *Food Hydrocolloids*, 25(5), 1009–1015. <https://doi.org/10.1016/j.foodhyd.2010.09.021>
- Mulvihill, D. M., & Donovan, M. (1987). Whey Proteins and Their Thermal Denaturation - A Review. *Irish Journal of Food Science and Technology*. (11), 43–75. Retrieved from <http://www.jstor.org/stable/25558153>
- Murphy, R. W., Farkas, B. E., & Jones, O. G. (2016). Dynamic and viscoelastic interfacial behavior of β -lactoglobulin microgels of varying sizes at fluid interfaces. *Journal of Colloid and Interface Science*, 466, 12–19. <https://doi.org/10.1016/j.jcis.2015.12.012>
- Murphy, R. W., Zhu, L., Narsimhan, G., & Jones, O. G. (2018). Impacts of Size and Deformability of β -Lactoglobulin Microgels on the Colloidal Stability and Volatile Flavor Release of Microgel-Stabilized Emulsions. *Gels (Basel, Switzerland)*, 4(3). <https://doi.org/10.3390/gels4030079>
- Nicolai, T., Britten, M., & Schmitt, C. (2011). β -Lactoglobulin and WPI aggregates: Formation, structure and applications. *Food Hydrocolloids*, 25(8), 1945–1962. <https://doi.org/10.1016/j.foodhyd.2011.02.006>
- Nicolai, T., & Durand, D. (2013). Controlled food protein aggregation for new functionality. *Current Opinion in Colloid & Interface Science*, 18(4), 249–256. <https://doi.org/10.1016/j.cocis.2013.03.001>
- Oetjen, K., Bilke-Krause, C., Madani, M., & Willers, T. (2014). Temperature effect on foamability, foam stability, and foam structure of milk. *Colloids and Surfaces A: Physicochemical and Engineering Aspects*, 460, 280–285. <https://doi.org/10.1016/j.colsurfa.2014.01.086>
- Pace, C. N. (1986). Determination and analysis of urea and guanidine hydrochloride denaturation curves. *Methods in Enzymology*, 131, 266–280. [https://doi.org/10.1016/0076-6879\(86\)31045-0](https://doi.org/10.1016/0076-6879(86)31045-0)
- Pace, C.N., & Marshall, H. F. (1980). A comparison of the effectiveness of protein denaturants for β -lactoglobulin and ribonuclease. *Archives of Biochemistry and Biophysics*, 199(1), 270–276. [https://doi.org/10.1016/0003-9861\(80\)90281-7](https://doi.org/10.1016/0003-9861(80)90281-7)
- Patocka, G., & Jelen, P. (1991). Calcium Association With Isolated Whey Proteins. *Canadian Institute of Food Science and Technology Journal*, 24(5), 218–223. [https://doi.org/10.1016/S0315-5463\(91\)70155-7](https://doi.org/10.1016/S0315-5463(91)70155-7)
- Permyakov, E. A., & Berliner, L. J. (2000). α -Lactalbumin: Structure and function. *FEBS Letters*, 473(3), 269–274. [https://doi.org/10.1016/S0014-5793\(00\)01546-5](https://doi.org/10.1016/S0014-5793(00)01546-5)
- Pessen, H., Purcell, J. M., & Farrell, H. M. (1985). Proton relaxation rates of water in dilute solutions of β -lactoglobulin. Determination of cross relaxation and correlation with structural changes by the use of two genetic variants of a self-associating globular protein. *Biochimica et Biophysica Acta (BBA) - Protein Structure and Molecular Enzymology*, 828(1), 1–12. [https://doi.org/10.1016/0167-4838\(85\)90002-0](https://doi.org/10.1016/0167-4838(85)90002-0)

- Picard, C., Garrigue, P., Tatry, M.-C., Lapeyre, V., Ravaine, S., Schmitt, V., & Ravaine, V. (2017). Organization of Microgels at the Air-Water Interface under Compression: Role of Electrostatics and Cross-Linking Density. *Langmuir : the ACS Journal of Surfaces and Colloids*, 33(32), 7968–7981. <https://doi.org/10.1021/acs.langmuir.7b01538>
- Pickering, S. U. (1907). CXCVI. — Emulsions. *J. Chem. Soc., Trans.*, 91(0), 2001–2021. <https://doi.org/10.1039/CT9079102001>
- Pierce, A., Colavizza, D., Benaissa, M., Maes, P., Tartar, A., Montreuil, J., & Spik, G. (1991). Molecular cloning and sequence analysis of bovine lactotransferrin. *European Journal of Biochemistry*, 196(1), 177–184. <https://doi.org/10.1111/j.1432-1033.1991.tb15801.x>
- Pinaud, F., Geisel, K., Massé, P., Catargi, B., Isa, L., Richtering, W., . . . Schmitt, V. (2014). Adsorption of microgels at an oil-water interface: Correlation between packing and 2D elasticity. *Soft Matter*, 10(36), 6963–6974. <https://doi.org/10.1039/C4SM00562G>
- Poole, L. B. (2015). The basics of thiols and cysteines in redox biology and chemistry. *Free Radical Biology & Medicine*, 80, 148–157. <https://doi.org/10.1016/j.freeradbiomed.2014.11.013>
- Pots, A. M., Gruppen, H., Hessing, M., van Boekel, M. A., & Voragen, A. G. (1999). Isolation and characterization of patatin isoforms. *Journal of Agricultural and Food Chemistry*, 47(11), 4587–4592. <https://doi.org/10.1021/jf981180n>
- Pots, A. M., Jongh, H. H. de, Gruppen, H., Hamer, R. J., & Voragen, A. G. (1998). Heat-induced conformational changes of patatin, the major potato tuber protein. *European Journal of Biochemistry*, 252(1), 66–72. <https://doi.org/10.1046/j.1432-1327.1998.2520066.x>
- Qi, X. L., Holt, C., McNulty, D., Clarke, D. T., Brownlow, S., & Jones, G. R. (1997). Effect of temperature on the secondary structure of beta-lactoglobulin at pH 6.7, as determined by CD and IR spectroscopy: A test of the molten globule hypothesis. *The Biochemical Journal*, 324 (Pt 1), 341–346. <https://doi.org/10.1042/bj3240341>
- Racusen, D., & Foote, M. (1980). A major soluble glycoprotein of potato tubers. *Journal of Food Biochemistry*, 4(1), 43–52. <https://doi.org/10.1111/j.1745-4514.1980.tb00876.x>
- Racusen, D., & Weller, D. L. (1984). Molecular Weight Of Patatin, A Major Potato Tuber Protein. *Journal of Food Biochemistry*, 8(2), 103–107. <https://doi.org/10.1111/j.1745-4514.1984.tb00318.x>
- Ravera, F., Loglio, G., & Kovalchuk, V. I. (2010). Interfacial dilational rheology by oscillating bubble/drop methods. *Current Opinion in Colloid & Interface Science*, 15(4), 217–228. <https://doi.org/10.1016/j.cocis.2010.04.001>
- Riddles, P. W., Blakeley, R. L., & Zerner, B. (1983). [8] Reassessment of Ellman's reagent. In C. H. W. Hirs (Ed.), *Methods in Enzymology: Vol. 91. Enzyme structure*

- (Vol. 91, pp. 49–60). New York, NY: Acad. Press. [https://doi.org/10.1016/S0076-6879\(83\)91010-8](https://doi.org/10.1016/S0076-6879(83)91010-8)
- Riener, C. K., Kada, G., & Gruber, H. J. (2002). Quick measurement of protein sulfhydryls with Ellman's reagent and with 4,4'-dithiodipyridine. *Analytical and Bioanalytical Chemistry*, 373(4-5), 266–276. <https://doi.org/10.1007/s00216-002-1347-2>
- Rodríguez Patino, J. M., Rodríguez Niño, M. R., & Sánchez, C. C. (1999). Adsorption of whey protein isolate at the oil-water interface as a function of processing conditions: a rheokinetic study. *Journal of Agricultural and Food Chemistry*, 47(6), 2241–2248. <https://doi.org/10.1021/jf981119i>
- Roefs, S. P. F. M., & Kruif, K. G. (1994). A Model for the Denaturation and Aggregation of beta-Lactoglobulin. *European Journal of Biochemistry*, 226(3), 883–889. <https://doi.org/10.1111/j.1432-1033.1994.00883.x>
- Rühs, P. A., Scheuble, N., Windhab, E. J., Mezzenga, R., & Fischer, P. (2012). Simultaneous control of pH and ionic strength during interfacial rheology of β -lactoglobulin fibrils adsorbed at liquid/liquid Interfaces. *Langmuir : the ACS Journal of Surfaces and Colloids*, 28(34), 12536–12543. <https://doi.org/10.1021/la3026705>
- Rullier, B., Novales, B., & Axelos, M. A.V. (2008). Effect of protein aggregates on foaming properties of β -lactoglobulin. *Colloids and Surfaces A: Physicochemical and Engineering Aspects*, 330(2-3), 96–102. <https://doi.org/10.1016/j.colsurfa.2008.07.040>
- Ryan, K. N., Zhong, Q., & Foegeding, E. A. (2013). Use of whey protein soluble aggregates for thermal stability-a hypothesis paper. *Journal of Food Science*, 78(8), R1105-15. <https://doi.org/10.1111/1750-3841.12207>
- Sarkar, A., & Dickinson, E. (2020). Sustainable food-grade Pickering emulsions stabilized by plant-based particles. *Current Opinion in Colloid & Interface Science*, 49, 69–81. <https://doi.org/10.1016/j.cocis.2020.04.004>
- Sawyer, L., & Kontopidis, G. (2000). The core lipocalin, bovine β -lactoglobulin. *Biochimica et Biophysica Acta (BBA) - Protein Structure and Molecular Enzymology*, 1482(1-2), 136–148. [https://doi.org/10.1016/S0167-4838\(00\)00160-6](https://doi.org/10.1016/S0167-4838(00)00160-6)
- Sawyer, L., Kontopidis, G., & Wu, S.-Y. (1999). beta-Lactoglobulin - a three-dimensional perspective. *International Journal of Food Science and Technology*, 34(5-6), 409–418. <https://doi.org/10.1046/j.1365-2621.1999.00320.x>
- Schmidt, S., Liu, T., Rutten, S., Phan, K.-H., Moller, M., & Richtering, W. (2011). Influence of microgel architecture and oil polarity on stabilization of emulsions by stimuli-sensitive core-shell poly(N-isopropylacrylamide-co-methacrylic acid) microgels: Mickering versus Pickering behavior? *Langmuir : the ACS Journal of Surfaces and Colloids*, 27(16), 9801–9806. <https://doi.org/10.1021/la201823b>
- Schmitt, C., Bovay, C., & Rouvet, M. (2014). Bulk self-aggregation drives foam stabilization properties of whey protein microgels. *Food Hydrocolloids*, 42, 139–148. <https://doi.org/10.1016/j.foodhyd.2014.03.010>
- Schmitt, C., Bovay, C., Rouvet, M., Shojaei-Rami, S., & Kolodziejczyk, E. (2007). Whey protein soluble aggregates from heating with NaCl: Physicochemical, interfacial,

- and foaming properties. *Langmuir : the ACS Journal of Surfaces and Colloids*, 23(8), 4155–4166. <https://doi.org/10.1021/la0632575>
- Schmitt, C., Bovetto, L., Buczkowski, J., Oliveira Reis, G. de, Pibarot, P., Amagliani, L., & Dombrowski, J. (2021). Plant proteins and their colloidal state. *Current Opinion in Colloid & Interface Science*, 56, 101510. <https://doi.org/10.1016/j.cocis.2021.101510>
- Schramm, L. L. (Ed.) (1994). *Foams: Fundamentals and Applications in the Petroleum Industry. Advances in Chemistry*. Washington, DC: AMERICAN CHEMICAL SOCIETY.
- Schramm, L. L., & Wassmuth, F. (1994). Foams: Basic Principles. In L. L. Schramm (Ed.), *Advances in Chemistry. Foams: Fundamentals and Applications in the Petroleum Industry* (Vol. 242, pp. 3–45). Washington, DC: AMERICAN CHEMICAL SOCIETY. <https://doi.org/10.1021/ba-1994-0242.ch001>
- Shi, A., Feng, X., Wang, Q., & Adhikari, B. (2020). Pickering and high internal phase Pickering emulsions stabilized by protein-based particles: A review of synthesis, application and prospective. *Food Hydrocolloids*, 109, 106117. <https://doi.org/10.1016/j.foodhyd.2020.106117>
- Shimada, K., & Cheftel, J. C. (1989). Sulfhydryl group/disulfide bond interchange reactions during heat-induced gelation of whey protein isolate. *Journal of Agricultural and Food Chemistry*, 37(1), 161–168. <https://doi.org/10.1021/jf00085a038>
- Sobhaninia, M., Nasirpour, A., Shahedi, M., & Golkar, A. (2017). Oil-in-water emulsions stabilized by whey protein aggregates: Effect of aggregate size, pH of aggregation and emulsion pH. *Journal of Dispersion Science and Technology*, 38(9), 1366–1373.
- Sorgentini, D. A., & Wagner, J. R. (2002). Comparative study of foaming properties of whey and isolate soybean proteins. *Food Research International*, 35(8), 721–729. [https://doi.org/10.1016/S0963-9969\(02\)00067-4](https://doi.org/10.1016/S0963-9969(02)00067-4)
- Stubenrauch, C., & Klitzing, R. von (2003). Disjoining pressure in thin liquid foam and emulsion films—new concepts and perspectives. *Journal of Physics: Condensed Matter*, 15(27), R1197-R1232. <https://doi.org/10.1088/0953-8984/15/27/201>
- Suttiprasit, P., Krisdhasima, V., & McGuire, J. (1992). The surface activity of α -lactalbumin, β -lactoglobulin, and bovine serum albumin. *Journal of colloid and interface science*, 154(2), 316–326. [https://doi.org/10.1016/0021-9797\(92\)90146-D](https://doi.org/10.1016/0021-9797(92)90146-D)
- Tadros, T. F. (2009). *Emulsion science and technology*. Weinheim: Wiley-VCH. Retrieved from <http://dx.doi.org/10.1002/9783527626564>
- Tadros, T. F. (2014). *Formulation of Disperse Systems*: Wiley.
- Talansier, E., Loisel, C., Dellavalle, D., Desrumaux, A., Lechevalier, V., & Legrand, J. (2009). Optimization of dry heat treatment of egg white in relation to foam and interfacial properties. *LWT*, 42(2), 496–503. <https://doi.org/10.1016/j.lwt.2008.09.013>

- Tanford, C., Bunville, L. G., & Nozaki, Y. (1959). The Reversible Transformation of β -Lactoglobulin at pH 7.5. *Journal of the American Chemical Society*, 81(15), 4032–4036. <https://doi.org/10.1021/ja01524a054>
- Tang, J., Quinlan, P. J., & Tam, K. C. (2015). Stimuli-responsive Pickering emulsions: Recent advances and potential applications. *Soft Matter*, 11(18), 3512–3529. <https://doi.org/10.1039/C5SM00247H>
- Tcholakova, S., Denkov, N. D., & Lips, A. (2008). Comparison of solid particles, globular proteins and surfactants as emulsifiers. *Physical Chemistry Chemical Physics : PCCP*, 10(12), 1608–1627. <https://doi.org/10.1039/B715933C>
- Tcholakova, S., Denkov, N. D., Sidzhakova, D., Ivanov, I. B., & Campbell, B. (2003). Interrelation between Drop Size and Protein Adsorption at Various Emulsification Conditions. *Langmuir*, 19(14), 5640–5649. <https://doi.org/10.1021/la034411f>
- Thompson, A., Singh, H., & Boland, M. (Eds.) (2009). *Milk proteins: From expression to food. Food science and technology international series*. San Diego, Calif, London: Academic Press. Retrieved from <http://www.sciencedirect.com/science/book/9780124051713>
- Timasheff, S. N., & Townend, R. (1964). Structure of the β -Lactoglobulin Tetramer. *Nature*, 203(4944), 517–519. <https://doi.org/10.1038/203517a0>
- Tolkach, A., & Kulozik, U. (2005). Effect of pH and temperature on the reaction kinetic parameters of the thermal denaturation of β -lactoglobulin. *Milchwissenschaft*. (60), 249–252.
- Tolkach, A. (2007). *Thermisches Denaturierungsverhalten von Molkenproteinfraktionen: Selektive Denaturierung - Fraktionierung mit Membranen - Reaktions-, Auffaltungs- und Aggregationskinetik* (Dissertation). Technische Universität München.
- Tolkach, A., & Kulozik, U. (2007). Reaction kinetic pathway of reversible and irreversible thermal denaturation of β -lactoglobulin. *Le Lait*, 87(4-5), 301–315. <https://doi.org/10.1051/lait:2007012>
- Töpel, A. (2016). *Chemie und Physik der Milch: Naturstoff, Rohstoff, Lebensmittel* (4. überarbeitete Auflage). Hamburg: Behr's Verlag. Retrieved from <http://www.behrs.de>
- Toro-Sierra, J., Tolkach, A., & Kulozik, U. (2013). Fractionation of α -Lactalbumin and β -Lactoglobulin from Whey Protein Isolate Using Selective Thermal Aggregation, an Optimized Membrane Separation Procedure and Resolubilization Techniques at Pilot Plant Scale. *Food and Bioprocess Technology*, 6(4), 1032–1043. <https://doi.org/10.1007/s11947-011-0732-2>
- Townsend, A.-A., & Nakai, S. (1983). Relationships Between Hydrophobicity and Foaming Characteristics of Food Proteins. *Journal of food science*, 48(2), 588–594. <https://doi.org/10.1111/j.1365-2621.1983.tb10796.x>
- Tripp, B. C., Magda, J. J., & Andrade, J. D. (1995). Adsorption of Globular Proteins at the Air/Water Interface as Measured via Dynamic Surface Tension: Concentration

- Dependence, Mass-Transfer Considerations, and Adsorption Kinetics. *Journal of colloid and interface science*, 173(1), 16–27. <https://doi.org/10.1006/jcis.1995.1291>
- Ulaganathan, V., Retzlaff, I., Won, J. Y., Gochev, G., Gehin-Delval, C., Leser, M., . . . Miller, R. (2017). β -Lactoglobulin adsorption layers at the water/air surface: 1. Adsorption kinetics and surface pressure isotherm: Effect of pH and ionic strength. *Colloids and Surfaces A: Physicochemical and Engineering Aspects*, 519, 153–160. <https://doi.org/10.1016/j.colsurfa.2016.03.008>
- Ulaganathan, V., Retzlaff, I., Won, J. Y., Gochev, G., Gunes, D. Z., Gehin-Delval, C., . . . Miller, R. (2017). β -Lactoglobulin adsorption layers at the water/air surface: 2. Dilational rheology: Effect of pH and ionic strength. *Colloids and Surfaces A: Physicochemical and Engineering Aspects*, 521, 167–176. <https://doi.org/10.1016/j.colsurfa.2016.08.064>
- Unterhaslberger, G., Schmitt, C., Sanchez, C., Appolonia-Nouzille, C., & Raemy, A. (2006). Heat denaturation and aggregation of β -lactoglobulin enriched WPI in the presence of arginine HCl, NaCl and guanidinium HCl at pH 4.0 and 7.0. *Food Hydrocolloids*, 20(7), 1006–1019. <https://doi.org/10.1016/j.foodhyd.2005.10.017>
- Verheul, M., Pedersen, J. S., Roefs, S. P. F. M., & Kruif, K. G. de (1999). Association behavior of native β -lactoglobulin. *Biopolymers*, 49(1), 11–20. [https://doi.org/10.1002/\(SICI\)1097-0282\(199901\)49:1<11::AID-BIP2>3.0.CO;2-1](https://doi.org/10.1002/(SICI)1097-0282(199901)49:1<11::AID-BIP2>3.0.CO;2-1)
- Verheul, M., Roefs, S. P. F. M., & Kruif, K. G. de (1998). Kinetics of Heat-Induced Aggregation of β -Lactoglobulin. *Journal of Agricultural and Food Chemistry*, 46(3), 896–903. <https://doi.org/10.1021/jf970751t>
- Visschers, R. W., & Jongh, H. H. J. de (2005). Disulphide bond formation in food protein aggregation and gelation. *Biotechnology Advances*, 23(1), 75–80. <https://doi.org/10.1016/j.biotechadv.2004.09.005>
- Walstra, P. (2003). *Physical chemistry of foods. Food science and technology: Vol. 121*. New York: Marcel Dekker. Retrieved from <http://site.ebrary.com/lib/alltitles/docDetail.action?docID=10050780>
- Wang, K., Sun, D.-W., Wei, Q., & Pu, H. (2018). Quantification and visualization of α -tocopherol in oil-in-water emulsion based delivery systems by Raman microspectroscopy. *LWT*, 96(9), 66–74. <https://doi.org/10.1016/j.lwt.2018.05.017>
- Watanabe, K., & Klostermeyer, H. (1976). Heat-induced changes in sulphhydryl and disulphide levels of β -lactoglobulin A and the formation of polymers. *Journal of Dairy Research*, 43(3), 411–418. <https://doi.org/10.1017/S0022029900015995>
- Watanabe, K., & Klostermeyer, H. (1977). Bildung von Dehydroalanin, Lanthionin und Lysinoalanin beim Erhitzen von beta-Lactoglobulin A [Formation of dehydroalanine, lanthionine and lysinoalanine during heat treatment of beta-lactoglobuline A (author's transl)]. *Zeitschrift fur Lebensmittel-Untersuchung und -Forschung*, 164(2), 77–79. <https://doi.org/10.1007/BF01354304>

- Wierenga, P. A., & Gruppen, H. (2010). New views on foams from protein solutions. *Current Opinion in Colloid & Interface Science*, 15(5), 365–373. <https://doi.org/10.1016/j.cocis.2010.05.017>
- Wierenga, P. A., Meinders, M. B. J., Egmond, M. R., Voragen, F. A. G. J., & Jongh, H. H. J. de (2003). Protein Exposed Hydrophobicity Reduces the Kinetic Barrier for Adsorption of Ovalbumin to the Air–Water Interface. *Langmuir : the ACS journal of surfaces and colloids*, 19(21), 8964–8970. <https://doi.org/10.1021/la034868p>
- Wierenga, P. A., Meinders, M. B. J., Egmond, M. R., Voragen, A. G. J., & Jongh, H. H. J. de (2005). Quantitative description of the relation between protein net charge and protein adsorption to air-water interfaces. *The Journal of Physical Chemistry. B*, 109(35), 16946–16952. <https://doi.org/10.1021/jp050990g>
- Wilde, P.J. (2000). Interfaces: Their role in foam and emulsion behaviour. *Current Opinion in Colloid & Interface Science*, 5(3-4), 176–181. [https://doi.org/10.1016/S1359-0294\(00\)00056-X](https://doi.org/10.1016/S1359-0294(00)00056-X)
- Wilde, P., Mackie, A., Husband, F., Gunning, P., & Morris, V. (2004). Proteins and emulsifiers at liquid interfaces. *Advances in Colloid and Interface Science*, 108-109, 63–71. <https://doi.org/10.1016/j.cis.2003.10.011>
- Williams, A., & Prins, A. (1996). Comparison of the dilational behaviour of adsorbed milk proteins at the air-water and oil-water interfaces. *Colloids and Surfaces A: Physicochemical and Engineering Aspects*, 114, 267–275. [https://doi.org/10.1016/0927-7757\(96\)03534-0](https://doi.org/10.1016/0927-7757(96)03534-0)
- Wilson, A. (1989). *Foams: Physics, Chemistry and Structure*. Springer Series in Applied Biology. London: Springer London; Imprint; Springer.
- Winkler, T., & Schörkl, R. (2011). Foam Behavior and Foam Stability of Aqueous Surfactant Solutions. *SOFW-Journal*. (4), 46–52.
- Wit, J. N. de (2009). Thermal behaviour of bovine β -lactoglobulin at temperatures up to 150°C. a review. *Trends in Food Science & Technology*, 20(1), 27–34. <https://doi.org/10.1016/j.tifs.2008.09.012>
- Wolz, M., & Kulozik, U. (2015). Thermal denaturation kinetics of whey proteins at high protein concentrations. *International Dairy Journal*, 49, 95–101. <https://doi.org/10.1016/j.idairyj.2015.05.008>
- Won, J. Y., Gochev, G. G., Ulaganathan, V., Krägel, J., Aksenenko, E. V., Fainerman, V. B., & Miller, R. (2017a). Dilational visco-elasticity of BLG adsorption layers at the solution/tetradecane interface – Effect of pH and ionic strength. *Colloids and Surfaces A: Physicochemical and Engineering Aspects*, 521, 204–210. <https://doi.org/10.1016/j.colsurfa.2016.08.054>
- Won, J. Y., Gochev, G. G., Ulaganathan, V., Krägel, J., Aksenenko, E. V., Fainerman, V. B., & Miller, R. (2017b). Effect of solution pH on the adsorption of BLG at the solution/tetradecane interface. *Colloids and Surfaces A: Physicochemical and Engineering Aspects*, 519, 161–167. <https://doi.org/10.1016/j.colsurfa.2016.05.042>

- Wu, J., Shi, M., Li, W., Zhao, L., Wang, Z., Yan, X., . . . Li, Y. (2015). Pickering emulsions stabilized by whey protein nanoparticles prepared by thermal cross-linking. *Colloids and Surfaces. B, Biointerfaces*, 127, 96–104. <https://doi.org/10.1016/j.colsurfb.2015.01.029>
- Www.krüss.de (2021).
- Zhou, B., Tobin, J. T., Drusch, S., & Hogan, S. A. (2021). Dynamic adsorption and interfacial rheology of whey protein isolate at oil-water interfaces: Effects of protein concentration, pH and heat treatment. *Food Hydrocolloids*, 116(11), 106640. <https://doi.org/10.1016/j.foodhyd.2021.106640>
- Zhou, X., Sala, G., & Sagis, L. M.C. (2020). Bulk and interfacial properties of milk fat emulsions stabilized by whey protein isolate and whey protein aggregates. *Food Hydrocolloids*, 109, 106100. <https://doi.org/10.1016/j.foodhyd.2020.106100>
- Zuniga, R. N., Tolkach, A., Kulozik, U., & Aguilera, J. M. (2010). Kinetics of formation and physicochemical characterization of thermally-induced beta-lactoglobulin aggregates. *Journal of Food Science*, 75(5), 8. <https://doi.org/10.1111/j.1750-3841.2010.01617.x>.